

Investigation of Interfaces in Flexible Polymer Lithium Ion Batteries

**by
Qiang Fu**

**A Dissertation Submitted to the
Materials Science and Engineering Program,
Cullen College of Engineering
in partial Fulfillment of the Requirements for the degree of**

DOCTOR OF PHILOSOPHY

in Materials Science and Engineering

Chair of Committee: Dr. Haleh Ardebili

Committee Member: Dr. Jae-Hyun Ryou

Committee Member: Dr. Alamgir Karim

Committee Member: Dr. John C. Wolfe

Committee Member: Dr. Hadi Ghasemi

**University of Houston
December 2021**

DEDICATION

This thesis is dedicated to the memory of my grandpa Chuanzhong Fu. Although he wanted to attend my dissertation for my Ph.D. degree, he was unable to see my graduation in person. He is still alive in my heart. His hard-working and kind personality always encourages me to face difficulties.

Thanks to my advisor Dr. Ardebili who guided me in the last four years, and the committee who kept me on track. I always remember her quote: What? Why? How? I need to prepare to ask myself these three questions before I start a project. Her kindness, patience, encouragement and push for tenacity ring in my ears. I appreciate for all she has done, especially research growth road, technology skills, and personality.

I dedicate this thesis to my parents and my young brother, who always encouraged me and inspired the pursuit of my major. It's the best time to have a 2 hours video chat with them every Saturday morning.

This thesis is dedicated to my colleagues and all my friends who motivate me to pursue my dream and finish my dissertation. They guide me from experiments to life. We talk about research and sports. I stay happy while living a busy life.

Lastly, I want to thank all the difficulties I have met. I know hardship is the basis for success. Without them, I do not have the experience, knowledge, and abilities to move forward. Curiosity is the light during the journey on this research road.

ACKNOWLEDGEMENT

Firstly, I want to thank my advisor Dr. Ardebili for her guidance on this thesis. I learn how to finish a research project in a scientific way from experiment design, assumptions, hands-on operation, batteries fabrication and analysis, modeling, and writing a report. I also thank her for help on my teaching assistant job. I become familiar with this challenging job. I also learned how to talk with students. I also learned about the grading approach that ensures grading is consistent and fair to all students. She gives me freedom for my research and lets me focus on the project I am interested in. Working on research and projects is fantastic.

I also want to thank my committee member Dr. Wolfe, Dr. Ryou, Dr. Karim, Dr. Ghasemi. They gave me a lot of suggestions.

I want to thank all my friends. I remember they told me to be practical and improve myself. Otherwise, you could not make it. I think having passion, enthusiasm, and curiosity is very important for my life and research.

I want to thank my family. They allow me to study abroad and encourage me to do my favorite subject: solar cells to batteries. They are always my supporters. I would like to explore more to find the true theories. I have found my passion career with their support.

Finally, a special thanks to all people I have met in Houston. It's so lucky to meet them in my life. This work will not be possible without your presence and help. Thank you, Houston.

ABSTRACT

Flexible and stretchable solid electrolyte-based lithium-ion batteries (LIBs) can potentially revolutionize our lives. They have wide range of applications, including flexible screen displays, wearable sensors, stretchable electronics, among others. Solid polymer electrolytes (SPEs) offer many advantages such as thermal and chemical stability, appropriate mechanical behavior, wide electrochemical window, safety, flexibility and low cost. However, SPE development faces several challenges, mainly, low ionic conductivity and problems pertaining to the interface between the electrodes and solid electrolytes. A stable and highly (ion) conductive interfacial layer is of utmost importance in LIB charge/discharge, rate capability, cyclability, and safety. This dissertation investigates the interface between SPE and electrodes in flexible and stretchable batteries. Several techniques to enhance the interfaces are explored including additives, specifically, tryptic soy broth (TSB) biomaterial and fluoroethylene carbonate (FEC), and enhanced SPE fabrication strategies (multi-layer fabrication method and hot-pressing). SPE-based LIB capacity improved significantly using 0.5 wt% TSB biomaterial due to the enhanced electrode-electrolyte interface. Furthermore, due to improved stable interfacial layer formation, flexible LIBs capacity more than doubled by using the FEC additives. Our flexible LIBs were shown to power light-emitting diode (LED) under 180 degree bending angles. Furthermore, spiral stretchable LIBs were demonstrated to work under 6000% out-of-plane stretching deformation. The investigation of interfacial phenomena and solid electrolytes in LIBs can provide deeper understanding of engineering strategies to improve LIBs properties and performance. The

developed SPE-based flexible and stretchable LIBs can be promising for high safety and high-capacity energy applications.

TABLE OF CONTENTS

DEDICATION.....	ii
ACKNOWLEDGEMENT.....	iii
ABSTRACT.....	iv
TABLE OF CONTENTS.....	vi
LIST OF TABLES.....	x
LIST OF FIGURES.....	xi
I. INTRODUCTION.....	1
1.1 Motivation.....	1
1.2 Materials and working principle of lithium ion batteries	3
1.3 Applications.....	7
1.4 Challenges.....	9
1.5 Thesis overview.....	10
II. MATERIALS REVIEW FOR LITHIUM ION BATTEIES.....	12
2.1 Background.....	12
2.2 Solid state electrolyte applied in the flexible Lithium ion battery.....	13
2.2.1 Poly-ethylene oxide (PEO) and its composite.....	14
2.2.2 Poly-acrylonitrile (PAN).....	22
2.2.3 Poly-methyl methacrylate (PMMA).....	26
2.2.4 Poly-vinylchloride (PVC).....	34
2.2.5 Poly-vinylidene fluoride (PVDF).....	36
2.2.6 Poly-propylene carbonate (PPC).....	41
2.2.7 Other polymer electrolyte and methods.....	44

2.2.8 Summary.....	47
2.3 Inorganic electrolytes.....	47
2.3.1 Li ₂ S based sulfides.....	49
2.3.2 Nasicon type - LAGP.....	51
2.3.3 Garnet type Li ₇ La ₃ Zr ₂ O ₁₂ (LLZO).....	52
2.3.4 LiPON.....	54
2.4 Electrodes.....	56
2.4.1 Anode.....	58
2.4.1.1 Carbon nanotubes and graphite.....	58
2.4.1.2 Silicon anode.....	60
2.4.1.3 Mn ₃ O ₄ , Co ₃ O ₄ , SnO ₂ , FeO _x , NiO anode materials.....	61
2.4.1.4 Others.....	63
2.4.2 Cathode.....	65
2.4.2.1 Transition metal oxide cathode.....	66
2.4.2.2 Layered LiCoO ₂ (LCO).....	68
2.4.2.3 Layered LiNi _x Co _y Mn _z O ₂ (NCM)	70
2.4.2.4 Layered Li(Ni _x Co _y Al _z)O ₂ (NCA)	71
2.4.2.5 Olive LiFePO ₄	71
2.4.2.6 Layered LiMn _x Fe _{1-x} PO ₄	72
2.4.2.7 Sulfur.....	73
2.4.2.8 Others.....	75
2.5 Current collectors.....	76
2.5.1 Current collectors for anodes.....	76

2.5.2 Current collectors for cathodes.....	78
2.6 Interface.....	79
2.6.1 Special techniques for the interface.....	81
2.6.2 Interface between the electrolyte and electrode.....	83
III. ENHANCING THE INTERFACIAL AND ELECTROCHEMICAL PERFORMANCE USING BIOMATERIALS	86
3.1 Background of bio materials.....	86
3.2 Experimental methods.....	93
3.3 Results and discussions.....	94
3.4 Conclusions.....	99
IV. FLEXIBLE LITHIUM ION BATTERIES	100
4.1 Background.....	100
4.2 Experimental methods.....	103
4.3 Results and discussions.....	105
4.4 Conclusions.....	112
V. STRETCHABLE BATTERIES.....	113
5.1 Background.....	113
5.2 Experimental methods.....	116
5.3 Results and discussions.....	117
5.4 Conclusions.....	125
VI. ENHANCING INTERFACES IN SOLID POLYMER BATTERIES	126
6.1 Background	126
6.2 Experimental methods.....	128

6.3 Results and discussions.....	129
6.4 Conclusions.....	143
VII. CONCLUSIONS AND FUTURE WORKS.....	145
7.1 Conclusions.....	145
7.2 Future works.....	146
REFERENCES.....	148
VIII. APPENDICES.....	218
A. Tables.....	218
B. Figures.....	220

LIST OF TABLES

Table 1. Different polymer electrolytes material properties	14
Table 2 Current research on PEO based electrolyte	21
Table 3 Research summary on PMMA based electrolyte.....	27
Table 4 Research summary on PVC based electrolyte	36
Table 5 Research summary on PVDF based electrolyte.....	40
Table 6 Work summary for PPC based electrolyte.....	43
Table 7 Electrochemical window of electrolyte, upper plot referred from Chemistry of Materials 2015 (Richards et al.,	55
Table 8 A summary of biomaterials used for batteries	87
Table 9 TSB components.....	91
Table 10 Amino Acids of TSB	91
Table 11 Summary of the work finished.....	101
Table 12 Summary of current flexibility test.....	103
Table 13 Summary of capacity loss during stretching.....	123
Table 14 Flexible commercial electronics and our lithium ion batteries.....	218
Table 15 Polymer electrolyte ionic conductivity comparison	218
Table 16 Flexible LIBs(LiBOB) performance summary for bending test.....	218
Table 17 Flexible LIBs (LiBOB) performance summary for thermal test	219
Table 18 Stretchable LIBs performance summary for stretchability test	219
Table 19 Summary of three types polymer electrolyte flexible LIBs.....	219

LIST OF FIGURES

Figure 1 (a) Electricity Source and (b) Energy Storage Deployed Type (Excluding Pumped Storage Hydropower) (U.S.	2
Figure 2(a): Common materials used for enhancing polymer electrolyte ionic conductivity; (b) Some LIBs properties;.....	3
Figure 3(a) Energy diagram of a full battery. The mismatch of HOMO/LUMO will results in the degradation of the	5
Figure 4 Flexible Lithium-ion batteries applications.....	9
Figure 5 PAN polymer chain model and methods for improving ionic conductivity.	24
Figure 6 PMMA based electrolyte.....	29
Figure 7 Ranking of PVC polymer properties.	35
Figure 8 PPC crosslinking process	42
Figure 9 Inorganic electrolyte properties.....	48
Figure 10 Ionic conductivity summary for inorganic material	55
Figure 11. Potential of electrodes materials (red) common cathodes, (blue) common anodes. Referred from Materials.....	58
Figure 12 Typical anodes materials structure analysis	64
Figure 13 Structure for common cathode materials.....	65
Figure 14 Interphase structure inside LIBs.....	80
Figure 15 Schematics of the TSB-solid polymer electrolyte and LiCoO ₂ cathode in lithium-ion battery and the main.....	93
Figure 16 Polarized light microscopy of (a) PEO+LiClO ₄ (b) PEO+LiClO ₄ +0.5wt.% TSB (c) PEO+LiClO ₄ +1wt.%.....	95
Figure 17 Electrochemical Window stability of PEO+ LiClO ₄ with TSB and without TSB	96
Figure 18 (a) Impedance spectra of batteries based on solid polymer electrolyte without TSB and their respective.....	97
Figure 19 Ion conductivity and electrochemical characterizations (a) solid polymer electrolyte ion conductivity vs.	98
Figure 20 Flexible LIBs structure and Flexibility measurement.	101
Figure 21 (a)Capacity performance of flexible pouch cells by using LiTFSI&LiBOB(1:1 molar ratio) salts;(b).....	104
Figure 22 (a) Rate capability test for pouch cells by using LiTFSI&LiBOB; (b) flexible LIBs rate capability.....	106
Figure 23 (a) Flexible LIBs capacity performance under different bending angles; (b) In-situ flexible LIBs capacity	108
Figure 24 (a) Flexible LIBs impedance performance before bending; (b) flexible LIBs impedance performance after.....	110
Figure 25 (a) Flexible LIBs open circuit potential tracking during bending; (b) Flexible LIBs open circuit potential.....	111
Figure 26 (a) Stretchable spiral LIBs capacity performance with 2.55cm ² area at unstretched state; (b) Stretchable	117
Figure 27 (a) Spiral LIBs Capacity performance for 9.81cm ² battery; (b) Spiral LIBs rate capability test with varied	119

Figure 28 (a) Spiral LIBs potential performance under different strain; (b) spiral LIBs in-situ test to track the potential	120
Figure 29 Spiral LIBs potential tracking when 6000% strain applied.....	121
Figure 30 Spiral LIBs capacity performance during stretching from 0 to 6000% strain deformation.	122
Figure 31 Spiral LIBs stretchability test under different strain deformations	123
Figure 32 (a) Spiral LIBs Impedance at different voltage ;(b) Spiral LIBs impedance at different strains deformation.....	124
Figure 33 Flexible LIBs and its structures	130
Figure 34 (a) Capacity performance of flexible batteries (SPE including PEO:TEGDME:LiBOB); (b) Effect of FEC	132
Figure 35 Cyclic voltammetry plot for full cells (LCO/SPE/G Structure) at 0.1mV/s...	134
Figure 36 Rate capability test of batteries (a): No FEC added in SPE based LIBs; (b): FEC mixed with SPE based LIBs.	135
Figure 37 FEC & SPE device performance under 0.12C rate	136
Figure 38 LIBs capacity performance under bending state (a) pristine electrolyte LIBs without FEC; (b) LIBs with	137
Figure 39 Impedance spectroscopy for SPE with FEC battery and FEC free battery	138
Figure 40 FEC decomposition mechanism	139
Figure 41 (a) Thermal cycling performance at different temperature for pristine polymer LIBs; (b) performance after	140
Figure 42 stress – strain plot of electrolyte	141
Figure 43 (a) Polarized optical microscopy plot of electrolyte with FEC; (b) S polarized optical microscopy plot of	142
Figure 44 CV plot for LCO+FEC based LIBs and G+FEC based LIBs, scan rate at 0.1mV/s.....	142
Figure 45 Impedance measurement for SPE with FEC processed Graphite electrode; FEC processed LCO electrode	143
Figure 46 Flexible polymer LIBs powered LED lights	220
Figure 47 (a) LiB powered LED light after puncture test; (b) LiB powered LED light after bending 180 degrees	220

CHAPTER I. INTRODUCTION

1.1 Motivation

Over the estimated 14 billion years of our universe, energy storage has played an essential role in all existing things. In recent years, we have become more dependent on reliable and stable electrical energy storage methods. The high demand for electrical energy storage is ubiquitous with the increasing population. However, our current energy source from fossil fuels faces problems pertaining to the increasing environmental risks, global warming, limited availability and future depletion (Zito et al. 2019). Electricity can be generated through various sources and methods including fossil fuels, natural gas, nuclear reaction, solar energy, and wind turbines (Li et al., 2018) (U.S. Department of Energy, 2019) (**Figure 1**). In 2021, Texas suffered from a power outage problem due to the winter ice storm and inefficient electricity storage. Therefore, developing stable and high energy density electrochemical energy storage devices is necessary. Among various types of energy storages methods, lithium-ion batteries (LIBs) are highly popular and used in our everyday life, including laptops, phones, and electric cars because of their high energy density, and efficiency (Li et al., 2018). Although LIBs, have reached a relatively high level of development, there is still a need for a deep understanding of LIBs capacity loss, cycling stability, materials degradation, and side reactions to enhance battery life and cycling performance (Tarascon & Armand, 2001).

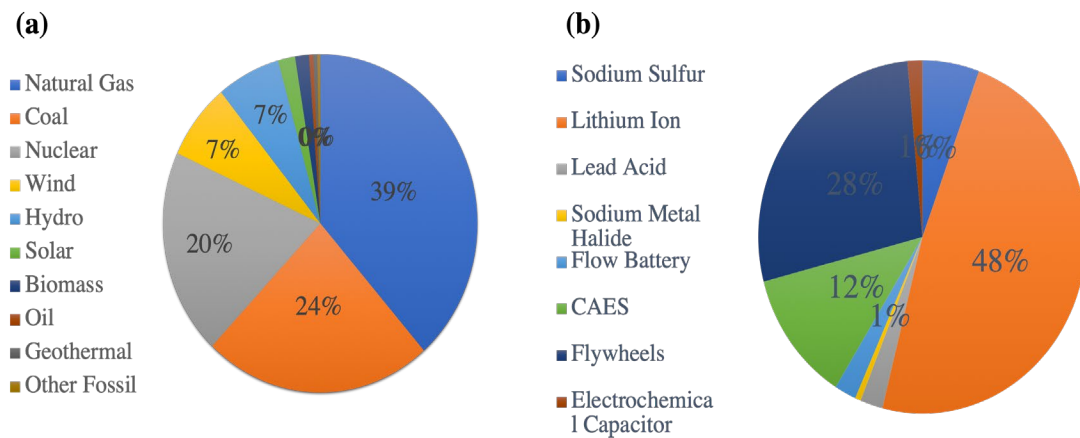


Figure 1 (a) Electricity Source and (b) Energy Storage Deployed Type (Excluding Pumped Storage Hydropower) (U.S. Department of Energy, 2019).

In addition, flexible and stretchable LIBs have been driven by a recent developing market for thin, flexible, stretchable and deformable electronics, such as flexible screen display, smart cards, wearable sensors, etc. (Nag et al., 2017) (Stoppa & Chiolerio, 2014). Conventional LIBs use liquid electrolytes, which have safety issues including electrolyte leakage, poor mechanical property, high flammability and thermal runaway. Replacing liquid electrolytes with solid materials could enhance LIBs safety (Stephan, 2006). This thesis work replaces the conventional liquid electrolyte with solid polymer electrolyte (SPE) due to its safety, flexibility and easy processing properties (Manuel Stephan, 2005). However, the low SPE ionic conductivity and poor interface between SPE and electrodes would reduce LIBs electrochemical performance (Ngai et al., 2016). Therefore, in this work, we specifically investigated and enhanced the interface of solid polymer-based lithium-ion batteries, including flexible and spiral stretchable LIBs. The formation of the solid electrolyte interface (SEI) layer (between anode and electrolyte) and cathode electrolyte interface (CEI) layer (between cathode and electrolyte) are related to electrolyte decomposition and reduction (Bard et al., 1993). The interfacial

layers play a crucial role in charge transfer, charging/discharging, capacity loss and cycling stability (Wang et al., 2020) (X. B. Cheng et al., 2015). To enhance the interface between electrodes and SPE, we focus on modifying electrolyte compositions using different LIBs additives, including tryptic soy broth (TSB) biomaterial and fluoroethylene carbonate (FEC). We also use different SPE fabrication strategies to enhance the interface between electrodes and SPE. We investigate LIBs electrochemical performance while the batteries are under bending, stretching and different temperature conditions. Our flexible and stretchable LIBs show an excellent reversible capacity and high mechanical properties.

1.2 Materials and working principle of lithium ion batteries

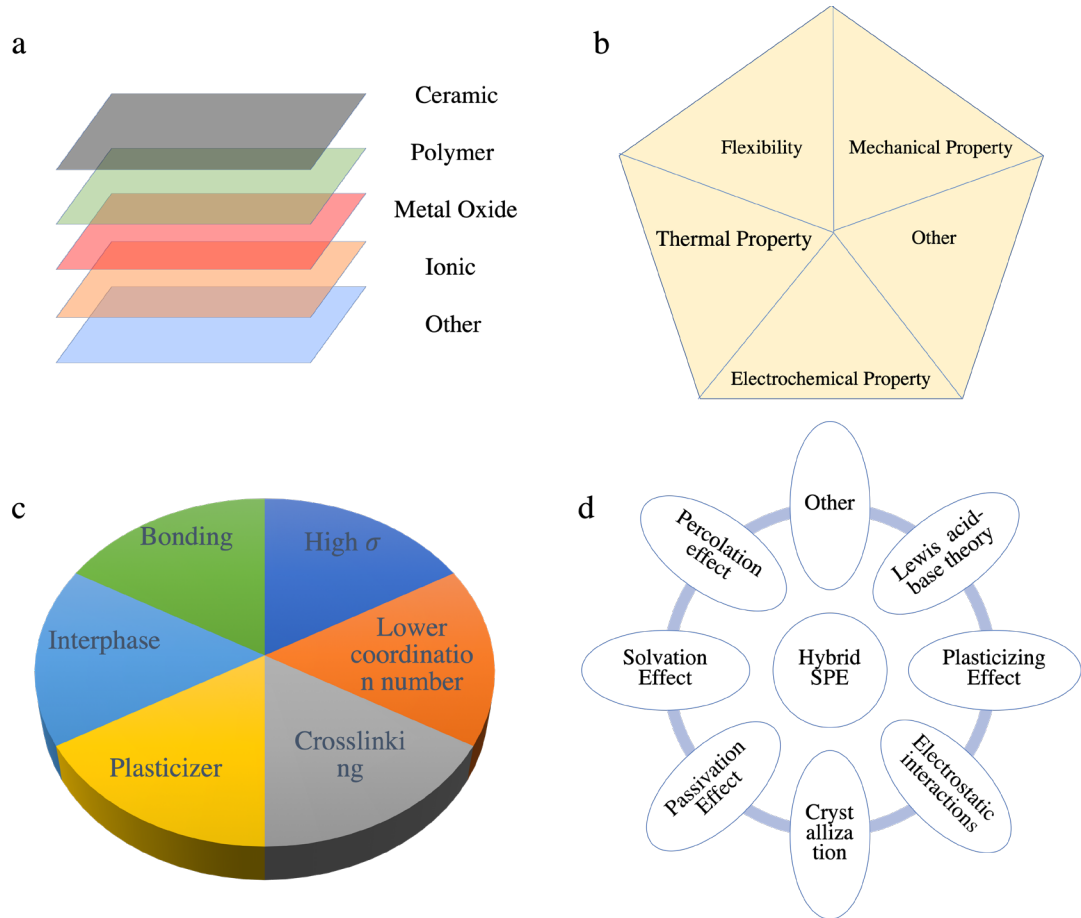


Figure 2(a): Common materials used for enhancing polymer electrolyte ionic conductivity; (b) Some LIBs properties; (c) Parameters or factors for LIBs high performance; (d) Theory for explaining high LIBs performance.

Lithium-ion batteries (LIBs) have achieved accelerated development since their early conception in the 1990s. Compared to the previous generations' batteries such as lead-acid and nickel cadmium batteries, LIBs offer higher power and energy densities. LIBs could be classified into different groups based on their electrode materials and designs. For example, C anode-lithium metal oxide cathode LIB can provide up to 275 Wh/Kg energy density, Li-O₂ shows 3505 Wh/kg energy density, and Li-S shows 2600 Wh/Kg energy densities (Yoshio et al., 2009) (X.-B. Cheng et al., 2017). Although different LIBs have varied materials and associated energy densities, LIBs are generally structured similarly. A liquid electrolyte-based LIB consists of anode, cathode, separator, electrolyte and current collectors. In solid polymer electrolyte (SPE)-based LIBs, separators and liquid electrolytes is replaced by solid ion conductive polymers (mixed with lithium salt and/or other additives). There are several polymer electrolytes, including poly (ethylene oxide) (PEO), poly (acrylonitrile) (PAN), poly (methyl methacrylate) (PMMA), Poly-vinyl chloride (PVC) and poly (vinylidene fluoride) (PVdF), etc. (Manuel Stephan, 2005). Polymer electrolytes can be mixed with different inorganic materials, lithium salts, ionic liquids, and plasticizers. The electrolyte mixtures can have different chemical compositions, which significantly influence SPE ionic conductivity and final LIBs electrochemical performance. **Figure 2** summarizes various methods of enhancing SPE ionic conductivities and consequent LIBs performances. Chapter II presents a more in-depth discussion of previous works and methods of enhancement in lithium-ion batteries.

The selection of the electrode materials in flexible and solid polymer-based LIBs is also a critical part of the design of batteries. Common cathode materials are lithium

metal oxide, including LiCoO_2 (LCO), $\text{LiMn}_x\text{Fe}_{1-x}\text{PO}_4$ (LFP), $\text{LiNi}_x\text{Co}_y\text{Mn}_z\text{O}_2$ (NCM), $\text{Li}(\text{Ni}_x\text{Co}_y\text{Al}_z)\text{O}_2$ (NCA), etc. Typical anode materials are graphite, Li metal, Si, etc. (Li et al., 2018). A more in-depth summary of the electrode materials and applications is presented in Chapter II. In this thesis, we chose LCO and graphite as our LIB electrodes owing to their high electrochemical window, high energy density, and good cycle stability compared with other electrodes materials.

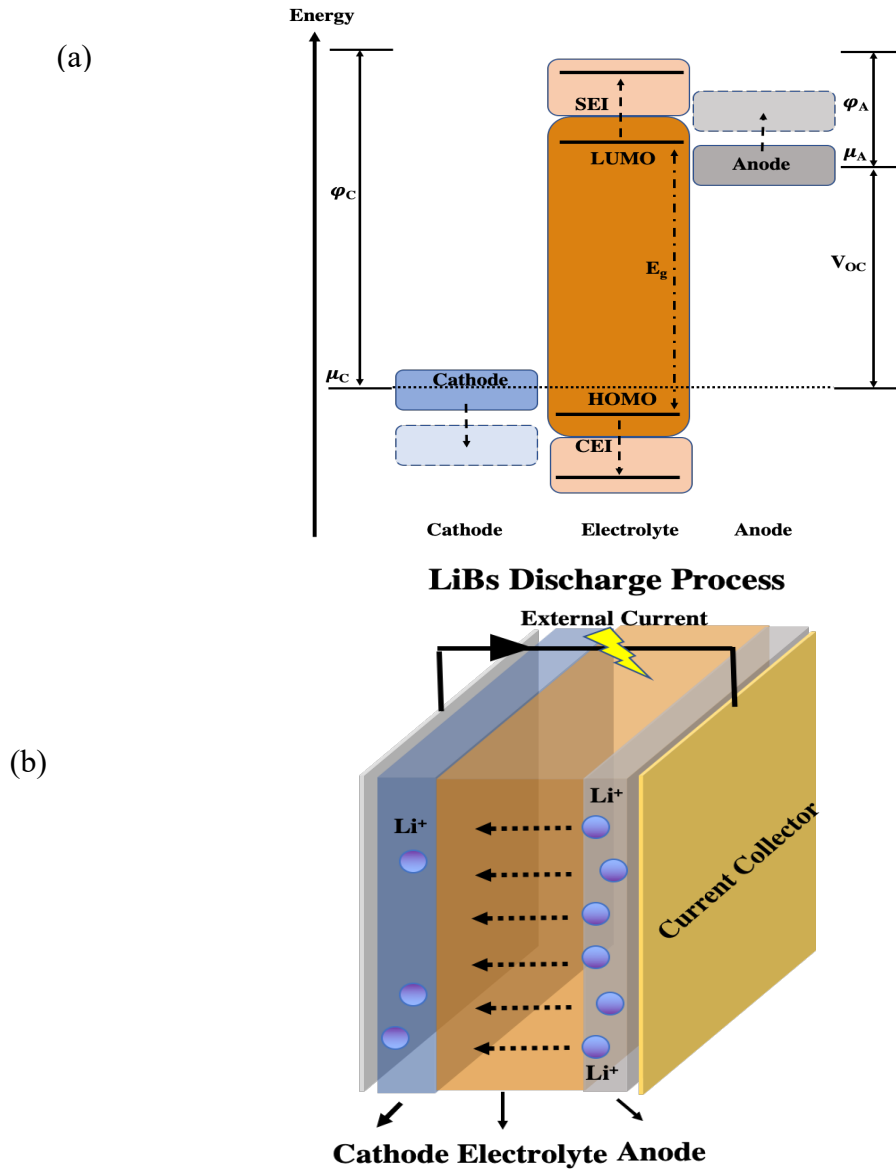


Figure 3(a) Energy diagram of a full battery. The mismatch of HOMO/LUMO will results in the degradation of the electrode and electrolyte; (b) Illustration of the working mechanism of batteries

SPE-based lithium-ion battery consists of an anode, cathode, solid polymer electrolyte (SPE), and two current collectors. This electrochemical cell converts electrical energy into electrochemical energy inside electrodes during the charging process and vice versa. Both electrodes store Li^+ by electrochemical reaction. During the discharging, Li^+ moves from anode to cathode through the SPE. Electrons move from the anode to cathode, too. Then electrical current flows from a positive current collector (connected to the cathode) to a negative current collector (connected to the anode) (Yoshio et al., 2009). During charging/discharging process, there is no electron flow inside the battery owing to electrolyte and separator blocking. The external current from the stored electrochemical energy can power various applications such as our cell phones and other electronics. During the charging process, the cathode is oxidized, and Li^+ ions transfer toward the anode. The reduction reaction will happen at the anode for the charging process (Pistoia et al., 2013). However, the cathode typically has a phase transition during the charging process, which will involve Li^+ extraction from metal oxide lattice and electrons dragging from transition metal ion d orbitals (if Li metal oxide is used as a cathode). So, Li^+ will enter the interstitial lattice back for discharging process. Electrons also go back to d orbitals during the discharging process, accompanying phase stabilization and electric potential energy decrease. In summary, there are several processes during charging/discharging, including electrochemical reactions at electrodes, electron and ion transport in electrodes, ionic transport in electrolytes, and ionic transfer on the interface between the electrodes and SPE (Kazemiabnavi et al., 2018). In order to fully understand LIB's working mechanisms, we can study the LIB energy diagram (**Figure 3a**) and LIB discharging process simulation diagram (**Figure 3b**). If cathode potential is higher than

the potential of electrolyte oxidation at a positive potential, it will oxidize the electrolyte. If anode potential is lower than the potential of electrolyte reduction at a negative potential, then the electrolyte will reduce. Because the intercalation potential of Li^+ into graphite is around 0-0.25V, the graphite potential is below the electrolyte stability window. Thus, the electrolyte will decompose at the graphite surface and form the SEI layer (Peljo & Girault, 2018) (An et al., 2016) (Xue et al., 2015).

At the electrode and electrolyte interface, electrolyte decomposition is strongly related to oxidation reactions at high potentials (Bard et al., 1993). Therefore, oxidized electrolytes (including the lithium salt, LIB additives, etc.) will have irreversible electrochemical reactions and form a surface layer on top of the electrode. We can obtain this irreversible electrochemical reaction information by doing surface product elements analysis. Some fundamental investigations about the interface compositional analysis were reported (Zhang et al., 2018) (Wang et al., 2020). However, a comprehensive understanding of this irreversible reaction process is still missing. This thesis will investigate the LIB interfacial layer impedance and LIB electrochemical performance under stretching, bending, and others to understand how interfacial layer influences our LIB performance.

1.3 Applications

Flexible LIBs can satisfy the portable and flexible electronic application requirements and standards (**Figure 4**). Alongside the advancement in miniaturized and lightweight electronics, wearable LIBs that can track biomedical information such as blood pressure, sleep patterns, heart rate, sweat, will be very promising and popular in near future (Nag et al., 2017). Therefore, compatible LIBs need to be flexible, safe, high

capacity, stable, and reliable with a wide operating temperature range. Flexible LIBs are applied for a variety of flexible electronics like foldable phones, watches, smart cards, wearable devices, etc. Recently, Microsoft Arc Mouse, Samsung Galaxy Fold, Huawei Mate X have attracted attention (Hager et al., 2020). Flexible healthcare heart rate monitor is another application in the medical area which could measure/display heart rate in real-time. In addition, surface-mounted devices have been used in biomedical areas like attached to the skin (Xiang et al., 2021). Other applications include keyboards, smart homes, building management systems, wearable healthcare electronics, which connect to each other for elaborate tasks (Mohanta et al., 2020).

However, flexible LIBs made with liquid electrolytes can suffer from liquid electrolyte leakage, delamination under mechanical deformation, LIB energy density fading or deterioration, and even internal short circuits under bending (J. Wen et al., 2012). To solve these flexible LIB problems, LIBs structural design and materials engineering will be necessary and practical to apply. For example, the liquid electrolyte must be replaced with a solid electrolyte. In this thesis work, our flexible LIBs based on the solid polymer electrolyte show relatively high thermal, mechanical and electrochemical performance, which is promising for the above-mentioned applications like wearable electronics, flexible smartphones, and flexible heart rate tracking monitors.

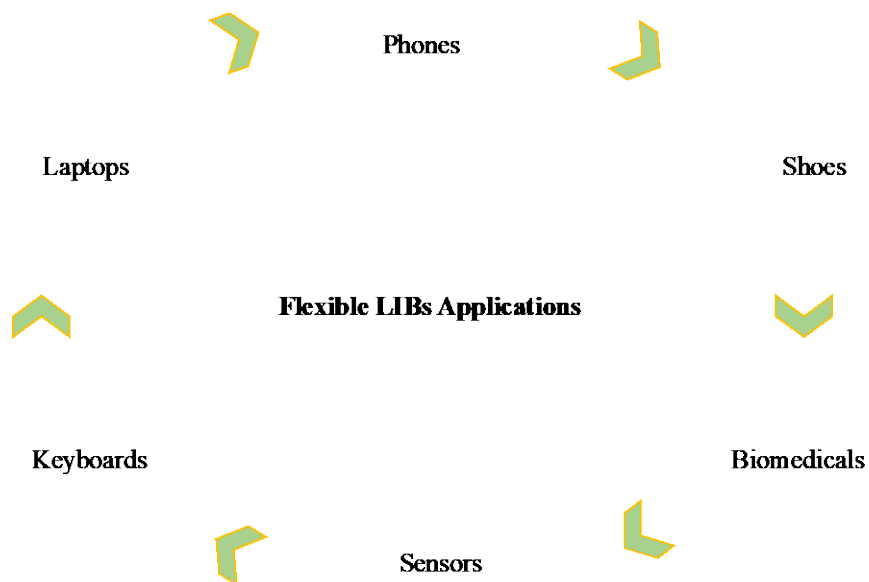


Figure 4 Flexible Lithium-ion batteries applications

1.4 Challenges

The investigation of LIBs interfacial layers is very challenging, because there are many factors such as electrodes materials particles sizes, electrodes crystal structures, electrodes phase transformations, electrodes electronic and ionic conductivity, electrolyte ionic conductivity, Li^+ transference number, electrochemical windows, solid polymer electrolyte thermal melting points, electrolyte mechanical modulus, electrolyte and electrodes materials affinity, etc. (Kasnatscheew et al., 2018)(Etacheri et al., 2011). Typically, many techniques are used to control the solid electrolyte's thickness and its compatibility with electrodes. Because Li^+ will go through the interfacial layer during charge/discharge, forming a stable interfacial layer between electrodes and electrolytes are quite crucial (Nair et al., 2019). Consequently, people have done a lot of work to improve interface stability. But processing is complex, and some processes need a high vacuum to deposit a thin film on top of electrodes (Tian et al., 2020). The ideal interfacial layer should have a high electrochemical window, high cycle stability, high ionic

conductivity, but lower electronic conductivity, high modulus, etc. Interfacial layers also should avoid short circuits, thermal runaway, side reactions, etc. (K. Wen et al., 2020).

Therefore, investigating the effects of different LIBs additives on interfacial layers will help us understand the reasons and mechanisms to enhance LIBs capacity (Yoshio et al., 2009). Here, we choose a simple blending method and combine different material advantages in one polymer composite material at room temperature. There is no vacuum needed for surface layer processing, which significantly enhances LIBs fabrication efficiency and LIBs performance.

1.5 Thesis overview

Chapter I covers motivations, typical electrolytes, and electrodes materials, LIBs working principles, challenges, and thesis overview. Chapter II provides a comprehensive review of relevant literature, including solid electrolytes, electrodes, and their modifications for higher performances, interfacial layers formations mechanism, and LIBs electrochemical performance results. Common electrodes and electrolyte materials will be also discussed. In Chapter III, polymer electrolyte-based LIBs are fabricated using TSB biomaterial additive, and TSB's influence on LIBs interface is investigated. High LIBs electrochemical performance observed could be attributed to an enhanced interfacial layer formed. By characterizing LIBs different electrochemical and mechanical properties, we explain the potential reasons for LIBs capacity enhancement. In Chapter IV flexible polymer LIBs are fabricated. Firstly, we compare two different lithium salts and their influences on flexible LIB capacity and interfaces. Then, we characterize flexible LIB electrochemical performance under varied bending states, charging rates and temperatures. Finally, we investigate LIB interface impedance changes

during the LIBs varied bending states. In Chapter V, we use new polymer electrolyte composition to prepare stretchable LIBs. Stretchable batteries differ from flexible LIBs because of the significant shape deformation. Our spiral stretchable batteries could work at 6000% out of plane strain deformation. We will analyze spiral LIBs capacity performance and interface impedance at different stretching deformations. In Chapter VI, we use new LIBs additive fluoroethylene carbonate (FEC) modified polymer electrolyte to fabricate high-performance flexible LIBs. The electrodes and electrolyte interfaces have enhanced and resulted in high LIBs capacity. This chapter also will cover electrolyte ionic conductivity test, flexible LIBs bending test, LIBs thermal test, LIBs rate capability test, interfacial layer impedance investigation, etc. In Chapter VII, a summary of all work in this thesis is presented. Based on previous and current work on LIBs, future work is discussed.

CHAPTER II. REVIEW OF MATERIALS FOR LITHIUM ION BATTERIES

2.1 Background

Lithium-ion batteries (LIBs) are widely used in our daily lives due to their relatively high energy densities and efficiencies. LIBs power our portable electronics, mobile phones, computer laptops, electric vehicles (EVs), etc. Compared to the gasoline vehicles as reported by the Department of Energy, EVs could reduce 70-80% CO₂ emission per year (U.S. Department of Energy, 2019). In addition, LIBs occupy 63% of worldwide sales with the estimated market of 116.6 billion dollars by 2030 (U.S. Department of Energy, 2019).

A conventional lithium-ion battery consists of an anode, cathode, liquid electrolyte, separator, and current collectors. In solid electrolyte-based LIB, the liquid electrolyte and separator are replaced with a solid electrolyte. Solid electrolytes can be divided into organic (polymers) and inorganic (ceramic, glass). The key requirements and features of a battery electrolyte consist of high ionic conductivity, wide electrochemical window, suitable working temperature range, safety, stability, etc. Li⁺ ion must transport between the cathode and anode through the solid electrolyte. An in-depth discussion of the electrochemical mechanisms of lithium-ion batteries was presented in Chapter I.

In this chapter, a comprehensive review of LIB materials and related research studies is provided. Current flexible commercial batteries will also be discussed. This chapter review aims to provide a deep insight into the past and current developments in LIBs and their evaluation standards with respect to lithium-ion battery designs, materials, mechanical flexibility, stretchability, and stability.

2.2 Solid polymer electrolytes used in flexible lithium-ion batteries

Polymer electrolytes can be classified into the following three categories according to their chemical composition: dry solid polymer electrolyte (no liquid additives), plasticized polymer electrolyte (mixed with plasticizers), gel polymer electrolyte (crosslinked polymer swollen with liquid additives), and composite solid electrolytes (mixed with inorganic solid) (Ngai et al., 2016). Although they have different ionic conductivity, thermal stability, and mechanical properties, some can offer mechanical flexibility, relatively easy processing, wide electrochemical window, and other suitable electrochemical properties (Ngai et al., 2016). Additionally, solid polymer electrolytes can prevent or suppress several safety issues (such as leakage, short circuit, dendrite growth) compared with liquid electrolytes. Here, we compare different polymer-based electrolytes in the following content (Bresser et al., 2013) (Kucinskis et al., 2013).

Decreasing SPE crystallization is necessary to achieve high SPE chain mobility (normally related to high ionic conductivity). As we all know, crystallization is related to polymer structures. Symmetrical, ordered and non-flexible chains structures would crystallize easily (Bresser et al., 2013) (Gedde, 1995). In order to solve the crystallization problem for high ionic conductivity, people used physical crosslinking, chemical crosslinking, copolymer, comb polymer, filler blending, polymer alloying methods. In addition, increasing charge carrier density and ionic conductivity could be obtained by introducing single ion (carboxylate, phosphate, methide, aluminate, sulfonate etc.), salt (imide, methide), and polymer in salt (molten onium salt) (Murata et al., 2000). However, SPE mechanical properties would change after introducing new chemicals. To enhance SPE mechanical strength, we can increase polar groups, hydrogen bonds, phenyl groups

density, crosslinking, crystallization, homogeneity, copolymerization, etc. (Gedde, 1995) (Kucinskis et al., 2013). Here, we compare some common polymers used as shown in **Table 1**, including polyethylene oxide (PEO), polyacrylonitrile (PAN), poly (methyl methacrylate) (PMMA), polyvinylidene fluoride (PVDF), polypropylene carbonate (PPC).

Table 1. Different polymer electrolytes material properties

Polymer	T_g °C	T_m °C	Electrochemical Window (V)	Tensile Strength	Ref
PEO	-67	65	4.0	1.5 Mpa	(X. Yang et al., 2020)(Kelly et al., 2016)
PAN	95	300	4.5	6.5 Mpa	(Jian Yao et al., 2014)
PMMA	105	160	4.7	5.7 Mpa	(Gonçalves et al., 2010)
PVDF	-35	177	5.0	3.1 Mpa	(Agyemang et al., 2016)
PPC	37	-	4.6	25.0 Mpa	(Jianjun Zhang et al., 2017)(Han et al., 2018)

2.2.1 Poly-ethylene oxide (PEO) and its composite

Since 1973, Wright et al. reported PEO semi-crystalline structure and alkali salts (Wright et al., 1973). Later, large research efforts were devoted to PEO-based electrolyte systems. According to the initial study, PEO-based systems show very low ambient temperature ion conductivities owing to low ion mobility, low mobile ions concentration, etc. The correlation between ionic conductivity with the amorphous region is also highlighted (H. Zhang et al., 2017). Polymers conductivity is related to PEO chains movement. Young's modulus could be 0.31GPa for 85 – 124 K M_w PEO (Y.-C. Cao et al., 2011). However, PEO-based LIBs cycling performance could be as low as 200~300 cycles because of poor electrolytes ionic conductivity. It was found that the Li⁺ might transfer in the crystallization region because of aligned chains. Li⁺ ion transfer occurs in the tunnels formed between PEO chains. Local crosslinking also promotes cation transfer

owing to the pairing chains (MacGlashan et al., 1999). The theoretical model based on Arrhenius (Crystalline phase) and Vogel-Tammann-Fulcher (Amorphous phase) model (Ratner et al., 2000) were reported. The ions combination and ions Lewis complexation with oxygen would result in fewer mobile cations. Here, we discuss the methods to enhance PEO ionic conductivity property.

Ionic liquid has high electrochemical stability, low volatility/flammability, low vapor pressure, and high ionic conductivity properties (Menne et al., 2014). Normally, it is composed of asymmetric organic cations and weakly coordinating inorganic/organic anions. The presence of free protons in cations will divide them into aprotic ILs and protic ILs. Protic ILs have lower lithium coordination numbers due to the interactions between cations and anions confirmed by Raman spectroscopy. So more free Li^+ will move and reduce charge transfer resistance (Vogl et al., 2014). Here is an example: Cyclic pyrrolidinium and piperidinium ILs are less viscous and cathodic stable than aliphatic cations. Using the aprotic ionic liquid 1-ethyl-3-methylimidazolium bis(trifluoromethyl sulfonyl) imide (EMIMTFSI) in PEO – Lithium difluoro (oxalato) borate (LiDFOB) electrolyte could get the maximum ionic conductivity $1.85 \times 10^{-4} \text{ S/cm}$ at 30°C because of ionic liquid high ionic conductivity, low viscosity, and wide electrochemical window (Macfarlane et al., 2014). Interaction among Li^+ , EMIM^+ and PEO oxygen atoms, electrolyte crystallinity decreased which were confirmed by XRD, FTIR (Polu & Rhee, 2017) (Y.-S. Ye et al., 2013) (MacFarlane et al., 2014). The smaller bis(fluorosulfonyl)imide anion (FSI^-) promoted the transport rates and formed an interfacial layer with graphitic carbon electrode compared with TFSI $^-$. The viscosity decreased owing to smaller anions. Reversibility also has been enhanced (Matsumoto et

al., 2006). However, the presence of TFSI⁻ or FSI⁻ would cause anodic dissolution and Al current collectors pitting when potentials exceed 4.0V vs Li/Li⁺. Higher viscosity and decreased lithium diffusivity are the main reason for LIBs poor performance at a high C-rate. Commonly used salt LiPF₆ could hydrolyze and release HF, which could degrade cathode materials. Al could be protected under fluorinated carbonate electrolyte owing to a chemical surface layer formation. Cations and anions effects need to be considered for future use (Shkrob et al., 2016) (Xianming Wang et al., 2000) (Balducci, 2017).

Using some nonionic conductive filler to ensure good mechanical property and ionic conductivity is also investigated. Inorganic fillers perform as the crosslinking centers to reduce polymer crystallinity (CEPAL, 1975) (Lin et al., 2015). In 1998, Croce et al. introduced TiO₂ and Al₂O₃ nanofillers into the electrolyte (F Croce et al., 1998). The enhancement by using Al₂O₃ and TiO₂ ceramic filler materials is related to maximizing amorphous region and promoting Li⁺ transfer at ceramic particles interface boundaries (Angulakshmi et al., 2012a). It was mentioned that nanometer-sized ceramic powders can perform as solid plasticizers for PEO instead of liquid plasticizers, which was the most common way to lower ambient region operation temperature of PEO–LiX polymer electrolytes (Angulakshmi et al., 2012a).

Nonionic fillers acting as solid plasticizers can effectively avoid liquid plasticizers' limited processability and high reactivity. All these materials and methods can help to reach the goal of obtaining a new class of solid polymer electrolyte with low-temperature ion conductivity, improved mechanical stability, and good compatibility with lithium electrode (Angulakshmi et al., 2012b). In 2001, Croce et al. used ceramic filler on P(EO)₂₀LiSO₃CF₃ electrolyte (F Croce et al., 2001). PEO chains crystallization and

surface groups interactions account for LIBs high performance (F Croce et al., 2001). Besides, nanofillers might act as anionic receptors according to Lewis- acid theory and help lithium salt dissociation (W. Wieczorek et al., 1996). The relatively high dielectric constant nano-oxide materials promote lithium salt dissociation, too (Varaprasad et al., 1979). Cui's group used SiO₂ nanospheres in PEO to suppress crystallization and facilitate polymers segmental motion for high ionic conductivity (Lin et al., 2016). A 4.4×10^{-5} S/cm at 30°C was obtained (Lin et al., 2016). Mesoporous SiO₂ mixed with PEO achieved $\sim 10^{-3}$ S/cm at room temperature (Y. Kim et al., 2017).

Our group used a hybrid clay-carbon nanotube hybrid nanofiller to enhance PEO electrolyte ionic conductivity (Tang et al., 2012). Fillers could facilitate lithium salt dissociation by weakening contact ion pairs force. Positive Li⁺ would interact with electrons cloud on the CNTs outer surface and negative oxygen atoms, resulting in contact ion pairs separation. Subsequent enhancement of charge carriers would improve ionic conductivity. Nanoscale fillers also expanded PEO chains free volume and decreased PEO crystallization. Nanofillers also improved the interface area between fillers and electrolyte owing to the large aspect ratio, leading to higher tensile strength (Tang et al., 2012). We also modeled the fillers enhancement mechanism based on free volume theory. Salt dissociation, free volume expansion and distribution, diffusion blocking, filler aggregation, ion trapping, and chain confinement have been considered (Q. Li et al., 2013) (Kammoun et al., 2015). Qin et al. also used molecular dynamics simulation to provide insights at the molecular level to study nanofillers shape and size effects on the static and dynamic properties (Q. Li & Ardebili, 2014). These nanofillers with Lewis acidic surface properties and porous large surface-volume fillers could

enhance miscibility, which was helpful for stabilizing the electrolyte/Li interface and other properties (F Croce et al., 2001) (Xi, Qiu, Cui, et al., 2006) (Y.-X. Jiang et al., 2008).

Nanostructured conductive materials mixed with PEO also have been investigated. Yu's group designed a 3-D nanostructured conductive $\text{Li}_{0.35}\text{La}_{0.55}\text{TiO}_3$ (LLTO) hydrogel framework combined with PEO (Bae et al., 2018). The improved ionic conductivity 8.8×10^{-5} S/cm at room temperature was obtained. Continuous interphase served as Li^+ pathway. Continuous Li^+ hopping sites at the surface is another reason for the ionic conductivity enhancement (Bae et al., 2018). Zhang et al. prepared polymer electrolyte by mixing $\text{Li}_{6.4}\text{La}_3\text{Zr}_{1.4}\text{Ta}_{0.6}\text{O}_{12}$ (LLZTO) with PEO and obtained ionic conductivity 2.1×10^{-4} S/cm at 30°C (Jingxian Zhang et al., 2016b). The LIBs showed 345Wh/kg by using $\text{LiFePO}_4/\text{Li}$ electrodes. The reason for this enhancement may be due to the percolation effect where Li^+ can transfer from LLZTO to PEO, which increases PEO vacancies (Jingxian Zhang et al., 2016b). However, nanostructured conductive materials face a disorder problem inside SPE. Zhai et al. used the ice templating process to align the ceramic particles for helping ions transfer (H. Zhai et al., 2017). High ionic conductivity 5.2×10^{-5} S/cm could be reached (H. Zhai et al., 2017). Pan's group also used the inorganic particles $\text{Li}_{1.3}\text{Al}_{0.3}\text{Ti}_{1.7}(\text{PO}_4)_3$ to enhance PEO mechanical properties and barricaded dendrite growth (L. Yang et al., 2017). By combining small molecular boronized polyethylene glycol (BPEG) to disorganize PEO domain crystallinity and facilitate interface contact, LIBs performance showed 158mAh/g at 60°C , 0.1 C charging rate (L. Yang et al., 2017). In 2013, metal-organic framework (MOF) nanoparticles were used to prepare PEO electrolyte, where 3.16×10^{-5} S/cm at 25°C was obtained (C. Yuan et

al., 2013). The high surface area, ordered micro-porous structure and thermal stability from MOF changed the crystallization and electrolyte ionic transportation (C. Yuan et al., 2013).

Blending with other polymers is another effective way to achieve a balanced property among mechanical properties, ionic conductivity, electrochemical stability, and electrochemical window for high-performance LIBs. It is a synthesis process simplification to control the mechanical property. In 1983, Tsuchida et al. blended PEO with PMMA to obtain hydrogen bonding type inter-macromolecular complex matrix with LiClO_4 salt (Tsuchida et al., 1983). A high conductivity 1.3×10^{-5} S/cm at 60°C was achieved (Tsuchida et al., 1983). Jinisha et al. used poly(vinylpyrrolidone) (PVP), PEO and LiNO_3 (Jinisha et al., 2017). They obtained 1.13×10^{-3} S/cm at room temperature. The presence of rigid pyrrolidone groups would enhance ionic conductivity. Carbonyl group ($\text{C}=\text{O}$) attached to PVP helped complexes formation with inorganic salts confirmed by XRD (Jinisha et al., 2017). Li et al. used the blending method to mix PEO, polyurethane (TPU) and lithium bis (trifluoromethane sulfonimide) (LiTFSI) (Y. J. Li et al., 2018). The hydrogen bond interaction between $\text{C}-\text{O}-\text{C}$ of PEO and $-\text{NH}$ from TPU increased the mechanical property and reduced the crystallinity. A 5.3×10^{-4} S/cm at 60°C ionic conductivity was achieved. Semi-interpenetrated network structure formed between PEO and TPU would restrict segments movement and result in low electrical conductivity. The assembled LIB by using $\text{LiFePO}_4/\text{SPE}/\text{Li}$ cell showed 140 mAh/g at 0.2C under 60°C (Y. J. Li et al., 2018).

Ji et al. synthesized a copolymer with Si and PEG. Ion conductivity was 3.2×10^{-5} S/cm at 10°C (Xiaoxiao Ji et al., 2017). Assembled $\text{LiFePO}_4/\text{Li}$ LIBs showed 84 mAh/g

at 10°C, 0.5C rate. High performance might be related to the separation of anions and cations movement inside Si-doped polymer (Xiaoxiao Ji et al., 2017). In addition, Kuo's group used PVDF-PAN copolymer blended with PEO to enhance ionic conductivity, thermal stability, and electrochemical stability (C. Y. Hsu et al., 2016).

Plasticizers are additives to enhance plasticity and improve ionic conductivity in polymers that dates to the 1970s (Wrightler et al. 1973). Plasticizers can include dimethyl carbonate (DMC), dioctyl adipate (DOA), dibutyl phthalate (DBP), diethylcarbamazine (DEC), propylene carbonate (PC), ethylene carbonate (EC), dimethyl formamide (DMF), diethyl phthalate (DEP), g-butyrolactone (BL), glycol sulfite (GS) and methylethyl carbonate. These plasticizers showed low flash points, high vapor pressure, and narrow electrochemical window. Some showed polar plasticizers reaction with Li metal electrode (Ngai et al., 2016).

Crosslinking PEO is another way to obtain stable electrolyte film (Choudhury, 2019). Passerini's group used benzophenone (Bp) as the crosslinking agent to crosslink PEO under UV light at different times (G.-T. Kim et al., 2010). The crosslinking point happened at that hydrogen which attaches to PEO chain. Bp would be abstracted to excited triplet state. Then, two PEO chains connected (G.-T. Kim et al., 2010). Rupp et al. used benzophenone as photoinitiator to UV crosslink PEO chains and mixed with ionic liquid, lithium salt Li-TFSI (Rupp et al., 2008). They achieved $4 * 10^{-4}$ S/cm at 30°C in 2008 (Rupp et al., 2008). Killis et al. obtained $5 * 10^{-5}$ S/cm at 25°C by crosslinking EO and PO block co-polymers (Killis et al., 1984). Hall et al. achieved $2 * 10^{-4}$ S/cm at 25°C by connecting PEO chains with polysiloxane chains in 1986 (Hall et al., 1986). Zhu et al. prepared 3D cross linking network by using SiO₂ as cross linking

agent and achieved 4.65×10^{-3} S/cm at 25°C for PEO-based SPE (Yinghua Zhu et al., 2019). By blending with ionic liquid N-alkyl-N-methyl pyrrolidinium TFSI and LiTFSI, $\sim 10^{-4}$ S/cm could be reached at room temperature. The crosslinking will not influence conductivity significantly. Higher performance attributed to ionic liquid and lithium salt addition (G.-T. Kim et al., 2010). Matsui et al. used cross-linked Poly(ethylene oxide – co -2 – (2-meth-oxyethoxy) ethyl glycidyl ether-co-allyl glycidyl ether) P(EO-MEEGE-AGE) as electrolyte in Li/LiCoO₂ LIBs and obtained 134 mAh/g at 60°C (Matsui et al., 2001). Kuratomi et al. also reported ethylene oxide and propylene oxide crosslinking PE (Kuratomi et al., 2001). In 2014, Lin et al. reported a crosslinked PE/PEO based PE. Ionic conductivity 1.6×10^{-4} S/cm at 25°C was achieved (Lin et al., 2016). Lehmann et al. crosslinked poly ethyleneimine (PEI) with PEO and obtained 1.2×10^{-3} S/cm at 80°C after mixing with plasticizer and lithium salt in 2020 (Lehmann et al., 2020).

In summary, crosslinked PEO polymer electrolyte could be promising for cyclic stability. Higher mechanical property and higher ionic conductivity could be achieved by decreasing crystallization. Ionic liquid, nonconductive inorganic fillers, plasticizer, and conductive inorganic electrolyte are common ways to achieve higher ionic conductivity. Combining facile crosslinking and blending with higher conductive fillers could be the future direction. In this thesis, plasticizer and LIB additives are selected and investigated owing to their facile processing and high performance.

Table 2 Current research on PEO based electrolyte

Polymer	Salt and solvent	Filler	Ionic conductivity (S/cm)	Electrical window	Tensile strength Mpa	Battery Performance	Ref
PEO-EMImTF SI	LiBOB		1.85×10^{-4} S/cm @ 30°C			Li/LiFePO ₄ 155mAh/g@0.1 C&RT	(Polu & Rhee, 2017)
PEO	LiClO ₄	SiO ₂	4.4×10^{-5} S/cm @ 30°C	5.5V		Li/LiFePO ₄ ~120mAh/g@1 C&90°C	(Lin et al., 2016)

Table 2 (Continued)

PEO		LLTO	8.8* 10 ⁻⁵ S/cm @RT			(Bae et al., 2018)
PEO	LiClO ₄	LLZTO	2.1*10 ⁻⁴ S/cm @ 30°C	4.75V	Li/LiFePO ₄ ~153.3mAh/g@ 0.05C&60°C	(Jingxian Zhang et al., 2016b)
PEO/BP EG	LiTFSI	LATP	2.5*10 ⁻⁴ S/cm @ 60°C		Li/LiFePO ₄ ~158.2mAh/g@ 0.1C&60°C	(L. Yang et al., 2017)
PEO/PE G	LiClO ₄	LATP	5.2*10 ⁻⁵ S/cm@ RT	3.6Mpa		(H. Zhai et al., 2017)
PEO/PV P	LiNO ₃		1.13*10 ⁻³ S/cm@ RT		0.332 Li transference number	(Jinisha et al., 2017)
PEO/TP U	LiTFSI		5.3*10 ⁻⁴ S/cm @ 60°C		140 mAh/g at 0.2C&60°C	(Y. J. Li et al., 2018)
PEO/pyrr olidinium TFSI	LiTFSI		10 ⁻³ S/cm @ 40°C	5.0V	Li/SPE/LiFeO ₄ 150mAh/g @0.05C, 30°C	(G.-T. Kim et al., 2010)

2.2.2 Poly-acrylonitrile (PAN)

Among the polymer hosts studied, poly-acrylonitrile (PAN) based electrolytes offer one type of homogenous electrolyte film in which salt and plasticizers are dispersed molecularly (J. Y. Song et al., 1999a). They show higher thermal stability, high ionic conductivity, and good compatibility owing to their polar groups. Good processability, flame resistance, resistance to oxidative degradation, and electrochemical stability make PAN a good candidate for the electrolyte. Using PAN to minimize dendrite growth is also reported (Tsutsumi et al., 2000) (Raghavan et al., 2011). The highest ionic conductivity 10⁻³ S/cm was obtained (Chen-Yang et al., 2009). PAN oxidation stability window could be 4.5V vs Li⁺/Li (Giovanni Battista Appetecchi et al., 1999). PAN fiber Young's modulus was around 80 MPa (L. Huang et al., 2014) (Tian et al., 2019).

The -C≡N group would result in higher crystallization. Large crystallization phase will block ions transfer, so incorporating inorganic nanoparticles will be one way to solve this problem, such as SiO₂ (Wetjen et al., 2013), TiO₂ (Plylahan et al., 2014), and

Al_2O_3 (Y. Wen et al., 2014) or with other metal oxides (Xiong et al., 2005) (Panero et al., 2007). But $-\text{C}\equiv\text{N}$ groups also could interact with Li^+ and increase the diffusion coefficients. PAN application is also limited by the low ionic conductivity (Fausto Croce et al., 1993). The addition of graphene oxide 2D material could alleviate the ion conductivity issue. Ion conductivity of 4×10^{-4} S/cm at 30°C was obtained, which can be attributed to the functional groups ($-\text{OH}$, $-\text{COOH}$, $-\text{C}=\text{O}$, $-\text{COC}$) alleviation with the polarity of $-\text{C}\equiv\text{N}$ group. A high discharge capacity 166 mAh/g at 0.2C was measured for Li/LiFePO₄ LIBs (Jia et al., 2018).

Watanabe et al. concluded that PAN host is inactive for ionic transport but acts as a matrix for structural stability (Watanabe et al., 1982). With PAN as host, some combinations of plasticizers, such as EC and DMC, have been used as salts to help produce membranes with high ionic conductivity and high stability. These unique characteristics make membranes more suitable for lithium battery applications than before (Watanabe et al., 1982) (Min et al., 2003). Wang's group used PAN fiber as a matrix. Dendrite growth has been hindered. High degree flexibility and thermal stability are exhibited (D. Zhang et al., 2017) (Xiuling Zhang et al., 2019). Wang et al. used PAN as the matrix for triethylene glycol diacetate-2-propenoic acid butyl ester (TEGDA-BA) electrolyte (Q. Wang et al., 2015). Gel polymer by using this 5wt% PAN showed 5.9×10^{-3} S/cm at 25°C . The LIBs by using LiFePO₄/Li₄Ti₅O₁₂ electrodes exhibited discharge capacity 125.2 mAh/g with high columbic efficiency greater than 98% after 100 cycles. Film Young's modulus was 0.9Mpa (Q. Wang et al., 2015).

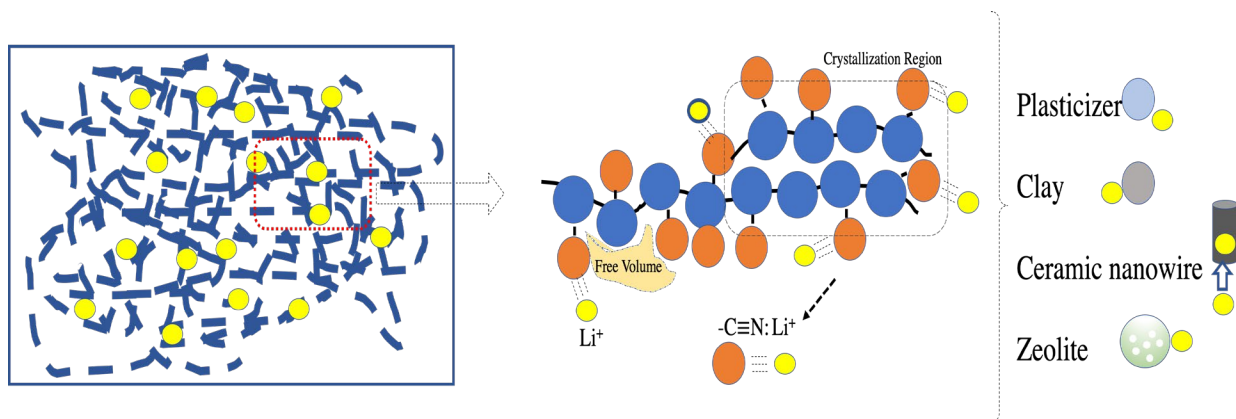


Figure 5 PAN polymer chain model and methods for improving ionic conductivity.

Nicotera's group used organo-clay blended with PAN and PEO (Simari et al., 2018). A higher transference number was achieved, which could be explained by the plasticizing effect, improving chains flexibility, and electrostatic interactions (between filler surface and lithium), creating the pathways for ions conduction (Simari et al., 2018). Mixing with PMMA and PVDF polymers improved PAN mechanical stability (Nicotera et al., 2006). Outstanding thermal stability up to 230°C was also achieved (Flora, Ulaganathan, Babu, et al., 2012).

Cui's group used ceramic nanowire $\text{Li}_{0.33}\text{La}_{0.557}\text{TiO}_3$ (LLTO), PAN, and LiClO_4 materials to fabricate composites (W. Liu et al., 2015b). High ionic conductivity 2.4×10^{-4} S/cm at room temperature was achieved. The reason was not from crystallization decrease but the fast Li^+ pathway on deficient perovskite structure sites. Nanowires surface area provides fast pathway for Li^+ diffusion. Li^+ replacing nearby vacancies in LLTO filled composite would reduce the activation energy (W. Liu et al., 2015b). Lewis acid-base theory proposed by Wiczorek et al. can explain the ionic conductivity enhancement using inorganic nanoparticles inside polymers electrolytes (Władysław Wiczorek et al., 1995). Duan et al. used the poly(acrylonitrile) (PAN), PEGDA as multi-layer electrolyte to hinder the dendrite formation and obtain a compact interface (Duan et

al., 2019). PAN was in contact with the cathode, PEGDA was contacted with Li metal anode, and PAN with $\text{Li}_{1.4}\text{Al}_{0.4}\text{Ge}_{1.6}(\text{PO}_4)_3$ (LAGP) composite as the middle layer. Stabilized discharge capacity around 170 mAh/g over 100 cycles has been obtained based on Li/NCM LIBs (Duan et al., 2019). The multilayered LIB also has been fabricated by using PAN& $\text{Li}_{1.3}\text{Al}_{0.3}\text{Ti}_{1.7}(\text{PO}_4)_3$ (LATP) and PEO&PAN&LATP (Xiuli Wang et al., 2019). PAN passivation effect has been hindered on the Li anode side by combining with PEO because of the intermolecular hydrogen bonds formed by hydroxyl and CN groups (Xiuli Wang et al., 2019).

Slane et al. used zeolite mixed with PAN and LiPF_6 liquid electrolyte (Slane & Salomon, 1995). Electrolyte solvent addition would form a ternary solvent mixture which would help ionic transfer (Slane & Salomon, 1995). The addition of zeolite would also improve surface stability which blocked the corrosive solvent flow (Watanabe et al., 1983) (Slane & Salomon, 1995). However, despite several PAN electrolyte advantages, its poor compatibility with lithium metal anode hinders practical applications (D. Y. Zhou et al., 2008). Besides, solvent exudation upon the long storage may happen for the gelled electrolyte. The high viscosity would decrease the ionic conductivity dramatically. Some studies even clearly revealed that the lithium electrode undergoes serious passivation when in contact with PAN-based electrolyte, leading to safety problems (Kucinskis et al., 2013). A polymer matrix of poly (acrylonitrile-polyhedral oligomeric silsesquioxane) (P(AN-POSS)) combining with liquid electrolyte showed 6.06×10^{-3} S/cm ionic conductivity at ambient temperature (Bo Liu et al., 2018). High transference number 0.59 and electrochemical stability potential 5.7 V were reported. Also, 148 mAh/g discharge capacity and 93.7% retention after 80 cycles were achieved in the LIB. The reasons for

enhancement were attributed to the crystallization decrease and stable interface compatibility (Bo Liu et al., 2018).

High T_g and low liquid electrolyte uptake would restrict chains movement and result in low ionic conductivity. Kuo et al. crosslinked PAN & PEO and obtained 5×10^{-3} S/cm at 25°C after uptaking liquid electrolyte in 2014 (Kuo et al., 2014). Kuo et al. chemical crosslinked polyacrylonitrile-glycidyl methacrylate (P(AN-GMA)) and achieved 8.23×10^{-3} S/cm at 25°C after immersing inside liquid electrolyte (Kuo et al., 2014). In 2019, Verdier et al. achieved 2.1×10^{-3} S/cm at 25°C by crosslinking PAN with nitrile butadiene rubber (NBR) (Verdier et al., 2019). High conductivity was attributed to the interaction between nitrile group with Li^+ (Verdier et al., 2019). Copolymers PAN and PMMA were also reported 2.5×10^{-3} S/cm and 3.5×10^{-3} S/cm with and without vinyl acetate added inside polymer electrolyte (Pu et al., 2006) (Y. H. Liao et al., 2009). The reason was related to the porous structures and amorphous region enhancement (Y. H. Liao et al., 2009).

In summary, PAN's thermal stability, mechanical strength can potentially help solve the dendrite growth problem. Ionic conductivity and crystallization could be achieved by crosslinking, copolymerization, and blending with different conductive or non-conductive fillers like PEO. The nitrile group concentration should be considered owing to the interaction with Li^+ and molecular reactions.

2.2.3 Poly-methyl methacrylate (PMMA)

In 1985, Iijima and Toyoguchi, two Japanese scientists, found that PMMA could be used as a gelatin agent (Iijima et al., 1985). Ionic conductivity of 10^{-3} S/cm was achieved at 25°C for 15wt.% PMMA mixed with LE. Young's modulus is 13.7 MPa for

PMMA, illustrating great mechanical property (Gonçalves et al., 2010) (Iijima et al., 1985). A few years later, Killis et al. focused on gel PMMA electrolytes with different plasticizers and found that the electrochemical stability depends on the polymer host and lithium salt complex (Killis et al., 1984). Although PMMA shows better scalability comparing with PAN, the LIBs efficiency tests revealed a consistent fraction lithium loss during charging/discharging. Thus a large amount of lithium would be required to assure an acceptable battery life eventually (G. B. Appetecchi et al., 1995) (J. Y. Song et al., 1999b). PMMA has good compatibility with Li metal anode, but the mechanical strength can be influenced by the PMMA porosity (C. Huang & Zhang, 2004) (N. Wu et al., 2011) (T. Ma et al., 2013). The ester groups can make a contribution to fast Li⁺ transfer because of their strong interaction with the oxygen group and liquid electrolyte uptaking (Flora, Ulaganathan, & Rajendran, 2012).

Table 3 Research summary on PMMA based electrolyte

Polymer	Salt and solvent		Ionic conductivity (S/cm)	Electrical window	Tensile strength (Mpa)	Battery Performance	Ref
PMMA	CH ₃ COOLi		8.21 *10 ⁻⁵ at 30°C				(Kurapati et al., 2019)
P(MMA-AN)	LiPF ₆ in DMC/EC=1:1		2.06*10 ⁻³ at RT	5.5V			(M. M. Rao et al., 2008)
PVP-co-PMMA	LiClO ₄		10 ⁻⁸ at RT				(Chiu et al., 2007)
P(MMA-Vac)			1.85*10 ⁻³ at RT				(L. Lu et al., 2007)
P(MMA-AN-Vac)	LiPF ₆ in EC/DMC/DEC=1:1:1		3.48*10 ⁻³ at RT	5.6V			(Y. H. Liao et al., 2009)
P(AN-MMA-St)	LiPF ₆ in EC/DMC/DEC=1:1:1		2.15*10 ⁻³ at RT	5V			(D. Kim & Sun, 1998)(CHEN et al., 2011)
P(MMA-Vac)-PEGDA	LiPF ₆ in EC/DMC/DEC=1:1:1		3.4*10 ⁻³ at RT	5V			(Y. H. Liao et al., 2011)
PMMA-IL-TFSI	--		5.12 *10 ⁻⁴ at 30°C	5.1V	1.83	Li/SPE/Li ₄ Ti ₅ O ₁₂ 120mAh/g at 1C &RT	(Yang Li et al., 2017)

Table 3 (Continued)

HBPS- (PMMA- b- PPEGM A)x	LiTFSI	8.3 *10 ⁻⁵ at 30°C	4.7V	(A. Wang et al., 2016)
PMMA- PC-TiO ₂	LiClO ₄	3 *10 ⁻⁴ at 30°C	Graphite/SPE /LiCoO ₂ 30 mAh/g @RT & C/16	(Pal & Ghosh, 2018)
PEO/PM MA/P(V DF-HFP)	LiPF ₆ in DMC/EC=1:1	8.1 *10 ⁻⁴ at 25°C	5.0V Li/GPE/LiCo O ₂ 152.7 mAh/g @0.1mA/cm ² and 25°C	(Shi et al., 2018)
POSS- PMMA	LiClO ₄ , PC	1.3*10 ⁻³ at RT	5.25V	(Y. Huang et al., 2015)

Zhang's group synthesized the multi-arm star polymers (A. Wang et al., 2016). The hyperbranched polystyrene (HBPS) is the core. PMMA block poly (ethylene glycol) methyl ether methacrylate (PEGMA) are the arms. Its ionic conductivity 8.3 *10⁻⁵ S/cm at 30°C was achieved after blending with LiTFSI, because CH₂CH₂O- segments from PEGMA and lower molecular weight polymer would increase the ionic conductivity significantly. Besides, the electrolyte electrochemical window could be 4.7V. (A. Wang et al., 2016). Free-volume transport theory suggests that polymer chain motion can be beneficial for free ions migration. A lower polymer T_g value contributed to higher ion conduction (Cohen & Turnbull, 1959) (Mindemark et al., 2015).

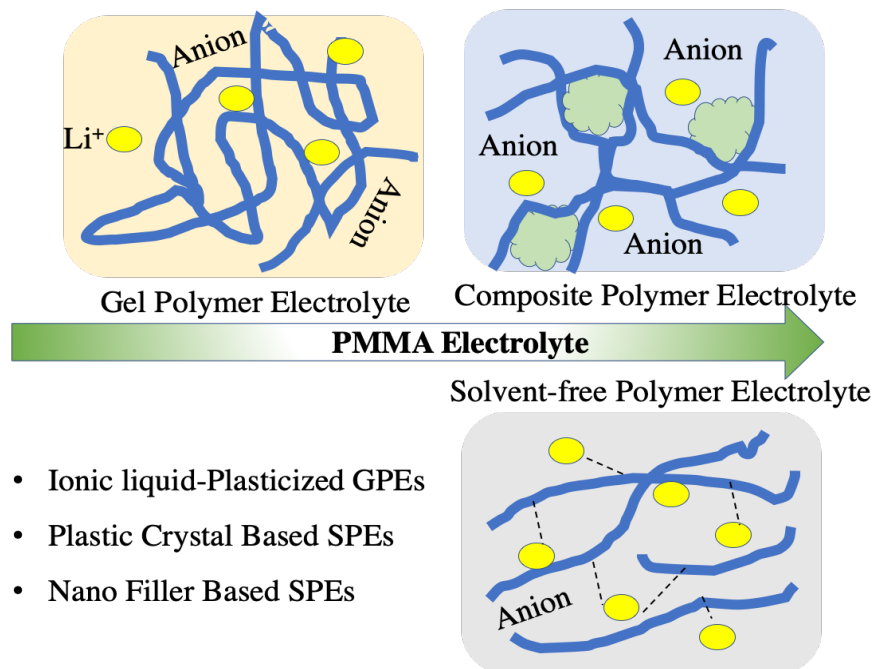


Figure 6 PMMA based electrolyte

Copolymerization can be a good solution to solve the polymer stability issue. Bi-polymers of poly (methyl methacrylate-acrylonitrile) (P(MMA-AN)) were synthesized. Acrylonitrile groups contributed to chemical stability and methyl methacrylate provided a high affinity with polar solvents. The high dielectric constant polymer could promise solvent retention (M. M. Rao et al., 2008). AN could also provide good processability (G. Wu et al., 2007). Electrochemical and thermal stability reduced polymer composite brittleness (K.-H. Lee et al., 2000) (S S Zhang et al., 2003) (S S Zhang & Jow, 2002). MMA could provide strong adhesion to electrodes and excellent mechanical stability (Baskaran et al., 2007). In addition, PEGDA and PEGDMA have two functional groups that react with other molecules to form three-dimensional network polymers which could absorb liquid electrolytes effectively (F.-M. Wang et al., 2009) (C. L. Cheng et al., 2004a) (Uchiyama et al., 2009). Sidechain carbonyl group (-COO-) from MMA would have strong interaction between MMA units. The aprotic solvent's strong interaction

made plasticizer difficult to phase separate from matrix polymer. This resulted in crystallization retardation (D. Kim & Sun, 1998).

Poly(methyl methacrylate-vinyl acetate) (P(MMA-Vac)) (L. Lu et al., 2007) and terpolymers of poly(methyl methacrylate acrylonitrile-vinyl acetate) (P(MMA-AN-Vac)) (Y. H. Liao et al., 2009), Poly (acrylonitrile -methyl methacrylate-styrene) (P(AN-MMA-St)) (CHEN et al., 2011), Poly(methyl methacrylate-vinyl acetate)-co-poly(ethylene glycol) diacrylate (P(MMA-Vac)-PEGDA) (Y. H. Liao et al., 2011) were also prepared. A higher concentration plasticizer would result in poor mechanical property. The weaker interaction between Li^+ and PMMA made it less able to dissociate lithium salt, which reduced ionic conductivity. A copolymer of PVP-PMMA was fabricated because strong PVP polar units helped lithium-ion dissolution (Chiu et al., 2007). Li et al. used poly (methyl methacrylate-acrylonitrile-ethyl acrylate) (P(MMA-AN-EA)) terpolymer as the host for GPE (P. Sun et al., 2014). The highest 3.82×10^{-3} S/cm conductivity was achieved. Soft EA chains would make crosslinking network soft. The electrochemical window voltage could be up to 5.2 V vs Li/Li^+ (P. Sun et al., 2014).

Anhydrides would oxidize during charging between cathode and electrolyte, forming a passivation layer that suppressed electrolyte decomposition, transition metal dissolution, and cathode erosion. Acrylate groups are helpful for higher ionic conductivity owing to the ester group. In 2017, Chen's group synthesized poly(acrylic anhydride-2- methyl-acrylic acid-2-oxirane-ethyl ester-methyl methacrylate) crosslinked polymer and achieved 6.79×10^{-4} S/cm ionic conductivity at 25°C, 27.5Mpa strength (Y. Ma et al., 2017). It was reported that copolymerized poly (methyl methacrylate-co-butyl acrylate-co-vinyl benzyl chloride) crosslinked polymer had the highest conductivity 2.5

10^{-2} S/cm at 80°C after soaking in the liquid electrolyte (Flora, Ulaganathan, & Rajendran, 2012). In addition, Bergman et al. prepared PMMA grafted poly (ethylene glycol) methyl ether methacrylate (PEGMA) polymer with LiTFSI salt (Bergman et al., 2015). Over 10^{-3} S/cm at 110°C was achieved owing to the arranged and continuous ion transport ways provided by polar polyether groups (Bergman et al., 2015).

Furthermore, inactive nanofillers such as SiO₂, Al₂O₃, SnO₂, TiO₂, etc. will enhance the Lewis acid-base interaction between polar surface groups of fillers and charge carriers. These fillers create additional channels for ions movement and help salts dissociation, enhancing the ionic conductivity (Nan et al., 2003) (Chandra et al., 2014) (Cui et al., 2013). The capillary action produced by nanoparticles could capture the plasticizer and increase ionic conductivity (Y. Liao et al., 2013). The large surface area of nanoparticles could improve the mechanical property (Xie et al., 2014). Rajendran et al. used CeO₂ as filler to enhance ionic conductivity to 8.32×10^{-3} S/cm at 75°C, where the enhancement was from the ionic interaction and ionic carriers enhancement (Rajendran et al., 2002).

Li's group synthesized polyhedral oligomeric silsesquioxane (POSS) based on PMMA matrix (Y. Huang et al., 2015). It had both organic and inorganic materials properties. Organic substitutes make it hydrophobic (Y. Huang et al., 2015). POSS/(PMMA₄₆)₈/PVDF electrolyte prepared by electrospinning on polypropylene (PP) substrate also has been investigated by Zhang et al. (M. Zhang et al., 2019). Enhanced mechanical property owing to the affinity between POSS/(PMMA₄₆)₈ with PVDF has been confirmed. The strong interaction between the star arm PMMA ester group and the carbonates oxygen group in LE may contribute to electrochemical property.

1.57×10^{-3} S/cm has been obtained at room temperature (M. Zhang et al., 2019). Another PMMA-Propylene carbonate (PC)-TiO₂-LiClO₄ electrolyte also was prepared (Pal & Ghosh, 2018).

PMMA has good compatibility with carbonate-based liquid electrolyte and high thermal stability (H. P. Zhang et al., 2007). It also has good liquid retention property (M. Rao et al., 2012) (J. Zhao et al., 2016). Li et al. used the PMMA in liquid electrolyte to assist Li deposition and dendrite-free anode preparation (Yang Li et al., 2017). Upon discharging, Li⁺ reacted with PMMA and became immobilized. Then pre-trapped Li⁺ is reduced into initial Li seeds to guide sequential Li deposition (Guo et al., 2019). Kurapati et al. used PMMA and CH₃COOLi to prepare solid electrolytes (Kurapati et al., 2019). Appetecchi et al. mixed PMMA electrolyte with PC/EC-LiClO₄. High ionic conductivity property 5×10^{-4} S/cm GPE at 25°C was achieved (G B Appetecchi et al., 1995). The anodic stability higher than 4.5 V vs Li/Li⁺ was also obtained (G B Appetecchi et al., 1995). Arof's group used the PMMA as host polymer mixing with EC/PC and LiBOB. 3.58×10^{-3} S/cm at 75°C was achieved. The gel polymer electrolyte showed 4.7V versus Li/Li⁺. The 130 mAh/g discharge capacity was obtained from Li/GPE/LiCoO₂ cell (Kufian et al., 2012).

Kufian et al. used PMMA and EPGDMA as electrolyte and found conductivity was over 10^{-3} S/cm at sub-ambient temperature (Kufian et al., 2012). The donor numbers explained high ionic conductivity from ethylene oxide unit on PEGDMA. The PMMA addition would increase composite viscosity, which would influence molecular motion (Kufian et al., 2012). It was reported that montmorillonite (MMT) clay and PMMA based gel polymer electrolyte showed 1.3×10^{-3} S/cm at room temperature. Higher clay surface

area could help sustain mechanical properties and lithium salts solubility. High liquid electrolyte uptaking and increasing composite dielectric constant improved ionic conductivity (J. Y. Song et al., 1999b) (Hayamizu et al., 1999). The presence of electronegative silicate platelets would increase the dielectric constant and dissolve more lithium salt, which resulted in higher ionic conductivity (Madhuryya Deka & Kumar, 2010).

Ng's group prepared surface-functionalized PMMA by using ionic liquid entity 1-methyl-3-propylimidazolium bis(trifluoromethyl sulfonyl)imide (IL-TFSI) (Yang Li et al., 2017). Additional IL based additive as the plasticizer was added. PMMA could hinder dendrite growth and enhance membrane strength. 5.12×10^{-4} S/cm at 30°C was achieved. Brush-like IL-TFSI matrix on the surface would intersect with each other and provide open and continuous channels for ion transport (Yang Li, Wong, & Ng, 2016) (Sato et al., 2011). The immobilized TFSI⁻ groups had weak interactions with Li⁺, enhancing ion mobility (Yang Li, Wong, Dou, et al., 2016) (Yingying Lu et al., 2012). The microscopic fluidic environment was also provided to help ions movement (W. Zhai et al., 2014) (P. Yang et al., 2014).

In summary, PMMA has higher modulus and lower ionic conductivity, higher thermal, and electrochemical stability, good affinity with polar solvent-based liquid electrolyte, strong interaction with Li⁺ from ester group, no crystallization, and strong mechanical properties. The chains mobility restricts its application for higher performance electrolyte. But blending with plasticizer and copolymerization with other polymer electrolytes could solve this problem. The appropriate PMMA can act as high mechanical strength host and improve SPE performance in the future.

2.2.4 Poly-vinyl chloride (PVC)

After polyethylene and polypropylene, amorphous poly-vinyl chloride (PVC) is the world's third-most widely produced synthetic plastic polymer (Alamgir & Abraham, 1995). PVC has two basic forms: rigid and flexible. It would be softer and more flexible after plasticizers addition. It's inexpensive and compatible with a large amount of plasticizers. PVC electrolyte-based LIBs cycling behavior were demonstrated by Alamgir and Abraham in 1995 (Alamgir & Abraham, 1995). PVC showed the ionic conductivity temperature dependence property. PVC membrane Young's modulus is reported to be around 4800 MPa (Hasan & Lee, 2014) (Stephan et al., 2000). The problem of poor PMMA mechanical strength was solved by blending with PVC (Alamgir & Abraham, 1995). But according to Stephan et al.'s investigation, the increased mechanical strength led to poor interfacial and poor cycling properties. So there still remained some difficulties to obtain a performance balanced solid material via using PVC as the host polymer electrolytes (Stephan et al., 1999). Shriver's group found that ion conduction depended on polymer chains segmental motion and PVC amorphous structure (Wei & Shriver, 1998).

Bhattacharya reported radiation crosslinked PVC with PE to enhance mechanical strength and thermal stability. It did not impart the matrix ionic conductivity (Bhattacharya, 2000). Yamakawa et al. grafted PVC with MMA and styrene. The thermal stability has been enhanced (Yamakawa & Stannett, 1974). Omichi et al. increased PVC mechanical property 8% after radiation-induced graft polymerization (Omichi et al., 1978).

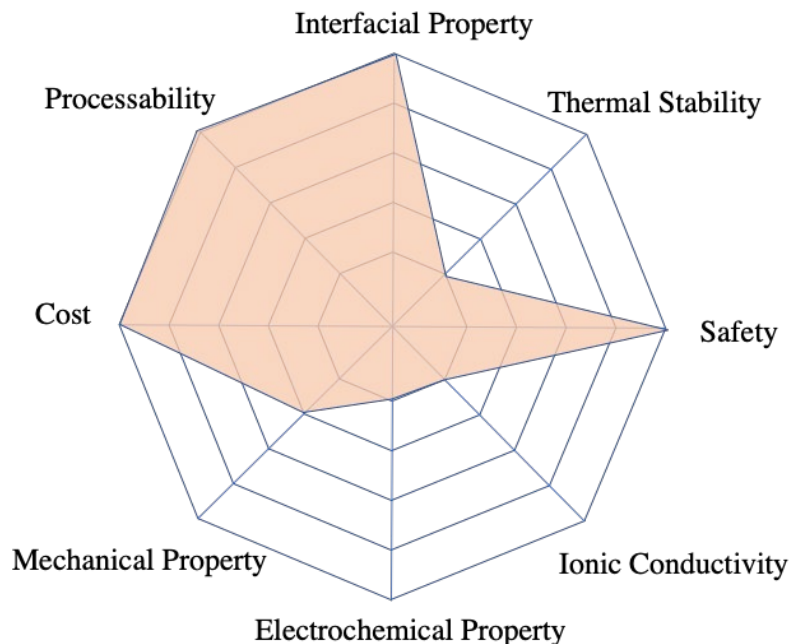


Figure 7 Ranking of PVC polymer properties.

Some PVC electrolyte-based research studies have been reported. Addition of PVC could suppress PEO crystallization (Castro et al., 2003) (Marco et al., 1993). PVDF blending with PVC could solve the phase separation problem because of immiscibility between PVC and plasticizer. PVC maintains the mechanical property. PVDF is absorbed by the electrolyte solution. PVDF has high anodic stability due to presence of strong electron-withdrawing C-F group and higher dielectric constant to help salt dissociation (Aravindan & Vickraman, 2007) (Vickraman et al., 2009) (Muniyandi et al., 2001) (Vickraman et al., 2007). Ramesh et al. blended PMMA with PVC and mixed it with LiTFSI salt (Ramesh et al., 2010). The increased segmental polymer chains and free voids decreased activation energy to 0.12eV. Sukeshini reported 10^{-4} S/cm ionic conductivity after mixing with plasticizer and Li^+ salt (Sukeshini et al., 1996).

Sivakumar's group recently proposed a composite: PVC with poly ethyl methacrylate (PEMA) as host material because PEMA had transparency, elasticity, and

good adhesion properties (Reiter et al., 2009) (Sim et al., 2012). PVC would enhance the LIB mechanical property. Also, its phase separation with plasticizer will help lithium ions transfer (Rhoo et al., 1997) (Jagadeesan et al., 2019). Pistoia reported 5×10^{-4} and 2×10^{-3} S/cm at room temperature for PAN and PVC matrices gel polymer electrolyte with LiClO_4 liquid electrolyte (Pistoia et al., 1996).

Table 4 Research summary on PVC based electrolyte

Polymer	Salt and plasticizer	Filler	Ionic conductivity(S/cm)	Battery Performance	Ref
PVDF/PVC	LiBOB, EC&DEC	TiO_2	4.38×10^{-4} @RT		(Aravindan & Vickraman, 2007)
PVDF/PVC	LiCF_3SO_3 , EC&DEC		1.47×10^{-5} @RT		(Vickraman et al., 2009)
PVDF/PVC	LiClO_4 , EC&DEC		1.74×10^{-3} @RT		(Vickraman et al., 2007)
PVC/ LiCF_3SO_3			1.0×10^{-4} @25°C		(Wei & Shriver, 1998)
PVC/ LiDFOB			2.23×10^{-5} @25°C	LiCoO_2/Li 73mAh/g @0.5C&25°C	(Chai et al., 2017)
PVC/PEMA	LiClO_4 , EC&DEC	BaTiO_3	6.17×10^{-3} @30°C		(Jagadeesan et al., 2019)

In summary, PVC-based electrolyte shows high electrochemical window and mechanical properties. The low price and easy processing properties make it compatible with many other polymer electrolytes. But the lower dielectric constant (~ 4) and poor solvating power for Li^+ limit its application as host electrolyte.

2.2.5 Poly-vinylidene fluoride (PVDF)

According to recent research studies, PVDF-based polymer electrolytes are highly stable, especially on the anode surface. This is because of the existence of a strong electron-withdrawing functional group and high dielectric constant, which are helpful for better dissolution. In 1997, it was reported that the PVDF-based electrolytes offer excellent electrochemical properties (Z. Jiang et al., 1997). Cyclic voltammetry showed that PVDF was more suitable for primary than secondary batteries when lithium metal is

used as anode (Z. Jiang et al., 1997). Tarascona et al. investigated PVDF and hexafluoropropylene (HFP) as polymer matrix electrolyte (Tarascona et al. year). PVDF crystalline parts would provide mechanical support. Amorphous PHFP trapped liquid electrolyte owing to the higher dielectric constant. The low volatility plasticizer was dimethyl-phthalate (DMP). After removing the plasticizer, a high ionic conductivity 0.2 mS/cm was achieved (Tarascona, 1996). In addition, PVDF fiber prepared by electrospinning demonstrated Young's modulus of 14.3 MPa (Agyemang et al., 2016).

Cheng et al. developed PVDF-HFP copolymer crosslinked with polyethylene glycol (PEG) and PEGDMA gel polymer electrolyte (C. L. Cheng et al., 2004b). It possessed higher thermal stability and tensile modulus (52MPa) as well as higher ionic conductivity around 10^{-3} S/cm (C. L. Cheng et al., 2004b). Yang et al. prepared PVDF-HFP/tetraethylammonium tetrafluoroborate-acetonitrile crosslinked electrolyte which had porous structures. 1.44×10^{-2} S/cm ionic conductivity was achieved. The tensile strength was 1.8Mpa (Chongyang Yang et al., 2015). In 2020, Zhou et al. crosslinked PVDF with crosslinker and LiPF_6 liquid electrolyte. They obtained 1.35×10^{-3} S/cm and higher cycle stability for 200 cycles (92% retention of initial capacity) (F. Zhou et al., 2020).

Wen et al. have investigated different diisocyanate-based waterborne polyurethanes (T. C. Wen et al., 2000). They are synthesized by using poly (propylene glycol) (PPG), dimethylol propionic acid (DMPA) and various diisocyanates. Lithium-ion transport would vary when the hard segments change. H-bonding in TPU played a role in the varied ionic conductivity (T. C. Wen et al., 2000). Liu et al. used PVDF/TPU/PAN gel electrolyte by electrospinning technique. The film showed 10.3Mpa tensile strength (Yuewen Liu et al., 2017).

Yang's group proposed a sandwich structure inspired by J. B. Goodenough group's idea to solve LLTO against lithium problem. $\text{Li}_{3x}\text{La}_{2/3-x}\text{TiO}_3$ high ionic conductivity (LLTO) was around 10^{-3} S/cm. It was simple and low-cost preparation (W. Liu et al., 2015a) (H. Li et al., 2018). PVDF/LLZTO Garnet type electrolyte is a promising candidate due to high ionic conductivity and excellent stability with Li metal (Jingxian Zhang et al., 2016a) (Xue Zhang et al., 2017). LLZTO addition is likely to create an alkaline-like condition and help PVDF dehydrofluorinate confirmed by Raman spectra (S. Zhang et al., 2006) (Bottino et al., 2000) (Hashim et al., 2011) (Sinirlioglu et al., 2014). The partial dehydrofluorinated PVDF with active region C=C could facilitate the interaction between PVDF, LiClO_4 , LLZTO, and other electrolyte materials (Wegener et al., 2006) (S. E. Hong et al., 2007). Fan's group used polyimide as the host with $\text{Li}_{6.75}\text{La}_3\text{Zr}_{1.75}\text{Ta}_{0.25}\text{O}_{12}$ (LLZO), PVDF, and Li-TFSI as electrolytes. The tensile strength was 11.5MPa (Hu et al., 2020).

Filler addition would introduce Lewis acid-base interaction between inorganic filler polar group and electrolyte ionic species. Ions migration will be achieved in those additional sites. It also minimized the cation and anion pairs formation, enhancing the ionic movement (Riley et al., 2002) (Prasanth et al., 2013) (Xiaosong Huang, 2013) (M Deka & Kumar, 2011). Electrospinning prepared PVDF membrane has been investigated (Cuiru Yang et al., 2009). Blending with cellulose acetate nanofiber increased the mechanical property (Kang et al., 2016). Polypropylene carbonate (PPC) /PVDF-based electrolyte showed high performance. The ester group from PPC was beneficial for ionic conduction by trapping and storing LE. The chains segmental motion was favorable for ions conduction (Xueyan Huang, Zeng, et al., 2015).

Some groups incorporated SiO₂-PAALi on the electrospinning prepared PVDF fibers because nanoparticles had influence on ionic conductivity, electrochemical stability, and mechanical strength (Y. Liao et al., 2013) (Angulakshmi et al., 2013) (Prasanth et al., 2013). The inorganic compound could improve heat resistance. Lewis-base interaction between SiO₂ and polymer could weaken F atom and Li⁺ interaction, enhancing free Li⁺ movement (Xiao et al., 2012). Because of the solvation effect, more charge carriers could be provided by SiO₂-PAALi. When film was attacked by an external force, nanoparticles will lead to a crazing effect and enhance the strength (W. Li et al., 2015) (Yusong Zhu et al., 2013).

Blending with other polymer electrolyte is an easy way to enhance electrolytes performance (Nunes-Pereira et al., 2015) (Z. Li et al., 2008) (Gopalan et al., 2008). The high ionic conductivity, high thermal stability, high cycling capacity, good interface, and low SPE crystallinity can be achieved (Y. M. Lee et al., 2005) (Xi, Qiu, Li, et al., 2006) (Prasanth et al., 2014) (Rajendran & Sivakumar, 2008). Hydroxyethyl cellulose (HEC) is water soluble polymer that has thickening binding, emulsifying, suspending, dispersing, and stabilizing properties. Its excellent mechanical property could avoid short circuit and promise good thermal stability (M. Y. Zhang et al., 2017). Wang's group incorporated a reversible silicone-capped electroactive polyfluorene into PVDF electrolyte to offer overcharge protection for high voltage cathodes (operating above 4 V). Because it has photoactive and electroactive property (Leclerc, 2006) (B. Wang et al., 2013) (G. Chen & Richardson, 2010). Electroactive polymers switched the conductive and insulating states by oxidation/reduction owing to overcharge protection agents in LIBs (G. Chen & Richardson, 2004) (Ni et al., 2016).

Table 5 Research summary on PVDF based electrolyte

Polymer	Salt and plasticizer	Filler	Ionic conductivity(S/cm)	Electric window	Tensile Strength	Battery Performance	Ref
PVDF/PVDF-LLTO/PVDF		LLTO	3.01×10^{-3} @RT	5.0V		LiCoO ₂ /Li 110mAh/g @2C & RT	(H. Li et al., 2018)
PVDF	LiClO ₄	LLZTO	5×10^{-4} @25°C			LiCoO ₂ /Li 136mAh/g @2C & 25°C	(Xue Zhang et al., 2017)
PVDF/HEC/PVDF	LiPF ₆ EC/DMC /EMC		8.8×10^{-4} @RT			LiFePO ₄ /Li 140mAh/g @0.2C & 25°C	(M. Y. Zhang et al., 2017)
PVDF/PMMA/PVDF	LiPF ₆ EC/DMC /EMC					LiCoO ₂ /Li 140mAh/g @0.2C & 25°C	(H. P. Zhang et al., 2007)
PFO-PSQ/P3BT-impregnated PVDF	LiPF ₆ EC/DMC			4.4V		LiCoO ₂ /Li 125mAh/g @0.5C & 25°C	(Ni et al., 2016)
PVDF	LiPF ₆ in EC:DMC :EMC	SiO ₂ -PAALi	3.5×10^{-3} @25°C	5.05V	48.8Mpa 25.6%	LiCoO ₂ /Li 152mAh/g @0.1C & 25°C	(W. Li et al., 2015)
PVDF	LiPF ₆ in EC:DMC :EMC	SiO ₂	1.13×10^{-3} @25°C			LiFePO ₄ /Li 118.7mAh/g @0.1C & 25°C	(Yusong Zhu et al., 2013)
PVDF	LiPF ₆ EC/DMC	montmorillonite	3.08×10^{-3} @RT			LiMn ₂ O ₄ /Li 118mAh/g @0.1C & 25°C	(Prasanth et al., 2013)
PVDF	LiClO ₄ PC/DEC	montmorillonite	2.3×10^{-3} @RT	4.6V			(M Deka & Kumar, 2011)
PVDF	LiPF ₆ EC/DMC	silica	1.27×10^{-3} @RT		7 MPa for yield strength	LiNi _{1/3} Co _{1/3} O ₂ /Graphite ~115mAh/g @0.1C & 25°C	(Xiaosong Huang, 2013)
PVDF+PMMA	LiPF ₆ EC/DMC		7.9×10^{-3} @25°C			LiCoO ₂ /Carbon 116.5 mAh/g @0.1C & 25°C	(Z. Li et al., 2008)
PVDF+PAN	LiClO ₄ PC		7.8×10^{-3} @25°C	5.1V		LiCoO ₂ /Li 120.4 mAh/g @0.1C & 25°C	(Gopalan et al., 2008)
PVDF+PE	LiPF ₆ in EC:DMC :EMC		8.9×10^{-4} @25°C	4.5V	271 Kg/cm ²	LiCoO ₂ /Carbon 2.5 mA/cm ² @1C & 25°C	(Y. M. Lee et al., 2005)
PVDF+PEO	LiClO ₄ PC		2.0×10^{-3} @25°C		30Mpa		(Xi, Qiu, Li, et al., 2006)

Table 5 (Continued)

PVDF+P EO	LiTFSI EC/DEC	4.0×10^{-3} @20°C	LiFePO ₄ /Li 168mAh/g @0.1C & 25°C	(Prasanth et al., 2014)
PVDF+P VC	LiClO ₄ EC/PC	3.7×10^{-3} @25°C		(Rajendra n & Sivakumar , 2008)

In order to reduce PVDF crystallinity and enhance electrolyte mechanical property, HFP segments have been induced. The amorphous HFP groups could reduce PVDF crystallinity and porosity, enhancing electrolyte mechanical property. Fluorine content increasing would enhance the hydrophobicity, which resulted in higher roughness and more pores. The long bond of C-F compared with C-H would give chains more free space to reduce electrolyte crystallinity (Xinya Wang et al., 2018) (Abbrent et al., 2001) (I. Kim et al., 2018).

In summary, PVDF possesses high electrochemical stability, low dissipation factor and high dielectric constant (~ 8) (Du Pasquier et al., 2000). The PVDF crystallization reduces ionic conductivity. HFP segments could solve this crystallization problem. Crosslinking and copolymerization are good ways to enhance the mechanical strength and liquid electrolyte uptaking. Because of the higher conductivity and comparable high mechanical strength, PVDF-HFP based gel polymer electrolyte would play an important role in future LIBs.

2.2.6 Poly propylene carbonate (PPC)

PPC is a copolymer of propylene carbonate and carbon dioxide. Ester group from PPC is conductive and could store liquid electrolytes. The PPC chains motion also contributes to ion transport. But the PPC mechanical strength degraded after mixing with liquid electrolyte. Bohnke et al. used the LiClO₄- propylene carbonate (PC) mono-

PMMA to fabricate polymer electrolyte (Bohnke et al., 1992). The high ionic conductivity 2.3×10^{-3} S/cm was achieved at 25°C. Fast ion movement was achieved with PC molecules. Besides, PMMA acted as stiffener because of high mechanical property. Ionic conductivity ranged from 5×10^{-3} S/cm to 2.3×10^{-5} S/cm when changing the amount of liquid electrolyte (Bohnke et al., 1992) (Bohnke et al., 1993a) (Bohnke et al., 1993b). Additionally, Nithya et al. used PPC as the plasticizer in PEO-based electrolyte systems (Nithya et al., 2012).

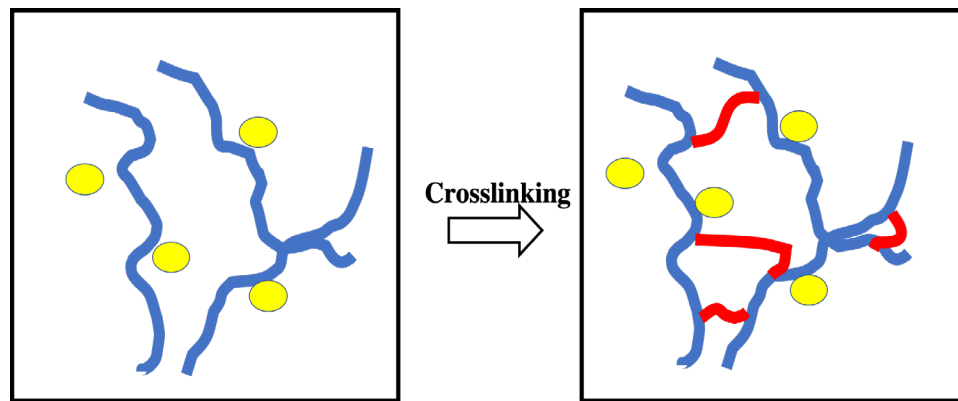


Figure 8 PPC crosslinking process

PPC copolymer of propylene oxide and carbon dioxide was also investigated. Amorphous aliphatic polycarbonate had local relaxation and segmental motion (Jianjun Zhang et al., 2015) (Jianjun Zhang et al., 2017) (Xiao-Yuan Yu et al., 2010). Zhou et al. used PPC as host, LiClO_4 salt, and 1-butyl-3-methylimidazolium tetrafluoroborate ($\text{BMIM}^+\text{BF}_4^-$) ionic liquid to prepare gel electrolyte (D. Zhou et al., 2013). 1.5 mS/cm electrolyte ionic conductivity was obtained. ILs based electrolytes could be helpful for solvent-free, nonvolatile, and high conductive GPE. The nonflammability, wide electrochemical window, safety and rate capability, cycle stability were displayed (J. Zhao et al., 2016) (D. Zhou et al., 2013) (Xiaoyuan Yu et al., 2010) (Xueyan Huang, Zeng, et al., 2015) (Jianjun Zhang et al., 2018).

Table 6 Work summary for PPC based electrolyte

Polymer	Salt and plasticizer	Filler or ceramic electrolyte	Ionic conductivity (S/cm) @25°C	Electrochemical window	Battery Performance	Ref
PPC	LiTFSI	cellulose	4.2×10^{-4} @25°C	4.6V	LiFePO ₄ /Li 75mAh/g @ 5C	(Jianjun Zhang et al., 2015)
PPC	LiTFSI	LLZTO	5.2×10^{-4} @25°C	4.6V	LiFePO ₄ /Li 90mAh/g @ 5C	(Jianjun Zhang et al., 2017)
PPC/PEO	LiClO ₄		6.83×10^{-5} @25°C	4.5V		(Xiao-Yuan Yu et al., 2010)
PPC	LiClO ₄	Ionic liquid	1.5×10^{-3} @25°C			(D. Zhou et al., 2013)
PPC	LiODFB in PC		1.14×10^{-3} @25°C	5.0V	LiNi _{0.5} Mn _{1.5} O ₄ /Li 66.5mAh/g @5C	(J. Zhao et al., 2016)
PPC	LiClO ₄ in EC:DMC		8.43×10^{-3} @25°C	4.2V	LiNi _{1/3} Co _{1/3} Mn _{1/3} O ₂ /Li 115mAh/g @0.1C	(Xiaoyuan Yu et al., 2010)
PPC/PVDF	LiPF ₆ in EC:DMC		4.05×10^{-3} @25°C	5.2V	LiFePO ₄ /Li 102mAh/g @ 2C	(Xueyan Huang, Zeng, et al., 2015)

Tu's group reported PPC into poly (vinylidene fluoride-hexafluoropropylene) (PVDF-HFP) as polymer host and swollen with LiPF₆ in EC/DEC (Liang et al., 2019). It showed 1.18 mS/cm for ionic conductivity, 4.8 V for electrochemical windows (Liang et al., 2019). The pristine PPC showed 3.8MPa reported by Zhang et al. Their LIBs also showed 140mAh/g at 1C and 120°C (Jianjun Zhang et al., 2015).

Huang et al. crosslinked polybutadiene, PPC, and PEG by using benzoyl peroxide (Xueyan Huang, Huang, et al., 2015). The mechanical strength has enhanced by crosslinking. BR acted as the binder and enhanced the contact between the electrodes and electrolyte, reducing the electrolyte cost. 1.25×10^{-3} S/cm ionic conductivity at room temperature was obtained (Xueyan Huang, Huang, et al., 2015). Song et al. produced cross-linkable PPC with 37.5 MPa tensile strength. Introducing cross-linkable moiety is a

facile way to enhance thermal stability and molecular weight (Pengfei Song et al., 2019) (Peng-fei Song et al., 2009). Miranda reported PPO-PEO-PPO block copolymer with cross-linkable ending groups achieved 6.4×10^{-4} S/cm at 25°C and storage modulus around 400 Kpa (Miranda et al., 2013).

In summary, PPC is a good electrolyte but has lower mechanical properties because it absorbs liquid electrolytes or ionic liquids. However, PPC's good compatibility with lithium salts offers a good interface with electrodes. PPC easily transfer to rubber state after adding ILs. The higher modulus could be achieved by crosslinking with other polymers, blending fillers, etc. PPC can be a promising electrolyte for the future owing to its high ionic conductivity.

2.2.7 Other polymer electrolyte and methods

Goodenough's group has used the double layer polymer electrolyte (PEO contact with the anode, PMMA contact with cathode) because of the limited electrical window for single polymer (W. Zhou et al., 2019). It avoided PEO oxidation at the cathode side when voltage is over 3.9V. In addition, it promised high alkali cation mobility on the anode surface. Malonic amide units could provide a main linear chain to facilitate the salt dissociation, Li^+ solvation and Li^+ transport (W. Zhou et al., 2019). Hersam's group used hexagonal boron nitride, ethyl cellulose as stabilizers and lithium ionic liquid gel electrolytes, achieving ~5 MP storage modulus (Hyun et al., 2019). Its ionic conductivity over 1mS/cm and over 5V electrochemical window were achieved (Hyun et al., 2019).

Cui's group recently combined the nanoporous polyimide (PI) filled with the PEO/LiTFSI as electrolyte and obtained 125 mAh/g under 1C charge condition (Wan et al. 2019). PI will provide an ultrathin, flexible, mechanically strong, non-flammable and

porous host for electrolyte film (Wan et al. 2019). Chen's group used the poly (ethylene glycol ether acrylate) PEGPEA gel polymer mixing with nano fumed silica-SiO₂ and LITFSI for flexible battery preparation (Niu et al., 2019). High ion conductivity 2.16×10^{-5} S/cm was obtained at room temperature (Niu et al., 2019). Meyer proposed that the polymer electrolyte should develop in two main directions: the higher conductive materials via crosslinking for gel electrolyte, the construction of SPEs with supramolecular architectures (Meyer, 1998). In 2020, Yu et al. used PVDF-PVAC-LLZTO and TMS as electrolyte to prepare flexible lithium-ion batteries. LIBs charged and discharged between 3.0 - 4.5V for 200 cycles at room temperature (Xinrun Yu et al., 2020).

Cui's group designed the easy *in situ* preparation method for poly vinylene carbonate (PVC) based material. Liquid VC would be polymerized by initiator at 60°C (Chai et al., 2017).. The superior interfacial stability and integrated interface were the main reason for higher performance (Chai et al., 2017). Wang et al. used the UV curving crystal electrolyte called ethoxylated trimethylolpropane triacrylate (ETPTA) monomer to form crosslinked electrolyte. The polymer electrochemical voltage window could be 4.78 V. Discharge capacity was 147.1 mAh/g at 0.5 C (room temperature) by assembling with LiFePO₄ and Li electrode (Yang Lu et al., 2019). Grewal et al. used the bifunctional PEGDGE and PEGDA based polymers as the crosslinked network electrolyte (Grewal et al., 2019). A small crosslinker would facilitate lithium ions movement and avoid ions paring or salt precipitation. The conductivity could be 1.1×10^{-6} S/cm at room temperature. In addition, the SPE transference number was 0.56 (Grewal et al., 2019).

Cui's group has reviewed the research about the Li^+ motion and frontier orbital energy levels of SPEs, including ion-dipole (salts with polymer), hydrogen bonds, $\pi - \pi$ stacking, and Lewis acid-base interaction (Q. Zhou et al., 2019). Due to the high potential μ_c for deintercalation in the cathode, a low HOMO of SPEs is needed. High PEO HOMO is lower than most lithium salts which may also decompose at higher potential applied (Q. Zhou et al., 2019). Salts decomposition in electrolytes can depend on ionic or covalent bonds energy, bond length, electron affinities, atoms sizes and overall molecule structures, which can be an overall complex process.

Plastic crystals could weaken the interaction strength between Li^+ and polymer, ionizing lithium salts owing to high polarity and entropy, resulting in high σ . Patel et al. proposed that the competitive interaction decreased the energy barrier for gauche-trans transformation and increased trans concentration, which could explain the high ionic conductivity 10^{-3} S/cm for PAN/PEO/SN/LiTFSI system (Patel et al., 2008) (Patel & Bhattacharyya, 2008). Polar group carbonyl on PEO derivative side chain increased σ . The reason attributes to Li^+ and flexible ether side group C-O-C (Tominaga, 2017). Introducing anion acceptor is another way to improve transference numbers. However, electrolyte ionic conductivity normally decreased owing to the acceptor agglomeration (Błażejczyk et al., 2004) (Mehta & Fujinami, 1997) (Hekselman et al., 2010) (Stephan et al., 2011). The interaction between the polar group and hydrogen bond could enhance Li^+ transfer. A new class polymer urea-cytosine end-capped polypropylene glycol (UrCy-PPG) had ordered phase separation and 10^{-4} S/cm to 10^{-6} S/cm ionic conductivity (H. Chen et al., 2004) (C.-C. Cheng & Lee, 2016). The $\pi - \pi$ stacking interaction in the

liquid crystal can also form lithium ion channels through phase segregation (Q. Zhou et al., 2019).

2.2.8 Summary

In conclusion, we compare different polymer electrolytes electrochemical performance and methods like blending with other polymers, ionic liquids, plasticizers, inorganic fillers, ceramic electrolytes, crosslinking, forming copolymers, etc. We elucidate ion conductivity enhancement mechanisms in polymer composite electrolytes. The ionic conductivity of all the polymer hosts mentioned above increases when they are plasticized. There is still a challenge to obtain the SPE high electrochemical performance and high mechanical property simultaneously. In addition, some problems can be solved by combining several hosts together.

In the present study, people are still looking for polymer electrolytes that possess advantages such as no internal shorting, electrolytes leakage, and non-combustible reaction to substitute commercial liquid electrolytes (Venkataraman Thangadurai et al., 2014) (Design et al., 2000). In this thesis, PEO is chosen as the polymer electrolyte because of its chemical stability, ionic conductivity, electrochemical window, etc. In addition, the future direction should focus on the new polymers' developments by chemical synthesis and physical process. Atomistic investigation of the nanoparticle size and shape effects on solid polymer electrolytes ionic conductivity also could be considered.

2.3 Inorganic electrolytes

Compared to liquid electrolyte and gel electrolyte, the inorganic solid electrolyte has the following advantages: 1) non-volatile; 2) working in a wide temperature range,

especially under high temperature; 3) wide electrochemical window; 4) high strength and hardness, which can effectively prevent lithium dendrite growth and improve battery safety, 5) generally not flammable (C. Cao et al., 2014). Inorganic solid electrolyte is divided into oxide solid electrolyte, sulfide solid electrolyte and polyanion solid electrolyte. In recent years, the conductivity of sulfide and garnet oxide solid electrolyte have made significant progress. Their room-temperature ionic conductivity has reached $10^{-3} \sim 10^{-2} \text{ S/cm}^{-1}$, which can meet the commercial battery electrolyte conductivity requirements (Aricò et al., 2005).

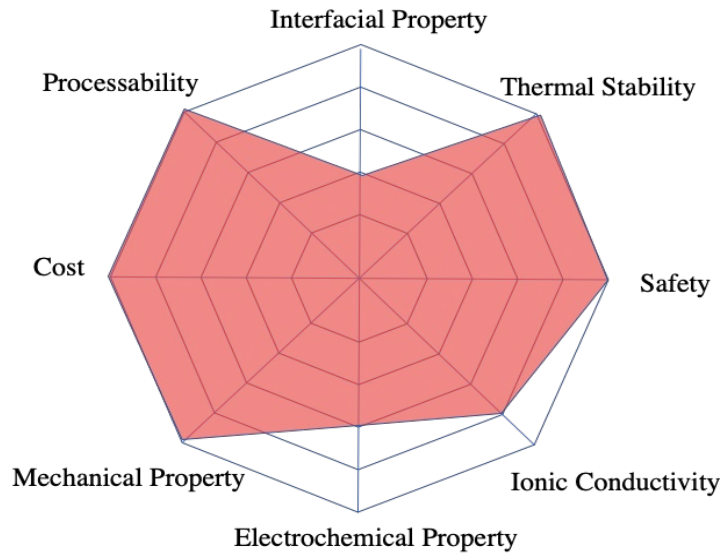


Figure 9 Inorganic electrolyte properties

High-performance inorganic electrolytes require high ionic conductivity and good electrochemical stability. The inorganic electrolytes that can meet the above requirements mainly include the two major systems: oxide system and sulfide system (Bresser et al., 2013). The sulfide system has high ionic conductivity advantages, a simple preparation method, and so on. Here is a brief review summary of these materials (Oh et al., 2015).

2.3.1 Li₂S based sulfides

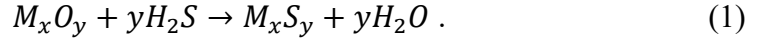
Sulfide electrolytes mainly include two systems of Li₂S-SiS₂ and Li₂S-P₂S₅ (Hayashi et al., 2014). The Li₂S-SiS₂ electrolyte conductivity is relatively low ($\sim 10^{-4}$ S/cm). So, the Li₂S-SiS₂ system conductivity development has become the focus of sulfide electrolyte research. At present, the development is mainly carried out to improve sulfide electrolyte ionic conductivity (Kudu et al., 2018). The traditional method to improve sulfide electrolytes conductivity is elements substitution in electrolyte lattice. Li₂S electrochemical window is stable in the range of 0 - 2.1 V, which means that its oxidation onset at lower voltage 2V (Sakuda et al., 2018). LGPS and Li₃PS₄ also have limited electrochemical windows because high potential will decompose SE. In addition, Li₂S-SiS₂ have a poor interface with LiCoO₂ electrode, leading to high interfacial resistance, degradation, and poor cycling (Yizhou Zhu et al., 2016).

Kudu et al. reviewed the relationship between structural properties and synthesis methods for Li₂S-P₂S₅ system (Kudu et al., 2018). It is found that using P₂S₃ and P₂O₃ partially replacing P₂S₅ can not only improve Li₂S-P₂S₅ electrolyte electrochemical stability but also improve the electrolyte conductivity. The sample [70Li₂S· (30-x) P₂S₅ · xP₂S₃] containing 1% P₂S₃ had the highest ionic conductivity, reaching to 5.4×10^{-3} S/cm. The battery exhibited excellent charge and discharge performance. When LIBs cycles number was more than 700 times, the battery capacity was still stable (Kudu et al., 2018). The superionic Li₇P₃S₁₁ was obtained by heating 70Li₂S· 30P₂S₅ system and showed 3.2×10^{-3} S/cm at RT (Hayashi et al., 2010). It was found that preparation methods like ball mill apparatus would influence ionic conductivity significantly (Minami et al., 2011).

Doping with halide is also helpful for ionic conductivity enhancement (Bresser et al., 2013). Halides are good additives which is widely used in $\text{Li}_2\text{S-P}_2\text{S}_5$ solid electrolyte system. Melt quenching prepared $\text{Li}_2\text{S-P}_2\text{S}_5$ is pretty common (Mercier et al., 1981). The greater the halogen ions radius, the more obvious conductivity increase. For glass-ceramic electrolytes, LiX phase effect on electrolyte conductivity is not clear. $\text{Li}_2\text{S-P}_2\text{S}_5$ electrolyte doped with LiBr phase conductivity is the highest, which could be 6.5×10^{-3} S/cm. Mixing $\text{Li}_2\text{S-P}_2\text{S}_5$ electrolytes with LiBH_4 crystals could produce glass state electrolyte $\text{Li}_2\text{S-P}_2\text{S}_5\text{-LiBH}_4$. When the LiBH_4 reached 50%(mol%), the conductivity reached the maximum point of 1.8×10^{-3} S/cm (Sakuda et al., 2018).

However, some sulfide electrolytes materials limitations are also being discussed (Bresser et al., 2013). Sulfide electrolytes have high lithium-ion conductivity and good process-ability, but their chemical stability is low in the air. The hygroscopic nature needs to be treated in the inert gas atmosphere to prevent hydrolysis in the air. It is easy to react with H_2O from air to produce harmful H_2S gas. So, the process must be treated in an inert atmosphere (or dry air) (Manuel Stephan, 2005). Hayashi et al. from Tatsumisago's group substituted P_2O_5 for P_2S_5 partially and decreased H_2S generation rate (Hayashi et al., 2014). Tatsumisago's group also reported ball-milled mixtures of sulfide glass with metal oxides like Fe_2O_3 , ZnO , and Bi_2O_3 , which would suppress H_2S generation effectively due to the chemical reaction between metal oxide and H_2S (**Equation -1**) (Hayashi et al., 2013). It requires the metal oxide must have a large negative Gibbs energy difference (ΔG) for this reaction. ZnO has -78.0 KJ/mol (Carnes & Klabunde, 2002). It is not clear how the H_2O product influences the LIB performance and should be addressed in the future work.

The reaction between metal oxides M_xO_y and H_2S is following (Hayashi et al., 2013) :



It is generally believed that the solid sulfide electrolyte cannot solve short circuit problems caused by lithium dendrite growth (Bresser et al., 2013). This is due to the preference for metal lithium to deposit in solid electrolytes gap and grain boundary during the Li deposition process (Sheng S Zhang & Tran, 2013). This phenomenon is particularly serious at large current density. Secondly, the solid sulfide electrolyte is unstable to the lithium metal, and it will be reduced after contact with Li metal, and the reduction product forms the interface layer on the contact surface. The interface layer electrochemical properties have an important effect on the solid-state LIB comprehensive performance. Lithium polysulfide are strong nucleophilic agents and react with many salts, electrolyte solvents, and polymer electrolytes (Sheng S Zhang & Tran, 2013) (Urbonaite et al., 2015). Therefore, limiting lithium dendrite growth along the solid electrolyte is the focus to achieve LIBs long-term cycles.

2.3.2 Nasicon type - LAGP

Lee et al. used $Li_{1.4}Al_{0.4}Ge_{1.6}(PO_4)_3$ (LAGP) particles as electrolytes (J. Lee et al., 2019). Because ceramic material LAGP has high ionic conductivity (10^{-4} S/cm) at room temperature, good stability and safety could help improve PEO-based LIBs electrochemical performance. High ceramic content will alleviate segmental motions. There is no strong interaction between PEO chains and LAGP fillers (J. Lee et al., 2019). It was reported that NASICON- type structured $Li_{1.5}Al_{0.5}Ge_{1.5}(PO_4)_3$ (LAGP) glass melt could fabricate glass-ceramic fibers electrolyte by a combination of melt spun and

annealing method. The diameter will be controlled by the drawing rate. The fibers ion conductivity depended on the crystal structure and tunnel size. High crystalline hexagonal structures exhibit the highest ionic conductivity performance (He et al., 2019).

Wang et al. used LAGP mixed with PEO to prepare uniform electrolytes owing to the difficulty of prepare dense electrolytes by raw LAGP material and the poor interface with an electrode (Chunhua Wang et al., 2017). Assembled LIBs showed 160.8mAh/g at 50°C (Chunhua Wang et al., 2017). Liu et al. tried to use sputtering Ge on top of Li metal and improved interface problem owing to Ge^{4+} to Ge^{2+} , Ge^0 reductions (Yijie Liu et al., 2018). Using LAGP electrolytes still has a long way to go because of the processing method and interface problem. Another Nasicon type electrolyte is LATP. Kosova et al. also investigated $\text{Li}_{1.3}\text{Al}_{0.3}\text{Ti}_{1.7}(\text{PO}_4)_3$ (LATP) electrolyte which showed 1mS/cm (Kosova et al., 2008). The LATP electrolyte is stable with Li metal. Kou et al. prepared $\text{Li}_{1.3}\text{Al}_{0.3}\text{Ti}_{1.7}(\text{PO}_4)_3$ (LATP) under varied pH (Kou et al., 2020). The assembled batteries LCO/LATP/Li showed 150 mAh/g at 0.1C and had 94.28% capacity retention after 300 cycles (Kou et al., 2020).

In summary, although LAGP shows high ionic conductivity, it has many intrinsic shortcomings like grain boundary resistance, electrochemical compatibility with electrodes, cycling stability, high cost, reaction with air, and high processing temperature. There is still a long way to achieve commercial applications.

2.3.3 Garnet type $\text{Li}_7\text{La}_3\text{Zr}_2\text{O}_{12}$ (LLZO)

It was found that garnet LLZO showed the lowest reduction potential 0.05V and least favorable decomposition energy -0.02eV per atom at 0V, which could be stabilized against Li metal (Bresser et al., 2013). These garnet materials show 1mS/cm ionic

conductivity and 0-6V electrochemical windows. Stoichiometric LLZO showed a tetragonal crystal structure (Bresser et al., 2013).

Linear elasticity analyses performed by Monroe and Newman, suggested that the shear modulus should be two times higher than the Li metal modulus for preventing dendrite growth (Monroe & Newman, 2005). Siegel's group calculated the LLZO Young's modulus around 147-154 Gpa. The shear moduli for Al/Ta doped LLZO showed 60 Gpa which was one order magnitude higher than the Li (S. Yu et al., 2016). Wen's group prepared Ta doped LLZO-MgO ceramics and reached 5.17×10^{-4} S/cm at 25°C (J. Lee et al., 2019). Fracture strength was 150Mpa. There were also some works have been done by doping with Al, Ga, Y, Si, Ge, Nb, Ta, and W for stabilizing LLZO structure (Xiao Huang et al., 2019).

Hu's group used garnet type $\text{Li}_{6.4}\text{La}_3\text{Zr}_2\text{Al}_{0.2}\text{O}_{12}$ (LLZO) lithium conductor material mixing with PEO as electrolyte (Kelvin et al., 2016). The polymer matrix showed 2.4×10^{-4} S/cm conductivity at room temperature (Kelvin et al., 2016). Lithium lanthanum titanate perovskite $\text{Li}_{0.33}\text{La}_{0.56}\text{TiO}_3$ (LLTO) also showed high ionic conductivity around 1mS/cm (Stramare et al., 2003).

However, the chemical stability with Li metal, low decomposition voltage, and sensitivity to moisture limited the application of LLTO, Li- β -alumina, Li_3N and Li_4SiO_4 based perovskite electrolytes (Robertson et al., 1997) (Adachi et al., 1996) (V Thangadurai & Weppner, 2006) (Stramare et al., 2003).

In summary, LLZO shows high potential owing to the high conductivity. However, the high processing temperature, crack propagation, grain boundaries, and stability still need to be overcome.

2.3.4 LiPON

LiPON had the chemical formula $\text{Li}_x\text{PO}_y\text{N}_z$ ($x=2y+3z-5$) and showed high ionic conductivity (Cherkashinin et al., 2020). The electrochemical window was reported between 0-5V versus Li/Li^+ . For SE materials, significant overpotential is expected for the oxidation reactions because of poor diffusion kinetics and gas evolution process. Yu et al. found bubbles formation in LiPON electrolyte (Xiaohua Yu et al., 1997). The gaps between the oxygen chemical potential and sulfur chemical potential suggested that the interface between sulfide SE and LCO was not stable (Venkataraman Thangadurai et al., 2014). An interfacial layer was needed. Both perovskite and garnet structure showed isotropic Li^+ conduction. The crystal structure played an important role in the Li^+ conduction. However, higher preparation temperature and special equipment limited ceramic electrolyte application. Its poor flexibility is another limitation factor (Venkataraman Thangadurai et al., 2014). Jaegermann's group demonstrated interfacial stability controlled by band bending direction (Cherkashinin et al., 2020). $\text{LiCoPO}_4/\text{LiPON}$ interface was more stable owing to the large ionization potential difference which implied that a small amount of electron charges transfers at interface even in high voltage. LiNiPO_4 Femi level upshift would provide more probability for electron transfer when in contact with LiPON. A sufficient energy gap between electrode and electrolyte was necessary for a stable interface (Cherkashinin et al., 2020). The processing method for LiPON would still be a limit for a large application. Dudney's group used the sputtering method to solve the interfacial problems and obtained high LIBs cycle stability results (Juchuan Li et al., 2015).

Table 7 Electrochemical window of electrolyte, upper plot referred from Chemistry of Materials 2015 (Richards et al., 2016)

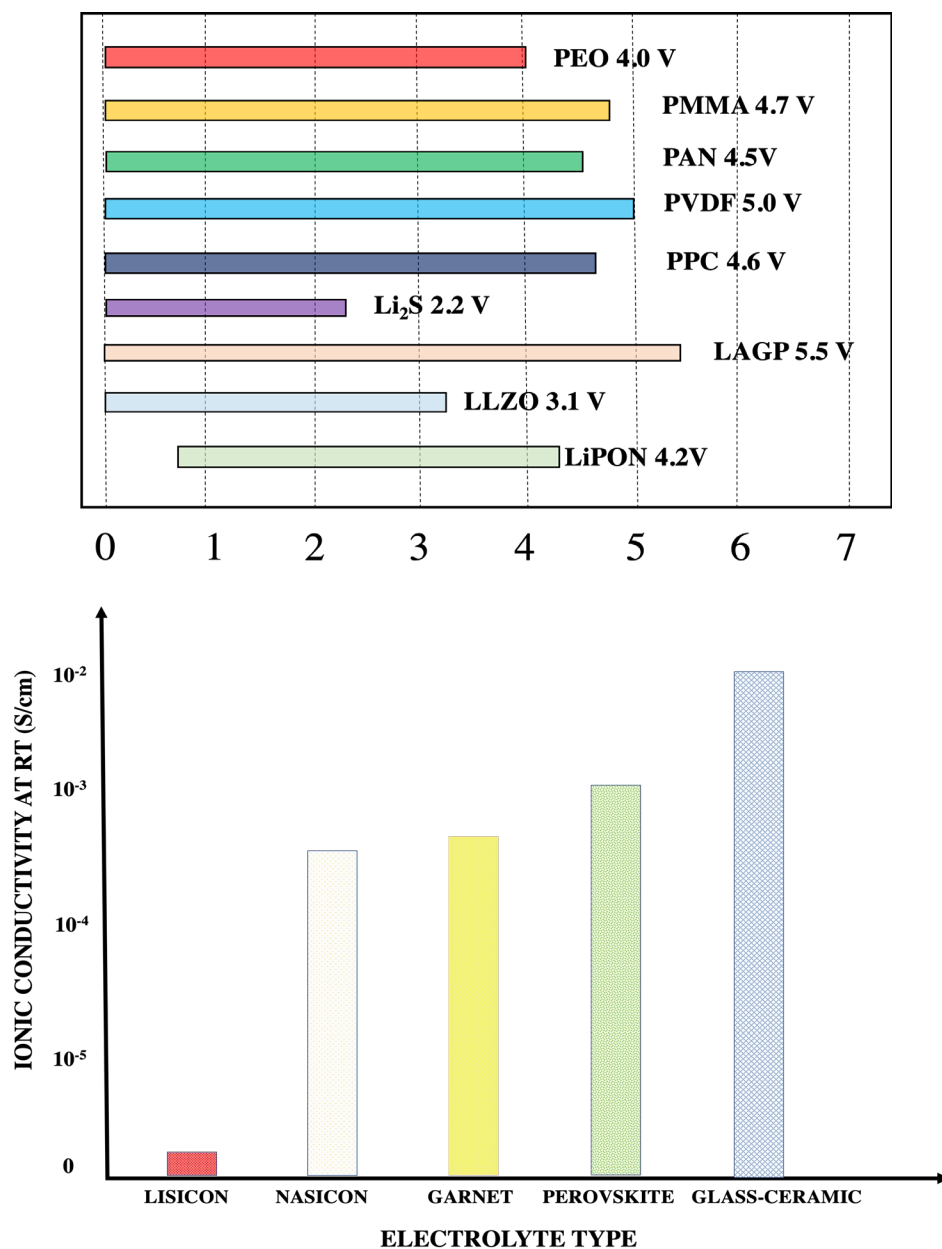


Figure 10 Ionic conductivity summary for inorganic material

In summary, although inorganic electrolytes show high ionic conductivity, some inorganic solid electrolyte suffers from instability with Li metal. As mentioned before, the interfacial problem between solid electrolyte and electrode, electrolyte preparing method, processing temperature still need more investigation.

2.4 Electrodes

Electrode materials theoretical capacity can be expressed by (Torabi & Ahmadi, 2020):

$$C_t = \frac{nF}{3.6M}, \quad (2)$$

where n is the number of reactive electrons per formula unit, F is the Faraday constant, M is electrode material molar weight.

We can calculate high-capacity electrode materials from above equation by using small molar weight and accommodating more electrons per formula. For example, Li metal shows 3850mAh/g. Pure Si shows 4200mAh/g if the alloying compound is $\text{Li}_{22}\text{Si}_4$ but high dealloying potential $>0.4\text{V}$, high volume expansion ($>300\%$), low electrical conductivity ($<10^{-5} \text{ S/cm}$ at RT), and instable SEI related to electrode volume change (Peng et al., 2017). Other anode materials like germanium (Ge), tin (Sn), phosphorous (P), Aluminum (Al), Zinc (Zn), Sodium (Na), and Potassium (K). Multivalent metal anodes showed 800-3000mAh/g but offset by higher redox potential (0.7-2.2V) (Peng et al., 2017). Graphite (redox potential 0.05V vs Li/Li^+ , 372mAh/g by forming LiC_6) has lithium deposition safety concern for overcharge. Here, we mainly talk about carbon, Si, and metal oxides anodes.

For cathode materials, LiCoO_2 shows 273mAh/g theoretically, but 140mAh/g practically obtained due to reaction reversibility and host lattice structure stability (Nitta et al., 2015). V_2O_5 shows 443mAh/g (Prosini et al., 1998). Other cathodes like halogens Bromine (Br_2), Iodine (I_2) have redox potential $>3.0\text{V}$ and 200-350 mAh/g energy density (Nitta et al., 2015). However, the limitations are their volatile and hazardous properties. Oxygen (O_2) shows 1675mAh/g capacity but tradeoff by short cycling life, poor cycle

stability, and atmospheric contamination such as CO₂ and N₂ (Aurbach et al., 2016). There are also some other chalcogen electrodes, like Sulfur (S) (Bruce et al., 2012), tellurium (Te) (Goodenough & Kim, 2010) (Nitta et al., 2015) (Choi & Aurbach, 2016). We compared lithium metal oxide and sulfur cathodes materials after considering the cost, specific capacity, preparation techniques, chemistry, safety, environmental issues.

Electronegativity is an essential factor in determining electrode electrochemical potential, which determines bond types between transition metal and anions or anion ligands (Nitta et al., 2015). The big electronegativity difference will form more ionic bonds, which have dense structure. This will influence the crystal stability, phase stability and Li⁺ site energy. The small differences will form covalent bonds and result in a loose packed system. The Gibbs free energy change and electrochemical potential depend on the valence state, ionic radius, electronegativity, and cations local environment for cathode materials.

Gibbs free energy change calculation is (C. Liu et al., 2016):

$$\Delta G = -nFE , \quad (3)$$

where ΔG denotes the internal energy difference during a reaction, n is the number of electrons involved, F is Faraday constant, E denotes the electrochemical potential (C. Liu et al., 2016).

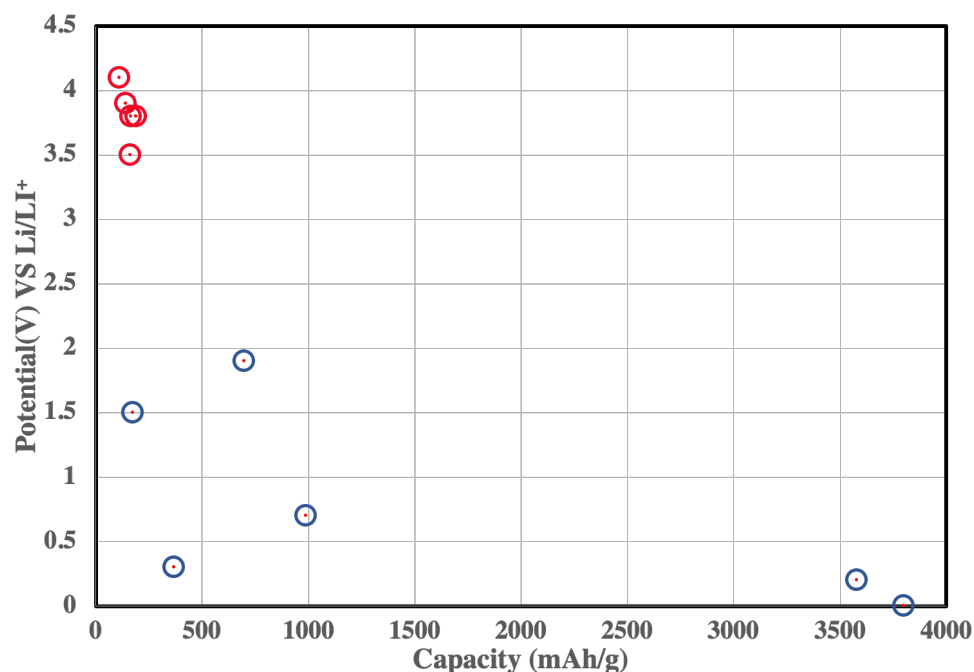


Figure 11. Potential of electrodes materials (red) common cathodes, (blue) common anodes. Referred from *Materials Today* 2016 (C. Liu et al., 2016)

2.4.1 Anode

2.4.1.1 Carbon nanotubes and graphite

In 1996, Thio's group reported nanotube electrical resistivity relationship with temperature and electrode particle size (Ebbesen et al., 1996). The resistivity ranged from 1.2×10^{-4} to $5.8 \Omega \cdot \text{cm}$ at room temperature. Nanotube electrical conductivity was around 0.17 to $8.3 \times 10^3 \text{ S/cm}$. Its reported crystalline graphite is $3.8 \times 10^{-5} \Omega \cdot \text{cm}$ ($2.6 \times 10^4 \text{ S/cm}$) (Ebbesen et al., 1996). Copper current collector is around $5.96 \times 10^5 \text{ S/cm}$ (Matula, 1979). In addition, it was found that graphene and nanotubes had high electrical conductivity, comparable structural stability, tunable surface functionality, and good mechanical properties (Article, 2015). The reason could be divided into two parts (Landi, 2009). Firstly, their high capacities normally happened during the first several cycles. Rapid performance degradation (30% - 50% charge consumption) could attribute to the irreversible lithiation and delithiation process, because strong Van der Waals forces

among layers will make the layer re-stacking and lithium consumption. The lithium storage mechanism is an adsorption mechanism, both in internal surfaces and empty nanopores. The second reason is related to graphene discharging at around 1-3 V. Graphene has large voltage hysteresis in the charge/discharge curve (Z. Wu et al., 2012).

Nowadays, carbon nanotubes and graphene have improved electrodes' electrical conductivity (Fang et al., 2019). However, they are not the active lithium storage materials but the support material for the lithium-ion transfer (Fang et al., 2019).

Graphite shows 372 mAh/g reversible capacity and LiC_6 formed after intercalation (Seino et al., 2005). Zhang et al. investigated low-temperature performance graphite and found that Li^+ diffusivity decreased significantly below 0 °C (S S Zhang et al., 2002). 10^{-9} - 10^{-10} cm^2/s at 20°C was observed (S S Zhang et al., 2002). Blyth et al. used XPS to study graphite surface after pretreatment (Blyth et al., 2000). They found that chemical modification occurred at prismatic planes. Various C-O bonds existed on the graphite (Blyth et al., 2000). Buqa et al. investigated LIBs high current rate performance by using different porosities (30-40%) graphite electrodes (Buqa et al., 2005). 20C rate could be achieved for low electrode loading ($1.5\text{mg}/\text{cm}^2$) LIBs. The key parameters influencing the current rate are the electrode materials loading, electrode thickness, and electrode porosity (Buqa et al., 2005).

In summary, graphite shows high stable cycle stability and electrochemical performance. In this thesis, we will use graphite anode in our LIBs. We will investigate the interface layer between graphite and SPE in Chapter VI.

2.4.1.2 Silicon anode

Silicon (Si) is a popular anode because of high theoretical capacity around 4200 mAh/g, almost ten times higher than conventional carbon anode (Cocke et al., 2003). However, Si volume change during the charge and discharge process could be up to 400% (Cocke et al., 2003). Wu et al. from Cui's group have proposed a double-walled silicon nanotube as the anode (H. Wu et al., 2012). The steady SEI layer formed. The mechanism was covering a clamping layer on top of the silicon hollow nanotube. This layer is composed of silicon oxide, which does not react with lithium. Lithium would penetrate inside and has the lithiation. In addition, electrode volume change toward hollow inside direction rather than outside direction. The Si volume change during the charge/discharge problem was solved. Besides, the high temperature around 500 degrees would oxidize outside silicon and exclude internal carbons, resulting in a hollow structure. After 6000 times cycle, the battery still retained 85% capacity (H. Wu et al., 2012).

Fu et al. used the chemical vapor deposition method (CVD) to prepare silicon-based anode on the carbon nanotubes (CNTs) (Fu et al., 2013). The flexibility is from self-sustained CNT. The wave-like deformation would help the electrode mitigate the stress formation during the lithiation and delithiation. The amorphous silicon has a very strong bonding on carbon nanofibers (C. M. Wang et al., 2012). The volume changed on radial direction rather than on the axis direction (Fu et al., 2013) (C. M. Wang et al., 2012). Bradford's group used electrospinning PMMA-Si nanofibers onto aligned CVD method prepared pyrolytic CNT sheets (Yildiz et al., 2019). Decomposing PMMA under the elevated temperature would form a uniform Si film. They obtained excellent cycle

capacity 1470 mAh/g and good capacity retention 88% after 150 cycles under 100 mA/g charging current (Yildiz et al., 2019).

In summary, although SiO₂ and SEI formation may cause capacity loss, Si still has a high theoretical capacity and would be promising for future LIBs. The electrode volume change during charge/discharge could be solved by engineering anode structure and combining it with other anode materials.

2.4.1.3 Mn₃O₄, Co₃O₄, SnO₂, FeO_x, NiO anode materials

Wang et al. synthesized Mn₃O₄-Graphene hybrid material as an anode (Hailiang Wang et al., 2010). The reason was related to Mn abundance, low cost, and environmental benignity. The poor electrical conductivity (around 10⁻⁷-10⁻⁸ S/cm) limited its application. By wiring up Mn₃O₄ nanoparticles to the conductive graphene substrate, 900mAh/g capacity (theoretical 936mAh/g) LIBs were fabricated (Hailiang Wang et al., 2010) (Poizot et al., 2000b).

Tae et al. synthesized virus-based Co₃O₄ nanowires anode because of high reversible capacity (Tae et al., 2002). The virus would help Co₃O₄ form a dense and integrality structure which resulted in the high electrochemical properties. The self-assemble property was achieved by virus-virus interaction. By controlling surface charge and fluidic force, free-standing, lightweight and flexibility properties were achieved (Tae et al., 2002). Lou et al. overcame poor LIBs capacity retention and rate capability barriers by building needlelike Co₃O₄ nanotubes (Lou et al., 2008). Finally, 918 mAh/g was retained after 30 cycles for Co₃O₄/Li half cells (Lou et al., 2008). Li et al. synthesized Co₃O₄ nanowires on Ti substrate and obtained around 700 mAh/g after 20 cycles under

1C charge rate (Yanguang Li et al., 2008). This template-free method would eliminate ancillary materials use (Yanguang Li et al., 2008).

Meduri et al. presented SnO₂ nanowires covered with Sn nanoclusters, exhibiting an exceptional 800 mAh/g capacity (Meduri et al., 2009). The reason was related to Sn nanoclusters which had less volume change, high surface area for Li alloying and dealloying. In addition, there were two phases formed by Sn and SnO (Meduri et al., 2009). Ye et al. prepared SnO₂ nanotubes by using the sacrificial silica mesostructured template method (J. Ye et al., 2010). LIBs showed 468mAh/g after 30 cycles at a current density of 100mAh/g (J. Ye et al., 2010). Xia et al. have used electrospinning method to prepare SnO₂/Carbon film and obtained 754 mAh/g reversible capacity at 300 cycles under 1A/g charge rate (Xia et al., 2016).

Additionally, Ban et al. used single-walled carbon nanotubes and FeOOH nanorods to prepare Fe₃O₄ anode without the binder (Ban et al., 2010). 1000 mAh/g capacity was achieved after 50 cycles at 1C (Ban et al., 2010). Zhong et al. made the hollow core-shell η -Fe₂O₃ microspheres by using PVP soft template (Zhong et al., 2010). The high discharge capacity 899.2mAh/g was achieved after 100 cycles under 150mA/g charge rate (Zhong et al., 2010). Xu's group has prepared a new anode using 3D graphene and Fe₂O₃ framework (T. Jiang et al., 2017). Ultrahigh capacity 1129 mAh/g at 0.2 A/g after 130 cycles was achieved (T. Jiang et al., 2017). The electrode structural strain could be alleviated (T. Jiang et al., 2017). Furthermore, Zhou et al. synthesized graphene-wrapped Fe₃O₄ anode material which showed high cyclic stability and rate capability (G. Zhou et al., 2010). Graphene nanosheets would provide electron-

conducting channels and confine Fe_3O_4 volume change. A high capacity 1026 mAh/g after 30 cycles at 35mA/g was obtained (G. Zhou et al., 2010).

Liu et al. also used the nanocasting method to prepare mesoporous NiO anode, which could retain 680mAh/g after running 50 cycles (H. Liu et al., 2011). The high performance was mainly from low activation energy (H. Liu et al., 2011). Then Kim et al. used Ag nanoparticles decorated SnO_2/NiO nanotubes as the anode by electrospinning process (C. Kim et al., 2016). One dimensional porous hollow structure solved the volume change problem. Finally, they obtained 826mAh/g capacity for 500 cycles at a high current density 1000 mA/g (C. Kim et al., 2016).

Poizot et al. also has already investigated transition metal oxide: CoO, FeO, and NiO with Li anode (Poizot et al., 2000a). The metal oxide particle size had a big influence on LIBs capacity. The capacity of MoO based lithium-ion batteries had doubled, compared with CoO_2/C based LIBs (Poizot et al., 2000a).

In summary, oxide-based anodes still have cycle stability, volume change problems during cycling. Electrical conductivity needs to be enhanced for future work. Combing different anode materials to form the composites anodes could be the future research direction.

2.4.1.4 Others

Deng et al. used MoS_2 and C hybrid 3D microporous structure to avoid MoS_2 stacking/restacking and volume expansion during the charge and discharge process (Deng et al., 2017). The high discharge capacity of 3.428 mAh/cm² at 0.1 mA/cm² and good cycling stability (93% capacity retention after 100 cycles) were achieved (Deng et al., 2017).

Chen et al. used the clean exfoliation method to prepare clean black phosphorus (BP) nanosheets (L. Chen et al., 2016). After combining BP with graphene, they obtained a high capacity 920 mAh/g at a current density 100 mA/g. Comparable stability (80.2% retention after 500 cycles at 500mAh/g) was achieved (L. Chen et al., 2016).

Liu et al. synthesized ZnCo_2O_4 nanowire arrays/carbon cloth anodes for flexible LIBs (Bin Liu et al., 2012). The final LIBs by using ZnCo_2O_4 /liquid electrolyte/ LiCoO_2 showed 1300mAh/g and kept 96% initial capacity after 40 cycles (Bin Liu et al., 2012).

In summary, some anode materials are still limited by volume change during the charge and discharge process, such as Si, oxides anode materials. However, nanosized materials will open a door for solving the volume change problem.

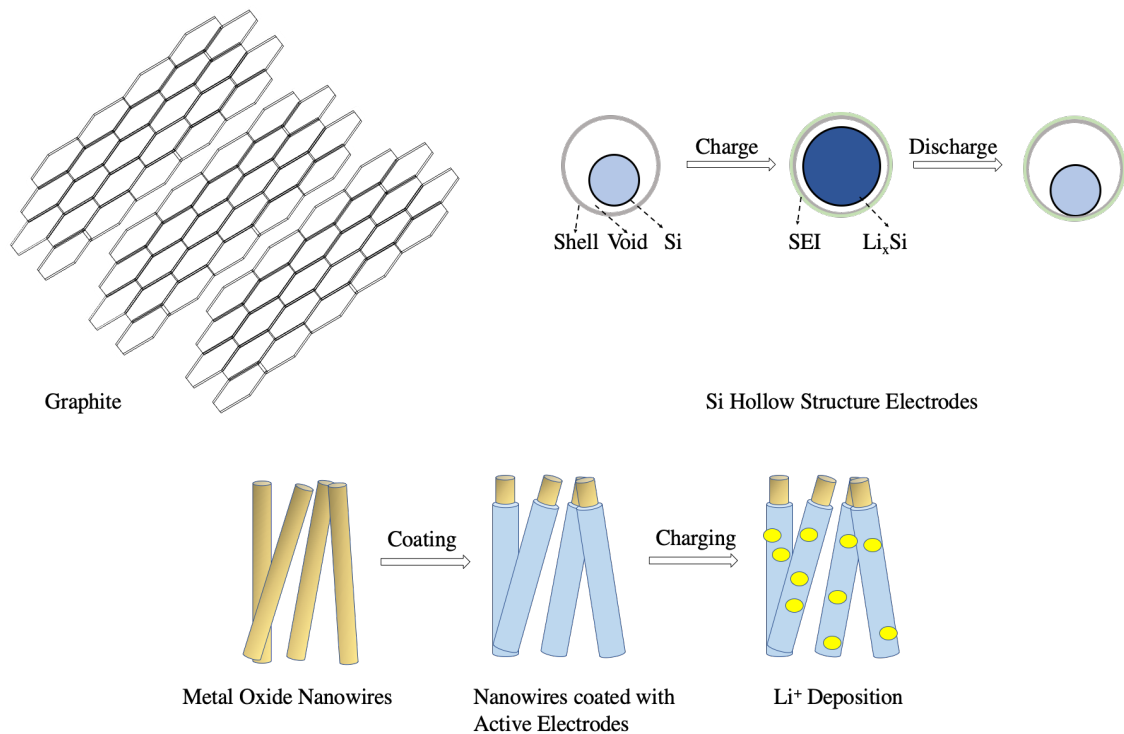


Figure 12 Typical anodes materials structure analysis

2.4.2 Cathode

Manthiram talked about the cathode chemistry about spinel, layered and polyanion cathodes materials in 2020 (Manthiram, 2020). LiMO_2 where $M = \text{V}, \text{Mn}$ and Fe , suffering from the structural transition from layered to spinel during the charging and discharging process due to the lower octahedral site stabilization energies. For NMC cathode, $\text{Mn}^{3+/4+}$ band energy lies above $\text{Ni}^{2+/3+}$ band energy and oxidizes easily. Mn does not suffer from any chemical stability issues due to band energy difference but has structural stability issues. LiMn_2O_4 spinel cathode suffered from Mn^{2+} dissolution when H^+ concentration is higher. Substituting a small portion Mn with Li would solve this problem (Manthiram, 2020).

Polyanion cathode suffers from poor electrical conductivity, which requires the addition of carbon during the synthesis process (Manthiram, 2020). Al^{3+} could increase the electron localization by perturbing the metal-metal interaction and reducing long-range metal-oxygen bond covalence. The cathode thermal stability and air stability have been improved (Manthiram, 2020).

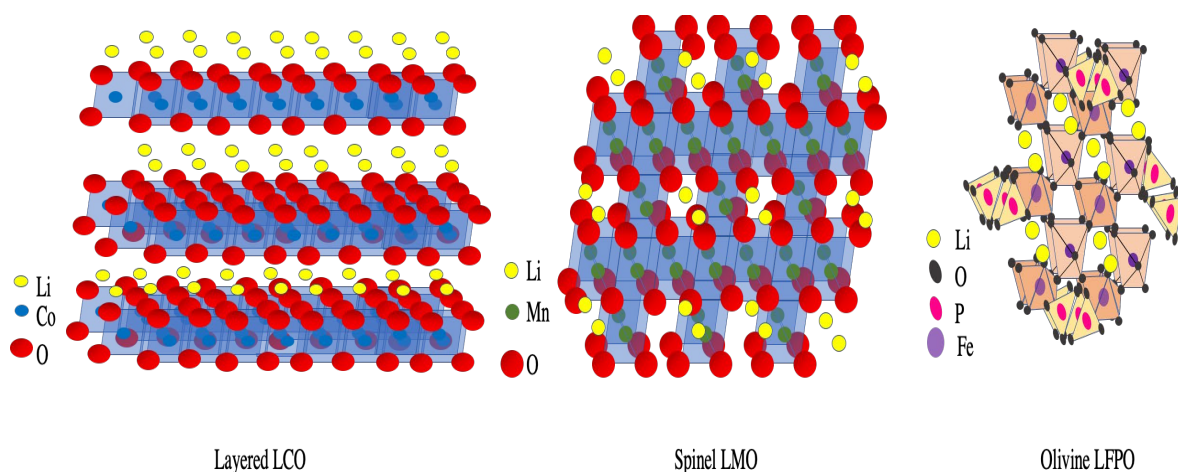


Figure 13 Structure for common cathode materials

2.4.2.1 Transition metal oxide cathode

Because of the high cobalt metal cost, LiMn_2O_4 is a good alternative for cathode material (Kannan & Manthiram, 2002). Tarascon et al. investigated LiMn_2O_4 cathode material which has 5-10% lower capacity than LiCoO_2 (G. Amatucci & Tarascon, 2002). LiMn_2O_4 was recommended as the promising cathode material to replace LiCoO_2 . The delithiation from LiMn_2O_4 happens at 4.1 V vs Li/Li^+ and inserts at 3 V for $\lambda\text{-MnO}_2$. The high potential 4.1 V was needed for extracting Li. In contrast to LiCoO_2 layered structure, LiMn_2O_4 was 3D structure. The cubic, tetragonal, orthorhombic structures would be obtained because of cation twisting and nonstoichiometric properties. Temperature and voltage were two major factors resulting in phases transition (G. Amatucci & Tarascon, 2002).

Li^+ inserted into LiMnO_4 , which is different from LiMn_2O_4 (Thackeray et al., 1983). Li^+ would move from 8a to 16c sites in both Fe_3O_4 and Mn_3O_4 because of the strong electrostatic repulsive field among Fe^{3+} , Mn^{2+} , and Li^+ . The interaction between Li^+ and neighboring cations would decrease LIBs open circuit voltage. Li^+ mobilities in $\text{Li}_{1-x}\text{Mn}_2\text{O}_4$ would be low because Li^+ occupied 8a sites (Thackeray et al., 1983).

LiMn_2O_4 suffers from Jahn-Teller distortion near room temperature, reducing capacity significantly (G. G. Amatucci et al., 2002). The LIBs capacity fade in 3V region is related to Jahn-Teller distortion in the spinel structure. Spinel also plays a role as the catalytic agent for electrolyte decomposition at the elevated temperature and elevated charge state (G. G. Amatucci et al., 2002). Fluorine-based salts LiPF_6 contained a small amount of HF, increasing manganese cations dissolution (Kannan & Manthiram, 2002). In order to enhance spinel electrode surface area, electrode surface treatment was needed

(Gao et al., 2002). One is lithium boron oxide (LBO) glass compositions. It was stable against high oxidation potential and had good wetting properties. Acetylacetone also would remove the active sites on the spinel manganese cations surface, which have catalytic properties (Gao et al., 2002).

It was found LiMn_2O_4 failure mechanism was related to $\text{LiAl}_x\text{Mn}_{2-x}\text{O}_{4-z}\text{F}_z$ (G. G. Amatucci et al., 2002) (X et al., 2002). The failure mechanism should be from two sides. One was Jahn-Teller distortion that cation had high-spin d^4 configuration which would result in energy levels differentiation. Crystal structure would change from cubic to tetragonal when trivalent manganese exceeds 50%. Another was manganese dissolution/proton exchange at elevated temperature. However, Aluminum (Al) had small ionic size and reduced crystal size. The LiMn_2O_4 bonding covalency and framework strength would be enhanced by Al doping (G. G. Amatucci et al., 2002) (X et al., 2002). Anodic substitution by F would also enhance LiMn_2O_4 capacity because it could reduce Mn oxidation state and improve cycle life (G. Amatucci & Tarascon, 2002). The substitution Mn by Al would enhance the $\text{LiAl}_x\text{Mn}_{2-x}\text{O}_{4-z}\text{F}_z$ thermodynamic stability. Small radius Al would perturb Mn atoms' mobility. The strong Mn-O bond will hinder Mn ions movement because Mn-O bond shrinkage would result in bond strength increase. 3D channels also helped Li^+ transfer and electron transfer for LiMn_2O_4 compared with LiFePO_4 (G. Amatucci & Tarascon, 2002).

Manthiram et al. used Li_xCoO_2 , $\text{LiNi}_{0.5}\text{Co}_{0.5}\text{O}_2$, Al_2O_3 , and MgO materials to modify LiMn_2O_4 because of fading (Kannan & Manthiram, 2002). $\text{LiNi}_{0.5}\text{Co}_{0.5}\text{O}_2$ modified LIBs showed 110mAh/g capacity and 2.8% fade after 100 cycles at 60°C. Al_2O_3 modified LIBs showed 130mAh/g and 16% fade after 100 cycles at 60°C.

$\text{Li}_{0.75}\text{CoO}_2$ modified LIBs showed 124mAh/g and 8% fade in 100 cycles at 60°C. The LiMn_2O_4 fading reason was related to manganese dissolution, oxygen deficiency formation, electrolyte decomposition, Jahn-Teller distortion, cation mixing and crystallization loss. If acidic species attacking from electrolyte decreased and Jahn-Teller distortion on the electrode surface was hindered, the final LIBs cycling stability will be enhanced (Kannan & Manthiram, 2002).

It was also found that 1.5wt% ZnO coated $\text{LiNi}_{0.5}\text{Mn}_{1.5}\text{O}_4$ electrode could deliver 137mAh/g capacity (Y. K. Sun et al., 2002). The 5V plateau originated from substituted transition metals(M) oxidation, while 4 V plateau was related with Mn^{3+} to Mn^{4+} transition during charge/discharge. At the same time, HF presence in electrolyte would deteriorate MnO dissolution where MnO from $\text{Li}_2\text{Mn}_2\text{O}_4$ and Li_2MnO_3 (Y. K. Sun et al., 2002).

In summary, LiMn_2O_4 has many advantages, such as being less toxic and much cheaper compared with LiCoO_2 . However, Jahn-Teller distortion near room temperature would reduce the LiMn_2O_4 capacity significantly. Enhancing the crystals bonding and improving LiMn_2O_4 based LIBs cycle stability need to be explored.

2.4.2.2 Layered LiCoO_2 (LCO)

LiCoO_2 has theoretical high capacity 274 mAh/g theoretically and a high operation temperature ($>130^\circ\text{C}$) (Venkatraman et al., 2000). The reversible capacity is around 140mAh/g when charged to 4.2V(x=0.5). However, the oxygen would release because of LiCoO_2 decomposition at elevated temperature. At the same time, the following irreversible chemical reaction between electrode and the organic electrolyte is an exothermic reaction, causing safety concern and capacity loss (Zou et al., 2003)

(Doughty, 2012). There are many works to enhance LiCoO_2 capacity and cycle stability. Nam et al. used the virus to synthesize electrodes (Nam et al., 2006). By incorporating gold-binding peptides into the electrode, gold-cobalt bonds would form. This would improve LIBs capacity (Nam et al., 2006). Park's group used Al_2O_3 coating for LCO electrodes to enhance LCO structural stability (Cho et al., 2000). The anisotropic expansion and contraction would lead to electrode microcracks formation and electrode structural degradation. The structural transition from a hexagonal to monoclinic phase happened at $x \sim 0.5$ when voltage is 4.1 - 4.2 V vs Li metal, accompanying 1.2% extension along c axis, which is higher than tolerance 0.1% for oxide elastic strain. The $\text{LiCo}_{1-y}\text{Al}_y\text{O}_2$ formation would result in contraction along c axis (Cho et al., 2000).

The LCO capacity retention was dependent on cut-off voltage because the high voltage will result in phase transformation and Co dissolution (Y.-K. Sun et al., 2006). There are several methods to improve the LCO stability at high voltage. Coating with ZrO_2 , MgO , SnO_2 , TiO_2 and SiO_2 had also been investigated (Y.-K. Sun et al., 2006). HF content would result in metal ion dissolution. Using varied coating layers could act as HF scavengers to reduce HF formation and reduce cathode decomposition (Y. K. Sun et al., 2002). The LCO electrode still would be a good choice for future application (Z. Chen & Dahn, 2004) (Y. K. Sun et al., 2002).

In Summary, LCO has comparable high potential, stable crystal structures at room temperature and high-capacity properties. We will use commercial LCO as our cathode materials due to its high capacity and cycle stability.

2.4.2.3 Layered $\text{LiNi}_x\text{Co}_y\text{Mn}_z\text{O}_2$ (NCM)

Layered NCM cathode has been widely used owing to its excellent capacity (Noh et al., 2013). $\text{LiNi}_{0.6}\text{Co}_{0.2}\text{Mn}_{0.2}\text{O}_2$ (NCM622) delivers a specific capacity of more than 170 mAh/g when the voltage from 3.0V to 4.3V vs Li metal. Increasing Ni content effectively improves cathode specific capacity but decreases electrode structural and thermal stability (Noh et al., 2013). The reason for rich Ni NCM cathode high capacity is related to $\text{Ni}^{2+}/\text{Ni}^{3+}$ and $\text{Ni}^{3+}/\text{Ni}^{4+}$ transition, which had two electrons transfer (De Biasi et al., 2019). However, Ni^{4+} would react with electrolyte solvent, leading to CO_2 and SEI formation. Besides, NCM lattice change would result in electrode degradation. Lattice change could result in volume contractions (Berkes et al., 2015). In addition, the mechanical stress at NCM and electrolyte interface would result in intergranular fracture (Kondrakov et al., 2017). There are many works to solve NCM cathode issues. It was reported that Li rich Mn-based cathode display hysteresis at around 2.5/3.3V, resulting in an irreversible phase transformation (Sohn et al., 2014). This phase transformation process had cation migration and oxygen redox reaction. Chandan et al. obtained 205mAh/g capacity by tuning cations ratio with 85% retention after 400 cycles (Chandan et al., 2019).

In summary, controlling transition metal redox couple dissolution and metal ions deposition on the electrode surface, obtaining a stable spinel structure, decreasing electrolyte dissolution, improving cycle stability would be helpful for future commercial LIBs cathode (over 200 mAh/g) applications.

2.4.2.4 Layered $\text{Li}(\text{Ni}_x\text{Co}_y\text{Al}_z)\text{O}_2$ (NCA)

LiNiO_2 has a theoretical capacity 275 mAh/g and a similar layer structure with NCA (Dahn et al., 1990). The theoretical NCA capacity was around 275mAh/g and developed for NCA materials in the last two decades (Dahn et al., 1990). The Ni materials are cheap compared with Co. Ni^{2+} formation during intercalation and deintercalation will block the Li^+ transfer pathway (Kalyani & Kalaiselvi, 2005). Co and Al atoms would enhance practical $\text{Li}(\text{Ni}_{0.8}\text{Co}_{0.15}\text{Al}_{0.05})\text{O}_2$ capacity to 199mAh/g. The average voltage could be 3.7V (Martha et al., 2011). Ni increase would increase capacity but reduce cycling performance and thermal safety (H.-H. Sun et al., 2015). There will be a phase transition when NCA is charged to 4.2V vs Li metal, resulting in LIBs capacity fading accompanying NCA microcracks formation. Microcracks facilitate electrolyte penetration and form the NiO-like (Ni^{4+} reaction with oxygen) impurity phases resulting in high impedance (Ryu et al., 2018). In addition, Sun's group has found Ni increase could result in high capacity but low capacity retention due to the microcracking formation at secondary particles (Park et al., 2019). Albano's group also reported TiO_2 and Al_2O_3 atomic layer deposition on NCA cathode surface to improve cutoff voltage and delivers high energy density (Mohanty et al., 2016).

In summary, NCA cathode's high voltage and high capacity are still the promising electrodes for global demand. The poor cycle stability at elevated temperature and high humidity would be enhanced by doping and coating new protection layer.

2.4.2.5 Olive LiFePO_4 (LFP)

LiFePO_4 has been used owing to a flat voltage profile, low cost, abundant supply, and better environmental compatibility (Ritchie & Howard, 2006). The limitations are

comparatively low capacity (170mAh/g), low density (3.6g/cm³). In addition, the strong covalent oxygen bonds lead to low ionic diffusivity (10⁻¹³ to 10⁻¹⁶ cm²/s) and poor electronic conductivity (~10⁻⁹ S/cm) (Jiying Li et al., 2008). During charging and discharging process, the phase transformation involved Li⁺ motion along b channels through phase boundaries nucleation sites. LFP capacity degradation includes Li⁺ loss by side reactions, active material loss during cracking and dissolution, impedance rise due to SEI formation, and structure degradation. Carbon coating is one effective way to improve LFP cathode stability and conductivity. (Shim & Striebel, 2003) (Amine et al., 2005) (Q. Zhang & White, 2007). Additionally, high-rate LIBs performance will be obtained by reducing LFP particle size because of ions and electrons distance decreasing. Some doping studies also had been done to improve electronic conductivity and Li diffusion rate, such as Nb⁵⁺, Zr⁴⁺, Ti⁴⁺ doping, etc. Because doping could induce Li⁺ charge compensation. Zhang et al. have reviewed these techniques (Q. Zhang & White, 2007). The cyclic life has been improved to 2000 cycles.

In summary, LFP materials show comparable low capacity compared with NCA and NMC electrodes. However, the high thermal stability (degradation temperature around 300°C) would enhance the LIBs safety. The large amount of Fe and P elements would also reduce materials preparation costs.

2.4.2.6 Layered LiMn_xFe_{1-x}PO₄ cathode

LiFePO₄(triphylite) material has reversible stability because of FePO₄ and LiFePO₄ similar structures during charge/discharge (W.-J. Zhang, 2011). However, high voltage (over 4 V) would decompose electrode materials (W.-J. Zhang, 2011). In addition, Fe⁴⁺/Fe³⁺ energy was lower than lithium anode fermi energy. Fe³⁺/Fe²⁺ was

close to anode fermi energy. Some polyanions would decrease $\text{Fe}^{3+}/\text{Fe}^{2+}$ energy such as $(\text{SO}_4)^{2-}$, $(\text{PO}_4)^{3-}$, $(\text{AsO}_4)^{3-}$ and $(\text{MoO}_4)^{2-}$ or $(\text{WO}_4)^{2-}$ (Damay et al., 2015). It was found that electrons polarization from O^{2-} in strong covalent bonding within polyanions would increase the LIBs V_{oc} and reduce $\text{Fe}^{3+}/\text{Fe}^{2+}$ energy after Mn doping. The Mn-O-Fe interaction raises $\text{Mn}^{3+}/\text{Mn}^{2+}$ energy and reduces $\text{Fe}^{3+}/\text{Fe}^{2+}$ energy, which coincides with V_{oc} increase compared with LiFePO_4 (Kannan & Manthiram, 2002). A few years later, Yao et al. characterized different Mn compositions in $\text{LiMn}_x\text{Fe}_{1-x}\text{PO}_4$ electrodes and found that increasing Mn would reduce electrochemical reactivity and cycle life (J Yao et al., 2006). The reason should be related to the poor electrochemical property after Mn addition, lattice size expanding, and decomposition (J Yao et al., 2006).

In summary, $\text{LiMn}_x\text{Fe}_{1-x}\text{PO}_4$ would be very promising electrode owing to its high capacity ~ 170 mAh/g and enhanced charge voltage but Mn addition would also decrease electrochemical performance like LIBs cycle stability.

2.4.2.7 Sulfur

Sulfur has the abundance, low cost, environmental benignity and high capacity as cathode material (Shim et al., 2002). The specific energy would be 1672 mAh/g, 1167 mAh/g for S and Li_2S cathode, respectively. Li-S batteries could show 2597 Wh/kg capacity (Shim et al., 2002). However, there are some disadvantages of the S electrode. Firstly, S electrode limitation is lithium polysulfides formation during charge/discharge, which could dissolve in electrolyte solvents. Secondly, it's low electronical conductivity (5×10^{-30} S/cm at 25°C) compared with lithium metal oxide materials (>0.1 mS/cm at 25°C). There are some ways reported to enhance S electrode electronic conductivity and capacity, for example, carbon and metal sulfide-based electrode has high electrical

conductivity 67 S/cm and over 650 mAh/g capacity at 25°C (Shim et al., 2002) (Hayashi et al., 2004). Thirdly, the large S electrode volume change (79%) happens during charge/discharge (Y.-Z. Sun et al., 2017). Volume change would result in less physical contact and cracks formation (H.-L. Wu et al., 2015).

In order to solve S electrode volume change problems, Su et al. prepared S(40wt%)-carbon nanotube cathode material (exhibited 541mAh/g), which could retain 68% initial capacity after 100 cycles at 1C (Su et al., 2012). Further surface functionalization also has been investigated, such as bottom-up strategy (Z. Yuan et al., 2014).

People have used polymer electrolyte to prevent polysulfide formation, but discharge capacity had 30% loss at 100°C (Machida et al., 2004). In addition, Yang et al. used CoS₃ as the catalyst for high loading S cathode and achieved 1008 mAh/g after 100 cycles (X. Yang et al., 2019), because the transfer process from Li₂S₂ to Li₂S had been boosted. This step contributes half the theoretical capacity (836 mAh/g). The first step from S₈ to Li₂S₄ and the second step from Li₂S₄ to Li₂S₂ take 25% theoretical capacity individually (Xiulei Ji & Nazar, 2010). It was also found that lots of dangling surface bonds on amorphous metal sulfides could behave as active sites for electrochemical reactions (X. Zhao et al., 2017).

Goodenough's group used vulcanized rubber as active materials and loaded it on flexible electrospinning prepared carbon nanofibers which showed 370mAh/g after 25 cycles at 5C (B.-C. Yu et al., 2017). Furthermore, Jin et al. combined graphene with sulfur (GS) owing to the graphene flexibility (sp² carbon lattice from a strong bond with neighbor carbon), large surface area(2630m²/g), high electron mobility etc. (Jin et al.,

2013). The GS/S showed 402 mAh/g after 100 cycles at 0.1C and retained 83% initial capacity (Jin et al., 2013). Polysulfide binding affinity and high electrical conductivity, carbon materials structural integrity would render the potential for future flexible LIBs (Jin et al., 2013).

At the same time, adding liquid electrolyte, ionic liquids on the electrode interface had been reported (Changhong Wang et al., 2018) (Zheng et al., 2018). The LIBs cycling performance had been enhanced. Shin et al. used LiTFSI in acetonitrile with TTE solvent as interface additives (Shin & Gewirth, 2019). Specific capacity 760 mAh/g at 100 cycles was obtained for Li-Li₂S batteries (Shin & Gewirth, 2019). Oh et al. also confirmed high stability for Li₃PS₄ and Li₁₀GeP₂S₁₂. Mixing with LiTFSI could decrease ethereal oxygen nucleophilicity owing to solvent-salt complexation (Oh et al., 2015).

In summary, understanding Li⁺ storage catalytic process still has a long way to go. But the high capacity over 1000 mAh/g was achieved for S/Carbon nanotube-based batteries, which gave us confidence for high-performance cathodes electrode.

2.4.2.8 Others

Compared with the 2D electrode, the 3D cathode has interdigitated contact with electrolytes (S. Sun et al., 2019). Xia's group used the direct current (DC) magnetron sputtering method to fabricate vertically aligned oxygen-deficient α -MoO_{3-x} nanoflake arrays (3D MO_x) (S. Sun et al., 2019). The LIBs had a high specific capacity 266 mAh/g at 50 mA/g. Their LIBs showed 92.7% capacity retention after 1000 cycles. The reason for this high stability was maximizing the interface between cathode and electrolyte and retaining short lithium ion diffusion length (S. Sun et al., 2019).

Another group had developed one Co free cathode $\text{LiNi}_x\text{Fe}_y\text{Al}_z\text{O}_2$ ($x+y+z=1$) cathode (Muralidharan et al., 2020). It showed ~ 200 mAh/g capacities and 80% retention after 100 cycles. This work opened the door for cobalt free lithium ion batteries (Muralidharan et al., 2020).

In summary, cathode development still needs to be explored because of the limited capacity compared with the anode. Multi electrons transfer will be the way for high capacity like $\text{Ni}^{2+}/\text{Ni}^{4+}$. Sulfur cathode shows almost 10 times higher capacity than Li metal oxide cathode and have a big potential future for next generation batteries. At the same time, nano techniques to prepare electrodes and LIBs would solve the common problem, including volume expansion, electrodes materials decomposition, electrodes lattice atoms loss, etc.

2.5 Current collectors

The current collector is the leading component in lithium ion batteries structures (Y. Yang et al., 2020). Its central role is attributed to transporting electrons for electrodes. Current collectors can be classified into two different categories. The first group is fabricated by conducting some surface modifications on the planner current collectors, such as Cu foils. Another group is 3D configuration (Y. Yang et al., 2020). Also, it can be divided to anode current collectors and cathode current collectors. A perfect current collector increases battery performance in a wide variety of aspects. Here, we will talk about current collectors based on the materials.

2.5.1 Current collectors for anodes

Metal foils have been considered as current collectors due to the following reasons: 1) Metal foils represent high thermal and electrical conductivity in comparison

with other presented materials; 2) High plasticity leads to great robustness; 3) Easy and low-cost manufacturing process; 4) Low density, providing high energy density for battery cell (Chu & Tuan, 2017) (Tai et al., 2017).

One of the conventional anode current collectors is Cu foil (Huimin Wang & Yu, 2019). The advantage of using Cu over other materials is its great electrical conductivity (5.96×10^5 S/cm), thermal conductivity (385 W/m K), and high plasticity (Huimin Wang & Yu, 2019) (J. Chen et al., 2018). Utilizing Cu foil as the current collector also has some inevitable disadvantages. Firstly, Cu foils as current collectors are planar structures and have lower mechanical properties. However, Cu foil flat surfaces cannot adhere to electrodes. Therefore, it prevents forming meshing interface between electrode materials and current collectors. In addition, for high-performance batteries, planar current collectors could not provide extra space for electrode stress releasing (Jie Li et al., 2018). Finally, electrode active material will delaminate from current collectors. This delamination leads to LIBs capacity decreasing and poor cycling life. Besides unloaded current collector will cause short circuit, resulting in a safety issue. Another challenge is related to electrons transport, small surface areas on flat Cu current collectors make it challenging for mass electrons transfer, decreasing current density. Another issue is that Cu has a high density (8.96 g/cm^3), which may cause LIBs specific energy density to decrease (Jie Li et al., 2018).

Therefore, designing different current collector structures has been attracted great attention in recent years. Noelle and Yao et al. have shown structuralized current collectors creating extra surface area, decreasing electrodes internal stress, and leading to high cycling stability (Noelle et al., 2018) (Z. Yao et al., 2018). Additionally, Kim and

Hsu et al. presented new techniques to create extra bonding strength between electrode materials and current collectors, enhancing LIBs safety (C.-H. Hsu et al., 2018) (S. Y. Kim et al., 2019). Chen et al. fabricated a rough-surface structuralized Cu current collector by FeCl_3 etching. The final LIBs coulombic efficiency was enhanced due to enhanced bonding between active materials and current collectors (J. C.-M. Chen et al., 2019). Yang et al. also had utilized Cu foil to fabricate Cu nanowire current collector (C.-P. Yang et al., 2015). They used the dehydration and reduction method for preparing $\text{Cu}(\text{OH})_2$ nanowires, enhancing LIBs cycle stability and decreasing Li dendrites growth (C.-P. Yang et al., 2015).

In summary, copper current collectors will continue to be used as anode current collectors due to their stability and high electronic conductivity. Simultaneously, the copper current collector will behave as a stable substrate for electrode materials.

2.5.2 Current collectors for cathodes

One of the most famous current cathodes collectors is Al foil (L. Cao et al., 2020). The electrochemical corrosion inside the battery needs to be considered for cathode current collectors. Li et al. applied high potential to prepare Al_2O_3 film on Al foil surface (S. Li & Church, 2017). This high potential prevents further corrosion. By applying a potential less than 0.6 V to the Al foil, Al_2O_3 is reduced to Al again owing to Li's reaction (S. Li & Church, 2017). A DC anodization approach fabricated a honeycomb surface structure Al foil (L. Cao et al., 2020).

Although Al has been considered as most popular current collector, some recent works have been trying to replace it in order to enhance LIBs performance. Wu et al. have utilized a graphite film (GF) as a current collector for both positive and negative

electrodes (Q. Wu et al., 2020). The main advantage of using GF is its light density, decreasing LIBs weight and enhancing LIB energy density. Furthermore, it will enhance LIBs cycle stability (Q. Wu et al., 2020).

In summary, although there are a lot of issues about current collectors, Cu and Al would still be the most popular current collectors for electrodes owing to the low cost, easy fabrication, mass production, high conductivity etc.

2.6 Interface

Solid Electrolyte Interphase (SEI) is a protecting layer formed on the negative electrode surface due to electrolyte decomposition (Z. Yuan et al., 2014). Normally, SEI formed in the first cycle. During the first charge cycle, electrolyte undergoes reduction at negatively polarized graphite surface forming a passive layer comprising organic and inorganic electrolyte decomposition products. The layer prevents further electrolyte degradation by blocking electron transport while concomitantly allowing Li-ions to pass through during cycling (Verma et al., 2010). Battery performance is highly dependent on SEI quality. Therefore, understanding SEI nature and composition is important to improve battery performance. In this thesis, we will mainly focus on the interface investigation by using different materials additives.

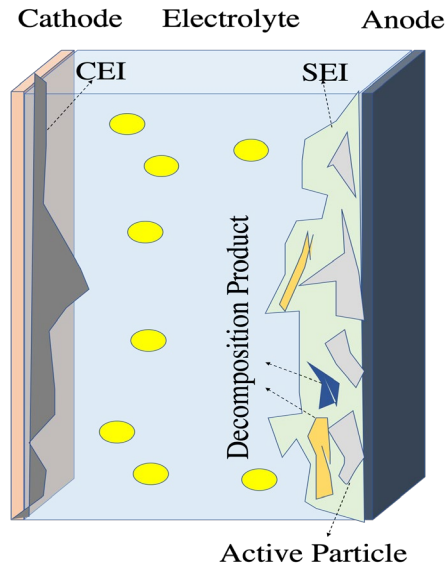


Figure 14 Interphase structure inside LIBs

Substantial works have been done in the past few decades on analyzing SEI and spelling out its components. Most literature compiled with a detailed compilation of X-ray photoelectron spectroscopy (XPS) and Fourier Transform Infrared (FTIR) data for SEI components (Fergus, 2010). Carbon anode type, carbon anode pretreatment, electrochemical conditions and electrolyte composition will also affect SEI composition. In addition, LIBs charge/discharge temperature is critical because it directly affects the electrochemical reaction kinetics (Fergus, 2010) (J. Y. Song et al., 1999a).

There are many techniques to investigate the interfacial layers. Scanning electron microscope (SEM) and Transmission electron microscopy (TEM) is used for imaging surface film (Verma et al., 2010). Vibration spectroscopies like FTIR and Raman provide valuable surface information regarding functionality. XPS and FTIR are highly surface sensitive and complementary to each other (Fergus, 2010). XPS limitation is radiation damage risk. FTIR limitation includes influencing SEI nature and spectroscopy self-limitation. There are abundant XPS, and FTIR data exists in the literature about SEI and its various components. It will be useful to compile this data into one table, which is

easier to compare, analyze, interpret and comprehend. This will also constructively define facts like relative error between different studies on similar material (Verma et al., 2010).

Julien et al. have investigated electrode surface modification and removed surface edges by mild oxidation (Mauger & Julien, 2014). They deposited metal oxide and coated polymers on the cathode surface, resulting in higher electronic conductivity, inhabiting cathode structural change. Metal oxide coating on the lithium transition metal oxide cathode will improve structural stability and decrease cations disorder in the crystal (Mauger & Julien, 2014). Peled et al. also proposed a model that the dominant SEI impedance was the grain boundary resistance which was related with ions crossover from particles to particles (Peled, 1997). Here we will discuss some techniques to investigate the interface.

2.6.1 Special techniques for the interface

Bard et al. investigated some characterization spectroscopies, interface dynamics, and interface materials (Bard et al., 1993). Firstly, they focus on electrode characterization using infrared reflection absorption spectroscopy (IRAS) and surface-enhanced raman spectroscopy (SERS), because Raman- allowed transitions were IR forbidden and low frequency (toward to 5 cm^{-1}). These methods could be used to study interface molecules (Bard et al., 1993).

In-situ techniques called scanning tunneling spectroscopy (STM) was also explained (Bard et al., 1993). The faradaic process could be minimized by maintaining the tips in some regions. Samples should be atomic clean and flat. Surface reconstruction was used to decrease free energy. Redox reaction would be monitored in STM. Under potential deposition (UPD) could produce anions monolayers which would affect the

observation. The difficulties for preparing metal oxides-based electrodes were from preparing the well-defined semiconductor surface (Bard et al., 1993).

Another technique is ultramicroelectrodes and scanning electrochemical spectroscopy (SECM) (Bard et al., 1993). The micrometer range electrode provides a plate for nonpolar solvents and supercritical fluid by electrochemical methods because of low current (pA-nA range). The resistance perturbation for IR is very small. SECM resolution could be 50 nm. SECM could measure both conductive and insulating layer, which is opposed to optical microscopy. In addition, XRD is used to study crystallized materials and electrolyte surfaces. However, crystal truncation rods (CTR) could study vertical direction electron density. X-ray standing wave (XSW) technique could measure interfacial species distribution by external reflection and Bragg diffraction (Bard et al., 1993).

Nonlinear optical methods are also used. Second harmonic generation (SHG) measures materials inversion symmetry rather than centrosymmetric crystals (Bard et al., 1993). The mixing wave (infrared and visible light) only occurs on less sensitive surface than infrared reflection spectroscopy. Surface forces microbalance (SFM) could measure interaction Debye length. Surface-enhanced Raman spectroscopy (SERS) could investigate interfacial solvent and ions distribution (Bard et al., 1993).

In summary, we talked about different techniques for characterization interfacial layers. AFM could differentiate the anode and SEI layers because of different mechanical properties. The feasibility is an advantage. However, the imaging range is narrow and AFM resolution is lower. Scanning probe microscopy (SPM) could be used to understand the topography and species distribution of the SEI.

2.6.2 Interface between the electrolyte and electrode

Ren et al. used the carbon nanotubes to enhance contact between electrolyte and LiFePO_4 electrodes (Ren et al., 2016). The higher sp^2 hybrid, smaller crystallite size, numerous surface defects, and large surface area would improve ionic and electronic conductivity. The cathode polarization will decrease after adding soft carbon (Ren et al., 2016).

Bis(fluorsulfonyl)imide (FSI^-) anion can form robust SEI protecting layer. The halogenated salt additives will decrease SEI resistance. The high modulus solid electrolyte not only be acted as an electrolyte but also suppressed dendrite growth (X. B. Cheng et al., 2015). Huang et al. used cryogenic-electron microscopy(cryo-EM) and electrochemical impedance spectroscopy (EIS) to investigate SEI formation and to grow in carbonate electrolytes (W. Huang et al., 2019). SEI thickness is growing up from 3 nm to 8 nm when the potential drop from 1 V to 0 V. Then 16 nm layer formed once the lithiation was finished (W. Huang et al., 2019).

Additionally, Hirayama et al. used the surface X-ray diffraction (SXRD) method to investigate electrolyte and LiMnO_4 cathode interface (Hirayama et al., 2010). They found that (111) plan stability was higher than (110) plan because manganese was loosely packed on (110) plan, which provided more opportunity to react with solvents and electrolyte. SEI formation would be thicker for the unsteady plan (Hirayama et al., 2010). Chan et al. used XPS and SEM to investigate anode and electrolyte interface (Chan et al., 2009). By charging and discharging in different voltages, the different SEI morphology and thickness formed. However, electrode volume change during the charging process will result in capacity loss. LiPF_6 is not stable in the low potential, which will decompose

into LiF as reported. Li_2CO_3 is another product produced from electrolyte electrochemical reduction rather than decomposition. In addition, they also found that the best discharge voltage should range from 0.4 V to 1.2 V based on electrochemical impedance spectroscopy (Chan et al., 2009).

Zhang et al. used several techniques for investigating interface decomposition between LiCoO_2 cathode and $\text{Li}_{10}\text{GeP}_2\text{S}_{12}$ electrolyte (W. Zhang et al., 2018). During galvanostatic cycling, Co diffusion happened because LiCoO_2 particles experienced severe mechanical deformation. Also, the generated microcracks accelerated decomposition and capacity fading (W. Zhang et al., 2018). Heterogeneous electron transfer in different potential and fast relaxation needs to be considered. The methylene unit attached to thiol will slow down electrons transfer. Electrons movement at interface was related to varied free energy which could be obtained by measuring ionic charge distribution. Faulkner et al. provided model to study interface capacitance formed by these charges (Bard & Faulkner, 1980).

Finally, the interface could be considered in several parts, surface atoms or defects, surface coating, and electrolyte materials. There is an example for solving interface problem: Wang et al. used the ionic liquid impregnated metal-organic framework nanocrystals (Li-IL@MOF) to solve the surface problem (Z. Wang et al., 2018). The high ion conductivity of $3 * 10^{-4} \text{ S/cm}$ is achieved. The transference number is 0.26. They obtained high performance of 145 mAh/g at 0.1 C charge rate for Li/LiFePO_4 structure (Z. Wang et al., 2018).

Materials crystallization temperature, electron crystallization, and multilayers structures also need to be considered. Self-assembled monomolecular films could form

by bringing chemical reagent to the surface and assembled by van der Waals attraction and hydrophobic effect. Sulfur containing chemicals will be strongly bonded to the surfaces and conveniently yield monomolecular films. The electrostatic binding is used to bind layers (H. G. Hong & Mallouk, 1991) (Evans et al., 1991). Furthermore, Thiol-based monolayers could be fabricated. Ion mobility depends on solvation properties, D/A sites are related with crosslinking and ion-ion interactions (Bard et al., 1993). These works would help us understand the interface.

Machine learning can get more accurate SEI information and best SEI structures or component materials from a wider perspective (Bengio, 2009). Take SEI efficiency as a function, $F(x_1, x_2, x_3, \dots)$, x_1, x_2, x_3, \dots represent the factors like the type of carbon, pretreatment of carbon, and electrolyte composition, electrochemical condition, cycling mode, polarization mode, etc. We can calculate which parts will contribute to SEI high efficiency. Some scientist used logistic regress algorithm to calculate easily. People can apply neural network algorithm to the system (Bengio, 2009) (Yizhou Zhu et al., 2016).

In summary, it is a challenge to obtain a steady, thin, high mechanical strength interface layer. The interface kinetics also need to be investigated to achieve high charge transfer. Interfacial layer plays a very important role in the LIBs performance. People used varied techniques to investigate its composition, growth, and morphology etc. This thesis will focus on obtaining stable interfacial layers by using different LIBs additives and characterize the interfacial layer impedance change with EIS spectroscopy.

CHAPTER III. ENHANCING THE INTERFACIAL AND ELECTROCHEMICAL PERFORMANCE USING BIOMATERIALS

3.1 Background of biomaterials

Biomaterials have increasingly been incorporated into electronics and energy storage devices (Willner, 2002) (Bettinger & Bao, 2010), including LIBs (Milczarek & Inganäs, 2012) (Kovalenko et al., 2011). For example, glucose and protein could enhance energy storage devices' electrochemical performance (J.-Y. Wang et al., 2012). Li et al. used mesoporous carbon and protein to improve mesoporous carbon electrode surface area (Z. Li et al., 2013). However, the Li^+ storage mechanism is not well investigated in nitrogen (N) riched carbons. But it is believed that N strong electronegativity and the hybridization of N lone pair electrons with carbon π electrons are beneficial for Li^+ transfer. The interaction between N and N riched carbon could help Li^+ transfer. Nitrogen concentration plays an essential role in electron transfer and energy conversion (Z. Li et al., 2013) (S. Li et al., 2013).

Protein has abundant oxygen active sites and nitrogen defects, improving electron conductive networks by forming a nitrogen-doped layer. The nitrogen-doped layer would improve redox reaction during the charge and discharge processes. Park et al. have used corn protein to synthesize new carbon-based electrocatalysts, which self-organized into two-dimensional ordered structures (Park et al., 2014). This corn protein would aggregate on carbon black surfaces and induce self-assembly (Park et al., 2014). A few years later, Lee et al. used hemoglobin blood protein to prepare iron/carbon composite microfiber catalyst using the electrospinning method (J.-S. Lee et al., 2019). Hemoglobin calcination resulted in smooth surfaces and planar structures, making the numerous microfibers lines

contacts (J.-S. Lee et al., 2019). Jia et al. used silk fibroin (a biodegradable protein) to stabilize chemicals owing to hydrogen bonds and polar groups in amino acids (Jia et al., 2017). The addition of silk fibroin-choline nitrate (SF-[Ch][NO₃]) weakened hydrogen bond and increased segments motion, thereby enhancing electrolyte flexibility. This material is an abundant, versatile, and naturally occurring cationic polyelectrolyte host (Jia et al., 2017). Cellulose is another candidate as the electrolyte host for lithium batteries (Jia et al., 2014) (Armand et al., 2011) (B. Wang et al., 2013). **Table-8** summarizes the recent years' works by using biological materials.

Table 8 A summary of biomaterials used for batteries

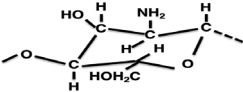
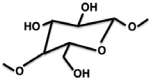
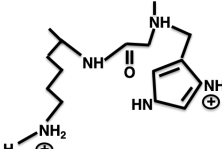
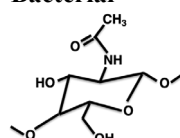
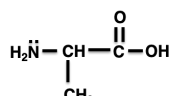
Biomaterial	Function	Reference
Chitosan <ul style="list-style-type: none"> Chitosan Biopolymer 	Binding with the negative surface. Mechanical support and stabilization as the electrolyte host.	Jia et al.(Jia et al., 2014)
Cellulose <ul style="list-style-type: none"> Pyrolyzed bacterial cellulose (PBC) 	Binder materials. Hydrogen bond accepting ability. Dissolved in ionic liquid to produce enzymatic reactions. 3-D mechanical and conducting properties. Interconnected conduction pathways.	Armand et al.(Armand et al., 2011) Wang et al.(B. Wang et al., 2013)

Table 8 (Continued)

<p>Protein</p> <ul style="list-style-type: none"> Silk (biodegradable protein) fibroin Sericin protein White egg Zein Gelatin protein Bovine serum albumin (Protein) Gelatin and soy protein isolate (SPI) Hemoglobin blood protein 	<p>Binder materials, peptide bonds with PEO chains.</p> <p>Entrapping chemicals or active molecules.</p> <p>Electrostatic interacting with cations.</p> <p>Mechanical support as electrolyte host, hydrogen bonds between units and suppress dendrite.</p> <p>Electrolyte oxidation negation.</p> <p>Strong hydrogen bonds, electrochemical stable.</p> <p>Polypeptide giving Lithophilic and anionphilic sites; Lone-pair Electrons of N facilitate Li^+ transfer.</p> <p>Unfolded configuration for ionic pathways.</p> <p>Electronegativity and hybridization.</p> <p>Ordered structure by self-organization or self-assemble.</p> <p>Discharge potentials stabilized.</p> <p>Prolonging the discharge plateau.</p> <p>Slowing down the loss of electrons.</p> <p>Binding effects owing to dipolar interactions.</p> <p>Attracting Li^+ of O atoms.</p> <p>Reducing aggregation.</p>	<p>Jia et al.(Jia et al., 2017)</p> <p>Tang et al.(Y. Tang et al., 2017)</p> <p>Li et al.(Z. Li et al., 2013)</p> <p>Park et al.(Park et al., 2014)</p> <p>Fu et al.(Fu, Li, Wang, Scudiero, et al., 2018)</p> <p>Li et al.(S. Li et al., 2013)</p> <p>Wang et al.(X. Wang et al., 2016)</p> <p>Fu et al.(Fu et al., 2019)</p> <p>Lee et al.(J.-S. Lee et al., 2019)</p>
<p>Virus</p> <ul style="list-style-type: none"> Tobacco mosaic Virus (TMV) M13 virus M13 & E4 virus 	<p>Molecular recognition and self-assembly.</p> <p>Well-ordered nanostructures owing to carboxylic acid with cations.</p> <p>Electrostatic repulsion.</p> <p>Strong interactions between thiol group of cysteine with metal.</p> <p>Peptides as scaffolds.</p> <p>Negative groups to react with cations for catalyst.</p> <p>Peptides for binding property.</p>	<p>Nam et al.(Nam et al., 2006)</p> <p>Chen et al.(X. Chen et al., 2010)</p> <p>Oh et al.(Oh et al., 2013)</p> <p>Nam et al.(Nam et al., 2008)</p> <p>Lee et al.(Y. J. Lee et al., 2009)</p>
<p>Bacterial</p> 	<p>Increase pH.</p> <p>Precipitating calcium carbonate.</p> <p>Metal oxide affinity with negative surfaces of bacterial; Biomineralization of metal oxides by nitrate as electron acceptor.</p>	<p>Ferris et al.(Ferris et al., 1997)</p> <p>Miot et al.(Miot et al., 2014)</p>
<p>TSB</p> 	<p>Binding with Li^+ and increasing its mobility</p> <p>Enhancing interfacial property between electrolyte and electrode</p> <p>Introducing new Li^+ transfer pathway</p> <p>Decreasing electrolyte crystallization</p>	<p>This Study</p>

Solid polymer electrolytes (SPEs), including polyethylene oxide (PEO) electrolytes, have attracted much attention because of their higher electrochemical stability, high ignition temperature, and thin-film manufacturability (Prosini et al., 1998) (Appetecchi et al., 2000). Although SPEs have many advantages, a low ion conductivity key challenge still remains. Because when Li^+ ions transport along the polymer chains, two main activation barriers need to be overcome. One is the salt ions solvation by coordinating ethylene oxide units. The other is ions hopping from one coordination site to another, which is related to polymer segmental motions (Fulcher, 1925) (Vogel, 1921) (Kelly et al., 2016).

Nanoscale materials, including nanosheets (Yoo et al., 2008), nanowires (Armstrong et al., 2005), nanotubes (Claye et al., 2000) (Sakamoto & Dunn, 2001), and 3D nanostructures (C. Tang et al., 2012), have been used in enhancing both the polymer electrolyte properties and the overall battery performance (Arico et al., 2011). Specifically, nanoparticles have improved polymer electrolytes ion conductivity by about 1 to 3 orders of magnitude (Sun et al., 2000). The enhancement is generally achieved because of the nanofillers large surface-area-to-volume ratio and their surface interactions with salt and polymer chains. For example, 2-D graphene oxide added solid polymer electrolyte ion conductivity could reach 10^{-5} S/cm (Yuan et al., 2014). Homogeneous nanomaterials, monodisperse, and hierarchical organizational control could maximize this potential. However, there are several disadvantages and challenges associated with nanoparticles, including complex fabrication, high cost, and chemical surface treatments, etc. (Y. J. Lee et al., 2009) (Wright, 1998) (Sheldon et al., 1989) (Croce et al., 1998).

Biosystems have inherent molecular recognition and self-assembly capabilities. Biosystems can be an attractive template for constructing and organizing nanostructures (Belcher et al., 1996). Lithium cobalt oxide shows excellent electrochemical performance as the cathode. Nam et al. investigated virus self-assembling nanowires for LIBs by controlling the protein chains' peptides and functional groups (Nam et al., 2006). The coated virus proteins could enhance the precise nanomaterial positioning. The anisotropic virus is suitable for nanowires growth and is stable in electrochemical conditions. The carboxylic acid, a side chain from glutamate, could bind the positive metal ions via ion exchange. Tetraglutamate would block the nanoparticle by electrostatic repulsion. E4 virus could interact with positively charged polymer electrolyte owing to the negativity. Self-assembly virus/cobalt oxide monolayer electrodes show high-capacity performance (Nam et al., 2006).

Polysulfide diffusion is a critical issue for Li-S batteries. Fu et al. introduced one interlayer inside the electrolyte (Fu et al., 2019). They found that self-assembled protein as nano-filter could trap the polysulfides owing to COO^- end group and oxygen's electrostatic interactions, facilitating the Li^+ transfer because of the porous structures. The porous structure was based on protein self-assembly (Fu, Li, Wang, Scudiero, et al., 2018) (Fu et al., 2019). Miot et al. used bacteria to synthesize iron oxide electrodes (Miot et al., 2014). Specifically, they used bacteria to precipitate and confine nanoparticle growth for electrode preparation due to surface negativity and protein micrometric porosity. After the heat treatment, the LIBs electrochemical reversibility and rate capability have enhanced (Miot et al., 2014).

Protein has been used as an ion conductor due to its unique functional group interactions (Fu et al., 2016). Tryptic soy broth (TSB) is commonly used as a culture broth for bacteria growth. About 70% of the TSB is made of protein, including tryptone and peptone (**Tables 9 and 10**). TSB can offer lower costs compared to pure protein solutions. Proteins consist of smaller units referred to as amino acids that are connected through peptide bonds, and the sequence of the amino acids can influence the protein surface interactions (Dee et al., 2003). The cathode-electrolyte interface in batteries has also been a research focus in recent years. The complex surface chemistry of the cathode material is one of the primary factors related to its long-term viability in batteries (D Aurbach et al., 1997) (Doron Aurbach et al., 2000).

Table 9 TSB components

Component	Percentage
Bacto™ Tryptone (Pancreatic Digest of ds)	57%
Bacto Soytone (Peptic Digest of Soybean Meal)	10%
Glucose (=Dextrose)	8%
Sodium Chloride	17%
Dipotassium Hydrogen Phosphate	8%

Table 10 Amino Acids of TSB

Name	Hydropathy Index*	Name	Hydropathy Index*
Glutamic Acid	-3.5	Lysine	-3.9
Proline	-1.6	Phenylalanine	2.8
Leucine	3.8	Cystine	2.5
Alanine	1.8	Histidine	-3.2
Aspartic Acid	-3.5	Serine	-0.8
Arginine	-4.5	Glycine	-0.4
Isoleucine	4.5	Threonine	-0.7
Tryptophan	-0.9	Valine	4.2
Methionine	1.9	Proline	-1.6
Tyrosine	-1.3		

Note: Quantitative score indicating the hydrophobicity of an amino acid

Surface properties such as LiMnO_x cathodes and cathode-electrolyte interface mechanisms have been studied in the past using electrochemical impedance spectroscopy (EIS) and other techniques (Thomas et al., 1985) (Levi et al., 1999) (C. H. Chen et al., 2001) (Balbuena & Wang, 2004). In addition, spinel LiNi_{0.5}Mn_{1.5}O₄(LNMO) cathode

suffered from severe oxidation and unstable SEI formation issues. Tang et al. found that electrochemical stable sericin protein could solve these problems (Y. Tang et al., 2017). The formed electrode reduced Li^+ ions diffusion barrier between electrolyte and cathode (Y. Tang et al., 2017). Soy protein and gelatin are also practical surfactants to disperse the nanoparticles inside the nanofiller-based ceramic electrolyte, where the ionic pathways could be enhanced. Strong adhesion interactions with the substrate may be achieved by charge–charge interaction, hydrogen bonding, van der Waals forces, and $\pi - \pi$ bonds. This work indicated that protein configuration could bring the novel strategy to build ion transfer channels inside solid electrolytes (Fu, Li, Wang, Kovatch, et al., 2018) (X. Wang et al., 2016). A significant number of studies conducted on the electrode-electrolyte interface generally involve conventional liquid electrolyte batteries (Doron Aurbach et al., 2000) (Yabuuchi et al., 2011) (Malmgren et al., 2013) (Cresce et al., 2014) (Carroll et al., 2013). However, interfaces in solid polymer electrolyte-based lithium-ion batteries have not been sufficiently explored.

This study investigates the TSB biomaterial effect on solid polyethylene oxide (PEO) electrolyte (**Figure 15**). The results show about one order of magnitude enhancement in ion conductivity of the solid polymer electrolyte with 0.5 to 1 wt% TSB. However, the battery capacity is found to be significantly higher than that of a pure-SPE-based battery. The observed higher energy density is attributed primarily to the enhanced interfacial ion diffusion between SPE and electrodes. The TSB consists of glucose, amino acid (protein unit), and K_2HPO_4 , which have played a critical role in the LIBs electrochemical performance. The interaction between Li^+ and these materials is

explained in **Figure -15**. The free electrons on N, O, C atoms may contain van der Waals forces, facilitating ion transfer.

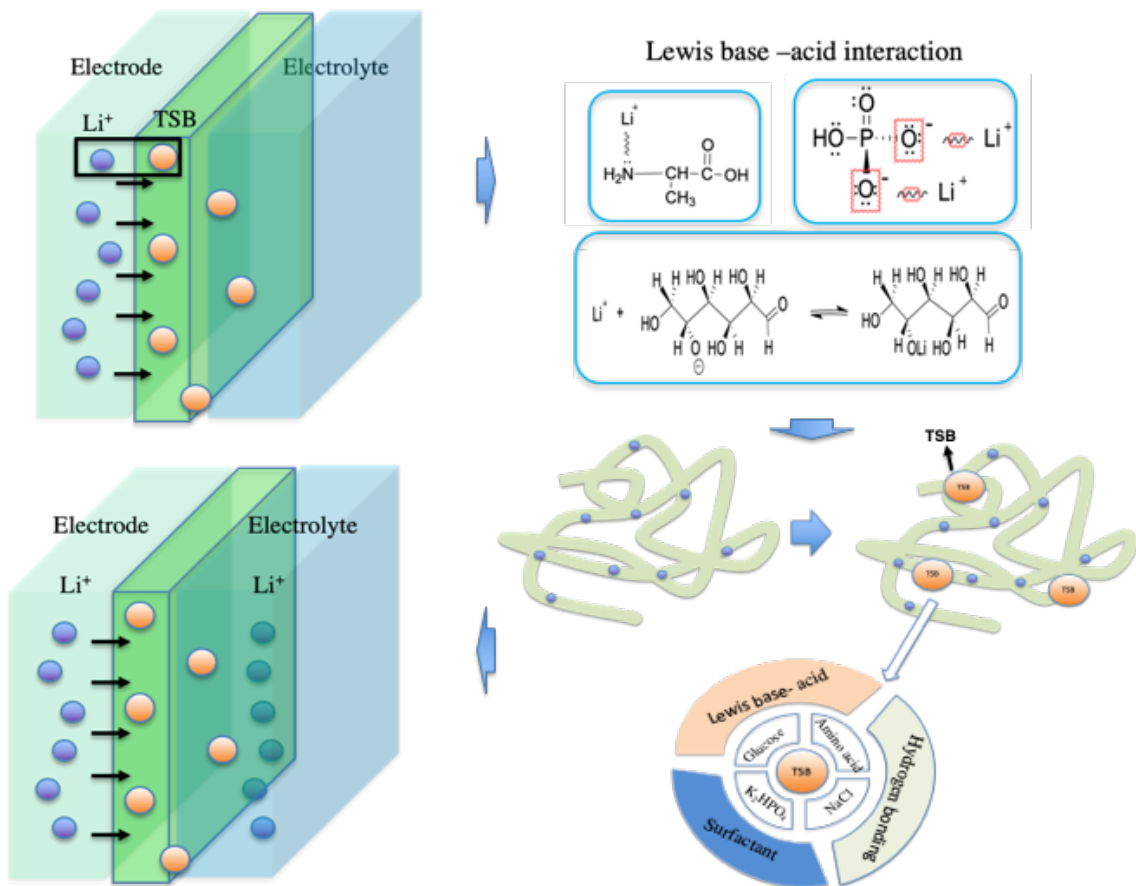


Figure 15 Schematics of the TSB-solid polymer electrolyte and LiCoO_2 cathode in lithium-ion battery and the main components of the Tryptic Soy Broth (TSB): Glucose, Amino Acid (protein unit); comparison of the interface and inter-diffusion region.

3.2 Experimental methods

The TSB-filled solid polymer electrolyte (SPE) film and Li-ion coin-cell batteries were fabricated, assembled, and characterized through various experimental techniques to investigate the effects of TSB biomaterial additive. SPE film was prepared as follows: The LiClO_4 salt powder (0.3 g) and the 100K M_w PEO powder (2 g) were dissolved in 30 mL acetonitrile in glass bottles. Next, 0.5, 1, 3, 5 wt% TSB powder mixed with salt, PEO, and solvent. Solution (including PEO, salt, solvent, and TSB) will stir for 6 hours. The

mixed solution was sonicated using a Branson 3510 ultrasonic cleaner for 25 mins. After sonication, the PEO/salt/TSB/solvent solutions were poured into different Teflon petri dishes and kept in the convection oven at 40 °C for 24 h until the solvent evaporated. The final film was transferred into the glovebox for LIBs fabrication. Assembling coin cell batteries were inside the dry glove box with lithium metal chip (anode), pure and composite solid PEO electrolyte, and lithium cobalt oxide (cathode). Both cathode and anode were 1.76 cm² circular shapes. The anode, cathode, and current collector materials were purchased from MTI Corp. A drop of liquid plasticizer (LiPF₆ in ethylene carbonate (EC) + dimethyl carbonate (DMC) + diethyl carbonate (DEC)), about 10wt% of the solid polymer electrolyte was deposited on the surface of each electrode during assembly to enhance interfacial contact. The battery components were assembled layer by layer and sealed using a coin cell-crimping machine.

My colleague Mengying Yuan worked with me on this project. SPE ion conductivities were determined using the complex impedance spectroscopy method carried out by Metrohm Autolab (N Series). The samples were sandwiched between two stainless steel electrode discs. The complex impedance spectra were obtained with the Autolab frequency response analyzer (FRA) module in the frequency range of 1 Hz–1 MHz. We also run charge/discharge LIBs test, electrochemical impedance spectroscopy (EIS) impedance test, polarized light microscopy (PLM) test (Advanced EPI Trinocular Infinity Polarizing Microscope 50x-1600x) for polymers investigation, etc.

3.3 Results and discussions

PLM images in **Figure 16** show the morphology of different TSB content SPEs. Both spherical crystals' size and number are observed to decrease after adding the TSB.

The reason can attribute to the urethane group in the TSB, which will reduce polymer electrolyte crystallization (Y.-D. Li et al., 2009). The protein self-assembling may enhance the nucleation rate of the PEO and form a more amorphous region between the crystals (Nam et al., 2008) (Fu, Li, Wang, Kovatch, et al., 2018).

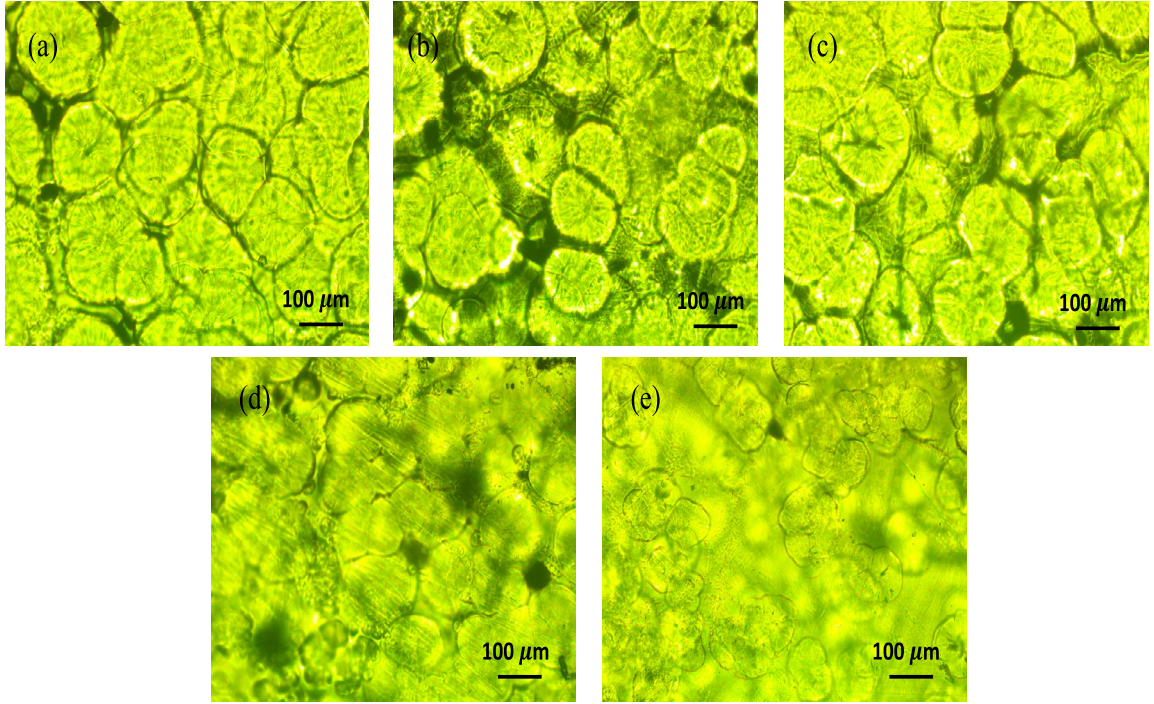


Figure 16 Polarized light microscopy of (a) PEO+LiClO₄ (b) PEO+LiClO₄+0.5wt.% TSB (c) PEO+LiClO₄+1wt.% TSB (d) PEO+LiClO₄+3wt.% TSB (e) PEO+LiClO₄+5wt.% TSB

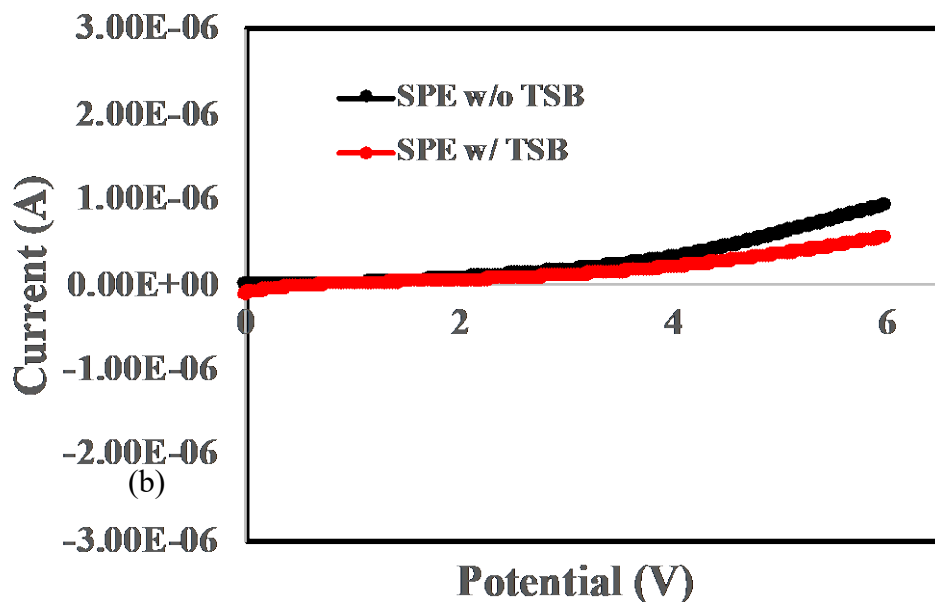
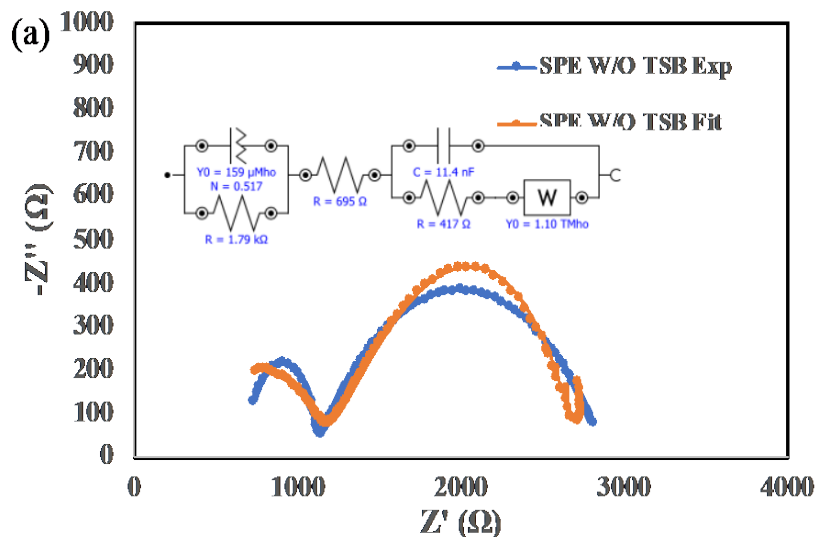


Figure 17 Electrochemical Window stability of PEO+ LiClO₄ with TSB and without TSB

To further understand the SPE electrochemical window information, we run the linear sweep voltammetry and characterize the SPE electrochemical window from 0 to 6V. The electrochemical window is 0.5V higher by using TSB (**Figure 17**). SPE is stable between 0 to 4.5V. The current is still lower than 1×10^{-6} A at 6V, which means that the stable SPE is prepared.



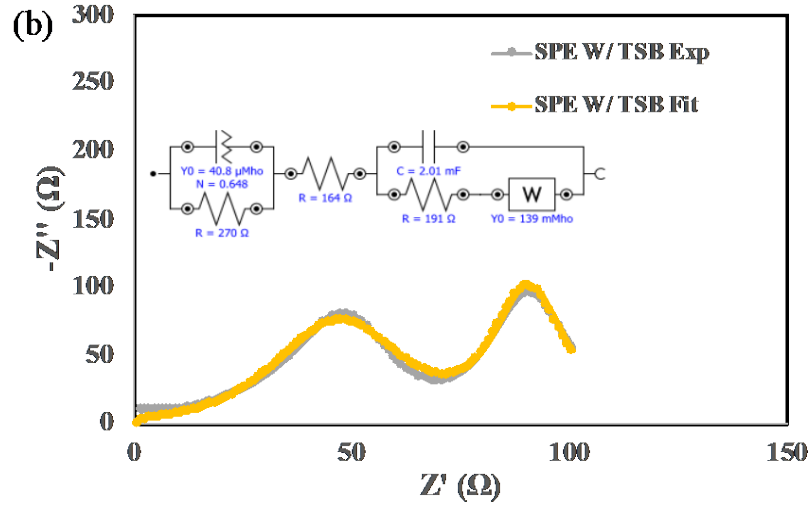


Figure 18 (a) Impedance spectra of batteries based on solid polymer electrolyte without TSB and their respective fitting circuit models: (b) Impedance spectra of batteries based on solid polymer electrolyte with TSB and their respective fitting circuit models.

The impedances spectra of the pure PEO-based LIBs and the TSB-PEO LIBs are compared in **Figure 18**. Significant improvement of battery performance is observed in the PEO/TSB-based battery. This is mainly attributed to the structural and interfacial properties of the protein, the main constituent of TSB. The electrode-electrolyte interfacial impedance is directly related to the contact and interfacial ion diffusion and conduction between the electrolyte and electrode. The interfacial layer (between the electrolyte and electrode) resistance decreases from 1790Ω to 270 Ω. PEO/TSB solid polymer electrolyte appears to reduce the interfacial resistance by providing higher ion conductivity and enhanced lithium-ion transfer across the electrode-electrolyte interface. Charge transfer resistance (second semi-circle from left) decreases from 417Ω to 191Ω, which attributes to high ionic conductivity SPE (**Figure 19a**).

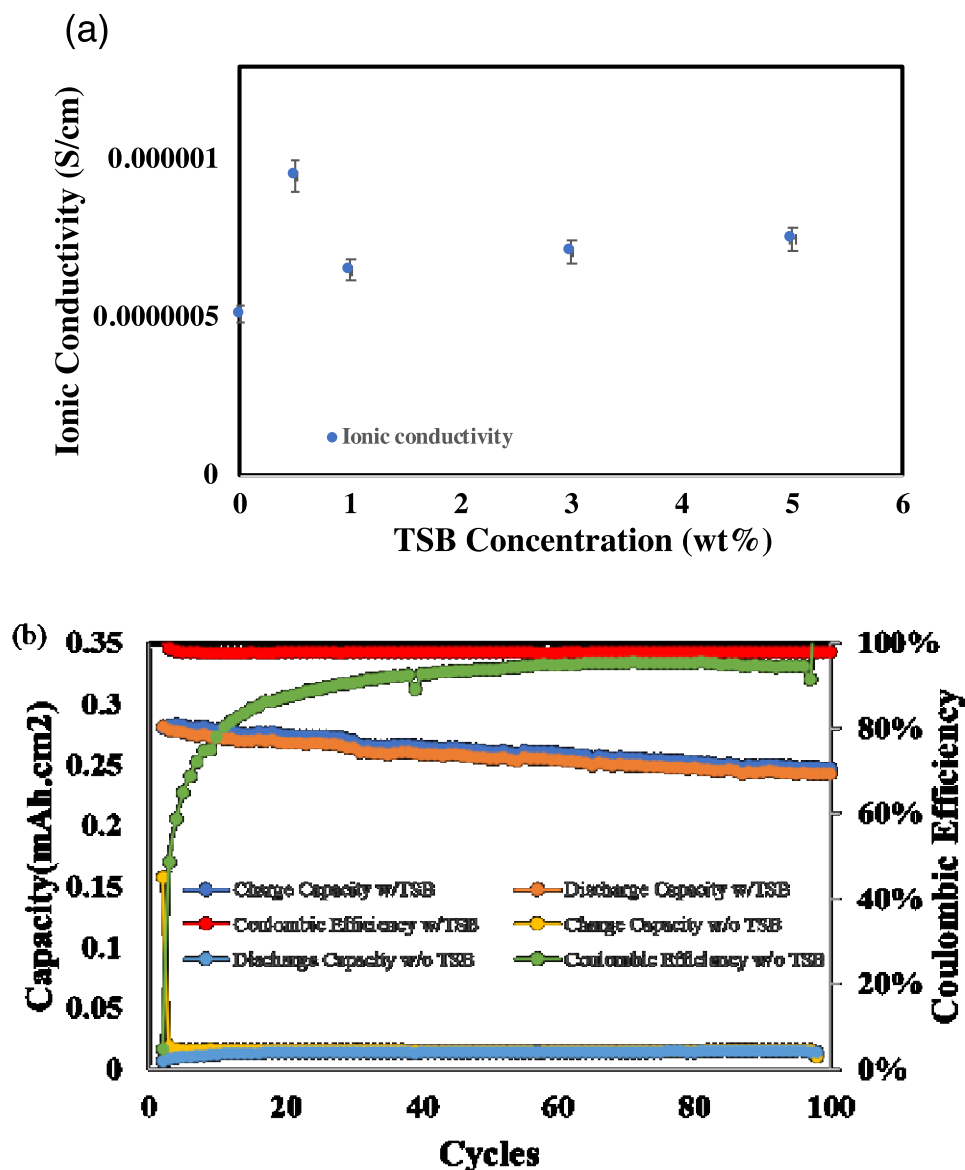


Figure 19 Ion conductivity and electrochemical characterizations (a) solid polymer electrolyte ion conductivity vs. TSB concentration; (b) flexible battery area capacity vs. cycle number.

Figure 19a shows the ion conductivity of the SPE electrolyte film for biomaterial content. The SPE ion conductivity is found to improve with the TSB addition from 8×10^{-7} S/cm to 7×10^{-6} S/cm. The optimum TSB biomaterial content (0.5wt% TSB) was selected for the SPE-based LIBs fabrication and testing. It is challenging to acquire a uniform film as we continue to increase the amount of TSB because entanglement and aggregation can occur (Y. Tang et al., 2017) (Zhu et al., 2016). High ionic conductivity SPE could

enhance Li^+ transfer in bulk and interfacial later. **Figure 19-b** shows PEO/TSB-based LIBs cycling performance, indicating significant improvement. For the specific capacity and columbic efficiency (electrochemical processes inside the battery appear to be relatively stable after the first few cycles. The protein can immobilize the anions and improve the Li transference number, which will reduce the polarization and improve the capacity. The adhesion property also improves because of the hydrogen bonding, Van Deer Waals force, electrostatic forces (X. Wang et al., 2016). The discharge capacity has changed from 0.03 mAh/cm^2 to 0.25 mAh/cm^2 . As mentioned previously, protein structure inside TSB can improve the contact between electrode and electrolyte and provide higher lithium-ion flux across the interface and in the interphase region, which will result in the high LIBs capacity.

3.4 Conclusions

In conclusion, SPE ionic conductivity increases by adding protein-based TSB biomaterial. The electrode-solid polymer electrolyte interfacial properties show significant improvement, specifically, one order of magnitude reduction in interfacial impedance (from 1790Ω to 270Ω) and improved battery capacity from 0.05mAh/cm^2 to 0.25mAh/cm^2 . We can see that TSB can improve device performance significantly. The enhancement could attribute to $-\text{NH}$ and $-\text{C}=\text{O}$ groups, increasing Li^+ movement and transfer. The higher density groups could liberate the polymer chains and help Li^+ ions transfer. Protein-based materials can be a promising biomaterial for solving the interfacial problem inside solid polymer-based batteries.

CHAPTER IV. FLEXIBLE LITHIUM-ION BATTERIES

4.1 Background

According to MarketsandMarkets reports, the flexible battery market will expand from 97 million dollars in 2016 to 958 million dollars by 2022 (Singh et al., 2018). The markets include medical devices, smart cards, battery-assisted tags, wireless sensor networks, real-time clock backup batteries, etc. For example, one Korean company called JENAX has fabricated flexible polymer LIBs, which could be subjected to bending at different angles (Hubl et al., 2016). Additionally, **Figure 20** shows common materials used in flexible batteries and flexibility test simulation plots. Here we summarize five major laminated battery fabrication companies: Automotive Energy Supply Corporation (AESC), Bright Volt, LG Chem, Murata Manufacturing, Panasonic in **Table 11**. For example, AESC currently uses NMC/Graphite as the electrode and obtains the 300 Wh/Kg for energy density. Murata has developed NCA/Gr, NCM/Gr, LFP/Gr, NCA/G + SiO-based flexible LIBs with 265 Wh/kg energy density. These flexible LIBs provide added mechanical features compared to conventional LIBs. They can be subject to bending, twisting, and folding. Apart from LIBs materials design, different flexible LIBs shapes have been investigated. Excluding planar batteries, cable-type batteries have attracted interest. New configurations could be assembled by paralleled or twisted anode and cathode wires. For instance, high-performance fiber-type flexible batteries were prepared by wet spinning electrodes into fiber (Zhang et al., 2016). Another coaxial cable-shaped flexible LIB shows 762mAh/g discharge capacity at 0.1C (Cao et al., 2016). From a materials perspective, metal-chalcogen shows inferior energy density than Li-S batteries but shows developing potential because of the high ionic conductivity and rate

performance. Although carbon cloth/fabric flexible electrodes have good electrical and flexible properties, these flexible electrodes also have the poor reversible capacity, low coulombic efficiency, and non-ideal insertion/extraction voltage, etc. In all, high flexible LIBs need to have high active materials surface area/volume ratio, flexible and steady electrode structure, reliable and high ionic conductivity SPE, good thermal and strain management, etc. (Peng et al., 2017). Searching for new electrode materials, optimizing components ratio, controlling conductivity and loading mass will be crucial (Zhou et al., 2014).

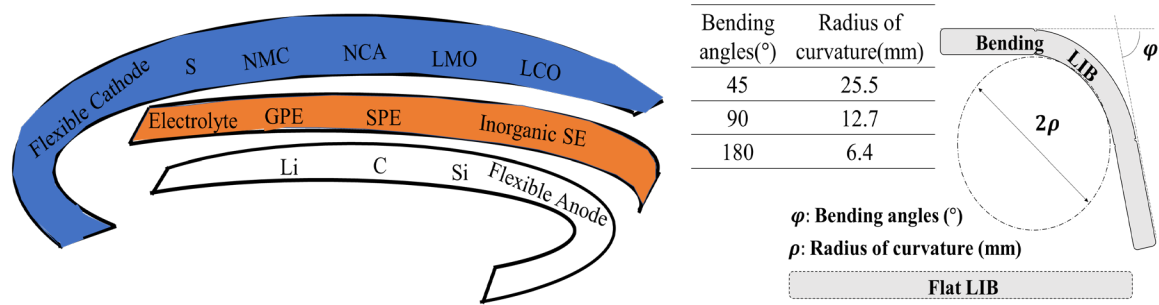


Figure 20 Flexible LIBs structure and Flexibility measurement.

Table 11 Summary of the work finished

Company	Capacity	Materials	Capacity retention	Bending radius and twisting angle	Country
JENAX 2017	2.3(mAh/cm ²)@0.1C	LCO/Gel Polymer/Graphite 5μm	80% @1C/1000 cycles		Korea
Panasonic 2016	1.6(mAh/cm ²)@1C 20 °C	Lithium oxide/gel/LE/Graphite	80% @1C/1000 cycles	Bending: R:25mm Twist: 25°/100mm	Japan
Samsung 2014	210mAh for (35*12*44mm)		50,000 bending cycles		Korea
LG Chem 2012		Ni-Sn/LE/LCO			Korea
Front Edge Technology	0.1mAh (20mm*25mm*0.1 mm)	LCO/LiPON/Lithium	Less 5% self-discharge per year	Bending and twisting ang angles	USA
Bright volt	35mAh for (45*23*0.45mm)	LiMnO ₂ /Polymer/Li			USA

Table 11 (continued)

ASEC	224 - 300Wh/Kg for (300*222*68mm)	NCM/Graphite		China
Blue Spark		Carbon-zinc MnO ₂	40mm Bending Radius	USA

Flexible LIBs still face electrodes delamination, inhomogeneous interfacial layer formation, low energy density issues (Peng et al., 2017). For example, metals tags (used to conduct current) physical contact with the current collector may induce high contact resistance (Sun et al., 2015). The connection and interfaces between each LIBs component still need to improve. Although some groups investigate delamination or fracture of different layers in LIBs (Zhou et al., 2015)(He et al., 2013), it is still unclear how interfacial layers and mechanical force influence flexible polymer LIBs. Our group has investigated extreme mechanical bending effects on the flexible LIBs interfacial properties. The relationship between contact pressure and conductance was discussed. The theoretical model also supported experimental results (Berg et al., 2017). Our group has also designed a 3D spiral shape thin film battery with out of plan stretching and flexible properties (Kammoun et al., 2016). To develop a higher performance flexible battery, we choose two different salt and investigate lithium salt influence on our flexible LIBs performance. We mix two different lithium salt with polymer electrolytes. The high viscosity mixture gives the appearance of a solid composite film. The final assembled flexible LIBs are analyzed by charge/discharge performance and impedance change. We refer to some standards during flexible LIBs characterization (**Table 12**) (Leber et al.,

2017). We find that our flexible LIBs have stable discharge capacity at different bending angles. The stable LIBs also show promising applications for flexible electronics.

Table 12 Summary of current flexibility test

Test name	Full Description	Key Parameters
JESD22-A110E (Highly accelerated temperature and humidity stress test-HAST)	Evaluating reliability for nonhermetic packaged devices in humid environments. Employing severe temperature, humidity, and bias to moisture penetration etc.	Severe temperature. Humidity
JESD220A102E (Accelerated moisture resistance- Unbiased HAST)	Similar with HAST. No bias applied	Severe temperature. Humidity
Table 12 (Continued)		
JESD22-A108D (Temperature bias and operating life)	Simulating operating condition in an accelerated temperature, a form of high temperature bias life at a short time(burn-in)	High temperature
ISO/IEC 7810 (Identification cards physical characteristics)	Physical dimensions; resistance to bending chemicals, temperature and humidity; toxicity	Dimensions. Resistance. Toxicity
ISO/IEC 7816-1 (Identification cards - integrated circuit cards)	Similar with ISO/IEC 7810. Mechanical strength included	Mechanical strength
ISO/IEC 10373-1 (Identification cards - Test methods)	Similar with ISO/IEC 7810, 7816	Test methods
IPC-TM-650 (Flexural fatigue life for a given bend radius)	Fatigue life at a bending radius; ductility determination	Fatigue life. Ductility
ASTM D522/D522M (Mandrel bend test of attached organic coatings)	Test covering resistance to cracking. Bending over a conical mandrel or cylindrical mandrels of varies diameters	Flexibility
MIL-STE-883K 1010.9 (Temperature cycling)	--	Temperature
MIL-STD-883K 2018.6 (SEM inspections)	Test standards for microcircuits; Temperature cycling, corrosion test, vibration fatigue, strength, loading functional testing, etc.	Mechanical, thermal, electrical test.

4.2 Experimental Methods

Solid polymer electrolyte (SPE) film and pouch cells were fabricated, assembled, and characterized through various experimental techniques to investigate bending angles effects. SPE film was prepared as follows: The lithium bib(oxalate)borate (LiBOB) salt powder (0.6 g) was dissolved in 2 mL tetraethylene glycol dimethyl ether (TEGDME). Next, 600K M_w PEO powder (2 g) was added to bottles and heated for 2 hours at 60°C. Then, the mixed composite was hot-pressed for 15 mins until the thin films formed.

Pouch cells were assembled inside a glove box with graphite(anode), composite solid PEO electrolyte, and lithium cobalt oxide (cathode). Both cathode and anode were cut into $2 \times 2 \text{ cm}^2$ circular shapes. The anode, cathode, and current collector materials were purchased from MTI Corp. The battery components were assembled layer by layer and sealed using a cell-sealing machine. Finally, the cells were hot-pressed for another 15s for a better interface between the electrolyte and electrodes.

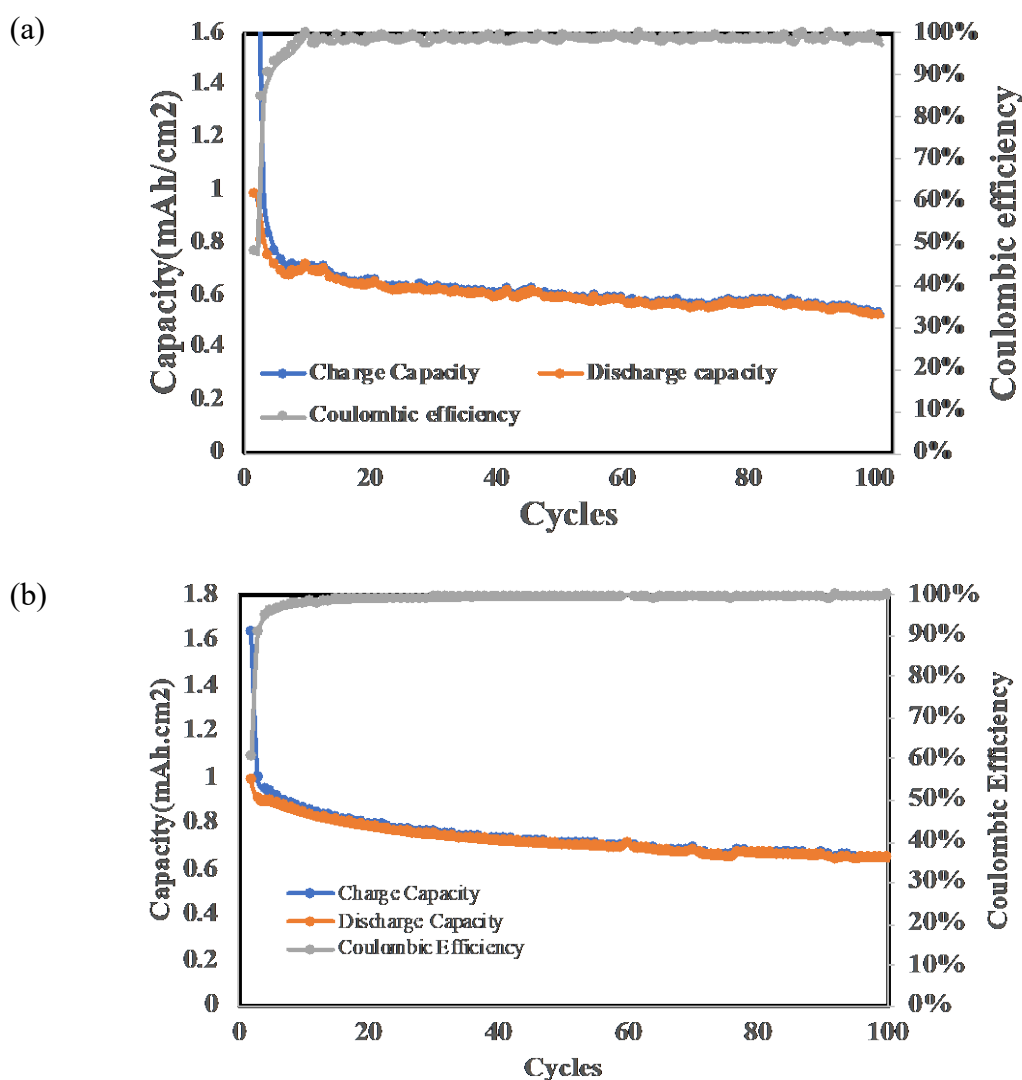


Figure 21 (a)Capacity performance of flexible pouch cells by using LiTFSI&LiBOB(1:1 molar ratio) salts;(b) capacity performance by using LiBOB salt.

4.3 Results and discussions

Figure 21 shows the flexible LIBs charge/discharge capacity and coulombic efficiency performance in the flat state before flexibility tests. We can see that the capacity reached ~ 0.6 and ~ 0.7 mAh/cm² after 100 cycles for LiTFSI&LiBOB(1:1) salt and LiBOB salt, respectively, which is higher than the previous cells prepared by the solution casting method. There is $\sim 70\%$ capacity retention after one hundred cycles. This high-capacity retention can attribute to higher amorphous regions and better interfaces between the electrolyte and electrodes. We can also observe that the coulombic efficiency is over 98% after ten cycles, indicating high discharge performance. The observed difference between the first and second cycles can attribute to the interface layer formation like SEI and cathode electrolyte interphase (CEI). The ion hopping mechanism dominates charge transfer inside SPE. However, interface ionic transfer is influenced by diffusion, intercalation, and hopping. We assume that the presence of fluorine (F) can improve the LIBs capacity by modifying and stabilizing the interfacial layer formation. However, using a fluorine-based salt, namely, LiTFSI did not lead to any improvement. So, a different salt, LiBOB, was selected, and fluorine's role was investigated in an additive form, namely, FEC (Chapter VI). Finally, we will investigate the interface resistance to confirm the capacity differences.

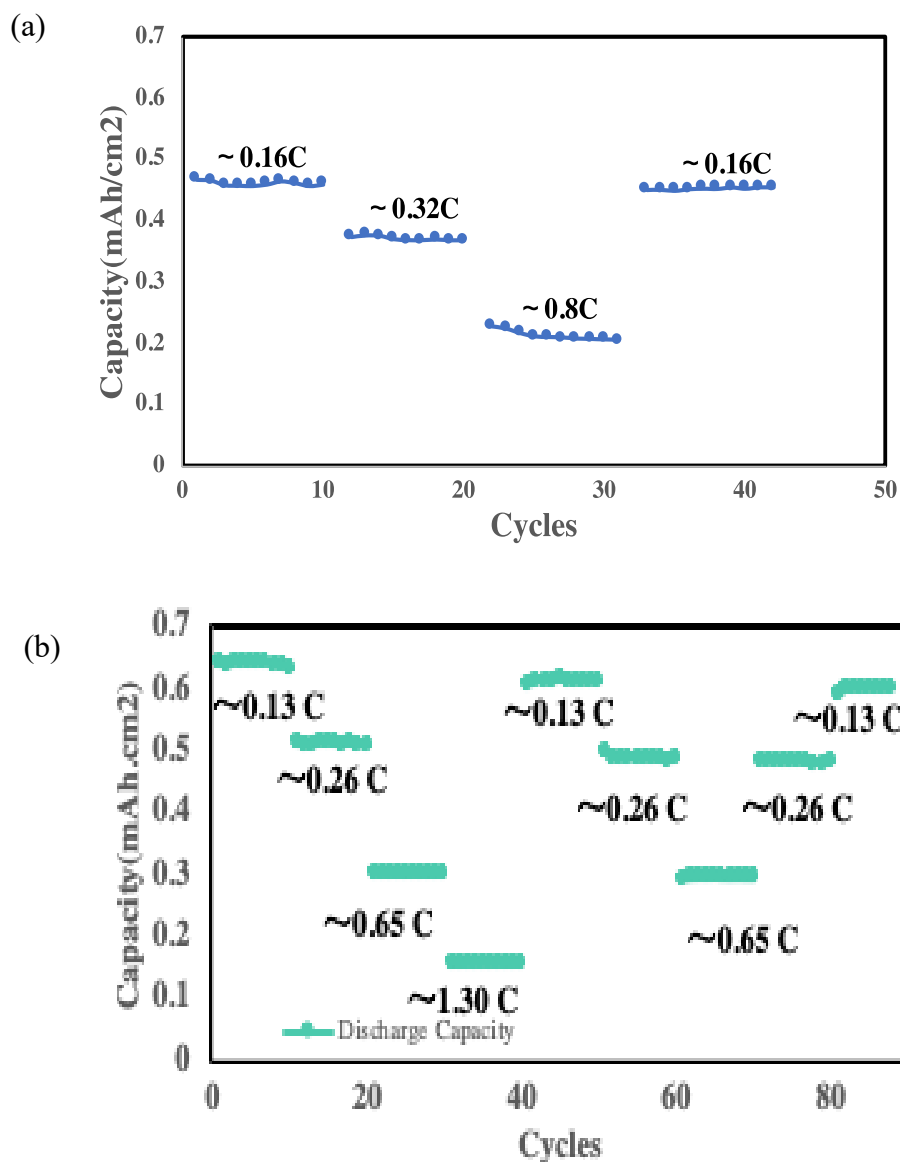
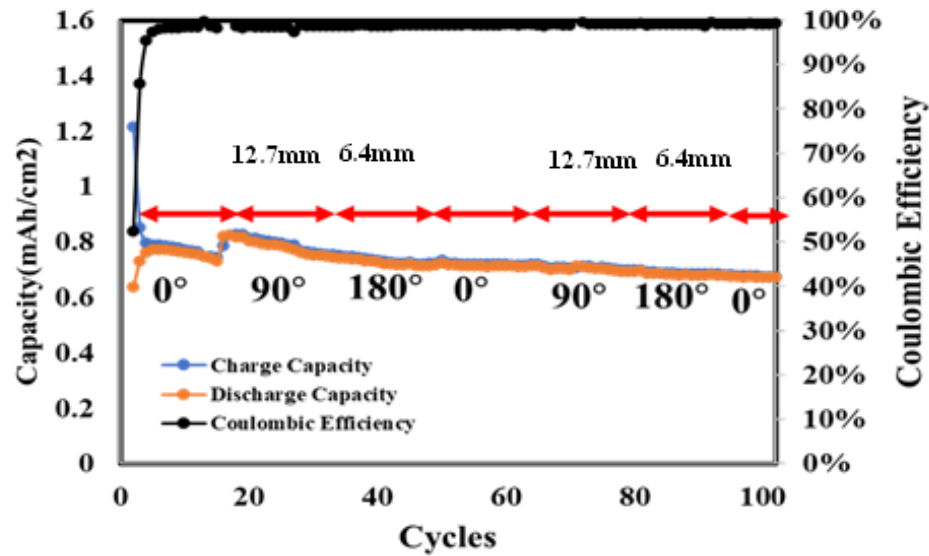


Figure 22 (a) Rate capability test for pouch cells by using LiTFSI&LiBOB; (b) flexible LIBs rate capability performance by using LiBOB.

Figure 22 shows the rate capability test for different charging rate cells. For LiTFSI&LiBOB based batteries, capacity changes from 0.48 mAh/cm² to 0.22 mAh/cm² when the C rate changes from 0.16C to 0.8C, respectively. For LiBOB based batteries, the charge and discharge current ranged from 0.14C to 1.30C. We can see that capacity decreases from 0.65 mAh/cm² to 0.14mAh/cm² after changing the charging rate. The

reason for this change attributes to the incomplete Li^+ intercalation inside the electrodes. We can also observe that the capacity decrease is not linear with respect to the charging rate increase. When the charging rate is 0.26C, capacity shows $\sim 0.50 \text{ mAh/cm}^2$. There is 0.15 mAh/cm^2 decrease. If we continue to increase to 0.65C (5 times higher than the first 0.13C rate), capacity is $\sim 0.30 \text{ mAh/cm}^2$. There is 0.35 mAh/cm^2 decrease compared with the initial value. If we further increase the rate to $\sim 1.30\text{C}$ (10 times higher than the first 0.13C rate), the capacity is $\sim 0.15 \text{ mAh/cm}^2$. There is a 0.50 mAh/cm^2 change. The capacity decreasing rate slows down if the charging rate is higher. So, there is a tradeoff between charging rate with capacity. Comparably higher charging rates can lead to surface electrochemical reactions. The surface reaction can consume most Li^+ ions. This phenomenon observed from the rate capability test also confirms the charging/discharging plots. Therefore, we focus on the LiBOB based batteries for further investigations.

(a)



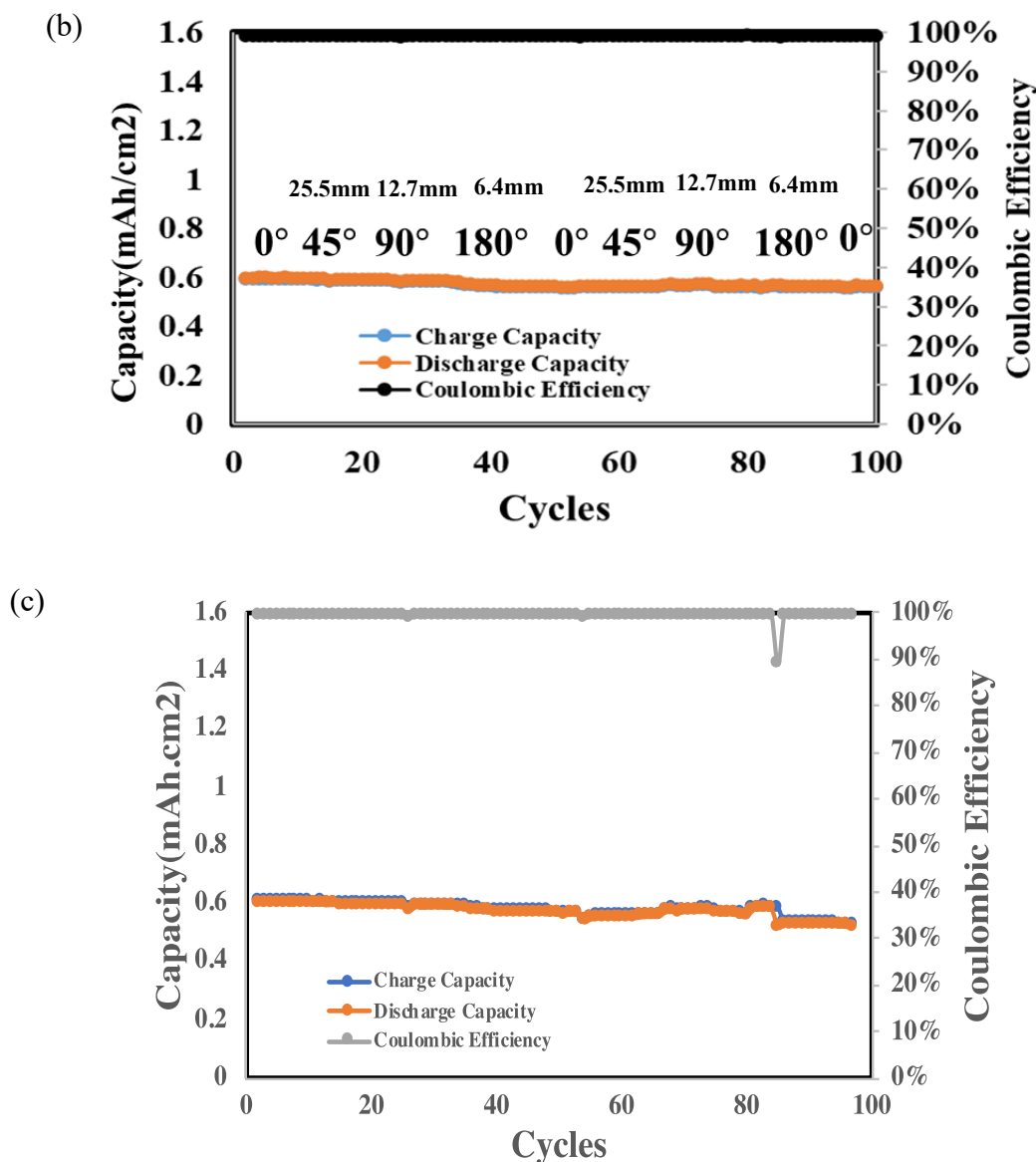
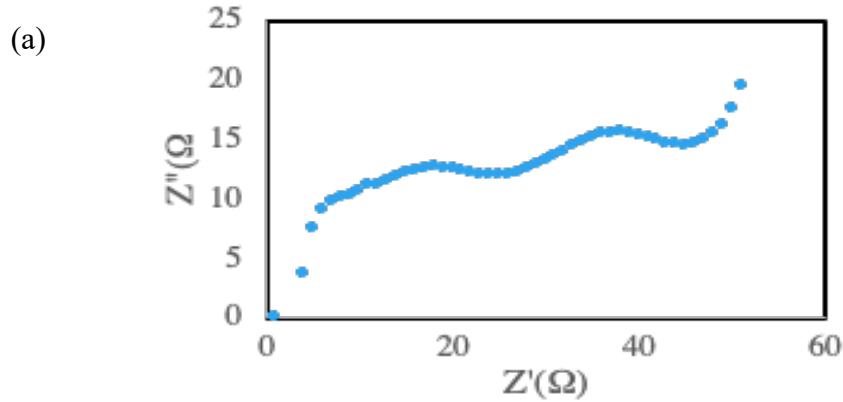


Figure 23 (a) Flexible LIBs capacity performance under different bending angles or different radius of curvature; (b) In-situ flexible LIBs capacity performance during different bending angles; (c) flexible LIBs capacity performance after bending 100 cycles at 0.13 C.

Figure 23 shows the flexible LIBs capacity subjected to mechanical bending test for ten cycles at different angles. The capacity is comparably stable after bending with a value of 0.61 mAh/cm² after 100 bending cycles. The slightly capacity decrease is likely due to electrolyte or electrode degradation and side reactions. We notice stable capacities from 0° to 180°. The steady capacity is related to the steady bulk structure. The stable capacity

performance means bending will not break down the inner electrode structures. Furthermore, the intercalation and deintercalation inside the cathode and anode appear to be stable. The robust SPE mechanical properties ensure good Li^+ ions transfer between electrodes. After the bending test, the flexible LIBs are subjected to charge/discharge cycles. The battery shows very stable electrochemical performance after bending (**Figure 23c**). After cycling around 100 cycles, capacity is 0.52 mA/cm^2 compared with 0.60 mA/cm^2 at the beginning. Capacity retention is around 87%. The bending test could influence the capacity due to the external force applied. Bending could improve the LIBs multi-layers structural stability. The applied mechanical force enhances the electrode and electrolyte interface. So homogeneous electrochemical reactions would take place on the surface of electrodes.



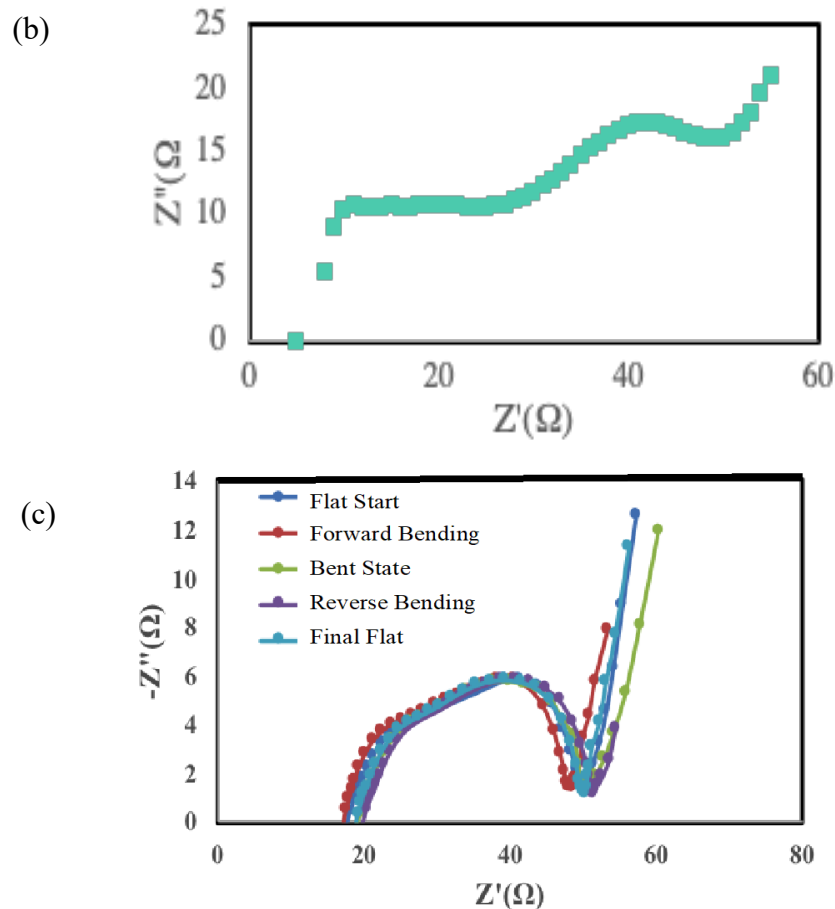


Figure 24 (a) Flexible LIBs impedance performance before bending; (b) flexible LIBs impedance performance after bending 100 cycles; (c) flexible LIBs impedance performance during bending process.

Figures 24 shows LIBs impedance performance before and after bending. We can see that the charge transfer resistance slightly changes from 18.3Ω (Before bending) to 19.7Ω (After bending). The interfacial layer resistance under the middle-frequency region shows 20.4Ω before bending and 24.6Ω after bending. This small resistance change may result from electrolyte decomposition during LIBs charge/discharge. But small change also illustrates good interphase formation between electrolyte and electrodes. We also see the stable impedance under the bending process (**Figure 24c**). We measure the impedance before bending, under bending, and after bending states. Similar two semi arc curves were observed from this plot. It means the bending process will not change battery

impedance significantly. The steady impedance could be influenced by solid adhesion between electrodes and electrolytes materials and high stable interfacial layer formation like SEI and CEI.

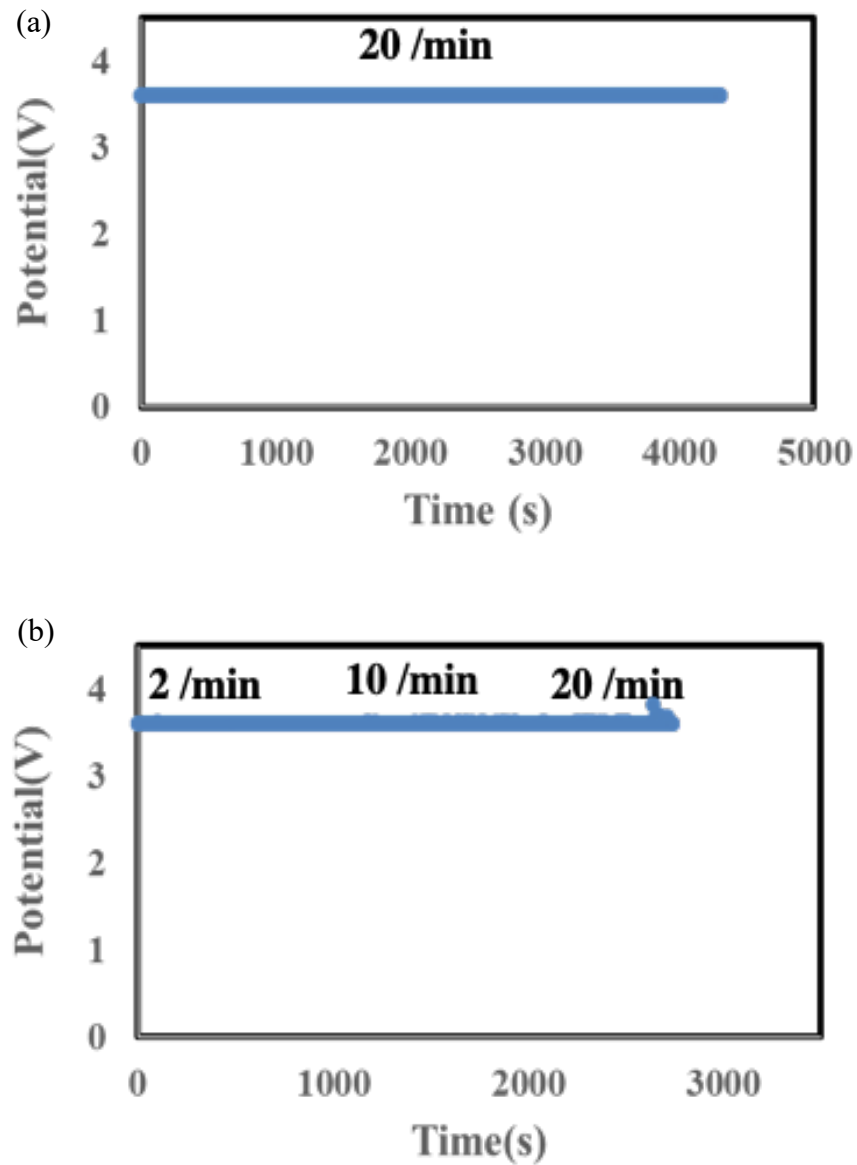


Figure 25 (a) Flexible LIBs open circuit potential tracking during bending; (b) Flexible LIBs open circuit potential tracking at different bending rate.

Figure 25 shows open circuit potential (OCV) change during bending. We can observe that bending rate influence on potential is minimal, as observed from **Figure**

35b. The flexible LIBs still maintained their original potential during the bending state. The stable OCV retention could be influenced by electrolyte and electrodes attachment because sudden dislocation between each component (cathode, anode, and SPE) would result in poor charge transfer and voltage loss. There is no OCV dropping during different bending rates. So, our battery could work very well under various bending states.

4.4 Conclusions

In summary, our all-solid-state flexible LIBs have 0.7 mAh/cm² capacity performance. Our flexible LIBs even could be subjected to bending under different angles (0-180°) and rates (0-20/min). The capacity is stable, which attributes to the better interfacial formed and stable polymer electrolyte. Compared with the second chapter using biomaterial TSB inside electrolyte, the significant capacity enhancement is mainly from the electrolyte preparation method (from solution casting to hot pressing). The high temperature would melt electrode surface polymers and ensure polymer chains mix with inorganic electrode particles well. The stable impedance under different bending states confirms the steady interfacial layers formation. During LIBs bending process, the external stress from LIBs encapsulation layer would enhance the electrodes and electrolyte interfaces. Flexible LIBs high electrochemical performance has been achieved. In the next chapter, we will continue to investigate interfacial layers inside stretchable LIBs.

CHAPTER V. STRETCHABLE BATTERIES

5.1 Background

Stretchable and wearable electronics have developed very quickly in recent years, for example, stretchable circuits, smart sportswear, implantable health monitoring sensors, wearable displays, military suits smart garments, and new generation smartwatches (Dagdeviren et al., 2016). Consequently, energy storage devices inside these stretchable and wearable electronics are crucial, especially supercapacitors and lithium-ion batteries (LIBs) that are lightweight, stretchable, and thin. Conventional batteries or capacitors could not be used due to the limited mechanical properties (Meoli & May-Plumlee, 2002) (Jost et al., 2014). Various strategies have been applied to prepare stretchable LIBs with high energy density and stretchability. Initially, flexible lithium-ion batteries were designed, fabricated, and reported to achieve stretchability (X. Chen et al., 2019) (Kang et al., 2020). Later on, stretchable batteries (and supercapacitors (Huang et al., 2015) (K. Liu et al., 2020) (Cheng et al., 2020)) were reported based on various designs and configurations such as buckling-structure (Yu et al., 2009), spring-like fiber (Zhang et al., 2014), etc. (N. Li et al., 2017) (J. Chen et al., 2013). Graphene hybrid hydrogen and silver nanowire current collectors are also applied in stretchable supercapacitors (Zhao et al., 2020) (Mu et al., 2021). In 2010, Rogers et al. reviewed the stretchable electronics mechanics and materials (Rogers et al., 2010). From a structure view, wavy shapes and bonding with elastomeric substrates could accommodate applied strain. The elastic substrate provided restoring force (Rogers et al., 2010). In addition, researchers have reported various stretchable LIBs based on the different structural designs. island-serpentine-architecture (Xu et al., 2013), spiral (Kammoun et al., 2016),

arched (Weng et al., 2015), origami (Song et al., 2014), and kirigami (Song et al., 2015) (Bao et al., 2020) are some of these non-fabric stretchable LIBs. Some studies demonstrate all-components stretchable batteries (X. Chen et al., 2019) (Liang et al., 2020) (Yan et al., 2014), while others have only one or more stretchable components, such as electrodes. The stable LIBs electrochemical performance could attribute to the interfacial layer stability and LIBs materials' compatibility (C. Wang et al., 2011) (Kaltenbrunner et al., 2010).

A fully stretchable battery is defined here as one battery where all components, including electrodes, solid electrolyte, and encapsulation, are stretchable. In addition, one technique to demonstrate fully stretchable LiBs is utilizing a wavy structural design. In this approach, the rigid components have been loaded on a flexible elastic stretched substrate to enhance the interfacial formation. Then the substrate has been released and returned to its unstrained position leading to a wavy configuration (W. Liu et al., 2017). Results have revealed the high electrochemical performance and long stability owing to the flexible PDMS porous substrate. Also, this wavy battery fabrication method has been reported to be considerably facile, simplifying commercial fabrication. Another documented example has utilized rigid components in an accordion-shaped structure (Shi et al., 2019). In 2017, Arias' group developed wire-shaped silver-zinc batteries based on helical band springs current collectors, resilient to fatigue due to stable interfacial layer formations (Zamarayeva et al., 2017). Electrochemical performance could retain after 17000 flexure cycles at a 0.5cm bending radius (Zamarayeva et al., 2017). Song et al. designed a kirigami pattern and achieved 150% LIBs stretchability (Song et al., 2015). Plastic rolling would reduce folding fractures and enhance electrodes and electrolyte

interface (Song et al., 2015). Weng et al. reported gum-like LIBs, which remained stable performance at 400% strain owing to the stable interfacial layer formation (Weng et al., 2015). Kim's group used stretchable polyurethane comprising gold nanoparticles as current collectors to enhance electrodes and current collector contact (Gu et al., 2019). In 2020, KIST fabricated a full stretchable LIB using two-dimensional micro honeycomb electrode material with a crosslinked gel electrolyte. The final capacity was 5.05mAh/cm² owing to the improved interfacial layer formation. The electrochemical performance showed up to 50% strain when the device was stretched 500 times without electrodes and electrolyte delamination (Kang et al., 2020) (X. Wang et al., 2020). Stretchable systems shared future opportunities.

Addressing aging and failure during frequent deformations is necessary. There are several ways to achieve it. Constructing a thermodynamically self-healing composite could facilitate the LIBs stability (Qi et al., 2021). 2D fractal-inspired patterns, 2D serpentine configurations, and 3D helical configurations encapsulation also improve structure strength (K. Li et al., 2019) (Mackanic et al., 2020). Wavy batteries, folding batteries, spiral form batteries, fiber-like batteries, and intrinsically stretchable batteries are pretty ordinary and promising (Kammoun et al., 2016). Stretchable LIBs have experienced a significant change in materials, mechanical design, and manufacturing strategies. Enormous strain (>1%) has been addressed. During the stretching process, LIBs experienced the elastic linear strain, bending, stretching, and twisting (Zhang et al., 2014) (Song et al., 2015). To solve LIBs failure and aging problems, we conducted stretchable LIBs experiments and focused on the electrochemical performance analysis under varied deformations. We found that enhanced interfacial layer stability is essential

for solving LIBs capacity fading and failure issues.

Here, we designed spiral shape batteries which could achieve high capacity and high strain deformation simultaneously. The stretchability could be 6000%, which is the highest strain reported as we know. In addition, we obtain 1.21 mAh/cm² stable capacity spiral LIBs. The stable spiral LIBs do not show open-circuit voltage (OCV) loss during stretching. The spiral LIBs high-performance could attribute to the enhanced interfacial layer formation. We conduct several electrochemical impedance spectroscopy (EIS) tests to investigate our stretchable LIBs interfacial layer. The EIS test design is accurate and convenient without chemical elementals analysis. From EIS test results, we show spiral LIBs long-term stability with low resistance change during stretching. Our stretchable spiral LIBs provide a contemplate for many stretchable electronics applications.

5.2 Experimental methods

The solid polymer electrolyte (SPE) film, spiral shape electrode (LiCoO₂ as cathode, graphite as the anode), self-sealing laminating sheets were prepared by Cricut Explore Air 2. Stretchable LIBs are assembled layer by layer inside the glovebox. Various experimental techniques investigate stretching strain effects. Tensile stress was applied from the Manual Mark Stress-Strain machine. The SPE film was prepared as follows: Lithium bib(oxalate)borate (LiBOB) salt powder (0.6 g) was dissolved in 2 ml tetraethylene glycol dimethyl ether (TEGDME) with 2ml fluoroethylene carbonate (FEC). Next, 600K M_w PEO powder (2 g) was added to the glass bottles and heated for 2 hours at 60°C. Then, the mixed composite was hot-pressed (80°C) for 15 mins until the thin films formed. Stretchable LIBs were assembled inside the dry glove box with graphite, SPE, and LCO. Both cathode and anode were cut into 2.55, 9.81, 19.81 cm²

spiral shapes. The anode, cathode, and current collector materials were purchased from MTI Corp. The battery components were assembled layer by layer and sealed using a cell-sealing machine. Finally, we will hot press cells for another 15 s for a better interface between electrolyte and electrodes. Spiral stretchable LIBs charge and discharge operated inside the glovebox.

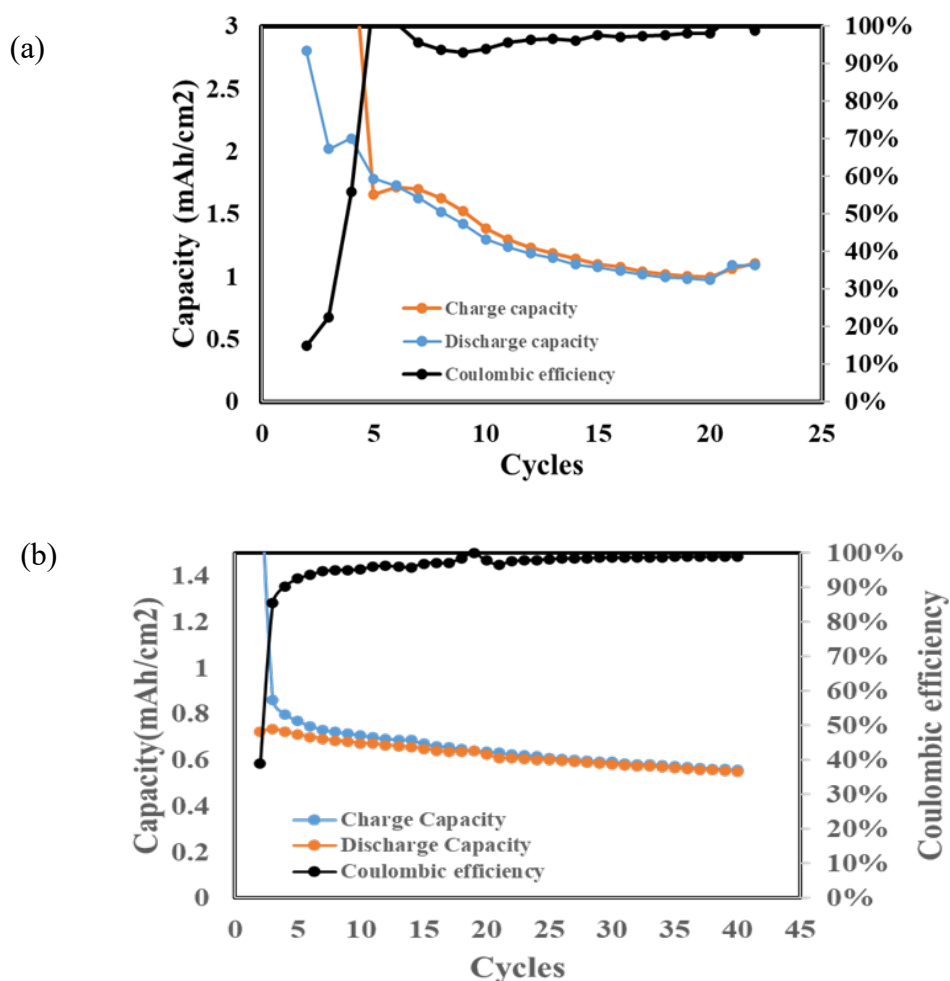


Figure 26 (a) Stretchable spiral LIBs capacity performance with 2.55 cm² area at unstretched state; (b) Stretchable spiral LIBs capacity performance with 19.81 cm² at unstretched state.

5.3 Results and discussions

Figure 26 shows spiral LIBs charge/discharge performance with different sizes. The high capacity can reach 1.55 mAh/cm² after five cycles. Then the capacity degrades

to 1.06mAh/cm² (31.6% degradation) after 15 cycles. The comparable high performance was from good interfaces between electrodes and electrolyte. LIBs capacity loss could be related to electrolyte and salt degradation during charging/discharging. To exclude size effect on device performance, we prepared different sizes of electrolytes and electrodes. Another 19.81 cm² battery has been prepared and charged/discharged. The higher performance 0.70mAh/ cm² (10.2% degradation) is obtained after cycling 15 cycles. The large spiral LIB degradation rate is lower than the smaller spiral LIB but suffers from low capacity. We find that LIBs size has a big impact on the device capacity. The reason could attribute to the incomplete electrochemical reaction on the electrodes. The interfacial layer between electrodes and electrolyte could change when LIBs size increases. During charging/discharging, the spiral LIBs current density distribution could be not homogenous compared with the smaller one (only one 5cm tab connecting with the terminal). Current distribution would also change when a LIB shape is bigger. The external encapsulation layer pressure could impact capacity, too. As discussed in the flexible battery (Chapter IV), bending would make each LIB component connect well, enhancing Li⁺ ions transfer between electrodes.

Therefore, improving LIBs capacity and cycle stability simultaneously was challenging. Here, we choose a medium size 9.8cm² as an experimental device. The reason was from the size effect and stretchability. Although smaller size batteries have a high capacity, it is hard to achieve 3D out-of-plane stretching. However, the complex processing and low-capacity performance limit the big-size spiral LIBs application. Consequently, we fabricate our spiral LIBs using 9.8 cm² electrodes. Our final spiral LIB

has high cycle stability ($\sim 90\%$ capacity retention after 15 cycles) and high capacity ($\sim 1.20 \text{ mAh/cm}^2$).

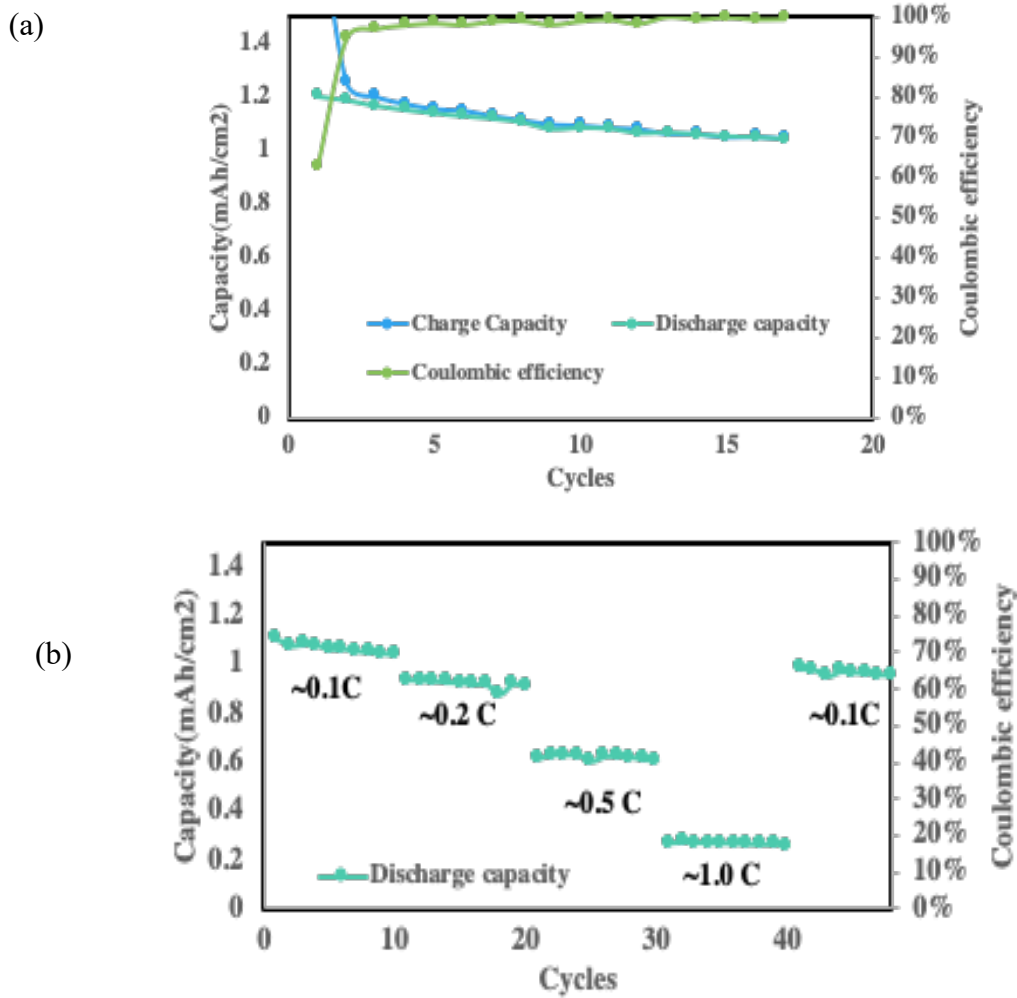


Figure 27 (a) Spiral LIBs Capacity performance for 9.81 cm^2 battery; (b) Spiral LIBs rate capability test with varied charging current rate.

Figure 27 shows the spiral LIBs capacity performance during charging/discharging. 1.21 mAh/cm^2 initial discharge capacity is achieved at 0.1 C . It decreases to 1.08 mAh/cm^2 (10.7% degradation) after 15 cycles, much lower than the previous smaller size spiral LIB. Then a rate capability test result is shown in **Figure 27b**. Spiral LIB is charged and discharged by applying different currents for the rate capability test. Spiral LIB capacity shows 1.08 mAh/cm^2 at 0.1 C , 0.95 mAh/cm^2 at 0.2 C ,

0.63 mAh/cm² at 0.5C and 0.24 mAh/cm² at 1C. Finally, spiral LIB charges and discharges at 0.1C, we still could get 1.03 mAh/cm² capacity. This battery could run over 60 cycles with 14.8% degradation. The coulombic efficiency is higher than 97% during cycling, confirming very stable interfacial layers formation. To further investigate spiral LIBs electrochemical performance, we have done some characterization like OCV tracking, EIS test, etc.

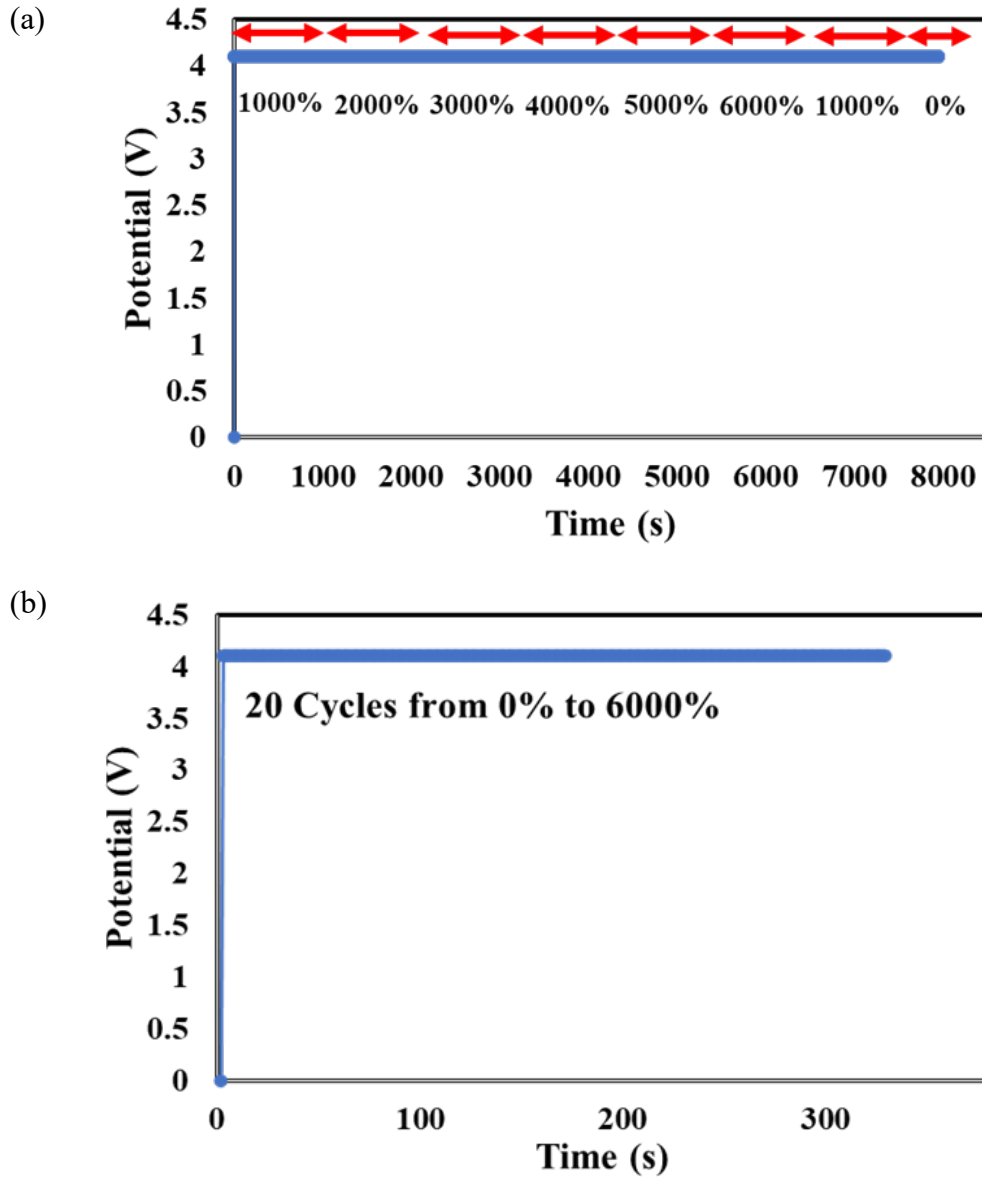


Figure 28 (a) Spiral LIBs potential performance under different strain; (b) spiral LIBs in-situ test to track the potential change during stretching.

Spiral LIBs' open circuit potential is measured during different strains (**Figure 28**). Open circuit voltage (OCV) does not change when the strain changed from 1000% to 6000% (**Figure 28a**). Because the battery thickness is around $700\mu m$, 1000% stretching means 7mm strain deformation. The stable OCV could attribute to stable LIBs structure under 1000% strain. Spiral LIB OCV also does not change when LIB stretches from 0 to 6000% for 20 cycles (**Figure 28b**), which means there is no capacity loss. This stable stretchable spiral LIB OCV also could be related to enhanced interfacial layer formation. To further understand the spiral LIB stability, we record OCV for 10 hours at a higher strain.

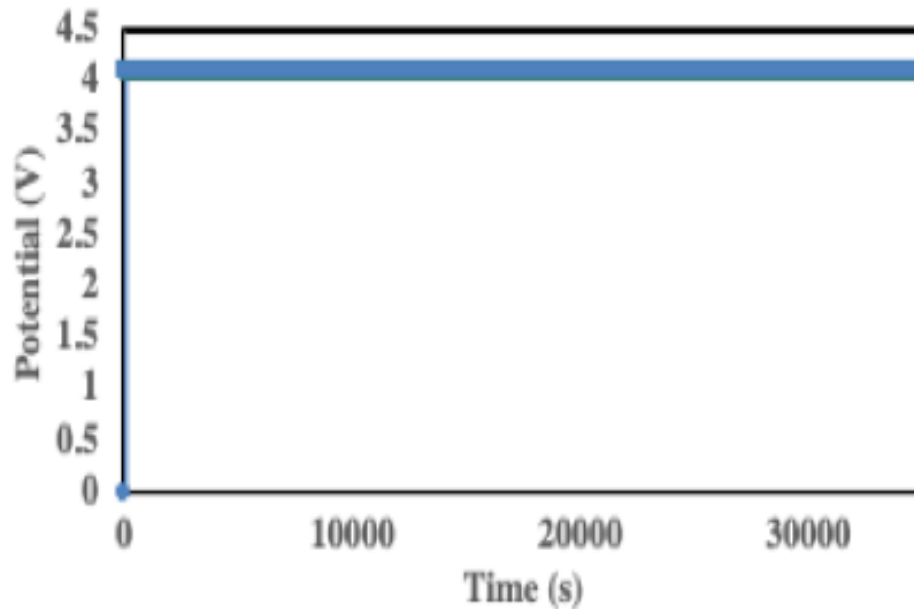


Figure 29 Spiral LIBs potential tracking when 6000% strain applied

Figure 29 records spiral LIBs potential during stretching for 10 hours. There was still no potential degradation at 6000% high strain. It confirmed LiBs high stability. There was no electrochemical reaction happening inside batteries to reduce open-circuit voltage.

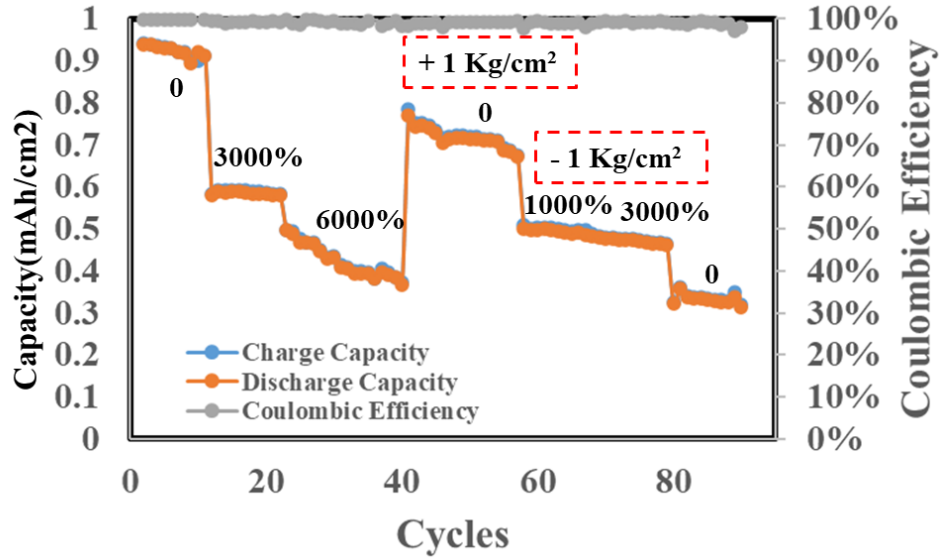


Figure 30 Spiral LIBs capacity performance during stretching from 0 to 6000% strain deformation.

Spiral stretchable LIBs charge and discharge capacity performance are shown and summarized (**Figure 30, Table 13**). Spiral stretchable LIBs could reach 0.59 mAh/cm² after stretching 3000%. It's very stable for ten cycles. LIBs capacity decreases after stretching 6000%. The spiral LIB capacity decrease could be related to encapsulation layer pressure because stretching LIBs would simultaneously experience twisting and stretching. The interface between electrodes and electrolytes would be influenced. Capacity decreases to 0.47 mAh/cm² finally. However, after applying new stress (encapsulation layer applied) between two electrodes, capacity increases to 0.72 mAh/cm², confirming our assumption that the pressure effect would play an essential role in LIBs capacity during stretching. When the stretching strain is 3000%, capacity shows 0.46 mAh/cm². Our spiral LIB is stable for 80 cycles. Finally, the LIB pressure is released, spiral LIB capacity shows 0.33mAh/cm².

Table 13 Summary of capacity loss during stretching

Stretching Percentage (%)	Capacity (mAh/cm ²)	Capacity Retention (%)
0	~0.92	100
3000	~0.59	64
6000	~0.47	51
0	~0.72	78
1000	~0.49	53
3000	~0.46	50
0	~0.33	36

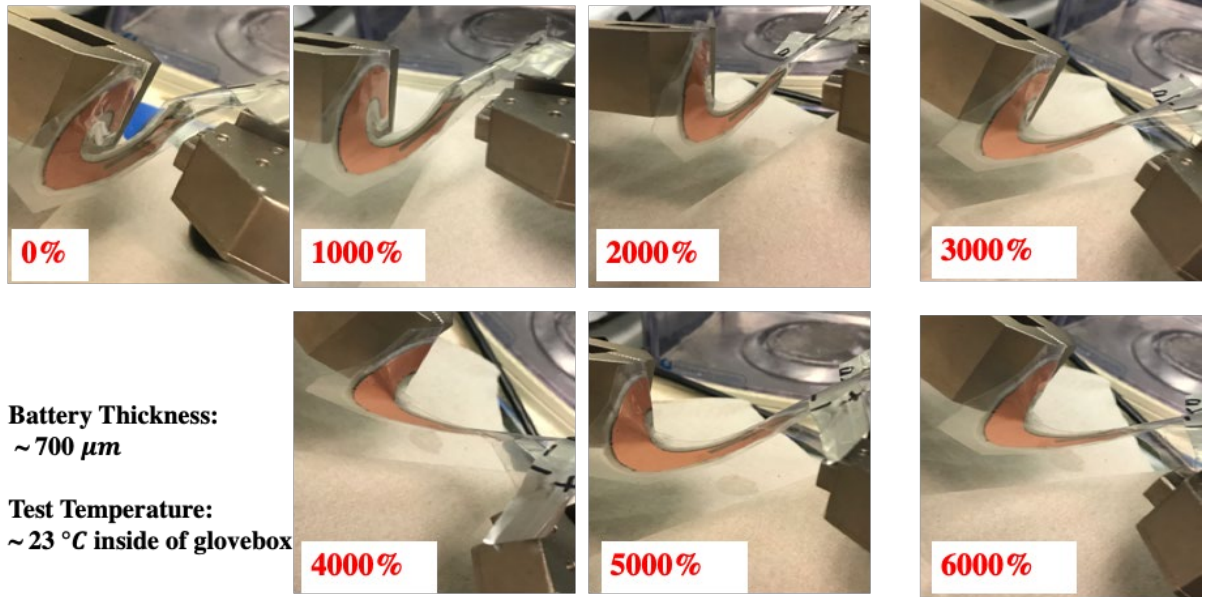


Figure 31 Spiral LIBs stretchability test under different strain deformations

Figure 31 shows stretchable LIBs deformation and shape change during the stretching. There is no crack observed during stretching. The battery thickness is around 700 μm .

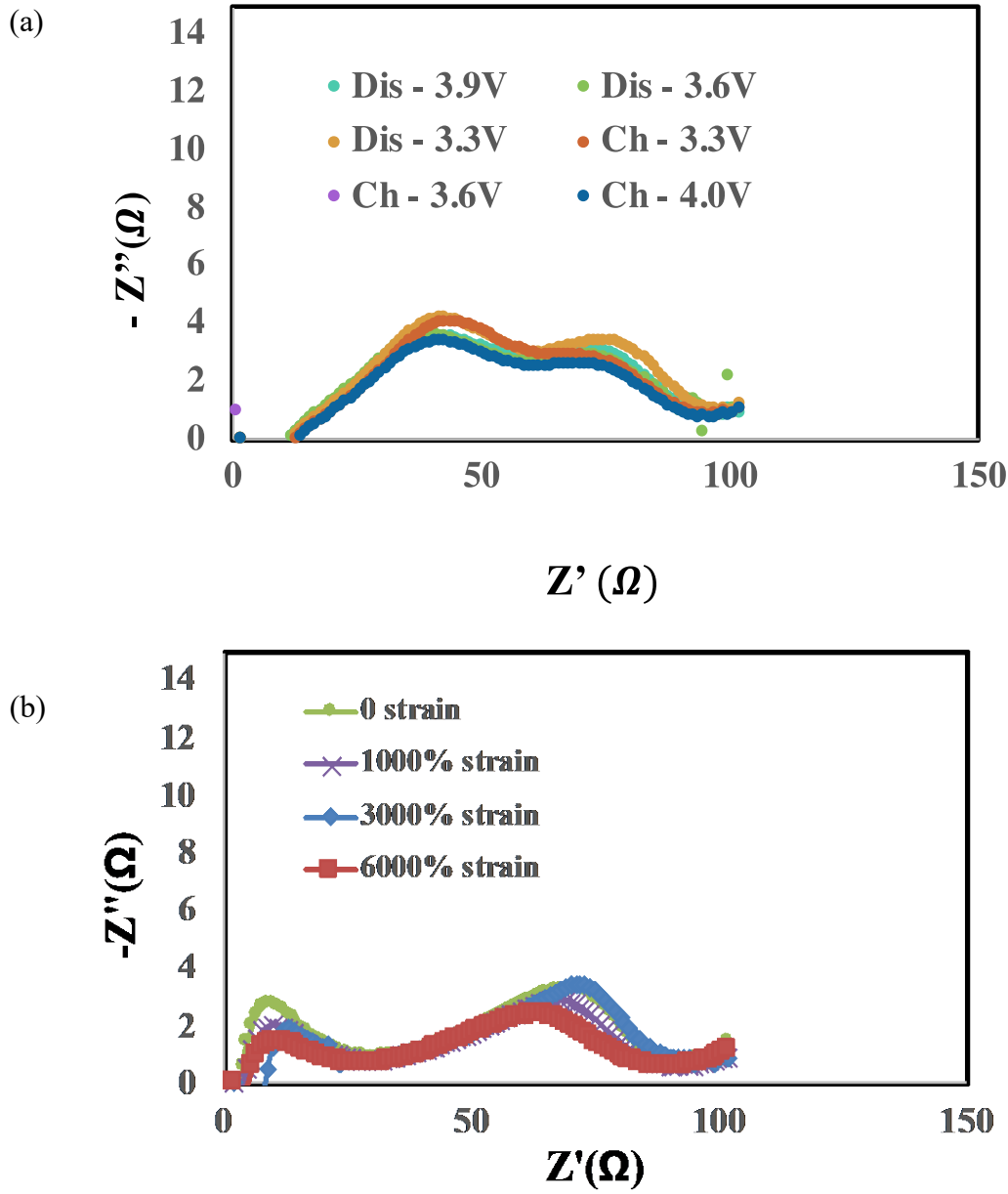


Figure 32 (a) Spiral LIBs Impedance at different voltage ;(b) Spiral LIBs impedance at different strains deformation.

Figure 32 shows spiral stretchable LIBs impedance. From **Figure 32a**, the open-circuit voltage (OCV) does not influence the LIBs impedance significantly. The LIBs could run very steadily under different voltages and cycles. Both bulk resistance and interfacial layer resistances do not change significantly during the charging/discharging

process owing to the similar semi-circle observed. From **Figure 32b**, we can also observe similar bulk resistance and interfacial layer resistance. Steady impedance could attribute to the steady interfacial later formation and stable materials structures. These EIS test results confirm the observed stable OCV potential under different strain deformation.

5.4 Conclusions

Here, we report the materials and schemes for future stretchable spiral LIBs with attractive forms and properties. A high capacity 1.21mAh/cm^2 is observed. The easy procedures for preparing materials and fabrication could make the whole process simplified. Furthermore, the higher deformation 6000% is achieved due to the enhanced interfacial layer formation. In addition, the external mechanical stress (LIBs under different strain deformation) influence on stretchable LIBs has been addressed. The stable interfacial impedance could attribute to the stable interfacial layer formation. For future work to achieve spiral LIBs high energy density, we should focus on the capacity loss under a high strain deformation and LIBs interfacial layer formation.

CHAPTER VI. ENHANCING INTERFACES IN SOLID POLYMER BATTERIES

6.1 Background

Lithium-ion batteries (LIBs) have attracted extensive research due to their high energy and power densities (Zhao et al., 2017) (Ma et al., 2015). LIBs have a wide range of applications in electric vehicles, smartwatches, drones, wheelchairs, scooters, phones, etc. (Grey & Hall, 2020). Commercial LIBs typically use liquid electrolytes with lithium metal oxide and graphite electrodes. The practical capacities of graphite and LCO are 372mAh/g and 140 mAh/g, respectively. Lithium inserted graphite at a low potential around <0.25 V vs Li/Li^+ reversibly. It is abundant and easy-to-produce properties make it be the most popular anode material (Aurbach et al., 2016). Here, we continue to use commercialized graphite as the anode and lithium cobalt oxide (LCO) as the cathode. Graphite and LCO show stable reversibility during the charge and discharge process without significant changes in electrode volume and electrode morphology. But conventional liquid LIBs suffer from electrolyte leakage, battery thermal runaway, unstable interfacial layer formation, among others (Wu et al., 2019). For next-generation LIBs, high capacity and safe solid-state batteries become the focus.

It is found that the inorganic solid electrolyte prepared LIBs have poor interfacial layer ionic conductivity and poor cycle stability. The main reason should be related to the inhomogeneous interfaces between the electrodes and electrolyte. Conventional liquid electrolyte LIBs have high capacity performance owing to formed cathode electrolyte interface (CEI) and solid electrolyte interface (SEI), etc. (Pinson & Bazant, 2012). The ion-permeable SEI would allow Li^+ to go through grain boundaries easily. This strong SEI would suppress corrosion reaction with SPE. The passivated and inhomogeneous

interfacial layer would result in lower capacity retention. Usually, these films consist of insoluble products like lithium alkyl carbonates, lithium carbonate, lithium alkoxide, polycarbonates, and others (An et al., 2016). However, flexible LIBs need high ionic conductive flexible electrolyte, high mechanical modulus electrolyte, and stable conductive interfacial layers. Both inorganic solid electrolyte and liquid electrolyte could not fulfill these requirements. Elastic polymer electrolytes could satisfy all these requirements, as discussed in Chapter II.

To achieve high SPE ionic conductivity, polymer electrolytes could mix with other LIBs additives. These additives have been used to improve LIBs cycles life and reduce LIBs capacity loss (Aurbach et al., 2002). Some would minimize capacity loss and improve the LIBs cycle life by surface modification like SO_2 , halogenated additives, alkyl or aryl sulfites (Aurbach et al., 1995) (Ein-Eli, 1997) (Naji et al., 2000) (Wrodnigg, Besenhard, et al., 1999) (Wrodnigg, Wrodnigg, et al., 1999). Among them, fluoroethylene carbonate (FEC) as LIBs electrolyte additive shows a low melting point, high stability for oxidation, and low flammability (less hydrogen available). Single F-C bonding energy (485 KJ/mol) would be more potent than C-O bond (358 KJ/mol) (Smart et al., 2003) (Etacheri et al., 2012). The use of fluorine graphite and fluorine electrolyte have already been investigated (Sato et al., 2011) (Möller et al., 2001). In 1999, McMillan et al. found that FEC could decrease the LIBs capacity loss to 37% after charging/discharging 200 cycles in graphite-based batteries (McMillan et al., 1999). High LIBs performance is attributed to higher electrodes surface area for Li^+ storage, decreasing charge transfer resistance, reduced interfacial layer resistance (Groult et al., 2005). Other fluorinated chemicals like MFE, TTFP have been used in LIBs (Choi et al.,

2006) (Nakai et al., 2011) (Sethuraman et al., 2011), too. Although many researchers reported electrodes surface layer modification in liquid electrolyte-based LIBs, solid-state flexible LIBs still have not been investigated. Additionally, mechanical bending's influence on flexible LIBs electrochemical performance is not clear. Our groups focus on the flexible LIBs but suffer from polymer electrolyte crystallization and low LIBs capacity. To improve our flexible polymer electrolyte electrochemical performance and improve interfacial layer stability, we used FEC as our flexible LIBs additive. We characterized flexible LIBs under different buckling states, environmental temperatures, charging rates. We found that the flexible LIBs capacity was enhanced by 114% after using FEC. The high capacity could attribute to the interfacial layer enhancement.

6.2 Experimental methods

Materials preparation and batteries fabrication: FEC filled and non-filled solid polymer electrolyte (SPE) film and pouch cells were fabricated and characterized through various experimental techniques to investigate the effects of FEC additive. The SPE film was prepared as follows: The lithium bis(oxalate)borate (LiBoB) salt powder (0.6 g) and tetraethylene glycol dimethyl ether (TEGDME) (2 g) were mixed at room temperature. Next, FEC solvent was added to the SPE and stirred mix for two hours at room temperature. Then, 600K M_w PEO powder (2 g) was added to the solution and heated for another 2 hours to obtain gel SPE. The gel electrolyte was hot-pressed at 80°C, 50 KN for 15 mins. Flexible batteries were assembled inside a dry glove box with graphite (anode), SPE, and lithium cobalt oxide (cathode). Both cathode and anode were cut into 4 cm² square shapes. The anode, cathode, and current collector materials were purchased from MTI Corp. Lithium bis(oxalato)borate (LiBoB), tetraethylene glycol dimethyl ether

(TEGDME), 600K Mw PEO bought from Sigma-Aldrich Inc. Ethylene carbonate (EC), diethyl carbonate (DEC), and FEC (around 5% wt. of the SPE) have been used to process electrodes surface during assembly. The reason was investigating the interfacial layer impedance and flexible LIBs energy density changes. The battery components were assembled layer by layer and sealed using a vacuum sealing machine.

Characterization: All of the electrochemical and buckling tests were carried out at $23.6 \pm 0.5^\circ\text{C}$. Flexible LIBs were placed on the mechanical stand Mark-10-ESM 301L. The batteries were bending under 45 degrees, 90 degrees, and 180 degrees by tuning different displacement lengths. The curvature radius at the center was measured using a circle fit method. Electrochemical Spectroscopy Impedance (EIS) of flexible batteries were obtained using Metrohm Autolab Frequency Response Analysis (FRA 2) with frequency range capability from 0.1Hz to 10 MHz and amplitude of 1mV. Nyquist plots simulation was used to create equivalent impedance circuits for analysis. The charge transfer resistance, SEI resistance, bulk resistance were obtained from the fitting plots.

6.3 Results and discussions

Figure 34a and Figure 34b show capacity performance for the flexible pouch cells. The highest capacity $\sim 1.5 \text{ mAh/cm}^2$ is from SPE with FEC based LIB compared with $\sim 0.7 \text{ mAh/cm}^2$ capacity without FEC based LIB. In order to figure out the reason for high performance, we try using the FEC processed graphite and LCO separately. From the yellow line, we observed that the severe capacity loss for FEC processed LCO based LIBs. This should be related to the increased stability toward oxidation. However, we obtain $\sim 1.2 \text{ mAh/cm}^2$ capacity after adding FEC on a graphite surface. The reductive

decomposition of FEC around -0.84 V vs Li/Li^+ would form a stable and homogeneous layer on top of the anode. FEC could not decompose at the cathode surface under pretty lower HOMO. It may form the Li^+ transfer barriers at the boundary between electrolyte and LCO (Dong et al., 2014).

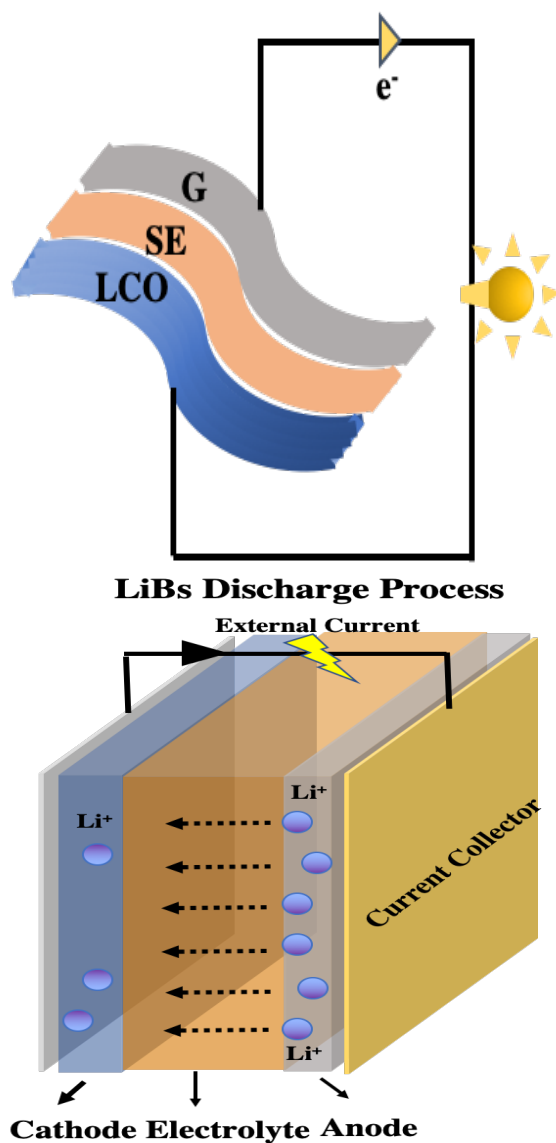
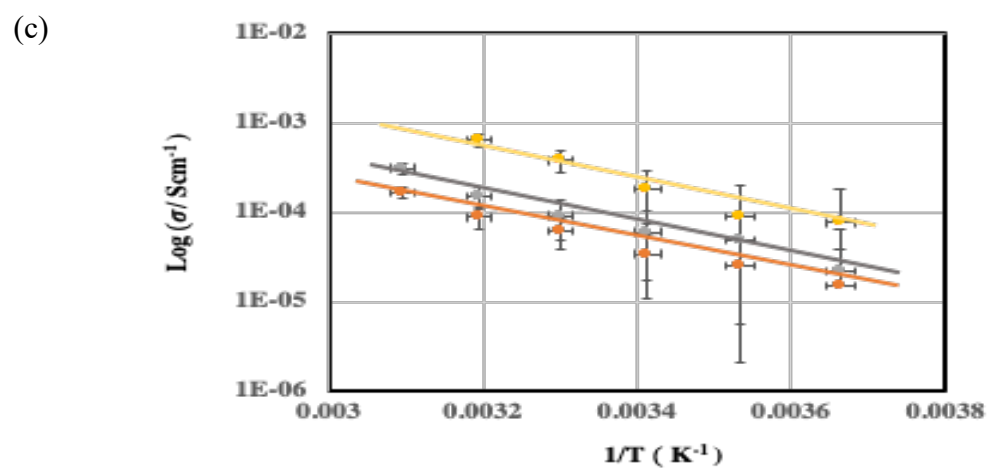
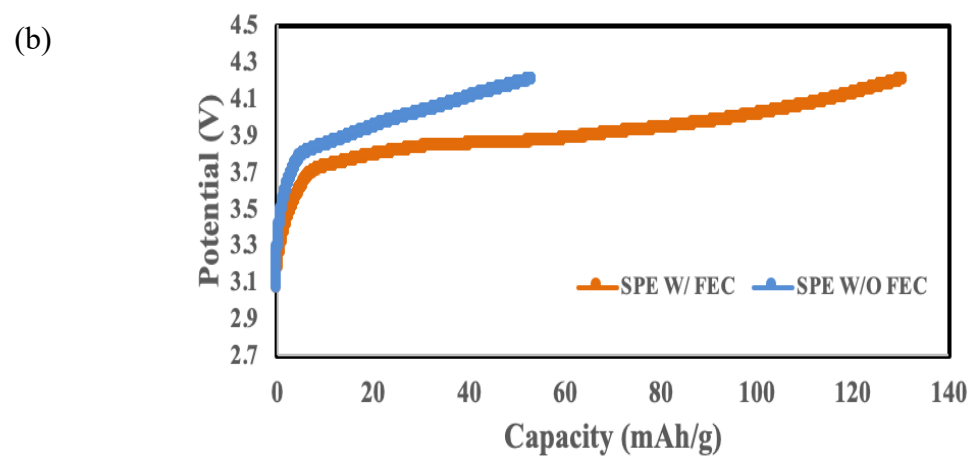
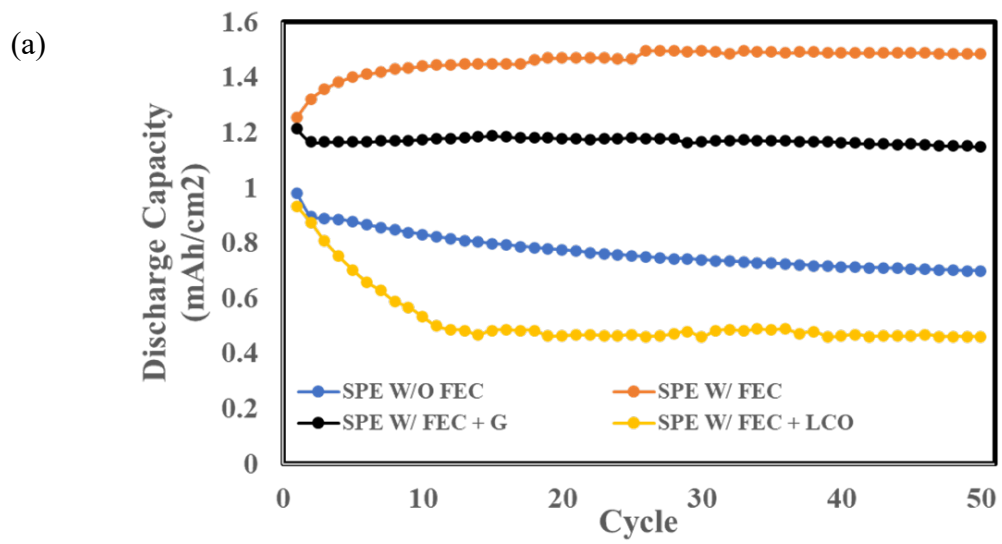


Figure 33 Flexible LiBs and its structures



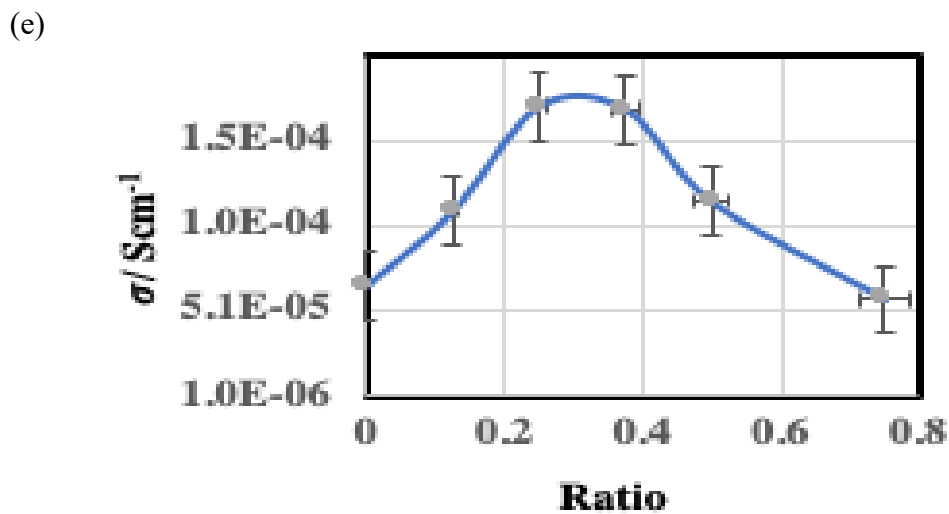
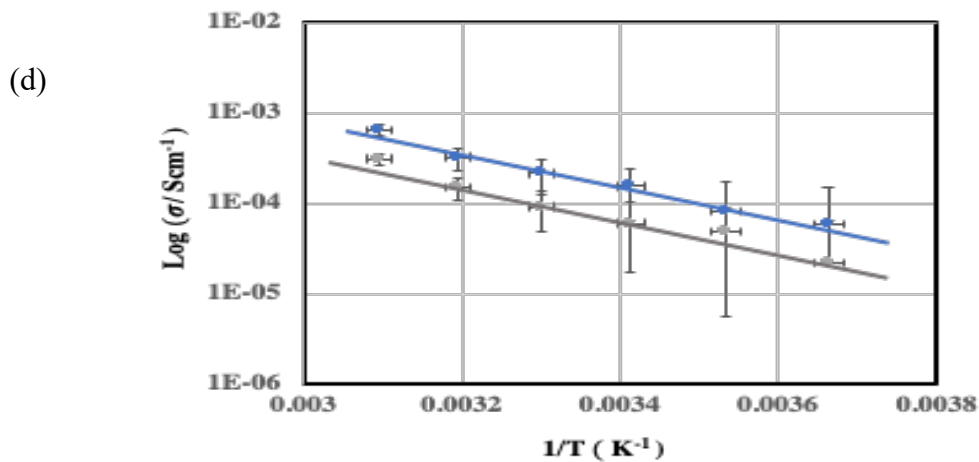


Figure 34 (a) Capacity performance of flexible batteries (SPE including PEO:TEGDME:LiBOB); (b) Effect of FEC on the electrodes' polarization during galvanostatic cycling at room temperature; (c) Ionic conductivity of polymer electrolyte without FEC but under different salt weight ratio (PEO: salt: 1:0.15; 1:0.3; 1:0.45) from bottom orange to upper yellow); (d) electrolyte conductivity with FEC (blue) and without FEC (0.3 salt ratio, gray); (e) different FEC weight ratio (FEC: PEO: 0.15:1; 0.25:1; 0.35:1; 0.5:1; 0.75:1) influence on electrolyte ionic conductivity.

Figure 34c show SPE ionic conductivity test at different temperature for SPE with different salt ratio. When lithium salt weight ratio increases from 0.15 to 0.3, ionic conductivity increases from 8.7×10^{-5} S/cm to 1.2×10^{-4} S/cm at room temperature (298K). When we continue to increase the ratio to 0.45, 6.4×10^{-4} S/cm shows at room temperature. However, the high salt ratio will melt at 45°C (328K). So, we choose 0.3

weight ratio salt SPE as the primary SPE. **Figure 34d** shows SPE ionic conductivity vs $1/T$ plot for 0.3 salt weight ratio SPE and FEC added SPE. Ionic conductivity increases at room temperature (298K). FEC could modify the solvation structure and electrolyte reduction behavior while being innocuous to transport properties. The small amount of FEC is found to have a higher Li^+ solvation structure which shows a higher contact-ion pair ratio (14%) than the parent EC electrolyte (6%). Moreover, Li^+ coordinated FEC would reduce to LiF and passivate anode surface at an early onset (ca. 0.3 V higher than EC) (Hou et al., 2019). From **Figure 34e**, we can see the weight ratio (FEC: PEO) influences on ionic conductivity. We use 0.25 ratio electrolyte for SPE due to the high ionic conductivity.

For FEC processed graphite (black line), we can see that LIB also shows a lower capacity after 1st cycle, which should be related to SEI formation. A steady and homogeneous interfacial layer could form after cycling because reduction reaction at negative potential of FEC -0.84 V vs Li/Li^+ would decompose at graphite surface. For bulk FEC-based SPE, higher dielectric constant SPE coordinates with Li^+ and results in charge carrier concentration increase. At higher concentration FEC, the dilution of Li^+ would result in poor capacity.

The high concentration LiF and Li_2CO_3 on top of graphite may blocks the electrons transfer and results in a high performance. For electrode with FEC processing, it shows high capacity. The reason could be divided into two parts. One is the smooth SEI formation. Second reason could be related to FEC increasing the free volume between chains. Their mechanical strength may also hinder the dendrite growth. Low crystallization region and high amorphous region should be another reason.

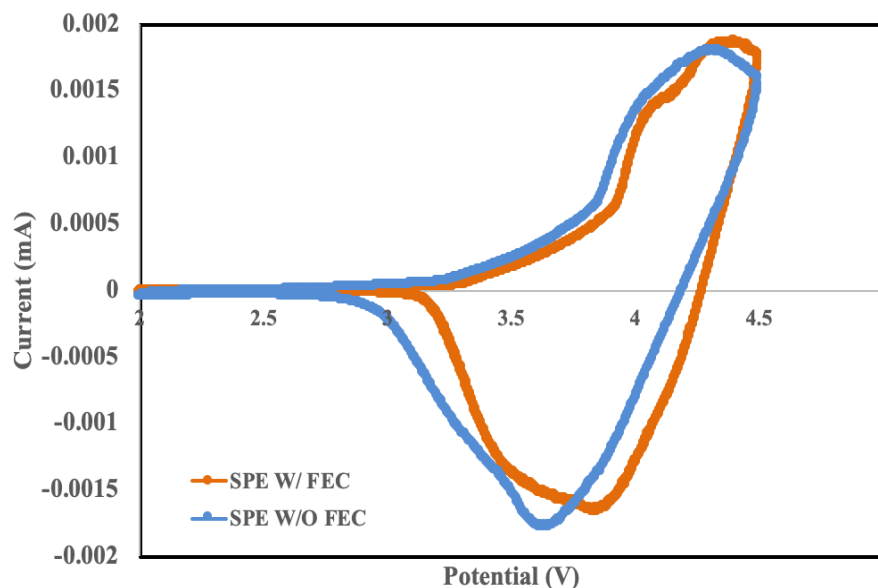


Figure 35 Cyclic voltammetry plot for full cells (LCO/SPE/G Structure) at 0.1mV/s

Figure 35 shows the CV test for FEC and FEC-free batteries. We could see that FEC batteries have clear two peaks (4.0V and 4.2 V, respectively) during the anodic scan. FEC-free batteries show one peak at around 4.1V. This should be related to Li^+ delithiation process from LCO where surface Li^+ would go through a more compact and homogeneous SEI layer at lower potential (4.0V) and mass Li^+ transfer at higher potential. During the cathodic scan, a reduction peak also moves right for FEC batteries. This shows the higher polarization for FEC batteries which also correspond with the higher bulk resistance observed in **Figure 39**. The clear polarization around 200 mV decreases after using FEC. This means a better interfacial film formation on top of the electrodes (Smart et al., 2003). **Figure 44** also shows the FEC processed LCO and Graphite electrode flexible LIBs. We could see the clear lower reduction and oxidation peak from FEC processed LCO LIBs. This should be related to incomplete electrochemical reactions at the LCO electrode surface.

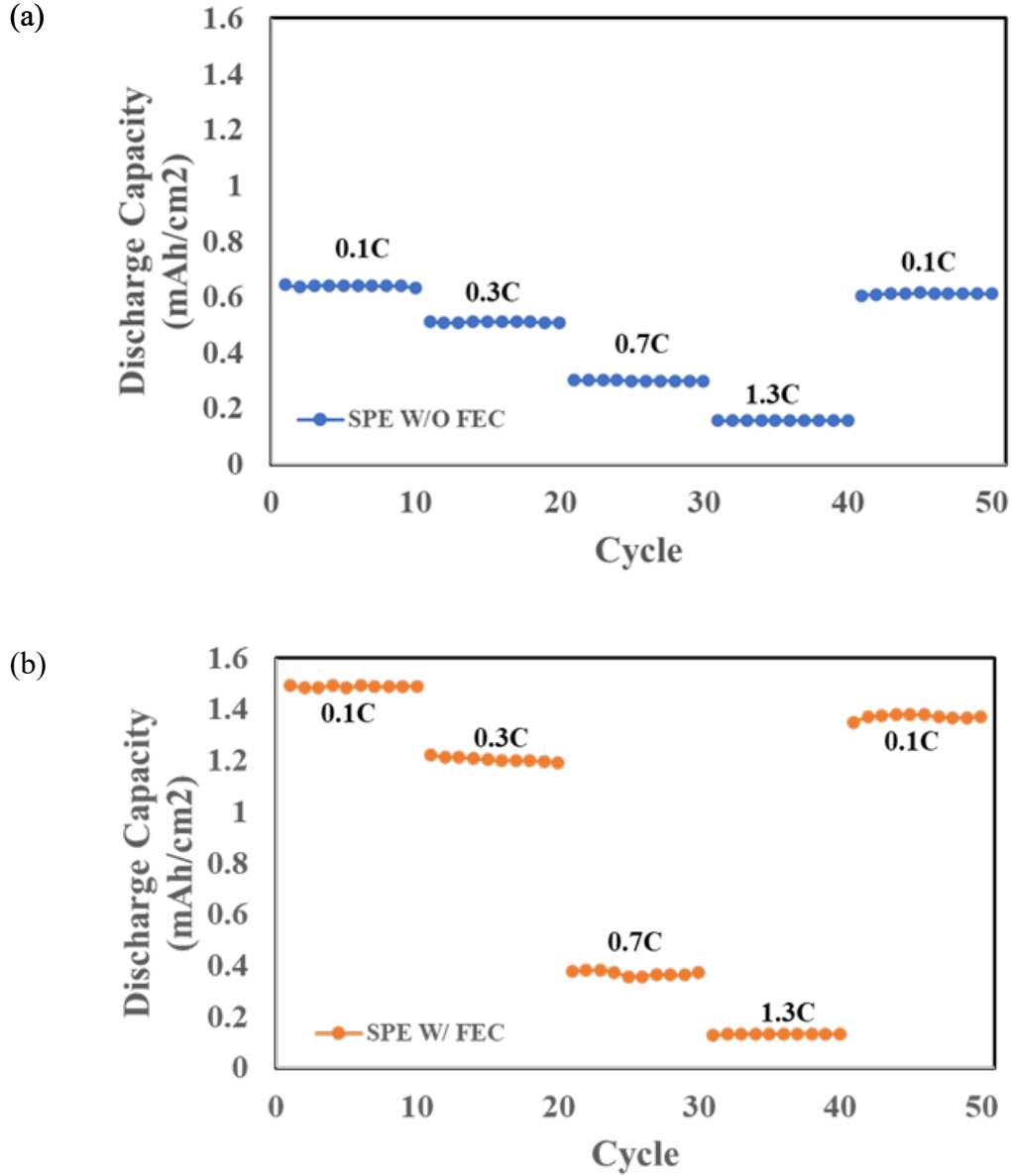


Figure 36 Rate capability test of batteries (a): No FEC added in SPE based LIBs; (b): FEC mixed with SPE based LIBs.

Figure 36 shows the rate capability test for batteries with and without FEC. We can see that at a higher C rate, the SPE-FEC-based flexible battery shows lower capacity performance. The specific mechanism leading to capacity decrease is not clear and needs to be investigated further. We charge our batteries at different current like 0.083 (0.1C),

0.166 (0.3C), 0.415 (0.7C), 0.830 (1.3C) mA/cm². 1.500 mAh/cm² and 0.700 mAh/cm² capacity showed at same current density. From 0.166 to 0.415 mA/cm², we found higher capacity loss for FEC added LIBs. The lower ionic conductivity limits the transfer at a higher charge and discharge current in batteries without FEC.

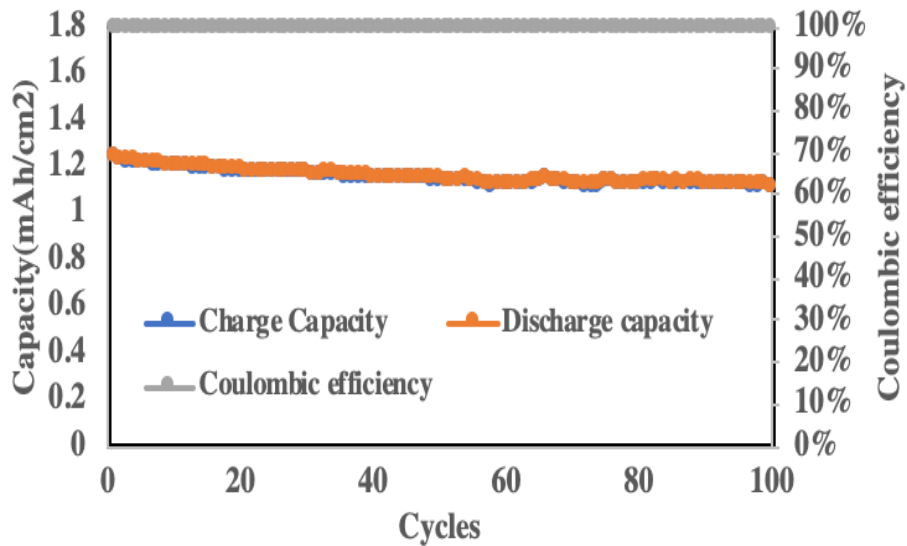


Figure 37 FEC & SPE device performance under 0.12C rate

Figure 37 shows LIB with FEC charges and discharges 100 cycles after rate capability test. It shows 1.25 mAh/cm² and has 94.1% capacity retention after 100 cycles. This illustrates the higher performance for steady flexible batteries. The smooth plot line illustrates steady LIBs.

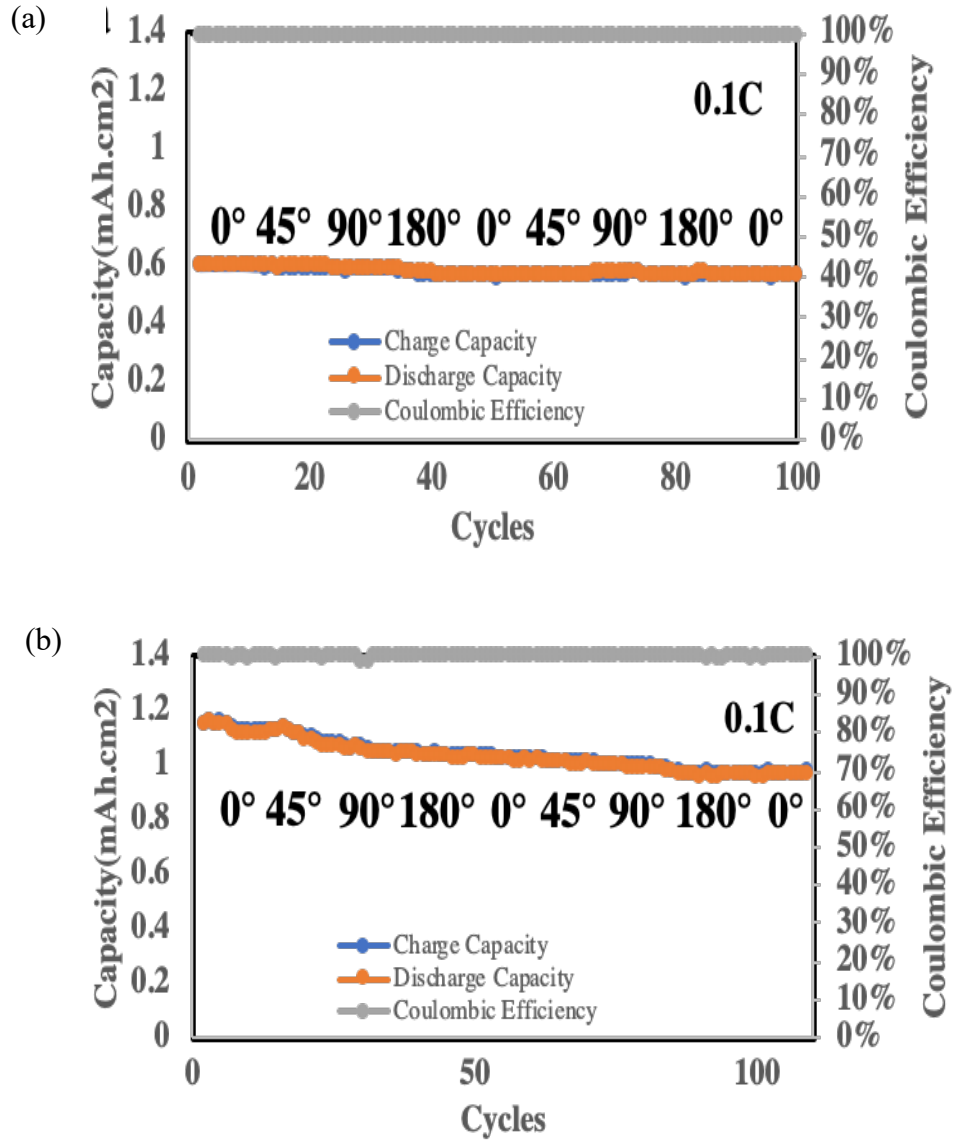


Figure 38 LIBs capacity performance under bending state (a) pristine electrolyte LIBs without FEC; (b) LIBs with FEC capacity performance.

Figure 38 shows batteries under different bending test from 45°, 90° to 180°. Commercial Samsung Galaxy Z Flip series smartphones could be folded at 180° degrees. We found that the capacity is steady in different bending angles, which means higher stability pouch cells fabricated. This type of battery could be used in future flexible electronics. The reason for the high performance under different buckling states is from

stable interfacial layer formation, which could tolerate the shape change. In addition, the bending state could enhance the compact interface between electrolyte and electrodes. The stress distribution on the surface has already been investigated in our group by both model and experiments (Berg et al., 2017). High modulus LiF (shear modulus around 55.1Gpa reported) could be steady under bucking conditions (Xu et al., 2014).

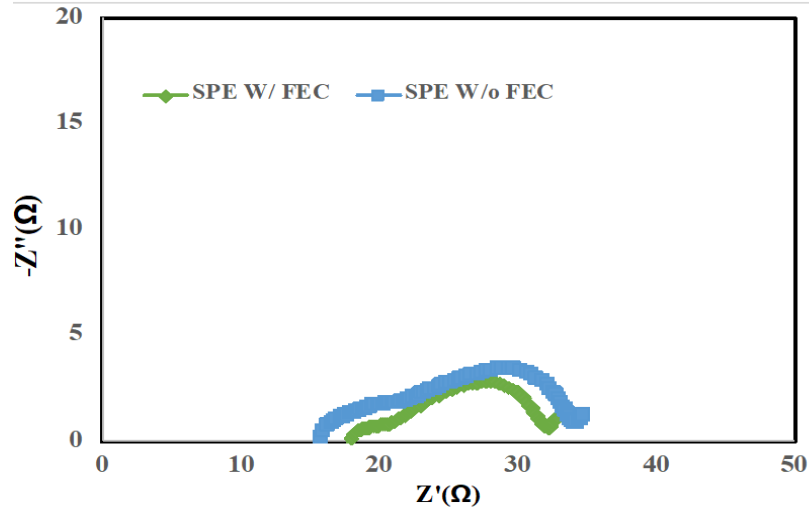


Figure 39 Impedance spectroscopy for SPE with FEC battery and FEC free battery

Figure 39 shows flexible LIBs impedance test for batteries with and without FEC. At the high frequency region, the first semi-circle is related to the SEI layer. In the middle frequency region, the semi-circle is related to the charge transfer. The low frequency region is related to Warburg resistance for the diffusion process (Groult et al., 2005). Bulk resistance from FEC based LIBs is 18.2Ω which is higher than 15.4Ω without FEC. However, charge transfer resistance decreases significantly from 16.9Ω to 9.0Ω . SEI resistance also decreases from 8.2Ω to 4.8Ω . This should be related to the stable buffer layer formation, which still needs to be investigated further. The lower impedance illustrates the faster charge transfer across the electrolyte and electrode interface because the Li^+ intercalation and deintercalation process change. Different

surface films have different Li^+ migration kinetics. From the impedance plot (**Figure 45**), we observe the capacitive effect in FEC processed LCO based LIB. A high imaginary number of impedances should be from the voids or imperfect interface. This could result in poor capacity performance. This impedance measurement addresses the varied charge transfer phenomenon across the surface films.

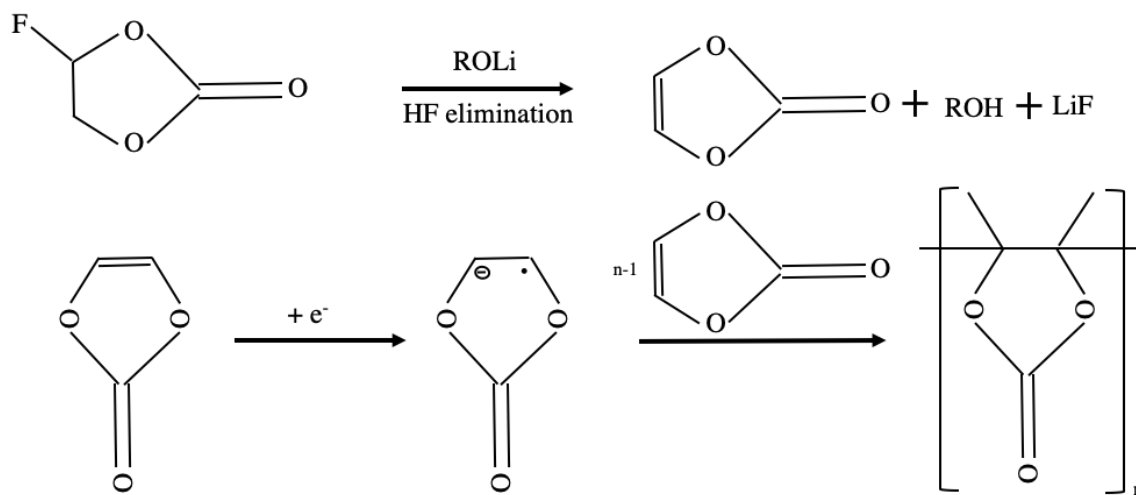


Figure 40 FEC decomposition mechanism

Etacheri et al. propose the FEC decomposition mechanism (**Figure - 40**) (Etacheri et al., 2012). HF elimination on the anode surface would form VC, which would polymerize and form the polycarbonate species. Then part of carbonate groups would form functional $-\text{OCO}_2\text{Li}$ groups.

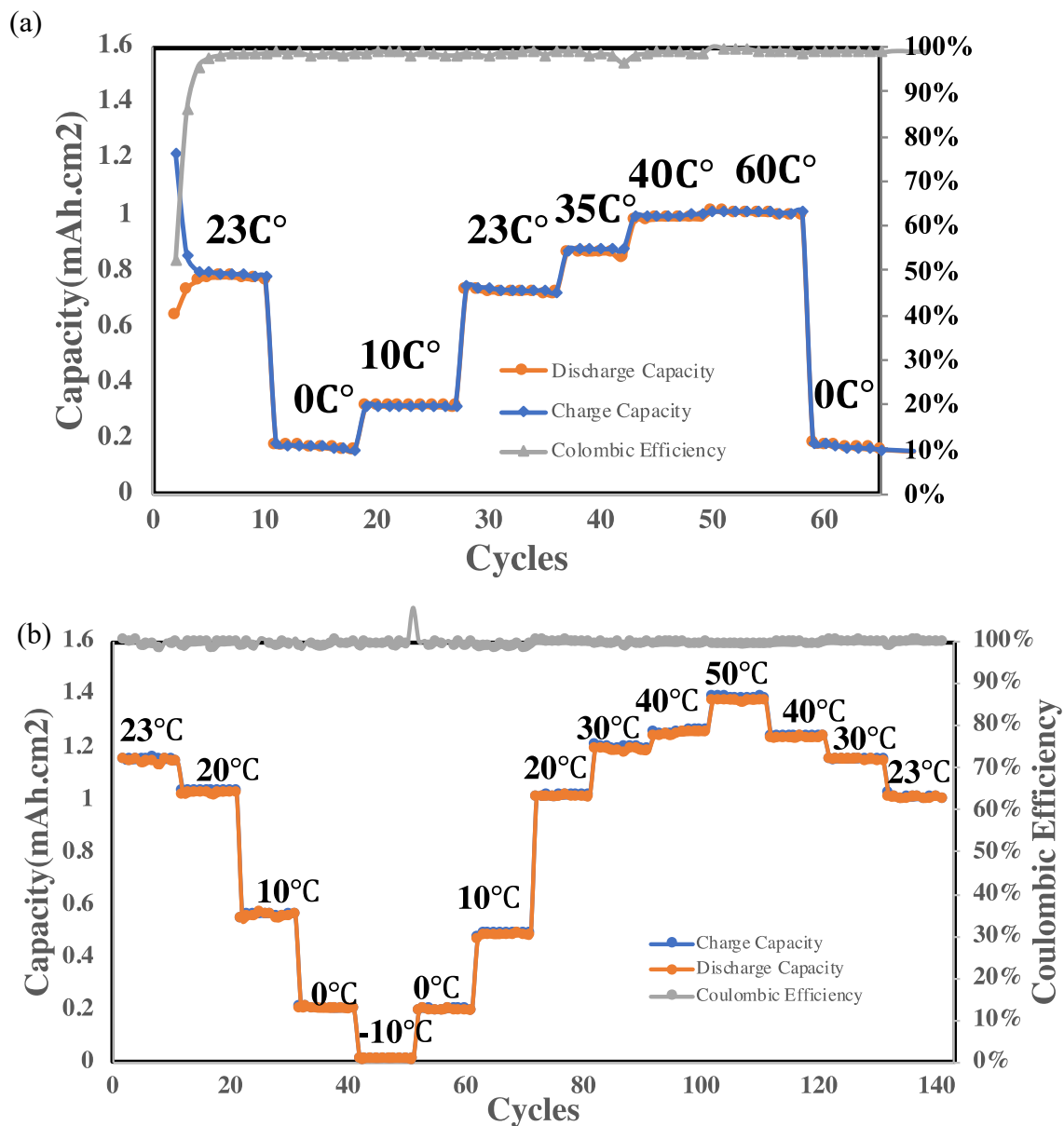


Figure 41 (a) Thermal cycling performance at different temperature for pristine polymer LIBs; (b) performance after adding FEC inside polymer electrolyte

Figure 41 shows the thermal performance of the batteries from -10 °C to 60 °C with and without FEC. We can see that the capacity decreases dramatically from RT to 10°C. This capacity decrease also coincides with the SPE chains lower mobility when the temperature decreases. If we continue to reduce the temperature, the capacity shows

0.164 mAh/cm², 0.196 mAh/cm² at 0°C, respectively. At -10°C, the capacity shows 0.006 mAh/cm² for FEC added batteries. At 23°C, the capacity shows 0.737 mAh/cm², 1.001 mAh/cm² for LIBs without FEC and with FEC, respectively. At 40°C, the capacity shows 0.998 and 1.247 mAh/cm² for LIBs without FEC and with FEC, respectively. At 50°C, FEC added LIBs capacity shows 1.360 mAh/cm², which is even higher than 1.008 mAh/cm² at 60°C FEC free LIBs.

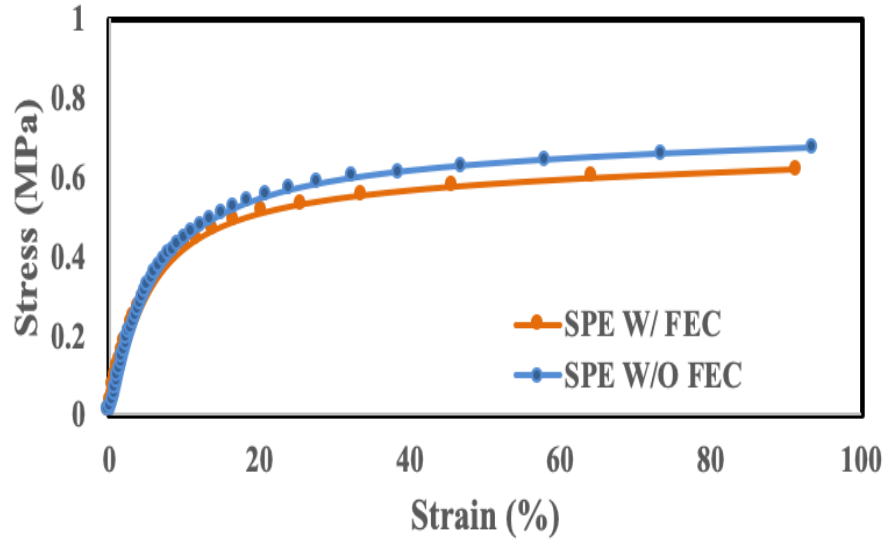


Figure 42 stress – strain plot of electrolyte

Figure 42 shows the stress–strain plot of the solid polymer electrolyte (SPE). The mechanical young's modulus is calculated to be 6.2 and 6.0 Mpa for the SPE with and without FEC, respectively. The mechanical modulus is similar. It means FEC added SPE does not influence SPE mechanical property significantly.

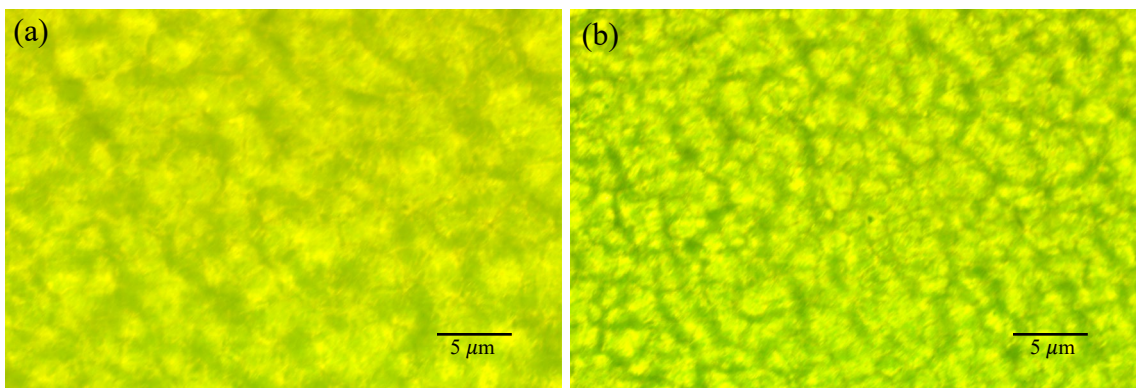


Figure 43 (a) Polarized optical microscopy plot of electrolyte with FEC; (b) S polarized optical microscopy plot of SPE without FEC.

Figure 43 shows polarized optical microscopy of the electrolyte with and without FEC. We could observe the clear crystals distribution and amorphous regions in the SPE sample without FEC. After mixing with FEC, more amorphous regions form and connect with each other. This can explain the reason for higher conductivity and better capacity achieved in the SPE-FEC-based flexible battery.

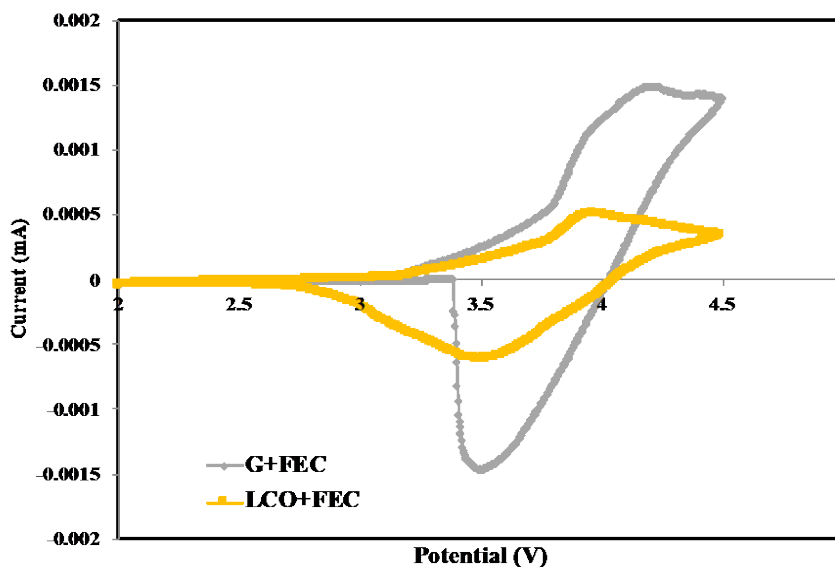


Figure 44 CV plot for LCO+FEC based LIBs and G+FEC based LIBs, scan rate at 0.1mV/s.

Figure 44 shows the CV curve for the FEC processed LCO LIBs and FEC processed graphite LIBs. Compared with **Figure 35**, FEC processed graphite shows a similar reduction and oxidation peak value, which has a good match with higher capacity

LIBs obtained. LCO processed LIBs show slightly higher oxidation potential which may attribute to the incomplete interfacial layer formation.

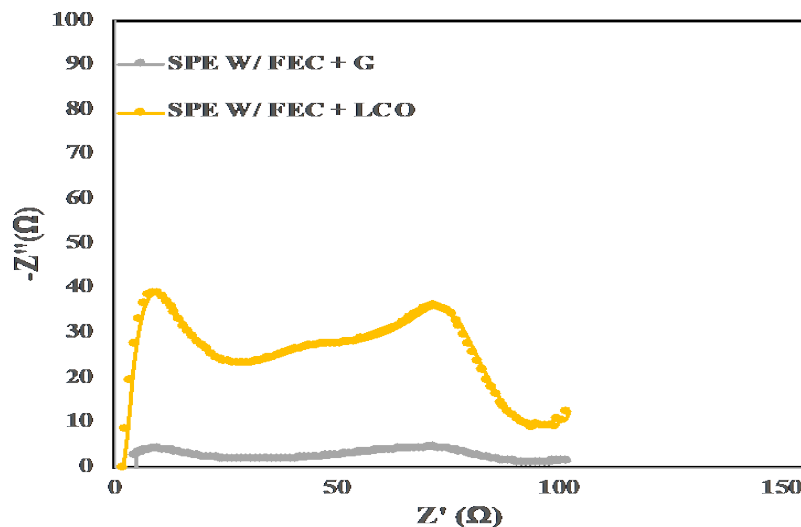


Figure 45 Impedance measurement for SPE with FEC processed Graphite electrode; FEC processed LCO electrode

Figure 45 shows impedance plots for FEC processed graphite LIBs and FEC processed LCO LIBs. The bulk resistances are 7.1Ω and 7.6Ω for FEC+G and FEC+LCO, respectively. The interfacial layer resistances are 21.4Ω and 38.2Ω , respectively. The difference between interlayer resistance also confirms the poor interface layer formation in FEC processed LIBs.

6.4 Conclusions

In all, fast Li^+ uptake and less resistance could be achieved by the formation of FEC-derived SEI. The Li^+ transport across the interface layer attributes to the higher fraction polar carbonate ($-\text{CO}_3^-$), Li_2CO_3 and stable disordered LiF structure, which has higher surface interfacial energy. The critical role of FEC in tailoring the Li^+ solvation structure and as-formed protective SEI composition provides both electrochemical and mechanistic insights that will aid in the rational future novel electrolytes design.

Fluoroethylene carbonate (FEC) as a battery additive has already been used in the last two decades in liquid electrolyte-based batteries. Here, we investigate the effect of FEC inside the solid polymer electrolyte system and on the surfaces of the electrodes. The electrochemical performance and surface chemistry have been characterized. Improved cycle stability (over 95% capacity retention after 100 cycles) and good capacity (130.7mAh/g) were achieved by stable and homogenous interfacial layer formation. The significant improved electrochemical performance is related to the FEC reduction and its effect on charge transfer inside the electrolyte. Our flexible LIBs show slight degradation after bending at 180 degrees. The wide working temperature range (-10°C to 60°C) also make LIBs applicable for varied environments.

CHAPTER VII. CONCLUSIONS AND FUTURE WORKS

7.1 Conclusions

This thesis investigates interfaces in solid polymer electrolyte (SPE) based flexible lithium-ion batteries (LIBs). Flexible LIBs and spiral stretchable LIBs are designed and fabricated. Several methods to enhance the interfaces in flexible LIBs are explored, including new fabrication strategies and using LIBs additives. From TSB modified LIBs (Chapter III) to FEC modified LIBs (Chapter VI), SPE-based LIBs capacity shows an increase to a maximum of 1.50 mAh/cm² due to the enhanced interfacial layer formed between electrodes and electrolyte. Here, we verify that flexible LIBs electrochemical performance is highly influenced by the LIBs materials and the interfacial layer stability. Specifically, TSB optimized SPE has reduced crystallization regions, enhancing SPE ionic conductivity and LIB capacity. Flexible LIBs show high cycle stability and energy density by using hot-pressing prepared SPE. The improved interfaces between electrodes and electrolytes could form stable interfacial layers. Furthermore, we use thermal pressing methods to enhance electrode surface particles' contact with polymer electrolyte chains because thermal pressing would decrease the interfacial layer resistance. Additionally, stable flexible LIBs were subjected to mechanical bending at different bending angles. It was found that varied bending angles did not influence the flexible battery's energy density and open-circuit voltage. Furthermore, our stretchable LIBs also have long-lasting capacity retention even under 6000% deformation due to the stable interfacial layer formation. These spiral-shaped LIBs show high electrochemical and mechanical properties. In addition to mixing FEC with SPE, we find that FEC additive also works on anode surface layer during battery assembly, which contributes stable and

high ionic conductive SEI layer. Flexible battery safety is also examined through a destructive test such as battery puncturing. We find that punctured flexible LIBs could still power the LED light. Owing to LIB's high energy density, our durable and safe solid polymer electrolyte flexible lithium-ion batteries are promising for future applications.

7.2 Future works

SPE-based LIBs would be very promising and suitable for wearable & flexible electronics applications. However, future solid-state flexible LIBs need to have fast charge/discharge, high energy density, high cycle stability, safety, high power density, and low cost. For quick charge/discharge, SPE-based LIBs suffer from low SPE ionic conductivity due to few polymer chains freedom regions at room temperature. In addition, polymer crystallization needs to be considered under 0°C. Improving SPE ionic conductivity, decreasing polymer crystallization, and increasing SPE electrochemical windows will be a good future plan. Inorganic solid electrolyte-based LIBs have a high working temperature range and do not have any crystallization or lower ionic conductivity issues. But inorganic solid electrolyte-based LIBs are limited by poor interfacial conductivity and compatibility between electrodes and electrolyte. Inorganic and organic composite electrolytes could be another future direction, but further investigation is needed, especially regarding the high cost of ceramic electrolytes. For prospective commercial LIBs, alternative anodes can be investigated. For example, lithium metal anode can provide high capacity. However, lithium metal anode faces dendrite growth, lithium plating, and safety issues. Si anode also provides high capacity but has ~400% volume change and capacity fading problems. Li-air batteries face cycle stability issues. The sulfur electrode has a shuttle effect, and capacity fading issues. LCO,

NCA, NCM materials as cathodes are limited by Co, Ni production, cost and low decomposition temperature (around 200 °C). The interface between solid electrodes and electrolyte needs more accurate methods for characterizations. Although our flexible LIBs work well, more research effort is needed to understand the self-discharge, interfacial layer formation, and electrode morphologies during the charging and discharging process.

REFERENCES

- Abbrent, S., Plestil, J., Hlavata, D., Lindgren, J., Tegenfeldt, J., & Wendsjö, Å. (2001). Crystallinity and morphology of PVdF–HFP-based gel electrolytes. *Polymer*, 42(4), 1407–1416.
- Adachi, G. Y., Imanaka, N., & Aono, H. (1996). *Fast Li⁺ conducting ceramic electrolytes*.
- Agyemang, F. O., Li, F., Momade, F. W. Y., & Kim, H. (2016). Effect of poly (ethylene oxide) and water on electrospun poly (vinylidene fluoride) nanofibers with enhanced mechanical properties as pre-filter for oil-in-water filtration. *Materials Chemistry and Physics*, 182, 208–218.
- Alamgir, M., & Abraham, K. M. (1995). POWER sggRm Room temperature rechargeable polymer electrolyte. *Journal of Power Sources*, 54, 40–45.
- Amatucci, G. G., Pereira, N., Zheng, T., & Tarascon, J.-M. (2002). Failure Mechanism and Improvement of the Elevated Temperature Cycling of LiMn₂O₄ Compounds Through the Use of the LiAl_xMn_{2-x}O₄-zFz Solid Solution. *Journal of The Electrochemical Society*, 148(2), A171. <https://doi.org/10.1149/1.1342168>
- Amatucci, G., & Tarascon, J.-M. (2002). Optimization of Insertion Compounds Such as LiMn₂O₄ for Li-Ion Batteries. *Journal of The Electrochemical Society*, 149(12), K31. <https://doi.org/10.1149/1.1516778>
- Amine, K., Liu, J., & Belharouak, I. (2005). High-temperature storage and cycling of C-LiFePO₄/graphite Li-ion cells. *Electrochemistry Communications*, 7(7), 669–673.
- Angulakshmi, N., Nahm, K. S., Nair, J. R., Gerbaldi, C., Bongiovanni, R., Penazzi, N., & Stephan, A. M. (2013). Cycling profile of MgAl₂O₄-incorporated composite electrolytes

- composed of PEO and LiPF₆ for lithium polymer batteries. *Electrochimica Acta*, 90, 179–185.
- Angulakshmi, N., Nahm, K. S., Swaminathan, V., Thomas, S., & Nimma Elizabeth, R. (2012a). Nanocomposite polymer electrolytes for lithium batteries. *Polymer Processing and Characterization*, 394(July), 55–65. <https://doi.org/10.1201/b13105>
- Angulakshmi, N., Nahm, K. S., Swaminathan, V., Thomas, S., & Nimma Elizabeth, R. (2012b). Nanocomposite polymer electrolytes for lithium batteries. *Polymer Processing and Characterization*, 394(July), 55–65. <https://doi.org/10.1201/b13105>
- Appetecchi, G. B., Croce, F., & Scrosati, B. (1995). Kinetics and stability of the lithium electrode in poly(methylmethacrylate)-based gel electrolytes. *Electrochimica Acta*, 40(8), 991–997. [https://doi.org/10.1016/0013-4686\(94\)00345-2](https://doi.org/10.1016/0013-4686(94)00345-2)
- Appetecchi, G B, Croce, F., & Scrosati, B. (1995). Kinetics and stability of the lithium electrode in poly (methylmethacrylate)-based gel electrolytes. *Electrochimica Acta*, 40(8), 991–997.
- Appetecchi, G B, Scaccia, S., & Passerini, S. (2000). Investigation on the stability of the lithium-polymer electrolyte interface. *Journal of the Electrochemical Society*, 147(12), 4448.
- Appetecchi, Giovanni Battista, Croce, F., Romagnoli, P., Scrosati, B., Heider, U., & Oesten, R. (1999). High-performance gel-type lithium electrolyte membranes. *Electrochemistry Communications*, 1(2), 83–86. [https://doi.org/10.1016/S1388-2481\(99\)00011-9](https://doi.org/10.1016/S1388-2481(99)00011-9)
- Aravindan, V., & Vickraman, P. (2007). A study on LiBOB-based nanocomposite gel polymer electrolytes (NCGPE) for Lithium-ion batteries. *Ionics*, 13(4), 277–280.
- Arico, A. S., Bruce, P., Scrosati, B., Tarascon, J.-M., & Van Schalkwijk, W. (2011).

- Nanostructured materials for advanced energy conversion and storage devices. In *Materials for sustainable energy: a collection of peer-reviewed research and review articles from Nature Publishing Group* (pp. 148–159). World Scientific.
- Aricò, A. S., Bruce, P., Scrosati, B., Tarascon, J. M., & Van Schalkwijk, W. (2005). Nanostructured materials for advanced energy conversion and storage devices. In *Nature Materials*. <https://doi.org/10.1038/nmat1368>
- Armand, M., Endres, F., MacFarlane, D. R., Ohno, H., & Scrosati, B. (2011). Ionic-liquid materials for the electrochemical challenges of the future. In *Materials For Sustainable Energy: A Collection of Peer-Reviewed Research and Review Articles from Nature Publishing Group* (pp. 129–137). World Scientific.
- Armstrong, A. R., Armstrong, G., Canales, J., García, R., & Bruce, P. G. (2005). Lithium-Ion Intercalation into TiO₂-B Nanowires. *Advanced Materials*, 17(7), 862–865.
- Raccichini, R., Varzi, A., Passerini, S., & Scrosati, B. (2015). The role of graphene for electrochemical energy storage. *Nature materials*, 14(3), 271-279.
- Aurbach, D., Zaban, A., Ein-Eli, Y., Weissman, I., Chusid, O., Markovsky, B., Levi, M., Levi, E., Schechter, A., & Granot, E. (1997). Recent studies on the correlation between surface chemistry, morphology, three-dimensional structures and performance of Li and Li-C intercalation anodes in several important electrolyte systems. *Journal of Power Sources*, 68(1), 91–98.
- Aurbach, Doron, Ein-Eli, Y., Markovsky, B., Zaban, A., Luski, S., Carmeli, Y., & Yamin, H. (1995). The study of electrolyte solutions based on ethylene and diethyl carbonates for rechargeable Li batteries: II. Graphite electrodes. *Journal of The Electrochemical Society*, 142(9), 2882.

- Aurbach, Doron, Gamolsky, K., Markovsky, B., Gofer, Y., Schmidt, M., & Heider, U. (2002). On the use of vinylene carbonate (VC) as an additive to electrolyte solutions for Li-ion batteries. *Electrochimica Acta*, 47(9), 1423–1439.
- Aurbach, Doron, Gamolsky, K., Markovsky, B., Salitra, G., Gofer, Y., Heider, U., Oesten, R., & Schmidt, M. (2000). The study of surface phenomena related to electrochemical lithium intercalation into Li_xMO_y host materials ($\text{M} = \text{Ni}, \text{Mn}$). *Journal of The Electrochemical Society*, 147(4), 1322.
- Aurbach, Doron, McCloskey, B. D., Nazar, L. F., & Bruce, P. G. (2016). Advances in understanding mechanisms underpinning lithium–air batteries. *Nature Energy*, 1(9), 1–11.
- Bae, J., Li, Y., Zhang, J., Zhou, X., Zhao, F., Shi, Y., Goodenough, J. B., & Yu, G. (2018). A 3D Nanostructured Hydrogel-Framework-Derived High-Performance Composite Polymer Lithium-Ion Electrolyte. *Angewandte Chemie - International Edition*, 57(8), 2096–2100. <https://doi.org/10.1002/anie.201710841>
- Balbuena, P. B., & Wang, Y. (2004). *Lithium-ion batteries: solid-electrolyte interphase*. Imperial college press.
- Balducci, A. (2017). Ionic liquids in lithium-ion batteries. In *Ionic Liquids II* (pp. 1–27). Springer.
- Ban, C., Wu, Z., Gillaspie, D. T., Chen, L., Yan, F., Blackburn, J. L., & Dillon, A. C. (2010). Nanostructured Fe_3O_4 /SWNT electrode: Binder-free and high-rate Li-ion anode. *Advanced Materials*. <https://doi.org/10.1002/adma.200904285>
- Bao, Y., Hong, G., Chen, Y., Chen, J., Chen, H., Song, W. L., & Fang, D. (2020). Customized Kirigami Electrodes for Flexible and Deformable Lithium-Ion Batteries. *ACS Applied*

- Materials and Interfaces*. <https://doi.org/10.1021/acsami.9b18232>
- Bard, A. J., Abruña, H. D., Chidsey, C. E., Faulkner, L. R., Feldberg, S. W., Itaya, K., Majda, M., Melroy, O., Murray, R. W., Porter, M. D., Soriaga, M. P., & White, H. S. (1993). The electrode/electrolyte interface - A status report. *Journal of Physical Chemistry*, 97(28), 7147–7173. <https://doi.org/10.1021/j100130a007>
- Bard, A. J., & Faulkner, L. R. (1980). : Fundamentals and Applications. In *Annual Review of Materials Science*. <https://doi.org/10.1146/annurev.matsci.30.1.117>
- Bard, A. J., & Faulkner, L. R. (2001). Fundamentals and applications. *Electrochemical Methods*, 2(482), 580–632.
- Baskaran, R., Selvasekarapandian, S., Kuwata, N., Kawamura, J., & Hattori, T. (2007). Structure, thermal and transport properties of PVAc–LiClO₄ solid polymer electrolytes. *Journal of Physics and Chemistry of Solids*, 68(3), 407–412.
- Batteries, R. L. (1997). *L 'fJ*. 144(4), 1–7.
- Belcher, A. M., Wu, X. H., Christensen, R. J., Hansma, P. K., Stucky, G. D., & Morse, D. E. (1996). Control of crystal phase switching and orientation by soluble mollusc-shell proteins. *Nature*, 381(6577), 56–58.
- Bengio, Y. (2009). Learning Deep Architectures for AI. In *Foundations and Trends® in Machine Learning* (Vol. 2, Issue 1). <https://doi.org/10.1561/22000000006>
- Berg, S., Akturk, A., Kammoun, M., & Ardebili, H. (2017). Flexible batteries under extreme bending: Interfacial contact pressure and conductance. *Extreme Mechanics Letters*, 13, 108–115.
- Bergman, M., Bergfelt, A., Sun, B., Bowden, T., Brandell, D., & Johansson, P. (2015). Graft copolymer electrolytes for high temperature Li-battery applications, using poly (methyl

- methacrylate) grafted poly (ethylene glycol) methyl ether methacrylate and lithium bis (trifluoromethanesulfonimide). *Electrochimica Acta*, 175, 96–103.
- Berkes, B. B., Jozwiuk, A., Sommer, H., Brezesinski, T., & Janek, J. (2015). Simultaneous acquisition of differential electrochemical mass spectrometry and infrared spectroscopy data for in situ characterization of gas evolution reactions in lithium-ion batteries. *Electrochemistry Communications*, 60, 64–69.
- Bettinger, C. J., & Bao, Z. (2010). Biomaterials-based organic electronic devices. *Polymer International*, 59(5), 563–567.
- Bhattacharya, A. (2000). Radiation and industrial polymers. *Progress in Polymer Science*, 25(3), 371–401.
- Błażejczyk, A., Wieczorek, W., & Kovarsky, R. (2004). d. Golodinsky, e. Peled, LG Scanlon GB Appatecchi, B. Scrosati, j. *Electrochem. Soc*, 151, A1762.
- Blyth, R. I. R., Buqa, H., Netzer, F. P., Ramsey, M. G., Besenhard, J. O., Golob, P., & Winter, M. (2000). XPS studies of graphite electrode materials for lithium ion batteries. *Applied Surface Science*, 167(1–2), 99–106.
- Bohnke, O., Frand, G., Rezrazi, M., Rousselot, C., & Truche, C. (1993a). Fast ion transport in new lithium electrolytes gelled with PMMA. 1. Influence of polymer concentration. *Solid State Ionics*, 66(1–2), 97–104.
- Bohnke, O., Frand, G., Rezrazi, M., Rousselot, C., & Truche, C. (1993b). Fast ion transport in new lithium electrolytes gelled with PMMA. 2. Influence of lithium salt concentration. *Solid State Ionics*, 66(1–2), 105–112.
- Bohnke, O., Rousselot, C., Gillet, P. A., & Truche, C. (1992). Gel Electrolyte for Solid-State Electrochromic Cell. *Journal of the Electrochemical Society*, 139(7), 1862–1865.

- Bottino, A., Capannelli, G., Monticelli, O., & Piaggio, P. (2000). Poly (vinylidene fluoride) with improved functionalization for membrane production. *Journal of Membrane Science*, 166(1), 23–29.
- Bresser, D., Passerini, S., & Scrosati, B. (2013). Recent progress and remaining challenges in sulfur-based lithium secondary batteries - a review. *Chemical Communications*, 49(90), 10545–10562. <https://doi.org/10.1039/c3cc46131a>
- Bruce, P. G., Freunberger, S. A., Hardwick, L. J., & Tarascon, J.-M. (2012). Li–O₂ and Li–S batteries with high energy storage. *Nature Materials*, 11(1), 19.
- Buqa, H., Goers, D., Holzapfel, M., Spahr, M. E., & Novák, P. (2005). High rate capability of graphite negative electrodes for lithium-ion batteries. *Journal of the Electrochemical Society*, 152(2), A474.
- Cahn, J. W. (1961). On spinodal decomposition. *Acta Metallurgica*, 9(9), 795–801.
- Cao, J., Chen, C., Zhao, Q., Zhang, N., Lu, Q., Wang, X., Niu, Z., & Chen, J. (2016). A Flexible Nanostructured Paper of a Reduced Graphene Oxide–Sulfur Composite for High-Performance Lithium–Sulfur Batteries with Unconventional Configurations. *Advanced Materials*, 28(43), 9629–9636.
- Cao, L., Li, L., Xue, Z., Yang, W., Zou, H., Chen, S., & Liu, Z. (2020). The aluminum current collector with honeycomb-like surface and thick Al₂O₃ film increased durability and enhanced safety for lithium-ion batteries. *Journal of Porous Materials*, 27(6), 1677–1683.
- Cao, Y.-C., Xu, C., Wu, X., Wang, X., Xing, L., & Scott, K. (2011). A poly (ethylene oxide)/graphene oxide electrolyte membrane for low temperature polymer fuel cells. *Journal of Power Sources*, 196(20), 8377–8382.

- Carnes, C. L., & Klabunde, K. J. (2002). Unique chemical reactivities of nanocrystalline metal oxides toward hydrogen sulfide. *Chemistry of Materials*, 14(4), 1806–1811.
- Carroll, K. J., Qian, D., Fell, C., Calvin, S., Veith, G. M., Chi, M., Baggetto, L., & Meng, Y. S. (2013). Probing the electrode/electrolyte interface in the lithium excess layered oxide Li 1.2 Ni 0.2 Mn 0.6 O 2. *Physical Chemistry Chemical Physics*, 15(26), 11128–11138.
- Castro, R. E. N., Toledo, E. A., Rubira, A. F., & Muniz, E. C. (2003). Crystallisation and miscibility of poly (ethylene oxide)/poly (vinyl chloride) blends. *Journal of Materials Science*, 38(4), 699–703.
- CEPAL, N. U. (1975). *Mujeres en América Latina: aportes para una discusión*. 156, 141–153.
- Chai, J., Liu, Z., Ma, J., Wang, J., Liu, X., Liu, H., Zhang, J., Cui, G., & Chen, L. (2017). In situ generation of poly (vinylene carbonate) based solid electrolyte with interfacial stability for LiCoO₂ lithium batteries. *Advanced Science*, 4(2), 1600377.
- Chandan, P., Chang, C.-C., Yeh, K.-W., Chiu, C.-C., Wu, D.-Z., Huang, T.-W., Wu, P. M., Chi, P.-W., Hsu, W.-F., & Su, K.-H. (2019). Voltage fade mitigation in the cationic dominant lithium-rich NCM cathode. *Communications Chemistry*, 2(1), 1–7.
- Chandra, A., Chandra, A., & Thakur, K. (2014). Synthesis, characterization and polymer battery fabrication of hot-pressed ion conducting nano-composite polymer electrolytes. *Composites Part B: Engineering*, 60, 292–296.
- Chen-Yang, Y. W., Chen, Y. T., Chen, H. C., Lin, W. T., & Tsai, C. H. (2009). Effect of the addition of hydrophobic clay on the electrochemical property of polyacrylonitrile/LiClO₄ polymer electrolytes for lithium battery. *Polymer*, 50(13), 2856–2862.
- Chen, C. H., Liu, J., & Amine, K. (2001). Symmetric cell approach and impedance spectroscopy of high power lithium-ion batteries. *Journal of Power Sources*, 96(2), 321–

- Chen, G., & Richardson, T. J. (2004). Overcharge protection for rechargeable lithium batteries using electroactive polymers. *Electrochemical and Solid-State Letters*, 7(2), A23–A26.
- Chen, G., & Richardson, T. J. (2010). Overcharge protection for 4 V lithium batteries at high rates and low temperatures. *Journal of The Electrochemical Society*, 157(6), A735–A740.
- Chen, H., Jiang, C., Wu, H., & Chang, F. (2004). Hydrogen bonding effect on the poly (ethylene oxide), phenolic resin, and lithium perchlorate–based solid-state electrolyte. *Journal of Applied Polymer Science*, 91(2), 1207–1216.
- Chen, J. C.-M., Yang, J., & Cheng, M. M.-C. (2019). Induced nanoscale roughness of current collectors enhances lithium ion battery performances. *Journal of Power Sources*, 430, 169–174.
- Chen, Ji, Li, C., & Shi, G. (2013). Graphene materials for electrochemical capacitors. In *Journal of Physical Chemistry Letters*. <https://doi.org/10.1021/jz400160k>
- Chen, Jian, Li, C., Zhang, J., Li, C., Chen, J., & Ren, Y. (2018). First-principles study on the adsorption and dissociation of impurities on copper current collector in electrolyte for Lithium-Ion Batteries. *Materials*, 11(7), 1256.
- Chen, L.-Q. (2002). Phase-field models for microstructure evolution. *Annual Review of Materials Research*, 32(1), 113–140.
- Chen, L., Rao, M., Li, W.-S., Xu, M., Liao, Y., Tan, C., & Yi, J. (2011). Performance improvement of polyethylene-supported PAMS electrolyte using urea as foaming agent. *Acta Physico-Chimica Sinica*, 27(7), 1689–1694.
- Chen, L., Zhou, G., Liu, Z., Ma, X., Chen, J., & Zhang, Z. (2016). Scalable Clean Exfoliation of High-Quality Few-Layer Black Phosphorus for a Flexible Lithium Ion Battery. 510–

517. <https://doi.org/10.1002/adma.201503678>

Chen, Xi, Huang, H., Pan, L., Liu, T., & Niederberger, M. (2019). Fully Integrated Design of a Stretchable Solid-State Lithium-Ion Full Battery. *Advanced Materials*.

<https://doi.org/10.1002/adma.201904648>

Chen, Xilin, Gerasopoulos, K., Guo, J., Brown, A., Wang, C., Ghodssi, R., & Culver, J. N. (2010). Virus-enabled silicon anode for lithium-ion batteries. *ACS Nano*, 4(9), 5366–5372.

Chen, Z., & Dahn, J. R. (2004). Methods to obtain excellent capacity retention in LiCoO₂ cycled to 4.5 V. *Electrochimica Acta*, 49(7), 1079–1090.

Cheng, C.-C., & Lee, D.-J. (2016). Supramolecular assembly-mediated lithium ion transport in nanostructured solid electrolytes. *RSC Advances*, 6(44), 38223–38227.

Cheng, C. L., Wan, C. C., & Wang, Y. Y. (2004a). Microporous PVdF-HFP based gel polymer electrolytes reinforced by PEGDMA network. *Electrochemistry Communications*, 6(6), 531–535.

Cheng, C. L., Wan, C. C., & Wang, Y. Y. (2004b). Preparation of porous, chemically cross-linked, PVdF-based gel polymer electrolytes for rechargeable lithium batteries. *Journal of Power Sources*, 134(2), 202–210.

Cheng, Q., Meng, C., Qian, Y., He, J., & Dong, X. (2020). Energy capacity enhancement of all-organic fabric supercapacitors by organic dyes: Old method for new application. *Progress in Organic Coatings*. <https://doi.org/10.1016/j.porgcoat.2019.105439>

Cheng, X.-B., Zhang, R., Zhao, C.-Z., & Zhang, Q. (2017). Toward safe lithium metal anode in rechargeable batteries: a review. *Chemical Reviews*, 117(15), 10403–10473.

Cheng, X. B., Zhang, R., Zhao, C. Z., Wei, F., Zhang, J. G., & Zhang, Q. (2015). A review of

- solid electrolyte interphases on lithium metal anode. *Advanced Science*, 3(3), 1–20.
<https://doi.org/10.1002/advs.201500213>
- Cherkashinin, G., Yu, Z., Eilhardt, R., Alff, L., & Jaegermann, W. (2020). The effect of interfacial charge distribution on chemical compatibility and stability of the high voltage electrodes (LiCoPO₄, LiNiPO₄)/solid electrolyte (LiPON) interface. *Advanced Materials Interfaces*, 2000276.
- Chiu, C.-Y., Yen, Y.-J., Kuo, S.-W., Chen, H.-W., & Chang, F.-C. (2007). Complicated phase behavior and ionic conductivities of PVP-co-PMMA-based polymer electrolytes. *Polymer*, 48(5), 1329–1342.
- Cho, J., Kim, Y. J., & Park, B. (2000). Novel LiCoO₂ cathode material with Al₂O₃ coating for a Li ion cell. *Chemistry of Materials*, 12(12), 3788–3791.
- Choi, J. W., & Aurbach, D. (2016). Promise and reality of post-lithium-ion batteries with high energy densities. *Nature Reviews Materials*, 1(4), 1–16.
- Choi, N.-S., Yew, K. H., Lee, K. Y., Sung, M., Kim, H., & Kim, S.-S. (2006). Effect of fluoroethylene carbonate additive on interfacial properties of silicon thin-film electrode. *Journal of Power Sources*, 161(2), 1254–1259.
- Choudhury, S. (2019). A Highly Reversible Room-Temperature Lithium Metal Battery Based on Cross-Linked Hairy Nanoparticles. In *Rational Design of Nanostructured Polymer Electrolytes and Solid–Liquid Interphases for Lithium Batteries* (pp. 35–57). Springer.
- Chu, H.-C., & Tuan, H.-Y. (2017). High-performance lithium-ion batteries with 1.5 μm thin copper nanowire foil as a current collector. *Journal of Power Sources*, 346, 40–48.
- Claye, A. S., Fischer, J. E., Huffman, C. B., Rinzler, A. G., & Smalley, R. E. (2000). Solid-state electrochemistry of the Li single wall carbon nanotube system. *Journal of the*

- Electrochemical Society*, 147(8), 2845.
- Cocke, D. L., Patil, P. K., Zhang, X.-W., Wang, C., Appleby, A. J., & Little, F. . (2003). Electrochemical performance of lithium ion battery, nano-silicon-based, disordered carbon composite anodes with different microstructures. *Journal of Power Sources*, 125(2), 206–213. <https://doi.org/10.1016/j.jpowsour.2003.07.019>
- Cohen, M. H., & Turnbull, D. (1959). Molecular transport in liquids and glasses. *The Journal of Chemical Physics*, 31(5), 1164–1169.
- Complexes of alkali metal ions with poly(ethylene oxide). (1973). *Polymer*, 14(11), 589. [https://doi.org/10.1016/0032-3861\(73\)90146-8](https://doi.org/10.1016/0032-3861(73)90146-8)
- Cresce, A. v, Russell, S. M., Baker, D. R., Gaskell, K. J., & Xu, K. (2014). In situ and quantitative characterization of solid electrolyte interphases. *Nano Letters*, 14(3), 1405–1412.
- Croce, F, Appetecchi, G. B., Persi, L., & Scrosati, B. (1998). Nanocomposite polymer electrolytes for lithium batteries. *Nature*, 394(6692), 456–458.
- Croce, F, Persi, L., Scrosati, B., Serraino-Fiory, F., Plichta, E., & Hendrickson, M. A. (2001). Role of the ceramic fillers in enhancing the transport properties of composite polymer electrolytes. *Electrochimica Acta*, 46(16), 2457–2461.
- Croce, Fausto, Brown, S. D., Greenbaum, S. G., Slane, S. M., & Salomon, M. (1993). Lithium-7 NMR and Ionic Conductivity Studies of Gel Electrolytes Based on Poly(acrylonitrile). *Chemistry of Materials*, 5(9), 1268–1272. <https://doi.org/10.1021/cm00033a014>
- Cui, W.-W., Tang, D.-Y., & Gong, Z.-L. (2013). Electrospun poly (vinylidene fluoride)/poly (methyl methacrylate) grafted TiO₂ composite nanofibrous membrane as polymer

- electrolyte for lithium-ion batteries. *Journal of Power Sources*, 223, 206–213.
- Dahn, J. R., von Sacken, U., & Michal, C. A. (1990). Structure and electrochemistry of $\text{Li}_{1\pm y}\text{NiO}_2$ and a new Li_2NiO_2 phase with the $\text{Ni}(\text{OH})_2$ structure. *Solid State Ionics*, 44(1–2), 87–97.
- Das, S., Prathapa, S. J., Menezes, P. V., Row, T. N. G., & Bhattacharyya, A. J. (2009). Study of ion transport in lithium perchlorate-succinonitrile plastic crystalline electrolyte via ionic conductivity and in situ cryo-crystallography. *The Journal of Physical Chemistry B*, 113(15), 5025–5031.
- De Biasi, L., Schwarz, B., Brezesinski, T., Hartmann, P., Janek, J., & Ehrenberg, H. (2019). Chemical, Structural, and Electronic Aspects of Formation and Degradation Behavior on Different Length Scales of Ni-Rich NCM and Li-Rich HE-NCM Cathode Materials in Li-Ion Batteries. *Advanced Materials*, 31(26), 1900985.
- Dee, K. C., Puleo, D. A., & Bizios, R. (2003). *An introduction to tissue-biomaterial interactions*. John Wiley & Sons.
- Deka, M., & Kumar, A. (2011). Electrical and electrochemical studies of poly (vinylidene fluoride)–clay nanocomposite gel polymer electrolytes for Li-ion batteries. *Journal of Power Sources*, 196(3), 1358–1364.
- Deka, Madhuryya, & Kumar, A. (2010). Enhanced electrical and electrochemical properties of PMMA–clay nanocomposite gel polymer electrolytes. *Electrochimica Acta*, 55(5), 1836–1842.
- Deng, Z., Jiang, H., Hu, Y., Liu, Y., Zhang, L., & Liu, H. (2017). *3D Ordered Macroporous MoS_2 @ C Nanostructure for Flexible Li-Ion Batteries*.
<https://doi.org/10.1002/adma.201603020>

- Design, N. C., Society, M., Computer, T., & Society, A. M. (2000). Nano-sized transition-metal oxides as negative-electrode materials for lithium-ion batteries. *Nature*, 407(September), 496–499. <https://doi.org/10.1038/35035045>
- Dong, H., Dorfman, S. M., Holl, C. M., Meng, Y., Prakapenka, V. B., He, D., & Duffy, T. S. (2014). Compression of lithium fluoride to 92 GPa. *High Pressure Research*, 34(1), 39–48.
- Doughty, D. H. (2012). *Vehicle battery safety roadmap guidance*. National Renewable Energy Lab.(NREL), Golden, CO (United States).
- Du Pasquier, A., Warren, P. C., Culver, D., Gozdz, A. S., Amatucci, G. G., & Tarascon, J.-M. (2000). Plastic PVDF-HFP electrolyte laminates prepared by a phase-inversion process. *Solid State Ionics*, 135(1–4), 249–257.
- Duan, H., Fan, M., Chen, W. P., Li, J. Y., Wang, P. F., Wang, W. P., Shi, J. L., Yin, Y. X., Wan, L. J., & Guo, Y. G. (2019). Extended Electrochemical Window of Solid Electrolytes via Heterogeneous Multilayered Structure for High-Voltage Lithium Metal Batteries. *Advanced Materials*, 31(12), 1–7. <https://doi.org/10.1002/adma.201807789>
- Duong, A. T., & Mumm, D. R. (2013). On the interaction of SSC and LSGM in composite SOFC electrodes. *Journal of Power Sources*, 241, 281–287.
- Ebbesen, T. W., Lezec, H. J., Hiura, H., Bennett, J. W., Ghaemi, H. F., & Thio, T. (1996). Electrical conductivity of individual carbon nanotubes. *Nature*, 382(6586), 54–56.
- Ein-Eli, Y. (1997). S. R. Thomas, R. Chadha, T. J. Blakley, and V. Koch. *J. Electrochem. Soc*, 144.
- Etacheri, V., Haik, O., Goffer, Y., Roberts, G. A., Stefan, I. C., Fasching, R., & Aurbach, D. (2012). Effect of fluoroethylene carbonate (FEC) on the performance and surface

- chemistry of Si-nanowire Li-ion battery anodes. *Langmuir*, 28(1), 965–976.
- Evans, S. D., Ulman, A., Goppert-Berarducci, K. E., & Gerenser, L. J. (1991). Self-Assembled Multilayers of ω -Mercaptoalkanoic Acids: Selective Ionic Interactions. *Journal of the American Chemical Society*, 113(15), 5866–5868. <https://doi.org/10.1021/ja00015a053>
- Fang, R., Chen, K., Yin, L., Sun, Z., Li, F., & Cheng, H. (2019). *The Regulating Role of Carbon Nanotubes and Graphene in Lithium-Ion and Lithium – Sulfur Batteries*. 1800863, 1–22. <https://doi.org/10.1002/adma.201800863>
- Fergus, J. W. (2010). Ceramic and polymeric solid electrolytes for lithium-ion batteries. *Journal of Power Sources*, 195(15), 4554–4569. <https://doi.org/10.1016/j.jpowsour.2010.01.076>
- Ferris, F. G., Stehmeier, L. G., Kantzas, A., & Mourits, F. M. (1997). Bacteriogenic mineral plugging. *Journal of Canadian Petroleum Technology*, 36(09).
- Fick, A. (1855). Ueber diffusion. *Annalen Der Physik*, 170(1), 59–86.
- Flora, X. H., Ulaganathan, M., Babu, R. S., & Rajendran, S. (2012). Evaluation of lithium ion conduction in PAN/PMMA-based polymer blend electrolytes for Li-ion battery applications. *Ionics*, 18(8), 731–736.
- Flora, X. H., Ulaganathan, M., & Rajendran, S. (2012). Influence of lithium salt concentration on PAN-PMMA blend polymer electrolytes. *Int. J. Electrochem. Sci*, 7(8), 7451–7462.
- Fu, K., Yildiz, O., Bhanushali, H., Wang, Y., Stano, K., Xue, L., Zhang, X., & Bradford, P. D. (2013). Aligned carbon nanotube-silicon sheets: A novel nano-architecture for flexible lithium ion battery electrodes. *Advanced Materials*, 25(36), 5109–5114. <https://doi.org/10.1002/adma.201301920>
- Fu, X., Jewel, Y., Wang, Y., Liu, J., & Zhong, W.-H. (2016). Decoupled ion transport in a

- protein-based solid ion conductor. *The Journal of Physical Chemistry Letters*, 7(21), 4304–4310.
- Fu, X., Li, C., Wang, Y., Kovatch, L. P., Scudiero, L., Liu, J., & Zhong, W. (2018). Building Ion-Conduction Highways in Polymeric Electrolytes by Manipulating Protein Configuration. *ACS Applied Materials & Interfaces*, 10(5), 4726–4736.
- Fu, X., Li, C., Wang, Y., Scudiero, L., Liu, J., & Zhong, W.-H. (2018). Self-Assembled Protein Nanofilter for Trapping Polysulfides and Promoting Li⁺ Transport in Lithium–Sulfur Batteries. *The Journal of Physical Chemistry Letters*, 9(10), 2450–2459.
- Fu, X., Scudiero, L., & Zhong, W.-H. (2019). A robust and ion-conductive protein-based binder enabling strong polysulfide anchoring for high-energy lithium–sulfur batteries. *Journal of Materials Chemistry A*, 7(4), 1835–1848.
- Fulcher, G. S. (1925). Analysis of recent measurements of the viscosity of glasses. *Journal of the American Ceramic Society*, 8(6), 339–355.
- Gao, Y., Richard, M. N., & Dahn, J. R. (2002). Photoelectron spectroscopy studies of Li_{1+x}Mn_{2-x}O₄ for Li ion battery applications. *Journal of Applied Physics*, 80(7), 4141–4152. <https://doi.org/10.1063/1.363287>
- Gedde, U. L. F. (1995). *Polymer physics*. Springer Science & Business Media.
- Gonçalves, G., Marques, P. A., Barros-Timmons, A., Bdkin, I., Singh, M. K., Emami, N., & Grácio, J. (2010). Graphene oxide modified with PMMA via ATRP as a reinforcement filler. *Journal of Materials Chemistry*, 20(44), 9927–9934.
- Goodenough, J. B., & Kim, Y. (2010). Challenges for rechargeable Li batteries. *Chemistry of Materials*, 22(3), 587–603.
- Gopalan, A. I., Santhosh, P., Manesh, K. M., Nho, J. H., Kim, S. H., Hwang, C.-G., & Lee,

- K.-P. (2008). Development of electrospun PVdF–PAN membrane-based polymer electrolytes for lithium batteries. *Journal of Membrane Science*, 325(2), 683–690.
- Grewal, M. S., Tanaka, M., & Kawakami, H. (2019). Bifunctional poly(ethylene glycol) based crosslinked network polymers as electrolytes for all-solid-state lithium ion batteries. *Polymer International*, 68(4), 684–693. <https://doi.org/10.1002/pi.5750>
- Groult, H., Nakajima, T., Perrigaud, L., Ohzawa, Y., Yashiro, H., Komaba, S., & Kumagai, N. (2005). Surface-fluorinated graphite anode materials for Li-ion batteries. *Journal of Fluorine Chemistry*, 126(7), 1111–1116.
- Gu, M., Song, W. J., Hong, J., Kim, S. Y., Shin, T. J., Kotov, N. A., Park, S., & Kim, B. S. (2019). Stretchable batteries with gradient multilayer conductors. *Science Advances*. <https://doi.org/10.1126/sciadv.aaw1879>
- Guo, Y., Ouyang, Y., Li, D., Wei, Y., Zhai, T., & Li, H. (2019). PMMA-assisted Li deposition towards 3D continuous dendrite-free lithium anode. *Energy Storage Materials*, 16, 203–211.
- Hall, P. G., Davies, G. R., McIntyre, J. E., Ward, I. M., & Bannister, D. J. (1986). Ion conductivity in polysiloxane comb polymers with ethylene glycol teeth. *Polymer Communications (Guildford)*, 27(4), 98–100.
- Han, D., Guo, Z., Chen, S., Xiao, M., Peng, X., Wang, S., & Meng, Y. (2018). Enhanced properties of biodegradable poly (propylene carbonate)/polyvinyl formal blends by melting compounding. *Polymers*, 10(7), 771.
- Hasan, M., & Lee, M. (2014). Enhancement of the thermo-mechanical properties and efficacy of mixing technique in the preparation of graphene/PVC nanocomposites compared to carbon nanotubes/PVC. *Progress in Natural Science: Materials International*, 24(6),

579–587.

- Hashim, N. A., Liu, Y., & Li, K. (2011). Preparation of PVDF hollow fiber membranes using SiO₂ particles: the effect of acid and alkali treatment on the membrane performances. *Industrial & Engineering Chemistry Research*, 50(5), 3035–3040.
- Hayamizu, K., Aihara, Y., Arai, S., & Martinez, C. G. (1999). Pulse-gradient spin-echo ¹H, ⁷Li, and ¹⁹F NMR diffusion and ionic conductivity measurements of 14 organic electrolytes containing LiN(SO₂CF₃)₂. *The Journal of Physical Chemistry B*, 103(3), 519–524.
- Hayashi, A., Muramatsu, H., Ohtomo, T., Hama, S., & Tatsumisago, M. (2013). Improvement of chemical stability of Li₃PS₄ glass electrolytes by adding M_xO_y (M= Fe, Zn, and Bi) nanoparticles. *Journal of Materials Chemistry A*, 1(21), 6320–6326.
- Hayashi, A., Muramatsu, H., Ohtomo, T., Hama, S., & Tatsumisago, M. (2014). Improved chemical stability and cyclability in Li₂S–P₂S₅–P₂O₅–ZnO composite electrolytes for all-solid-state rechargeable lithium batteries. *Journal of Alloys and Compounds*, 591, 247–250.
- Hayashi, A., Ohtomo, T., Mizuno, F., Tadanaga, K., & Tatsumisago, M. (2004). Rechargeable lithium batteries, using sulfur-based cathode materials and Li₂S–P₂S₅ glass-ceramic electrolytes. *Electrochimica Acta*, 50(2–3), 893–897.
- He, K., Xie, P., Zu, C., Wang, Y., Li, B., Han, B., Rong, M. Z., & Zhang, M. Q. (2019). A facile and scalable process to synthesize flexible lithium ion conductive glass-ceramic fibers. *RSC Advances*, 9(8), 4157–4161. <https://doi.org/10.1039/C8RA08401G>
- He, X., Wu, Y., Zhao, F., Wang, J., Jiang, K., & Fan, S. (2013). Enhanced rate capabilities of Co₃O₄/carbon nanotube anodes for lithium ion battery applications. *Journal of*

- Materials Chemistry A*, 1(37), 11121–11125.
- Hekselman, M. K., Plewa-Marczewska, A., Żukowska, G. Z., & Sasim, E. (2010). W. 19
Wieczorek and M. Siekierski. *Electrochim. Acta*, 55, 1298–1307.
- Hirayama, M., Ido, H., Kim, K., & Cho, W. (2010). *Dynamic Structural Changes at LiMn 2 O
4 / Electrolyte Interface*. 14, 15268–15276.
- Ho, C., Raistrick, I. D., & Huggins, R. A. (1980). Application of A-C techniques to the study
of lithium diffusion in tungsten trioxide thin films. *Journal of the Electrochemical
Society*, 127(2), 343.
- Hong, H. G., & Mallouk, T. E. (1991). Electrochemical Measurements of Electron Transfer
Rates through Zirconium 1,2-Ethanediybis(phosphonate) Multilayer Films on Gold
Electrodes. *Langmuir*, 7(10), 2362–2369. <https://doi.org/10.1021/la00058a065>
- Hong, S. E., Kim, D.-K., Jo, S. M., Kim, D. Y., Chin, B. D., & Lee, D. W. (2007). Graphite
nanofibers prepared from catalytic graphitization of electrospun poly (vinylidene
fluoride) nanofibers and their hydrogen storage capacity. *Catalysis Today*, 120(3–4),
413–419.
- Hou, T., Yang, G., Rajput, N. N., Self, J., Park, S.-W., Nanda, J., & Persson, K. A. (2019).
The influence of FEC on the solvation structure and reduction reaction of LiPF₆/EC
electrolytes and its implication for solid electrolyte interphase formation. *Nano Energy*,
64, 103881.
- Hsu, C.-H., Lin, H.-H., Liu, Y.-H., & Lin, H.-P. (2018). Carbon fibers as three-dimensional
current collectors for silicon/reduced graphene oxide lithium ion battery anodes with
improved rate performance and cycle life. *New Journal of Chemistry*, 42(11), 9058–9064.
- Hsu, C. Y., Liu, R. J., Hsu, C. H., & Kuo, P. L. (2016). High thermal and electrochemical

- stability of PVDF-graft-PAN copolymer hybrid PEO membrane for safety reinforced lithium-ion battery. *RSC Advances*, 6(22), 18082–18088.
<https://doi.org/10.1039/c5ra26345j>
- Hu, J.-M., Liang, L., Ji, Y., Hong, L., Gerdes, K., & Chen, L.-Q. (2014). Interdiffusion across solid electrolyte-electrode interface. *Applied Physics Letters*, 104(21), 213907.
- Hu, J., He, P., Zhang, B., Wang, B., & Fan, L.-Z. (2020). Porous film host-derived 3D composite polymer electrolyte for high-voltage solid state lithium batteries. *Energy Storage Materials*, 26, 283–289.
- Huang, C., & Zhang, L. (2004). Miscibility of poly (vinylidene fluoride) and atactic poly (methyl methacrylate). *Journal of Applied Polymer Science*, 92(1), 1–5.
- Huang, L., Arena, J. T., Manickam, S. S., Jiang, X., Willis, B. G., & McCutcheon, J. R. (2014). Improved mechanical properties and hydrophilicity of electrospun nanofiber membranes for filtration applications by dopamine modification. *Journal of Membrane Science*, 460, 241–249.
- Huang, W., Boyle, D. T., Li, Y., Li, Y., Pei, A., Chen, H., & Cui, Y. (2019). Nanostructural and Electrochemical Evolution of the Solid-Electrolyte Interphase on CuO Nanowires Revealed by Cryogenic-Electron Microscopy and Impedance Spectroscopy. *ACS Nano*.
<https://doi.org/10.1021/acsnano.8b08012>
- Huang, Xiao, Lu, Y., Song, Z., Xiu, T., Badding, M. E., & Wen, Z. (2019). Preparation of dense Ta-LLZO/MgO composite Li-ion solid electrolyte: Sintering, microstructure, performance and the role of MgO. *Journal of Energy Chemistry*, 39, 8–16.
- Huang, Xiaosong. (2013). Cellular porous polyvinylidene fluoride composite membranes for lithium-ion batteries. *Journal of Solid State Electrochemistry*, 17(3), 591–597.

- Huang, Xueyan, Huang, J., Wu, J., Yu, X., Gao, Q., Luo, Y., & Hu, H. (2015). Fabrication and properties of polybutadiene rubber-interpenetrating cross-linking poly (propylene carbonate) network as gel polymer electrolytes for lithium-ion battery. *RSC Advances*, 5(65), 52978–52984.
- Huang, Xueyan, Zeng, S., Liu, J., He, T., Sun, L., Xu, D., Yu, X., Luo, Y., Zhou, W., & Wu, J. (2015). High-performance electrospun poly (vinylidene fluoride)/poly (propylene carbonate) gel polymer electrolyte for lithium-ion batteries. *The Journal of Physical Chemistry C*, 119(50), 27882–27891.
- Huang, Yan, Hu, H., Huang, Y., Zhu, M., Meng, W., Liu, C., Pei, Z., Hao, C., Wang, Z., & Zhi, C. (2015). From industrially weavable and knittable highly conductive yarns to large wearable energy storage textiles. *ACS Nano*. <https://doi.org/10.1021/acsnano.5b00860>
- Huang, Yun, Gong, S.-D., Huang, R., Cao, H.-J., Lin, Y.-H., Yang, M., & Li, X. (2015). Polyhedral oligomeric silsesquioxane containing gel polymer electrolyte based on a PMMA matrix. *RSC Advances*, 5(57), 45908–45918.
- Hyun, W. J., De Moraes, A. C. M., Lim, J.-M., Downing, J. R., Park, K.-Y., Tan, M. T. Z., & Hersam, M. C. (2019). High-modulus hexagonal boron nitride nanoplatelet gel electrolytes for solid-state rechargeable lithium-ion batteries. *ACS Nano*, 13(8), 9664–9672.
- Iijima, T., Toyoguchi, Y., & Eda, N. (1985). Quasi-solid organic electrolytes gelatinized with polymethyl-methacrylate and their applications for lithium batteries. *Denki Kagaku*, 53(8), 619–623.
- Jagadeesan, A., Sasikumar, M., Jeevani, R., Therese, H. A., Ananth, N., & Sivakumar, P. (2019). Fabrication of BaTiO₃ ceramic filler incorporated PVC-PEMA based blend

- nanocomposite gel polymer electrolytes for Li ion battery applications. *Journal of Materials Science: Materials in Electronics*, 1–14.
- Ji, Xiaoxiao, Zeng, H., Gong, X., Tsai, F., Jiang, T., Li, R. K. Y., Shi, H., Luan, S., & Shi, D. (2017). A Si-doped flexible self-supporting comb-like polyethylene glycol copolymer (Si-PEG) film as a polymer electrolyte for an all solid-state lithium-ion battery. *Journal of Materials Chemistry A*, 5(46), 24444–24452. <https://doi.org/10.1039/c7ta07741f>
- Ji, Xiulei, & Nazar, L. F. (2010). Advances in Li–S batteries. *Journal of Materials Chemistry*, 20(44), 9821–9826.
- Jia, W., Li, Z., Wu, Z., Wang, L., Wu, B., Wang, Y., Cao, Y., & Li, J. (2018). Graphene oxide as a filler to improve the performance of PAN-LiClO₄ flexible solid polymer electrolyte. *Solid State Ionics*, 315, 7–13.
- Jia, X., Wang, C., Ranganathan, V., Napier, B., Yu, C., Chao, Y., Forsyth, M., Omenetto, F. G., MacFarlane, D. R., & Wallace, G. G. (2017). A biodegradable thin-film magnesium primary battery using silk fibroin–ionic liquid polymer electrolyte. *ACS Energy Letters*, 2(4), 831–836.
- Jia, X., Yang, Y., Wang, C., Zhao, C., Vijayaraghavan, R., MacFarlane, D. R., Forsyth, M., & Wallace, G. G. (2014). Biocompatible ionic liquid–biopolymer electrolyte-enabled thin and compact magnesium–air batteries. *ACS Applied Materials & Interfaces*, 6(23), 21110–21117.
- Jiang, T., Bu, F., Feng, X., Shakir, I., Hao, G., & Xu, Y. (2017). *Porous Fe₂O₃ Nanoframeworks Encapsulated within Three-Dimensional Graphene as High-Performance Flexible Anode for Lithium-Ion Battery*. <https://doi.org/10.1021/acsnano.7b02198>

- Jiang, Y.-X., Xu, J.-M., Zhuang, Q.-C., Jin, L.-Y., & Sun, S.-G. (2008). A novel PEO-based composite solid-state polymer electrolyte with methyl group-functionalized SBA-15 filler for rechargeable lithium batteries. *Journal of Solid State Electrochemistry*, 12(4), 353–361.
- Jiang, Z., Carroll, B., & Abraham, K. M. (1997). Studies of some poly(vinylidene fluoride) electrolytes. *Electrochimica Acta*, 42(17), 2667–2677. [https://doi.org/10.1016/S0013-4686\(97\)00005-4](https://doi.org/10.1016/S0013-4686(97)00005-4)
- Jin, J., Wen, Z., Ma, G., Lu, Y., Cui, Y., Wu, M., Liang, X., & Wu, X. (2013). Flexible self-supporting graphene–sulfur paper for lithium sulfur batteries. *RSC Advances*, 3(8), 2558–2560.
- Jinisha, B., KM, A., Manoj, M., Pradeep, P., & Jayalekshmi, J. (2017). Development of a novel type of solid polymer electrolyte for solid state lithium battery applications based on lithium enriched poly (ethylene oxide) (PEO)/poly (vinyl pyrrolidone) (PVP) blend polymer. *Electrochimica Acta*, 235, 210–222. <https://doi.org/10.1016/j.electacta.2017.03.118>
- Jost, K., Dion, G., & Gogotsi, Y. (2014). Textile energy storage in perspective. In *Journal of Materials Chemistry A*. <https://doi.org/10.1039/c4ta00203b>
- Kaltenbrunner, M., Kettlgruber, G., Siket, C., Schwödiauer, R., & Bauer, S. (2010). Arrays of ultracompliant electrochemical dry gel cells for stretchable electronics. *Advanced Materials*. <https://doi.org/10.1002/adma.200904068>
- Kalyani, P., & Kalaiselvi, N. (2005). Various aspects of LiNiO₂ chemistry: A review. *Science and Technology of Advanced Materials*, 6(6), 689.
- Kammoun, M., Berg, S., & Ardebili, H. (2016). Stretchable spiral thin-film battery capable of

- out-of-plane deformation. *Journal of Power Sources*, 332, 406–412.
- Kammoun, M., Lundquist, L., & Ardebili, H. (2015). High proton conductivity membrane with coconut shell activated carbon. *Ionics*, 21(6), 1665–1674.
- Kang, S., Hong, S. Y., Kim, N., Oh, J., Park, M., Chung, K. Y., Lee, S. S., Lee, J., & Son, J. G. (2020). Stretchable Lithium-Ion Battery Based on Re-entrant Micro-honeycomb Electrodes and Cross-Linked Gel Electrolyte. *ACS Applied Materials and Interfaces*. <https://doi.org/10.1021/acsnano.0c00187>
- Kang, W., Ma, X., Zhao, H., Ju, J., Zhao, Y., Yan, J., & Cheng, B. (2016). Electrospun cellulose acetate/poly (vinylidene fluoride) nanofibrous membrane for polymer lithium-ion batteries. *Journal of Solid State Electrochemistry*, 20(10), 2791–2803.
- Kannan, A. M., & Manthiram, A. (2002). Surface/Chemically Modified LiMn_2O_4 Cathodes for Lithium-Ion Batteries. *Electrochemical and Solid-State Letters*, 5(7), A167. <https://doi.org/10.1149/1.1482198>
- Kazemiabnavi, S., Malik, R., Orvananos, B., Abdellahi, A., Ceder, G., & Thornton, K. (2018). The effect of surface-bulk potential difference on the kinetics of intercalation in core-shell active cathode particles. *Journal of Power Sources*, 382, 30–37.
- Kelly, T., Ghadi, B. M., Berg, S., & Ardebili, H. (2016). In situ study of strain-dependent ion conductivity of stretchable polyethylene oxide electrolyte. *Scientific Reports*, 6, 20128.
- Kelvin, K., Gong, Y., Dai, J., Gong, A., Han, X., Yao, Y., & Wang, C. (2016). *garnet nanofiber networks for lithium batteries*. 1–6. <https://doi.org/10.1073/pnas.1600422113>
- Kim, C., Jung, J.-W., Yoon, K. R., Yoon, D.-Y., Park, S., & Kim, I.-D. (2016). A high-capacity and long-cycle-life lithium-ion battery anode architecture: silver nanoparticle-decorated SnO_2/NiO nanotubes. *ACS Nano*, 10(12), 11317–11326.

- Kim, D., & Sun, Y. (1998). Polymer Electrolytes Based on Acrylonitrile-Methyl Methacrylate-Styrene Terpolymers for Rechargeable Lithium-Polymer Batteries. *Journal of The Electrochemical Society*, 145(6), 1958–1963.
- Kim, G.-T., Appetecchi, G. B., Carewska, M., Joost, M., Balducci, A., Winter, M., & Passerini, S. (2010). UV cross-linked, lithium-conducting ternary polymer electrolytes containing ionic liquids. *Journal of Power Sources*, 195(18), 6130–6137.
- Kim, I., Kim, B. S., Nam, S., Lee, H. J., Chung, H. K., Cho, S. M., Luu, T. H. T., Hyun, S., & Kang, C. (2018). Cross-linked poly(vinylidene fluoride-cohexafluoropropene) (PVDF-co-HFP) gel polymer electrolyte for flexible li-ion battery integrated with organic light emitting diode (OLED). *Materials*, 11(4), 1–11. <https://doi.org/10.3390/ma11040543>
- Kim, S. G., Kim, W. T., & Suzuki, T. (1999). Phase-field model for binary alloys. *Physical Review E*, 60(6), 7186.
- Kim, S. Y., Song, Y. Il, Wee, J.-H., Kim, C. H., Ahn, B. W., Lee, J. W., Shu, S. J., Terrones, M., Kim, Y. A., & Yang, C.-M. (2019). Few-layer graphene coated current collectors for safe and powerful lithium ion batteries. *Carbon*, 153, 495–503.
- Kim, Y., Kwon, S. J., Jang, H., Jung, B. M., Lee, S. B., & Choi, U. H. (2017). High ion conducting nanohybrid solid polymer electrolytes via single-ion conducting mesoporous organosilica in poly (ethylene oxide). *Chemistry of Materials*, 29(10), 4401–4410.
- Kondrakov, A. O., Schmidt, A., Xu, J., Geßwein, H., Mönig, R., Hartmann, P., Sommer, H., Brezesinski, T., & Janek, J. (2017). Anisotropic lattice strain and mechanical degradation of high-and low-nickel NCM cathode materials for Li-ion batteries. *The Journal of Physical Chemistry C*, 121(6), 3286–3294.
- Kosova, N. V., Devyatkina, E. T., Stepanov, A. P., & Buzlukov, A. L. (2008). Lithium

- conductivity and lithium diffusion in NASICON-type $\text{Li}_{1+x}\text{Ti}_{2-x}\text{Al}_x(\text{PO}_4)_3$ ($x=0$; 0.3) prepared by mechanical activation. *Ionics*, 14(4), 303–311.
- Kou, Z., Miao, C., Mei, P., Zhang, Y., Yan, X., Jiang, Y., & Xiao, W. (2020). Enhancing the cycling stability of all-solid-state lithium-ion batteries assembled with $\text{Li}_{1.3}\text{Al}_{0.3}\text{Ti}_{1.7}(\text{PO}_4)_3$ solid electrolytes prepared from precursor solutions with appropriate pH values. *Ceramics International*, 46(7), 9629–9636.
- Kovalenko, I., Zdyrko, B., Magasinski, A., Hertzberg, B., Milicev, Z., Burtovyy, R., Luzinov, I., & Yushin, G. (2011). A major constituent of brown algae for use in high-capacity Li-ion batteries. *Science*, 334(6052), 75–79.
- Kucinskis, G., Bajars, G., & Kleperis, J. (2013). Graphene in lithium ion battery cathode materials: A review. *Journal of Power Sources*, 240, 66–79.
<https://doi.org/10.1016/j.jpowsour.2013.03.160>
- Kudu, Ö. U., Famprikis, T., Fleutot, B., Braida, M.-D., Le Mercier, T., Islam, M. S., & Masquelier, C. (2018). A review of structural properties and synthesis methods of solid electrolyte materials in the Li_2S – P_2S_5 binary system. *Journal of Power Sources*, 407, 31–43.
- Kufian, M. Z., Aziz, M. F., Shukur, M. F., Rahim, A. S., Ariffin, N. E., Shuhaimi, N. E. A., Majid, S. R., Yahya, R., & Arof, A. K. (2012). PMMA-LiBOB gel electrolyte for application in lithium ion batteries. *Solid State Ionics*, 208, 36–42.
<https://doi.org/10.1016/j.ssi.2011.11.032>
- Kuo, P.-L., Wu, C.-A., Lu, C.-Y., Tsao, C.-H., Hsu, C.-H., & Hou, S.-S. (2014). High performance of transferring lithium ion for polyacrylonitrile-interpenetrating crosslinked polyoxyethylene network as gel polymer electrolyte. *ACS Applied Materials &*

Interfaces, 6(5), 3156–3162.

- Kurapati, S., Gunturi, S. S., Nadella, K. J., & Erothu, H. (2019). Novel solid polymer electrolyte based on PMMA: CH₃ COOLi effect of salt concentration on optical and conductivity studies. *Polymer Bulletin*, 1–19.
- Kuratomi, J., Iguchi, T., Bando, T., Aihara, Y., Ono, T., & Kuwana, K. (2001). Development of solid polymer lithium secondary batteries. *Journal of Power Sources*, 97, 801–803.
- Landi, B. J. (2009). *Energy & Environmental Science*. 2(6). <https://doi.org/10.1039/b904116h>
- Leber, D. E., Chaney, R. L., Hackler, D. R., Meek, B. N., Leija, S. D., DeGregorio, K. J., Wald, S. F., & Wilson, D. G. (2017). Advances in flexible hybrid electronics reliability. *2017 IEEE Workshop on Microelectronics and Electron Devices (WMED)*, 1–4.
- Leclerc, M. J. (2006). *Sci.*, Part A: Polym. Chem., 2001, 39, 2867–2873;(b) AC Grimsdale and K. Müllen. *Adv. Polym. Sci*, 199, 1–82.
- Lee, J.-S., Kim, H.-S., & Ryu, W.-H. (2019). Iron/carbon composite microfiber catalyst derived from hemoglobin blood protein for lithium-oxygen batteries. *Applied Surface Science*, 466, 562–567.
- Lee, J., Howell, T., Rottmayer, M., Boeckl, J., & Huang, H. (2019). *Free-Standing PEO / LiTFSI / LAGP Composite Electrolyte Membranes for Applications to Flexible Solid-State Lithium-Based Batteries*. 166(2), 416–422. <https://doi.org/10.1149/2.1321902jes>
- Lee, K.-H., Lee, Y.-G., Park, J.-K., & Seung, D.-Y. (2000). Effect of silica on the electrochemical characteristics of the plasticized polymer electrolytes based on the P (AN-co-MMA) copolymer. *Solid State Ionics*, 133(3–4), 257–263.
- Lee, Y. J., Yi, H., Kim, W.-J., Kang, K., Yun, D. S., Strano, M. S., Ceder, G., & Belcher, A. M. (2009). Fabricating genetically engineered high-power lithium-ion batteries using

- multiple virus genes. *Science*, 324(5930), 1051–1055.
- Lee, Y. M., Kim, J.-W., Choi, N.-S., Lee, J. A., Seol, W.-H., & Park, J.-K. (2005). Novel porous separator based on PVdF and PE non-woven matrix for rechargeable lithium batteries. *Journal of Power Sources*, 139(1–2), 235–241.
- Lehmann, M. L., Yang, G., Nanda, J., & Saito, T. (2020). Well-designed Crosslinked Polymer Electrolyte Enables High Ionic Conductivity and Enhanced Salt Solvation. *Journal of The Electrochemical Society*, 167(7), 70539.
- Levi, M. D., Salitra, G., Markovsky, B., Teller, H., Aurbach, D., Heider, U., & Heider, L. (1999). Solid-state electrochemical kinetics of Li-Ion intercalation into $\text{Li}_{1-x}\text{CoO}_2$: simultaneous application of electroanalytical techniques SSCV, PITT, and EIS. *Journal of the Electrochemical Society*, 146(4), 1279.
- Li, H., Li, M., Siyal, S. H., Zhu, M., Lan, J. Le, Sui, G., Yu, Y., Zhong, W., & Yang, X. (2018). A sandwich structure polymer/polymer-ceramics/polymer gel electrolytes for the safe, stable cycling of lithium metal batteries. *Journal of Membrane Science*, 555(February), 169–176. <https://doi.org/10.1016/j.memsci.2018.03.038>
- Li, Jie, Adewuyi, K., Lotfi, N., Landers, R. G., & Park, J. (2018). A single particle model with chemical/mechanical degradation physics for lithium ion battery State of Health (SOH) estimation. *Applied Energy*, 212, 1178–1190.
- Li, Jiying, Yao, W., Martin, S., & Vaknin, D. (2008). Lithium ion conductivity in single crystal LiFePO_4 . *Solid State Ionics*, 179(35–36), 2016–2019.
- Li, Juchuan, Ma, C., Chi, M., Liang, C., & Dudney, N. J. (2015). Solid electrolyte: the key for high-voltage lithium batteries. *Advanced Energy Materials*, 5(4), 1401408.
- Li, K., Cheng, X., Zhu, F., Li, L., Xie, Z., Luan, H., Wang, Z., Ji, Z., Wang, H., Liu, F., Xue,

- Y., Jiang, C., Feng, X., Li, L., Rogers, J. A., Huang, Y., & Zhang, Y. (2019). A Generic Soft Encapsulation Strategy for Stretchable Electronics. *Advanced Functional Materials*. <https://doi.org/10.1002/adfm.201806630>
- Li, N., Huang, X., Zhang, H., Li, Y., & Wang, C. (2017). Transparent and Self-Supporting Graphene Films with Wrinkled- Graphene-Wall-Assembled Opening Polyhedron Building Blocks for High Performance Flexible/Transparent Supercapacitors. *ACS Applied Materials and Interfaces*. <https://doi.org/10.1021/acsami.7b00487>
- Li, Q., & Ardebili, H. (2014). Atomistic investigation of the nanoparticle size and shape effects on ionic conductivity of solid polymer electrolytes. *Solid State Ionics*, 268, 156–161.
- Li, Q., Wood, E., & Ardebili, H. (2013). Elucidating the mechanisms of ion conductivity enhancement in polymer nanocomposite electrolytes for lithium ion batteries. *Applied Physics Letters*, 102(24), 243903.
- Li, Sha, Guo, Z. P., Wang, C. Y., Wallace, G. G., & Liu, H. K. (2013). Flexible cellulose based polypyrrole–multiwalled carbon nanotube films for bio-compatible zinc batteries activated by simulated body fluids. *Journal of Materials Chemistry A*, 1(45), 14300–14305.
- Li, Shengyi, & Church, B. C. (2017). Electrochemical stability of aluminum current collector in aqueous rechargeable lithium-ion battery electrolytes. *Journal of Applied Electrochemistry*, 47(7), 839–853.
- Li, W., Xing, Y., Wu, Y., Wang, J., Chen, L., Yang, G., & Tang, B. (2015). Study the effect of ion-complex on the properties of composite gel polymer electrolyte based on Electrospun PVdF nanofibrous membrane. *Electrochimica Acta*, 151, 289–296.

- Li, Y.-D., Zeng, J.-B., Li, W.-D., Yang, K.-K., Wang, X.-L., & Wang, Y.-Z. (2009). Rheology, crystallization, and biodegradability of blends based on soy protein and chemically modified poly (butylene succinate). *Industrial & Engineering Chemistry Research*, 48(10), 4817–4825.
- Li, Y. J., Fan, C. Y., Zhang, J. P., & Wu, X. L. (2018). A promising PMHS/PEO blend polymer electrolyte for all-solid-state lithium ion batteries. *Dalton Transactions*, 47(42), 14932–14937. <https://doi.org/10.1039/C8DT02904K>
- Li, Yang, Wong, K.-W., & Ng, K.-M. (2016). Ionic liquid decorated mesoporous silica nanoparticles: a new high-performance hybrid electrolyte for lithium batteries. *Chemical Communications*, 52(23), 4369–4372.
- Li, Yang, Wong, K. W., Dou, Q., & Ng, K. M. (2016). A single-ion conducting and shear-thinning polymer electrolyte based on ionic liquid-decorated PMMA nanoparticles for lithium-metal batteries. *Journal of Materials Chemistry A*, 4(47), 18543–18550.
- Li, Yang, Wong, K. W., Dou, Q., Zhang, W., Wang, L., & Ng, K. M. (2017). A highly elastic and flexible solid-state polymer electrolyte based on ionic liquid-decorated PMMA nanoparticles for lithium batteries. *New Journal of Chemistry*, 41(21), 13096–13103.
- Li, Yanguang, Tan, B., & Wu, Y. (2008). Mesoporous Co₃O₄ nanowire arrays for lithium ion batteries with high capacity and rate capability. *Nano Letters*. <https://doi.org/10.1021/nl0725906>
- Li, Zhi, Xu, Z., Tan, X., Wang, H., Holt, C. M. B., Stephenson, T., Olsen, B. C., & Mitlin, D. (2013). Mesoporous nitrogen-rich carbons derived from protein for ultra-high capacity battery anodes and supercapacitors. *Energy & Environmental Science*, 6(3), 871–878.
- Li, Zhiming, Shan, F., Wei, J., Yang, J., Li, X., & Wang, X. (2008). High ionic conductive

PVDF-based fibrous electrolytes. *Journal of Solid State Electrochemistry*, 12(12), 1629–1635.

Liang, J., Wang, S., Yu, H., Zhao, X., Wang, H., Tong, Y., Tang, Q., & Liu, Y. (2020).

Solution-processed PDMS/SWCNT porous electrodes with high mass loading: toward high performance all-stretchable-component lithium ion batteries. *Sustainable Energy and Fuels*. <https://doi.org/10.1039/c9se01120j>

Liang, Y. F., Xia, Y., Zhang, S. Z., Wang, X. L., Xia, X. H., Gu, C. D., Wu, J. B., & Tu, J. P.

(2019). A preeminent gel blending polymer electrolyte of poly (vinylidene fluoride-hexafluoropropylene)-poly (propylene carbonate) for solid-state lithium ion batteries. *Electrochimica Acta*, 296, 1064–1069.

Liao, Y. H., Li, X. P., Fu, C. H., Xu, R., Rao, M. M., Zhou, L., Hu, S. J., & Li, W. S. (2011).

Performance improvement of polyethylene-supported poly (methyl methacrylate-vinyl acetate)-co-poly (ethylene glycol) diacrylate based gel polymer electrolyte by doping nano-Al₂O₃. *Journal of Power Sources*, 196(16), 6723–6728.

Liao, Y. H., Zhou, D. Y., Rao, M. M., Li, W. S., Cai, Z. P., Liang, Y., & Tan, C. L. (2009).

Self-supported poly (methyl methacrylate–acrylonitrile–vinyl acetate)-based gel electrolyte for lithium ion battery. *Journal of Power Sources*, 189(1), 139–144.

Liao, Y., Sun, C., Hu, S., & Li, W. (2013). Anti-thermal shrinkage nanoparticles/polymer and ionic liquid based gel polymer electrolyte for lithium ion battery. *Electrochimica Acta*, 89, 461–468.

Lin, D., Liu, W., Liu, Y., Lee, H. R., Hsu, P.-C., Liu, K., & Cui, Y. (2015). High ionic

conductivity of composite solid polymer electrolyte via in situ synthesis of monodispersed SiO₂ nanospheres in poly (ethylene oxide). *Nano Letters*, 16(1), 459–465.

- Lin, D., Liu, W., Liu, Y., Lee, H. R., Hsu, P. C., Liu, K., & Cui, Y. (2016). High Ionic Conductivity of Composite Solid Polymer Electrolyte via in Situ Synthesis of Monodispersed SiO₂ Nanospheres in Poly(ethylene oxide). *Nano Letters*, 16(1), 459–465. <https://doi.org/10.1021/acs.nanolett.5b04117>
- Liu, Bin, Zhang, J., Wang, X., Chen, G., Chen, D., Zhou, C., & Shen, G. (2012). Hierarchical three-dimensional ZnCo₂O₄ nanowire arrays/carbon cloth anodes for a novel class of high-performance flexible lithium-ion batteries. *Nano Letters*, 12(6), 3005–3011. <https://doi.org/10.1021/nl300794f>
- Liu, Bo, Huang, Y., Cao, H., Zhao, L., Huang, Y., Song, A., Lin, Y., Li, X., & Wang, M. (2018). A novel porous gel polymer electrolyte based on poly (acrylonitrile-polyhedral oligomeric silsesquioxane) with high performances for lithium-ion batteries. *Journal of Membrane Science*, 545, 140–149.
- Liu, C., Neale, Z. G., & Cao, G. (2016). Understanding electrochemical potentials of cathode materials in rechargeable batteries. *Materials Today*, 19(2), 109–123.
- Liu, H., Wang, G., Liu, J., Qiao, S., & Ahn, H. (2011). Highly ordered mesoporous NiO anode material for lithium ion batteries with an excellent electrochemical performance. *Journal of Materials Chemistry*, 21(9), 3046–3052.
- Liu, K., Yao, Y., Lv, T., Li, H., Li, N., Chen, Z., Qian, G., & Chen, T. (2020). Textile-like electrodes of seamless graphene/nanotubes for wearable and stretchable supercapacitors. *Journal of Power Sources*. <https://doi.org/10.1016/j.jpowsour.2019.227355>
- Liu, W., Chen, J., Chen, Z., Liu, K., Zhou, G., Sun, Y., Song, M. S., Bao, Z., & Cui, Y. (2017). Stretchable Lithium-Ion Batteries Enabled by Device-Scaled Wavy Structure and Elastic-Sticky Separator. *Advanced Energy Materials*.

<https://doi.org/10.1002/aenm.201701076>

- Liu, W., Liu, N., Sun, J., Hsu, P.-C., Li, Y., Lee, H.-W., & Cui, Y. (2015a). Ionic conductivity enhancement of polymer electrolytes with ceramic nanowire fillers. *Nano Letters*, 15(4), 2740–2745.
- Liu, W., Liu, N., Sun, J., Hsu, P. C., Li, Y., Lee, H. W., & Cui, Y. (2015b). Ionic Conductivity Enhancement of Polymer Electrolytes with Ceramic Nanowire Fillers. *Nano Letters*, 15(4), 2740–2745. <https://doi.org/10.1021/acs.nanolett.5b00600>
- Liu, Yijie, Li, C., Li, B., Song, H., Cheng, Z., Chen, M., He, P., & Zhou, H. (2018). Germanium Thin Film Protected Lithium Aluminum Germanium Phosphate for Solid-State Li Batteries. *Advanced Energy Materials*, 8(16), 1702374.
- Liu, Yuewen, Peng, X., Cao, Q., Jing, B., Wang, X., & Deng, Y. (2017). Gel polymer electrolyte based on poly (vinylidene fluoride)/thermoplastic polyurethane/polyacrylonitrile by the electrospinning technique. *The Journal of Physical Chemistry C*, 121(35), 19140–19146.
- Lou, X. W., Deng, D., Lee, J. Y., Feng, J., & Archer, L. A. (2008). Self-supported formation of needlelike Co₃O₄ nanotubes and their application as lithium-ion battery electrodes. *Advanced Materials*. <https://doi.org/10.1002/adma.200702412>
- Lu, L., Zuo, X., Li, W., Liu, J., & Xu, M. (2007). Study on the preparation and performances of PMMA-Vac polymer electrolyte for lithium ion battery use. *ACTA CHIMICA SINICA-CHINESE EDITION*-, 65(6), 475.
- Lu, Yang, He, K. W., Zhang, S. J., Zhou, Y. X., & Wang, Z. B. (2019). UV-curable-based plastic crystal polymer electrolyte for high-performance all-solid-state Li-ion batteries. *Ionics*, 25(4), 1607–1615. <https://doi.org/10.1007/s11581-018-2788-8>

- Lu, Yingying, Moganty, S. S., Schaefer, J. L., & Archer, L. A. (2012). Ionic liquid-nanoparticle hybrid electrolytes. *Journal of Materials Chemistry*, 22(9), 4066–4072.
- Ma, L., Hendrickson, K. E., Wei, S., & Archer, L. A. (2015). Nanomaterials: Science and applications in the lithium–sulfur battery. *Nano Today*, 10(3), 315–338.
- Ma, T., Cui, Z., Wu, Y., Qin, S., Wang, H., Yan, F., Han, N., & Li, J. (2013). Preparation of PVDF based blend microporous membranes for lithium ion batteries by thermally induced phase separation: I. Effect of PMMA on the membrane formation process and the properties. *Journal of Membrane Science*, 444, 213–222.
- Ma, Y., Ma, J., Chai, J., Liu, Z., Ding, G., Xu, G., Liu, H., Chen, B., Zhou, X., & Cui, G. (2017). Two players make a formidable combination: in situ generated poly (acrylic anhydride-2-methyl-acrylic acid-2-oxirane-ethyl ester-methyl methacrylate) cross-linking gel polymer electrolyte toward 5 V high-voltage batteries. *ACS Applied Materials & Interfaces*, 9(47), 41462–41472.
- MacFarlane, D. R., Tachikawa, N., Forsyth, M., Pringle, J. M., Howlett, P. C., Elliott, G. D., Davis, J. H., Watanabe, M., Simon, P., & Angell, C. A. (2014). Energy applications of ionic liquids. *Energy & Environmental Science*, 7(1), 232–250.
- Macfarlane, D. R., Tachikawa, N., Forsyth, M., Pringle, J. M., Howlett, P. C., Elliott, G. D., Davis, J. H., Watanabe, M., Simon, P., Angell, C. A., Macfarlane, D. R., Tachikawa, N., Forsyth, M., Pringle, J. M., & Patrick, C. (2014). *Energy applications of ionic liquids To cite this version* : 7(1). <https://doi.org/10.1039/c3ee42099j>
- MacGlashan, G. S., Andreev, Y. G., & Bruce, P. G. (1999). Structure of the polymer electrolyte poly (ethylene oxide) 6: LiAsF 6. *Nature*, 398(6730), 792–794.
- Machida, N., Kobayashi, K., Nishikawa, Y., & Shigematsu, T. (2004). Electrochemical

- properties of sulfur as cathode materials in a solid-state lithium battery with inorganic solid electrolytes. *Solid State Ionics*, 175(1–4), 247–250.
- Mackanic, D. G., Kao, M., & Bao, Z. (2020). Enabling Deformable and Stretchable Batteries. In *Advanced Energy Materials*. <https://doi.org/10.1002/aenm.202001424>
- Malmgren, S., Ciosek, K., Hahlin, M., Gustafsson, T., Gorgoi, M., Rensmo, H., & Edström, K. (2013). Comparing anode and cathode electrode/electrolyte interface composition and morphology using soft and hard X-ray photoelectron spectroscopy. *Electrochimica Acta*, 97, 23–32.
- Manthiram, A. (2020). A reflection on lithium-ion battery cathode chemistry. *Nature Communications*, 11(1), 1–9.
- Manuel Stephan, A. (2005). Review on gel polymer electrolytes for lithium batteries. *European Polymer Journal*, 42(1), 21–42.
<https://doi.org/10.1016/j.eurpolymj.2005.09.017>
- Marco, C., Gómez, M. A., Fatou, J. G., Etxeberria, A., Elorza, M. M., & Iruin, J. J. (1993). Miscibility of poly (vinyl chloride)/poly (ethylene oxide) blends—I. Thermal properties and solid state ¹³C-NMR study. *European Polymer Journal*, 29(11), 1477–1481.
- Martha, S. K., Haik, O., Zinigrad, E., Exnar, I., Drezen, T., Miners, J. H., & Aurbach, D. (2011). On the thermal stability of olivine cathode materials for lithium-ion batteries. *Journal of the Electrochemical Society*, 158(10), A1115.
- Matsui, S., Muranaga, T., Higobashi, H., Inoue, S., & Sakai, T. (2001). Liquid-free rechargeable Li polymer battery. *Journal of Power Sources*, 97, 772–774.
- Matsumoto, H., Sakaebe, H., Tatsumi, K., Kikuta, M., Ishiko, E., & Kono, M. (2006). Fast cycling of Li/LiCoO₂ cell with low-viscosity ionic liquids based on bis (fluorosulfonyl)

- imide [FSI]–. *Journal of Power Sources*, 160(2), 1308–1313.
- Matula, R. A. (1979). Electrical resistivity of copper, gold, palladium, and silver. *Journal of Physical and Chemical Reference Data*, 8(4), 1147–1298.
- Mauger, A., & Julien, C. (2014). Surface modifications of electrode materials for lithium-ion batteries: Status and trends. *Ionics*, 20(6), 751–787. <https://doi.org/10.1007/s11581-014-1131-2>
- McMillan, R., Sleg, H., Shu, Z. X., & Wang, W. (1999). Fluoroethylene carbonate electrolyte and its use in lithium ion batteries with graphite anodes. *Journal of Power Sources*, 81, 20–26.
- Meduri, P., Pendyala, C., Kumar, V., Sumanasekera, G. U., & Sunkara, M. K. (2009). Hybrid tin oxide nanowires as stable and high capacity anodes for li-ion batteries. *Nano Letters*. <https://doi.org/10.1021/nl802864a>
- Mehta, M. A., & Fujinami, T. (1997). Li⁺ transference number enhancement in polymer electrolytes by incorporation of anion trapping boroxine rings into the polymer host. *Chemistry Letters*, 26(9), 915–916.
- Menne, S., Vogl, T., & Balducci, A. (2014). Lithium coordination in protic ionic liquids. *Physical Chemistry Chemical Physics*, 16(12), 5485–5489.
- Meoli, D., & May-Plumlee, T. (2002). Interactive electronic textile development: A review of technologies. *Journal of Textile and Apparel, Technology and Management*.
- Mercier, R., Malugani, J.-P., Fahys, B., & Robert, G. (1981). Superionic conduction in Li₂S-P₂S₅-LiI-glasses. *Solid State Ionics*, 5, 663–666.
- Meyer, W. H. (1998). Polymer electrolytes for lithium-ion batteries. *Advanced Materials*. [https://doi.org/10.1002/\(SICI\)1521-4095\(199804\)10:6<439::AID-ADMA439>3.0.CO;2-I](https://doi.org/10.1002/(SICI)1521-4095(199804)10:6<439::AID-ADMA439>3.0.CO;2-I)

- Milczarek, G., & Inganäs, O. (2012). Renewable cathode materials from biopolymer/conjugated polymer interpenetrating networks. *Science*, 335(6075), 1468–1471.
- Min, H.-S., Ko, J.-M., & Kim, D.-W. (2003). Preparation and characterization of porous polyacrylonitrile membranes for lithium-ion polymer batteries. *Journal of Power Sources*, 119, 469–472.
- Minami, K., Hayashi, A., Ujiie, S., & Tatsumisago, M. (2011). Electrical and electrochemical properties of glass–ceramic electrolytes in the systems Li₂S–P₂S₅–P₂S₃ and Li₂S–P₂S₅–P₂O₅. *Solid State Ionics*, 192(1), 122–125.
- Mindemark, J., Sun, B., Törmä, E., & Brandell, D. (2015). High-performance solid polymer electrolytes for lithium batteries operational at ambient temperature. *Journal of Power Sources*, 298, 166–170.
- Miot, J., Recham, N., Larcher, D., Guyot, F., Brest, J., & Tarascon, J.-M. (2014). Biomaterialized α -Fe₂O₃: texture and electrochemical reaction with Li. *Energy & Environmental Science*, 7(1), 451–460.
- Miranda, D. F., Versek, C., Tuominen, M. T., Russell, T. P., & Watkins, J. J. (2013). Cross-linked block copolymer/ionic liquid self-assembled blends for polymer gel electrolytes with high ionic conductivity and mechanical strength. *Macromolecules*, 46(23), 9313–9323.
- Mohanty, D., Dahlberg, K., King, D. M., David, L. A., Sefat, A. S., Wood, D. L., Daniel, C., Dhar, S., Mahajan, V., & Lee, M. (2016). Modification of Ni-rich FCG NMC and NCA cathodes by atomic layer deposition: preventing surface phase transitions for high-voltage lithium-ion batteries. *Scientific Reports*, 6, 26532.

- Möller, K.-C., Hodal, T., Appel, W. K., Winter, M., & Besenhard, J. O. (2001). Fluorinated organic solvents in electrolytes for lithium ion cells. *Journal of Power Sources*, 97, 595–597.
- Monroe, C., & Newman, J. (2005). The impact of elastic deformation on deposition kinetics at lithium/polymer interfaces. *Journal of The Electrochemical Society*, 152(2), A396.
- Mu, H., Wang, W., Yang, L., Chen, J., Li, X., Yuan, Y., Tian, X., & Wang, G. (2021). Fully integrated design of intrinsically stretchable electrodes for stretchable supercapacitors. *Energy Storage Materials*. <https://doi.org/10.1016/j.ensm.2021.04.017>
- Muniyandi, N., Kalaiselvi, N., Periyasamy, P., Thirunakaran, R., Gopukumar, S., Premkumar, T., Renganathan, N. G., & Raghavan, M. (2001). Optimisation of PVdF-based polymer electrolytes. *Journal of Power Sources*, 96(1), 14–19.
- Muralidharan, N., Essehli, R., Hermann, R. P., Amin, R., Jafta, C., Zhang, J., Liu, J., Du, Z., Meyer III, H. M., & Self, E. (2020). Lithium Iron Aluminum Nickelate, LiNixFeyAlzO2—New Sustainable Cathodes for Next-Generation Cobalt-Free Li-Ion Batteries. *Advanced Materials*, 2002960.
- Murata, K., Izuchi, S., & Yoshihisa, Y. (2000). An overview of the research and development of solid polymer electrolyte batteries. *Electrochimica Acta*, 45(8–9), 1501–1508.
- Naji, A., Ghanbaja, J., Willmann, P., & Billaud, D. (2000). New halogenated additives to propylene carbonate-based electrolytes for lithium-ion batteries. *Electrochimica Acta*, 45(12), 1893–1899.
- Nakai, H., Kubota, T., Kita, A., & Kawashima, A. (2011). Investigation of the solid electrolyte interphase formed by fluoroethylene carbonate on Si electrodes. *Journal of The Electrochemical Society*, 158(7), A798.

- Nam, K. T., Kim, D.-W., Yoo, P. J., Chiang, C.-Y., Meethong, N., Hammond, P. T., Chiang, Y.-M., & Belcher, A. M. (2006a). Virus-enabled synthesis and assembly of nanowires for lithium ion battery electrodes. *Science*, *312*(5775), 885–888.
- Nam, K. T., Kim, D., Yoo, P. J., Chiang, C., Meethong, N., Hammond, P. T., Chiang, Y., & Belcher, A. M. (2006b). Virus-Enabled Synthesis and Assembly Battery Electrodes. *Science*, *312*(October), 885–889. <https://doi.org/10.1126/science.1122716>
- Nam, K. T., Wartena, R., Yoo, P. J., Liao, F. W., Lee, Y. J., Chiang, Y.-M., Hammond, P. T., & Belcher, A. M. (2008). Stamped microbattery electrodes based on self-assembled M13 viruses. *Proceedings of the National Academy of Sciences*, *105*(45), 17227–17231.
- Nan, C.-W., Fan, L., Lin, Y., & Cai, Q. (2003). Enhanced Ionic Conductivity of Polymer Electrolytes Containing Nanocomposite SiO₂ Particles. *Physical Review Letters*, *91*(26), 266104.
- Ngai, K. S., Ramesh, S., Ramesh, K., & Juan, J. C. (2016). A review of polymer electrolytes: fundamental, approaches and applications. *Ionics*, *22*(8), 1259–1279.
- Ni, W., Yang, D., Cheng, J., Li, X., Guan, Q., & Wang, B. (2016). Gel-type polymer separator with higher thermal stability and effective overcharge protection of 4.2 V for secondary lithium-ion batteries. *RSC Advances*, *6*(58), 52966–52973.
- Nicotera, I., Coppola, L., Oliviero, C., Castriota, M., & Cazzanelli, E. (2006). Investigation of ionic conduction and mechanical properties of PMMA–PVdF blend-based polymer electrolytes. *Solid State Ionics*, *177*(5–6), 581–588.
- Nithya, H., Selvasekarapandian, S., Selvin, P. C., Kumar, D. A., & Kawamura, J. (2012). Effect of propylene carbonate and dimethylformamide on ionic conductivity of P (ECH-EO) based polymer electrolyte. *Electrochimica Acta*, *66*, 110–120.

- Nitta, N., Wu, F., Lee, J. T., & Yushin, G. (2015). Li-ion battery materials: present and future. *Materials Today*, 18(5), 252–264.
- Niu, C., Liu, J., Chen, G., Liu, C., Qian, T., Zhang, J., Cao, B., Shang, W., Chen, Y., Han, J., Du, J., & Chen, Y. (2019). Anion-regulated solid polymer electrolyte enhances the stable deposition of lithium ion for lithium metal batteries. *Journal of Power Sources*, 417(January), 70–75. <https://doi.org/10.1016/j.jpowsour.2019.02.004>
- Noelle, D. J., Wang, M., & Qiao, Y. (2018). Improved safety and mechanical characterizations of thick lithium-ion battery electrodes structured with porous metal current collectors. *Journal of Power Sources*, 399, 125–132.
- Noh, H.-J., Youn, S., Yoon, C. S., & Sun, Y.-K. (2013). Comparison of the structural and electrochemical properties of layered Li [NixCoyMnz] O2 (x= 1/3, 0.5, 0.6, 0.7, 0.8 and 0.85) cathode material for lithium-ion batteries. *Journal of Power Sources*, 233, 121–130.
- Nunes-Pereira, J., Costa, C. M., & Lanceros-Méndez, S. (2015). Polymer composites and blends for battery separators: state of the art, challenges and future trends. *Journal of Power Sources*, 281, 378–398.
- Oh, D., Qi, J., Lu, Y.-C., Zhang, Y., Shao-Horn, Y., & Belcher, A. M. (2013). Biologically enhanced cathode design for improved capacity and cycle life for lithium-oxygen batteries. *Nature Communications*, 4(1), 1–8.
- Oh, D. Y., Nam, Y. J., Park, K. H., Jung, S. H., Cho, S., Kim, Y. K., Lee, Y., Lee, S., & Jung, Y. S. (2015). Excellent Compatibility of Solvate Ionic Liquids with Sulfide Solid Electrolytes: Toward Favorable Ionic Contacts in Bulk-Type All-Solid-State Lithium-Ion Batteries. *Advanced Energy Materials*, 5(22), 1500865.
- Omichi, H., Yoshida, K., Suzuki, K., & Araki, K. (1978). Development of a continuous

- process for radiation-induced graft polymerization of butadiene onto poly (vinyl chloride). *Radiation Physics and Chemistry* (1977), 11(6), 327–334.
- Pal, P., & Ghosh, A. (2018). Influence of TiO₂ nano-particles on charge carrier transport and cell performance of PMMA-LiClO₄ based nano-composite electrolytes. *Electrochimica Acta*, 260, 157–167.
- Panero, S., Scrosati, B., Sumathipala, H. H., & Wieczorek, W. (2007). Dual-composite polymer electrolytes with enhanced transport properties. *Journal of Power Sources*, 167(2), 510–514.
- Park, K.-J., Hwang, J.-Y., Ryu, H.-H., Maglia, F., Kim, S.-J., Lamp, P., Yoon, C. S., & Sun, Y.-K. (2019). Degradation mechanism of Ni-enriched NCA cathode for lithium batteries: are microcracks really critical? *ACS Energy Letters*, 4(6), 1394–1400.
- Park, M., Ryu, J., Kim, Y., & Cho, J. (2014). Corn protein-derived nitrogen-doped carbon materials with oxygen-rich functional groups: a highly efficient electrocatalyst for all-vanadium redox flow batteries. *Energy & Environmental Science*, 7(11), 3727–3735.
- Patel, M., & Bhattacharyya, A. J. (2008). Plastic–polymer composite electrolytes: Novel soft matter electrolytes for rechargeable lithium batteries. *Electrochemistry Communications*, 10(12), 1912–1915.
- Patel, M., Chandrappa, K. G., & Bhattacharyya, A. J. (2008). Increasing ionic conductivity and mechanical strength of a plastic electrolyte by inclusion of a polymer. *Electrochimica Acta*, 54(2), 209–215.
- Peled, E. (1997). Advanced Model for Solid Electrolyte Interphase Electrodes in Liquid and Polymer Electrolytes. *Journal of The Electrochemical Society*, 144(8), L208.
<https://doi.org/10.1149/1.1837858>

- Peng, H.-J., Huang, J.-Q., & Zhang, Q. (2017). A review of flexible lithium–sulfur and analogous alkali metal–chalcogen rechargeable batteries. *Chemical Society Reviews*, 46(17), 5237–5288.
- Pistoia, G., Antonini, A., & Wang, G. (1996). Impedance study on the reactivity of gel polymer electrolytes towards a lithium electrode. *Journal of Power Sources*, 58(2), 139–144.
- Pylahan, N., Letiche, M., Barr, M. K. S., & Djenizian, T. (2014). All-solid-state lithium-ion batteries based on self-supported titania nanotubes. *Electrochemistry Communications*, 43, 121–124.
- Poizot, P., Laruelle, S., Grugeon, S., Dupont, L., & Tarascon, J.-M. (2000a). Nano-sized transition-metal oxides as negative-electrode materials for lithium-ion batteries. *Nature*, 407(September), 496.
<https://doi.org/10.1038/35035045>
<http://10.0.4.14/35035045>
<https://www.nature.com/articles/35035045#supplementary-information>
- Poizot, P., Laruelle, S., Grugeon, S., Dupont, L., & Tarascon, J. M. (2000b). Nano-sized transition-metal oxides as negative-electrode materials for lithium-ion batteries. *Nature*.
<https://doi.org/10.1038/35035045>
- Polu, A. R., & Rhee, H. W. (2017). Ionic liquid doped PEO-based solid polymer electrolytes for lithium-ion polymer batteries. *International Journal of Hydrogen Energy*, 42(10), 7212–7219. <https://doi.org/10.1016/j.ijhydene.2016.04.160>
- Prasanth, R., Shubha, N., Hng, H. H., & Srinivasan, M. (2013). Effect of nano-clay on ionic conductivity and electrochemical properties of poly (vinylidene fluoride) based nanocomposite porous polymer membranes and their application as polymer electrolyte

- in lithium ion batteries. *European Polymer Journal*, 49(2), 307–318.
- Prasanth, R., Shubha, N., Hng, H. H., & Srinivasan, M. (2014). Effect of poly (ethylene oxide) on ionic conductivity and electrochemical properties of poly (vinylidene fluoride) based polymer gel electrolytes prepared by electrospinning for lithium ion batteries. *Journal of Power Sources*, 245, 283–291.
- Prosini, P. P., Passerini, S., Vellone, R., & Smyrl, W. H. (1998). V₂O₅ xerogel lithium–polymer electrolyte batteries. *Journal of Power Sources*, 75(1), 73–83.
- Pu, W., He, X., Wang, L., Tian, Z., Jiang, C., & Wan, C. (2006). Preparation of P (AN–MMA) microporous membrane for Li-ion batteries by phase inversion. *Journal of Membrane Science*, 280(1–2), 6–9.
- Pyun, S.-I., & Bae, J.-S. (1996). The ac impedance study of electrochemical lithium intercalation into porous vanadium oxide electrode. *Electrochimica Acta*, 41(6), 919–925.
- Qi, D., Zhang, K., Tian, G., Jiang, B., & Huang, Y. (2021). Stretchable Electronics Based on PDMS Substrates. *Advanced Materials*. <https://doi.org/10.1002/adma.202003155>
- Raghavan, P., Manuel, J., Zhao, X., Kim, D.-S., Ahn, J.-H., & Nah, C. (2011). Preparation and electrochemical characterization of gel polymer electrolyte based on electrospun polyacrylonitrile nonwoven membranes for lithium batteries. *Journal of Power Sources*, 196(16), 6742–6749.
- Rajendran, S., Mahendran, O., & Kannan, R. (2002). Ionic conductivity studies in composite solid polymer electrolytes based on methylmethacrylate. *Journal of Physics and Chemistry of Solids*, 63(2), 303–307.
- Rajendran, S., & Sivakumar, P. (2008). An investigation of PVdF/PVC-based blend electrolytes with EC/PC as plasticizers in lithium battery applications. *Physica B*:

Condensed Matter, 403(4), 509–516.

- Ramesh, S., Liew, C.-W., Morris, E., & Durairaj, R. (2010). Effect of PVC on ionic conductivity, crystallographic structural, morphological and thermal characterizations in PMMA–PVC blend-based polymer electrolytes. *Thermochimica Acta*, 511(1–2), 140–146.
- Rao, M., Geng, X., Liao, Y., Hu, S., & Li, W. (2012). Preparation and performance of gel polymer electrolyte based on electrospun polymer membrane and ionic liquid for lithium ion battery. *Journal of Membrane Science*, 399, 37–42.
- Rao, M. M., Liu, J. S., Li, W. S., Liang, Y., & Zhou, D. Y. (2008). Preparation and performance analysis of PE-supported P (AN-co-MMA) gel polymer electrolyte for lithium ion battery application. *Journal of Membrane Science*, 322(2), 314–319.
- Ratner, M. A., Johansson, P., & Shriver, D. F. (2000). Polymer electrolytes: ionic transport mechanisms and relaxation coupling. *Mrs Bulletin*, 25(3), 31–37.
- Reiter, J., Krejza, O., & Sedlářiková, M. (2009). Electrochromic devices employing methacrylate-based polymer electrolytes. *Solar Energy Materials and Solar Cells*, 93(2), 249–255.
- Ren, W., Wang, K., Yang, J., Tan, R., Hu, J., Guo, H., Duan, Y., Zheng, J., Lin, Y., & Pan, F. (2016). Soft-contact conductive carbon enabling depolarization of LiFePO₄ cathodes to enhance both capacity and rate performances of lithium ion batteries. *Journal of Power Sources*, 331, 232–239. <https://doi.org/10.1016/j.jpowsour.2016.09.049>
- Rhoo, H.-J., Kim, H.-T., Park, J.-K., & Hwang, T.-S. (1997). Ionic conduction in plasticized PVC/PMMA blend polymer electrolytes. *Electrochimica Acta*, 42(10), 1571–1579.
- Richards, W. D., Miara, L. J., Wang, Y., Kim, J. C., & Ceder, G. (2016). Interface Stability in

Solid-State Batteries. *Chemistry of Materials*.

<https://doi.org/10.1021/acs.chemmater.5b04082>

- Riley, M., Fedkiw, P. S., & Khan, S. A. (2002). Transport properties of lithium hectorite-based composite electrolytes. *Journal of the Electrochemical Society*, 149(6), A667–A674.
- Ritchie, A., & Howard, W. (2006). Recent developments and likely advances in lithium-ion batteries. *Journal of Power Sources*, 162(2), 809–812.
- Robertson, A. D., West, A. R., & Ritchie, A. G. (1997). Review of crystalline lithium-ion conductors suitable for high temperature battery applications. *Solid State Ionics*, 104(1–2), 1–11.
- Rogers, J. A., Someya, T., & Huang, Y. (2010). Materials and mechanics for stretchable electronics. In *Science*. <https://doi.org/10.1126/science.1182383>
- Rubinstein, L. I. (1971). The Stefan Problem, Vol. 27. *Providence, RI: American Mathematical Society*.
- Rupp, B., Schmuck, M., Balducci, A., Winter, M., & Kern, W. (2008). Polymer electrolyte for lithium batteries based on photochemically crosslinked poly (ethylene oxide) and ionic liquid. *European Polymer Journal*, 44(9), 2986–2990.
- Ryu, H.-H., Park, K.-J., Yoon, C. S., & Sun, Y.-K. (2018). Capacity Fading of Ni-Rich Li [Ni_x Co_y Mn_{1-x-y}] O₂ (0.6 ≤ x ≤ 0.95) Cathodes for High-Energy-Density Lithium-Ion Batteries: Bulk or Surface Degradation? *Chemistry of Materials*, 30(3), 1155–1163.
- Sakamoto, J. S., & Dunn, B. (2001). Vanadium oxide-carbon nanotube composite electrodes for use in secondary lithium batteries. *Journal of the Electrochemical Society*, 149(1), A26.

- Sakuda, A., Yamauchi, A., Yubuchi, S., Kitamura, N., Idemoto, Y., Hayashi, A., & Tatsumisago, M. (2018). Mechanochemically Prepared Li_2S – P_2S_5 – LiBH_4 Solid Electrolytes with an Argyrodite Structure. *ACS Omega*, 3(5), 5453–5458.
- Santhosha, A. L., Medenbach, L., Palaniselvam, T., & Adelhelm, P. (2020). Sodium-Storage Behavior of Exfoliated MoS_2 as an Electrode Material for Solid-State Batteries with Na_3PS_4 as the Solid Electrolyte. *The Journal of Physical Chemistry C*, 124(19), 10298–10305.
- Sato, K., Zhao, L., Okada, S., & Yamaki, J. (2011). LiPF_6 /methyl difluoroacetate electrolyte with vinylene carbonate additive for Li-ion batteries. *Journal of Power Sources*, 196(13), 5617–5622.
- Sato, T., Morinaga, T., Marukane, S., Narutomi, T., Igarashi, T., Kawano, Y., Ohno, K., Fukuda, T., & Tsujii, Y. (2011). Novel Solid-State Polymer Electrolyte of Colloidal Crystal Decorated with Ionic-Liquid Polymer Brush. *Advanced Materials*, 23(42), 4868–4872.
- Schmalzried, H., & Pelton, A. D. (1981). *Solid state reactions*.
- Sethuraman, V. A., Kowolik, K., & Srinivasan, V. (2011). Increased cycling efficiency and rate capability of copper-coated silicon anodes in lithium-ion batteries. *Journal of Power Sources*, 196(1), 393–398.
- Sheldon, M. H., Glasse, M. D., Latham, R. J., & Linford, R. G. (1989). The effect of plasticiser on zinc polymer electrolytes. *Solid State Ionics*, 34(1–2), 135–138.
- Shi, C., Wang, T., Liao, X., Qie, B., Yang, P., Chen, M., Wang, X., Srinivasan, A., Cheng, Q., Ye, Q., Li, A. C., Chen, X., & Yang, Y. (2019). Accordion-like stretchable Li-ion batteries with high energy density. *Energy Storage Materials*.

<https://doi.org/10.1016/j.ensm.2018.11.019>

- Shi, J., Yang, Y., & Shao, H. (2018). Co-polymerization and blending based PEO/PMMA/P(VDF-HFP) gel polymer electrolyte for rechargeable lithium metal batteries. *Journal of Membrane Science*, 547, 1–10.
- Shim, J., & Striebel, K. A. (2003). Cycling performance of low-cost lithium ion batteries with natural graphite and LiFePO₄. *Journal of Power Sources*, 119, 955–958.
- Shim, J., Striebel, K. A., & Cairns, E. J. (2002). The lithium/sulfur rechargeable cell: effects of electrode composition and solvent on cell performance. *Journal of the Electrochemical Society*, 149(10), A1321.
- Shin, M., & Gewirth, A. A. (2019). Incorporating Solvate and Solid Electrolytes for All-Solid-State Li₂S Batteries with High Capacity and Long Cycle Life. *Advanced Energy Materials*, 9(26), 1900938.
- Shkrob, I. A., Pupek, K. Z., & Abraham, D. P. (2016). Allotropic control: How certain fluorinated carbonate electrolytes protect aluminum current collectors by promoting the formation of insoluble coordination polymers. *The Journal of Physical Chemistry C*, 120(33), 18435–18444.
- Sim, L. N., Majid, S. R., & Arof, A. K. (2012). FTIR studies of PEMA/PVdF-HFP blend polymer electrolyte system incorporated with LiCF₃SO₃ salt. *Vibrational Spectroscopy*, 58, 57–66.
- Simari, C., Lufrano, E., Coppola, L., & Nicotera, I. (2018). Composite gel polymer electrolytes based on organo-modified nanoclays: Investigation on lithium-ion transport and mechanical properties. *Membranes*, 8(3). <https://doi.org/10.3390/membranes8030069>
- Sinirlioglu, D., Muftuoglu, A. E., & Bozkurt, A. (2014). Investigation of proton conductivity

- of inorganic–organic hybrid membranes based on boronic acid and tetrazole. *Journal of Polymer Research*, 21(8), 526.
- Slane, S., & Salomon, M. (1995). Composite gel electrolyte for rechargeable lithium batteries. *Journal of Power Sources*, 55(1), 7–10. [https://doi.org/10.1016/0378-7753\(94\)02148-V](https://doi.org/10.1016/0378-7753(94)02148-V)
- Smart, M. C., Ratnakumar, B. V, Ryan-Mowrey, V. S., Surampudi, S., Prakash, G. K. S., Hu, J., & Cheung, I. (2003). Improved performance of lithium-ion cells with the use of fluorinated carbonate-based electrolytes. *Journal of Power Sources*, 119, 359–367.
- Sohn, H., Gordin, M. L., Xu, T., Chen, S., Lv, D., Song, J., Manivannan, A., & Wang, D. (2014). Porous spherical carbon/sulfur nanocomposites by aerosol-assisted synthesis: the effect of pore structure and morphology on their electrochemical performance as lithium/sulfur battery cathodes. *ACS Applied Materials & Interfaces*, 6(10), 7596–7606.
- Song, J. Y., Wang, Y. Y., & Wan, C. C. (1999a). Review of gel-type polymer electrolytes for lithium-ion batteries. *Journal of Power Sources*, 77(2), 183–197. [https://doi.org/10.1016/S0378-7753\(98\)00193-1](https://doi.org/10.1016/S0378-7753(98)00193-1)
- Song, J. Y., Wang, Y. Y., & Wan, C. C. (1999b). Review of gel-type polymer electrolytes for lithium-ion batteries. *Journal of Power Sources*, 77(2), 183–197.
- Song, Peng-fei, Wang, S., Xiao, M., Du, F., Gan, L., Liu, G., & Meng, Y. (2009). Cross-linkable and thermally stable aliphatic polycarbonates derived from CO₂, propylene oxide and maleic anhydride. *Journal of Polymer Research*, 16(2), 91–97.
- Song, Pengfei, Ran, B., Shang, Y., Kang, L., Chen, Y., & Sun, L. (2019). A facile strategy for the preparation of end-capped and cross-linkable poly (propylene carbonate) with high performance. *Advanced Industrial and Engineering Polymer Research*, 2(4), 161–166.
- Song, Z., Ma, T., Tang, R., Cheng, Q., Wang, X., Krishnaraju, D., Panat, R., Chan, C. K., Yu,

- H., & Jiang, H. (2014). Origami lithium-ion batteries. *Nature Communications*.
<https://doi.org/10.1038/ncomms4140>
- Song, Z., Wang, X., Lv, C., An, Y., Liang, M., Ma, T., He, D., Zheng, Y. J., Huang, S. Q., Yu, H., & Jiang, H. (2015). Kirigami-based stretchable lithium-ion batteries. *Scientific Reports*. <https://doi.org/10.1038/srep10988>
- Stephan, A. M., Kumar, T. P., Renganathan, N. G., Pitchumani, S., Thirunakaran, R., & Muniyandi, N. (2000). Ionic conductivity and FT-IR studies on plasticized PVC/PMMA blend polymer electrolytes. *Journal of Power Sources*, 89(1), 80–87.
- Stephan, A. M., Prem Kumar, T., Angulakshmi, N., Salini, P. S., Sabarinathan, R., Srinivasan, A., & Thomas, S. (2011). Influence of calix [2]-p-benzo [4] pyrrole on the electrochemical properties of poly (ethylene oxide)-based electrolytes for lithium batteries. *Journal of Applied Polymer Science*, 120(4), 2215–2221.
- Stephan, A. M., Thirunakaran, R., Renganathan, N. G., Sundaram, V., Eg, E. I. S. Ž., & Instruments, G. (1999). <Jpowsrc1999_752.Pdf>. 752–758.
- Stramare, S., Thangadurai, V., & Weppner, W. (2003). Lithium Lanthanum Titanates: A Review; *Chem. Mater*, 15, 3974–3990.
- Su, Y.-S., Fu, Y., & Manthiram, A. (2012). Self-weaving sulfur–carbon composite cathodes for high rate lithium–sulfur batteries. *Physical Chemistry Chemical Physics*, 14(42), 14495–14499.
- Sukeshini, A. M., Nishimoto, A., & Watanabe, M. (1996). Transport and electrochemical characterization of plasticized poly (vinyl chloride) solid electrolytes. *Solid State Ionics*, 86, 385–393.
- Sun, H.-H., Choi, W., Lee, J. K., Oh, I.-H., & Jung, H.-G. (2015). Control of electrochemical

- properties of nickel-rich layered cathode materials for lithium ion batteries by variation of the manganese to cobalt ratio. *Journal of Power Sources*, 275, 877–883.
- Sun, H. Y., Takeda, Y., Imanishi, N., Yamamoto, O., & Sohn, H. (2000). Ferroelectric materials as a ceramic filler in solid composite polyethylene Oxide-Based electrolytes. *Journal of the Electrochemical Society*, 147(7), 2462.
- Sun, P., Liao, Y., Xie, H., Chen, T., Rao, M., & Li, W. (2014). Poly (methyl methacrylate–acrylonitrile–ethyl acrylate) terpolymer based gel electrolyte for LiNi_{0.5}Mn_{1.5}O₄ cathode of high voltage lithium ion battery. *Journal of Power Sources*, 269, 299–307.
- Sun, Q., Fang, X., Weng, W., Deng, J., Chen, P., Ren, J., Guan, G., Wang, M., & Peng, H. (2015). An aligned and laminated nanostructured carbon hybrid cathode for high-performance lithium–sulfur batteries. *Angewandte Chemie International Edition*, 54(36), 10539–10544.
- Sun, S., Xia, Q., Liu, J., Xu, J., Zan, F., Yue, J., Savilov, S. V., Lunin, V. V., & Xia, H. (2019). Self-standing oxygen-deficient α -MoO_{3-x} nanoflake arrays as 3D cathode for advanced all-solid-state thin film lithium batteries. *Journal of Materiomics*, 5(2), 229–236. <https://doi.org/10.1016/j.jmat.2019.01.001>
- Sun, Y.-K., Han, J.-M., Myung, S.-T., Lee, S.-W., & Amine, K. (2006). Significant improvement of high voltage cycling behavior AlF₃-coated LiCoO₂ cathode. *Electrochemistry Communications*, 8(5), 821–826.
- Sun, Y.-Z., Huang, J.-Q., Zhao, C.-Z., & Zhang, Q. (2017). A review of solid electrolytes for safe lithium-sulfur batteries. *Science China Chemistry*, 60(12), 1508–1526.
- Sun, Y. K., Hong, K. J., Prakash, J., & Amine, K. (2002). Electrochemical performance of nano-sized ZnO-coated LiNi_{0.5}Mn_{1.5}O₄ spinel as 5 V materials at elevated

- temperatures. *Electrochemistry Communications*, 4(4), 344–348.
[https://doi.org/10.1016/S1388-2481\(02\)00277-1](https://doi.org/10.1016/S1388-2481(02)00277-1)
- Tae, K., Kim, D., Yoo, P. J., Chiang, C., Meethong, N., Hammond, P. T., Chiang, Y., & Belcher, A. M. (2002). American Association for the Advancement of Science (Continued). *The American Naturalist*, 23(274), 935–939. <https://doi.org/10.1086/275028>
- Tai, Z., Liu, Y., Zhang, Q., Zhou, T., Guo, Z., Liu, H. K., & Dou, S. X. (2017). Ultra-light and flexible pencil-trace anode for high performance potassium-ion and lithium-ion batteries. *Green Energy & Environment*, 2(3), 278–284.
- Tang, C., Hackenberg, K., Fu, Q., Ajayan, P. M., & Ardebili, H. (2012). High ion conducting polymer nanocomposite electrolytes using hybrid nanofillers. *Nano Letters*, 12(3), 1152–1156.
- Tang, Y., Deng, J., Li, W., Malyi, O. I., Zhang, Y., Zhou, X., Pan, S., Wei, J., Cai, Y., & Chen, Z. (2017). Water-Soluble Sericin Protein Enabling Stable Solid–Electrolyte Interphase for Fast Charging High Voltage Battery Electrode. *Advanced Materials*, 29(33), 1701828.
- Tarascona, J. (1996). Performace of Bellcore's Plastic rechargeable Li-ion batteries . *Solid State Ionics*, 86, 49-54
- Thackeray, M. M., David, W. I. F., Bruce, P. G., & Goodenough, J. B. (1983). Lithium Insertion into Magnesium Spinel. *Materials Research Bulletin*, 18, 461–472.
[https://doi.org/10.1016/0025-5408\(83\)90138-1](https://doi.org/10.1016/0025-5408(83)90138-1)
- Thangadurai, V., & Weppner, W. (2006). Recent progress in solid oxide and lithium ion conducting electrolytes research. *Ionics*, 12(1), 81–92.
- Thangadurai, Venkataraman, Narayanan, S., & Pinzaru, D. (2014). Garnet-type solid-state fast

- Li ion conductors for Li batteries: Critical review. *Chemical Society Reviews*, 43(13), 4714–4727. <https://doi.org/10.1039/c4cs00020j>
- Thomas, M., David, W. I. F., Goodenough, J. B., & Groves, P. (1985). Synthesis and structural characterization of the normal spinel Li [Ni₂] O₄. *Materials Research Bulletin*, 20(10), 1137–1146.
- Tian, X., Xin, B., Lu, Z., Gao, W., & Zhang, F. (2019). Electrospun sandwich polysulfonamide/polyacrylonitrile/polysulfonamide composite nanofibrous membranes for lithium-ion batteries. *RSC Advances*, 9(20), 11220–11229.
- Tominaga, Y. (2017). Ion-conductive polymer electrolytes based on poly (ethylene carbonate) and its derivatives. *Polymer Journal*, 49(3), 291–299.
- Tsuchida, E., Ohno, H., Tsunemi, K., & Kobayashi, N. (1983). Lithium ionic conduction in poly (methacrylic acid)-poly (ethylene oxide) complex containing lithium perchlorate. *Solid State Ionics*, 11(3), 227–233.
- Tsutsumi, H., Matsuo, A., Takase, K., Doi, S., Hisanaga, A., Onimura, K., & Oishi, T. (2000). Conductivity enhancement of polyacrylonitrile-based electrolytes by addition of cascade nitrile compounds. *Journal of Power Sources*, 90(1), 33–38.
- U.S. Department of Energy. (2019). Emissions from Hybrid and Plug-In Electric Vehicles. Retrieved from U.S Department of Energy: https://afdc.energy.gov/vehicles/electric_emissions.html. In *U.S. Department of Energy*.
- Uchiyama, R., Kusagawa, K., Hanai, K., Imanishi, N., Hirano, A., & Takeda, Y. (2009). Development of dry polymer electrolyte based on polyethylene oxide with co-bridging agent crosslinked by electron beam. *Solid State Ionics*, 180(2–3), 205–211.
- Urbonaitė, S., Poux, T., & Novák, P. (2015). Progress towards commercially viable Li–S

- battery cells. *Advanced Energy Materials*, 5(16), 1500118.
- Varaprasad, A. M., Shashi Mohan, A. L., Chakrabarty, D. K., & Biswas, A. B. (1979). Structural and dielectric studies of some perovskite-type titanates. *Journal of Physics C: Solid State Physics*, 12(3), 465–472. <https://doi.org/10.1088/0022-3719/12/3/014>
- Venkatraman, S., Subramanian, V., Kumar, S. G., Renganathan, N. G., & Muniyandi, N. (2000). Capacity of layered cathode materials for lithium-ion batteries—a theoretical study and experimental evaluation. *Electrochemistry Communications*, 2(1), 18–22.
- Verdier, N., Lepage, D., Zidani, R., Prébé, A., Ayme-Perrot, D., Pellerin, C., Dolle, M., & Rochefort, D. (2019). Cross-Linked Polyacrylonitrile-Based Elastomer Used as Gel Polymer Electrolyte in Li-Ion Battery. *ACS Applied Energy Materials*, 3(1), 1099–1110.
- Verma, P., Maire, P., & Novák, P. (2010). A review of the features and analyses of the solid electrolyte interphase in Li-ion batteries. *Electrochimica Acta*, 55(22), 6332–6341. <https://doi.org/10.1016/j.electacta.2010.05.072>
- Vickraman, P., Aravindan, V., Selvambikai, M., & Shankarasubramanian, N. (2009). Ionic transport, thermal, XRD, and phase morphological studies on LiCF₃SO₃-based PVC–PVdF gel electrolytes. *Ionics*, 15(4), 433–437.
- Vickraman, P., Aravindan, V., & Shankarasubramanian, N. (2007). A study on the blending effect of polyvinylidene fluoride in the ionic transport mechanism of plasticized polyvinyl chloride+ lithium perchlorate gel polymer electrolytes. *Ionics*, 13(5), 355–360.
- Vogel, H. (1921). The law of the relation between the viscosity of liquids and the temperature. *Phys. Z*, 22, 645–646.
- Vogl, T., Menne, S., Kühnel, R.-S., & Balducci, A. (2014). The beneficial effect of protic ionic liquids on the lithium environment in electrolytes for battery applications. *Journal*

of Materials Chemistry A, 2(22), 8258–8265.

Wan, J., Xie, J., Kong, X., Liu, Z., Liu, K., Shi, F., Pei, A., Chen, H., Chen, W., Chen, J.,

Zhang, X., Zong, L., Wang, J., Chen, L., & Qin, J. (n.d.). *for lithium batteries*.

<https://doi.org/10.1038/s41565-019-0465-3>

Wang, A., Xu, H., Zhou, Q., Liu, X., Li, Z., Gao, R., Wu, N., Guo, Y., Li, H., & Zhang, L.

(2016). A new all-solid-state hyperbranched star polymer electrolyte for lithium ion batteries: synthesis and electrochemical properties. *Electrochimica Acta*, 212, 372–379.

Wang, B., Li, X., Luo, B., Yang, J., Wang, X., Song, Q., Chen, S., & Zhi, L. (2013).

Pyrolyzed bacterial cellulose: a versatile support for lithium ion battery anode materials. *Small*, 9(14), 2399–2404.

Wang, B., Richardson, T. J., & Chen, G. (2013). Stable and high-rate overcharge protection for rechargeable lithium batteries. *Physical Chemistry Chemical Physics*, 15(18), 6849–6855.

Wang, C. M., Li, X., Wang, Z., Xu, W., Liu, J., Gao, F., Kovarik, L., Zhang, J. G., Howe, J.,

Burton, D. J., Liu, Z., Xiao, X., Thevuthasan, S., & Baer, D. R. (2012). In situ TEM investigation of congruent phase transition and structural evolution of nanostructured silicon/carbon anode for lithium ion batteries. *Nano Letters*, 12(3), 1624–1632.

<https://doi.org/10.1021/nl204559u>

Wang, Caiyun, Zheng, W., Yue, Z., Too, C. O., & Wallace, G. G. (2011). Buckled, stretchable

polypyrrole electrodes for battery applications. *Advanced Materials*.

<https://doi.org/10.1002/adma.201101067>

Wang, Changhong, Sun, Q., Liu, Y., Zhao, Y., Li, X., Lin, X., Banis, M. N., Li, M., Li, W., &

Adair, K. R. (2018). Boosting the performance of lithium batteries with solid-liquid

- hybrid electrolytes: Interfacial properties and effects of liquid electrolytes. *Nano Energy*, 48, 35–43.
- Wang, Chunhua, Yang, Y., Liu, X., Zhong, H., Xu, H., Xu, Z., Shao, H., & Ding, F. (2017). Suppression of lithium dendrite formation by using LAGP-PEO (LiTFSI) composite solid electrolyte and lithium metal anode modified by PEO (LiTFSI) in all-solid-state lithium batteries. *ACS Applied Materials & Interfaces*, 9(15), 13694–13702.
- Wang, F.-M., Wu, H.-C., Cheng, C.-S., Huang, C.-L., & Yang, C.-R. (2009). High ionic transfer of a hyperbranched-network gel copolymer electrolyte for potential electric vehicle (EV) application. *Electrochimica Acta*, 54(14), 3788–3793.
- Wang, Hailiang, Cui, L. F., Yang, Y., Sanchez Casalongue, H., Robinson, J. T., Liang, Y., Cui, Y., & Dai, H. (2010). Mn₃O₄-graphene hybrid as a high-capacity anode material for lithium ion batteries. *Journal of the American Chemical Society*.
<https://doi.org/10.1021/ja105296a>
- Wang, Huimin, & Yu, D., (2019). 3 V Cu–Al Rechargeable Battery Enabled by Highly Concentrated Aprotic Electrolyte. *ACS Applied Energy Materials*, 2(7), 4936–4942.
- Wang, J.-Y., Nien, P.-C., Chen, C.-H., Chen, L.-C., & Ho, K.-C. (2012). A glucose bio-battery prototype based on a GDH/poly (methylene blue) bioanode and a graphite cathode with an iodide/tri-iodide redox couple. *Bioresource Technology*, 116, 502–506.
- Wang, Q., Song, W. L., Fan, L. Z., & Shi, Q. (2015). Effect of polyacrylonitrile on triethylene glycol diacetate-2-propenoic acid butyl ester gel polymer electrolytes with interpenetrating crosslinked network for flexible lithium ion batteries. *Journal of Power Sources*, 295, 139–148. <https://doi.org/10.1016/j.jpowsour.2015.06.152>
- Wang, Xianming, Yasukawa, E., & Mori, S. (2000). Inhibition of anodic corrosion of

aluminum cathode current collector on recharging in lithium imide electrolytes.

Electrochimica Acta, 45(17), 2677–2684.

Wang, Xiaodan, Lu, Y., Geng, D., Li, L., Zhou, D., Ye, H., Zhu, Y., & Wang, R. (2020).

Planar Fully Stretchable Lithium-Ion Batteries Based on a Lamellar Conductive Elastomer. *ACS Applied Materials and Interfaces*.

<https://doi.org/10.1021/acsami.0c15305>

Wang, Xiaolin, Fu, X., Wang, Y., & Zhong, W. (2016). A protein-reinforced adhesive composite electrolyte. *Polymer*, 106, 43–52.

Wang, Xinya, Xiao, C., Liu, H., Huang, Q., & Fu, H. (2018). Fabrication and properties of PVDF and PVDF-HFP microfiltration membranes. *Journal of Applied Polymer Science*, 135(40), 46711.

Wang, Xiuli, Hao, X., Xia, Y., Liang, Y., Xia, X., & Tu, J. (2019). A polyacrylonitrile (PAN)-based double-layer multifunctional gel polymer electrolyte for lithium-sulfur batteries. *Journal of Membrane Science*, 37–47. <https://doi.org/10.1016/j.memsci.2019.03.048>

Wang, Z., Tan, R., Wang, H., Yang, L., Hu, J., Chen, H., & Pan, F. (2018). A Metal–Organic-Framework-Based Electrolyte with Nanowetted Interfaces for High-Energy-Density Solid-State Lithium Battery. *Advanced Materials*, 30(2), 1–7.

<https://doi.org/10.1002/adma.201704436>

Watanabe, M., Kanba, M., Nagaoka, K., & Shinohara, I. (1982). Ionic conductivity of hybrid films based on polyacrylonitrile and their battery application. *Journal of Applied Polymer Science*, 27(11), 4191–4198. <https://doi.org/10.1002/app.1982.070271110>

Watanabe, M., Kanba, M., Nagaoka, K., & Shinohara, I. (1983). IONIC CONDUCTIVITY OF HYBRID FILMS COMPOSED OF POLYACRYLONITRILE, ETHYLENE

- CARBONATE, AND LiClO₄. *Journal of Polymer Science. Part A-2, Polymer Physics*, 21(6), 939–948.
- Wegener, M., Künstler, W., & Gerhard-Multhaupt, R. (2006). Poling behavior and optical absorption of partially dehydrofluorinated and uniaxially stretched polyvinylidene fluoride. *Ferroelectrics*, 336(1), 3–8.
- Wei, X., & Shriver, D. F. (1998). Highly conductive polymer electrolytes containing rigid polymers. *Chemistry of Materials*, 10(9), 2307–2308.
- Wen, T. C., Luo, S. S., & Yang, C. H. (2000). Ionic conductivity of polymer electrolytes derived from various diisocyanate-based waterborne polyurethanes. *Polymer*, 41(18), 6755–6764. [https://doi.org/10.1016/S0032-3861\(00\)00023-9](https://doi.org/10.1016/S0032-3861(00)00023-9)
- Wen, Y., Lian, F., Ren, Y., & Guan, H. (2014). Enhanced electrochemical properties of a novel polyvinyl formal membrane supporting gel polymer electrolyte by Al₂O₃ modification. *Journal of Polymer Science Part B: Polymer Physics*, 52(8), 572–577.
- Weng, W., Sun, Q., Zhang, Y., He, S., Wu, Q., Deng, J., Fang, X., Guan, G., Ren, J., & Peng, H. (2015). A gum-like lithium-ion battery based on a novel arched structure. *Advanced Materials*. <https://doi.org/10.1002/adma.201405127>
- Wetjen, M., Navarra, M. A., Panero, S., Passerini, S., Scrosati, B., & Hassoun, J. (2013). Composite poly (ethylene oxide) electrolytes plasticized by N-alkyl-N-butylpyrrolidinium Bis (trifluoromethanesulfonyl) imide for lithium batteries. *ChemSusChem*, 6(6), 1037–1043.
- Wieczorek, W., Stevens, J. R., & Florjańczyk, Z. (1996). Composite polyether based solid electrolytes. The Lewis acid-base approach. *Solid State Ionics*, 85(1–4), 67–72.
- Wieczorek, Władysław, Florjanczyk, Z., & Stevens, J. R. (1995). Composite polyether based

- solid electrolytes. *Electrochimica Acta*, 40(13–14), 2251–2258.
- Willner, I. (2002). Biomaterials for sensors, fuel cells, and circuitry. *Science*, 298(5602), 2407–2408.
- Wright, P. V. (1998). Polymer electrolytes—the early days. *Electrochimica Acta*, 43(10–11), 1137–1143.
- Wrodnigg, G. H., Besenhard, J. O., & Winter, M. (1999). Ethylene Sulfite as Electrolyte Additive for Lithium-Ion Cells with Graphitic Anodes. *Journal of The Electrochemical Society*, 146(2), 470.
- Wrodnigg, G. H., Wrodnigg, T. M., Besenhard, J. O., & Winter, M. (1999). Propylene sulfite as film-forming electrolyte additive in lithium ion batteries. *Electrochemistry Communications*, 1(3–4), 148–150.
- Wu, G., Yang, H.-Y., Chen, H.-Z., Yuan, F., Yang, L.-G., Wang, M., & Fu, R.-J. (2007). Novel porous polymer electrolyte based on polyacrylonitrile. *Materials Chemistry and Physics*, 104(2–3), 284–287.
- Wu, H.-L., Huff, L. A., Esbenshade, J. L., & Gewirth, A. A. (2015). In situ EQCM study examining irreversible changes the sulfur–carbon cathode in lithium–sulfur batteries. *ACS Applied Materials & Interfaces*, 7(37), 20820–20828.
- Wu, H., Chan, G., Choi, J. W., Ryu, I., Yao, Y., Mcdowell, M. T., Lee, S. W., Jackson, A., Yang, Y., Hu, L., & Cui, Y. (2012). Stable cycling of double-walled silicon nanotube battery anodes through solid-electrolyte interphase control. *Nature Nanotechnology*, 7(5), 310–315. <https://doi.org/10.1038/nnano.2012.35>
- Wu, N., Cao, Q., Wang, X., Li, X., & Deng, H. (2011). A novel high-performance gel polymer electrolyte membrane basing on electrospinning technique for lithium rechargeable

- batteries. *Journal of Power Sources*, 196(20), 8638–8643.
- Wu, Q., Yang, J., Zhao, Y., Song, R., Wang, Z., Huang, Z., Shi, M., Ye, Y., He, D., & Mu, S. (2020). Lifting the energy density of lithium ion batteries using graphite film current collectors. *Journal of Power Sources*, 455, 227991.
- Wu, Z., Zhou, G., Yin, L., & Ren, W. (2012). Graphene / metal oxide composite electrode materials for energy storage. *Nano Energy*, 1(1), 107–131.
<https://doi.org/10.1016/j.nanoen.2011.11.001>
- Park, S., Kim, Y., Han, S., Ahn, S., Ku, C., & Lee, J. (2002). *The elevated temperature performance of LiMn₂O₄ coated*. 107, 2–7.
- Xi, J., Qiu, X., Cui, M., Tang, X., Zhu, W., & Chen, L. (2006). Enhanced electrochemical properties of PEO-based composite polymer electrolyte with shape-selective molecular sieves. *Journal of Power Sources*, 156(2), 581–588.
- Xi, J., Qiu, X., Li, J., Tang, X., Zhu, W., & Chen, L. (2006). PVDF–PEO blends based microporous polymer electrolyte: Effect of PEO on pore configurations and ionic conductivity. *Journal of Power Sources*, 157(1), 501–506.
- Xia, L., Wang, S., Liu, G., Ding, L., Li, D., & Wang, H. (2016). *Flexible SnO₂ / N-Doped Carbon Nanofiber Films as Integrated Electrodes for Lithium-Ion Batteries with Superior Rate Capacity and Long Cycle Life*. 7, 853–859.
<https://doi.org/10.1002/sml.201503315>
- Xiao, W., Li, X., Guo, H., Wang, Z., Zhang, Y., & Zhang, X. (2012). Preparation of core–shell structural single ionic conductor SiO₂@ Li⁺ and its application in PVDF–HFP-based composite polymer electrolyte. *Electrochimica Acta*, 85, 612–621.
- Xie, H., Liao, Y., Sun, P., Chen, T., Rao, M., & Li, W. (2014). Investigation on polyethylene-

- supported and nano-SiO₂ doped poly (methyl methacrylate-co-butyl acrylate) based gel polymer electrolyte for high voltage lithium ion battery. *Electrochimica Acta*, 127, 327–333.
- Xiong, H., Wang, Z., Liu, D., Chen, J., Wang, Y., & Xia, Y. (2005). Bonding polyether onto ZnO nanoparticles: An effective method for preparing polymer nanocomposites with tunable luminescence and stable conductivity. *Advanced Functional Materials*, 15(11), 1751–1756.
- Xu, S., Zhang, Y., Cho, J., Lee, J., Huang, X., Jia, L., Fan, J. A., Su, Y., Su, J., Zhang, H., Cheng, H., Lu, B., Yu, C., Chuang, C., Kim, T. Il, Song, T., Shigeta, K., Kang, S., Dagdeviren, C., Petrov I., Braun P., Huang Y., Paik U., Rogers, J. A. (2013). Stretchable batteries with self-similar serpentine interconnects and integrated wireless recharging systems. *Nature Communications*. <https://doi.org/10.1038/ncomms2553>
- Xu, W., Wang, J., Ding, F., Chen, X., Nasybulin, E., Zhang, Y., & Zhang, J.-G. (2014). Lithium metal anodes for rechargeable batteries. *Energy & Environmental Science*, 7(2), 513–537.
- Xue, Z., He, D., & Xie, X. (2015). Poly (ethylene oxide)-based electrolytes for lithium-ion batteries. *Journal of Materials Chemistry A*, 3(38), 19218–19253.
- Yabuuchi, N., Yoshii, K., Myung, S.-T., Nakai, I., & Komaba, S. (2011). Detailed studies of a high-capacity electrode material for rechargeable batteries, Li₂MnO₃–LiCo_{1/3}Ni_{1/3}Mn_{1/3}O₂. *Journal of the American Chemical Society*, 133(12), 4404–4419.
- Yamakawa, S., & Stannett, V. (1974). The thermal stability of radiation-grafted poly (vinyl chlorides). *Journal of Applied Polymer Science*, 18(7), 2177–2193.
- Yan, C., Wang, X., Cui, M., Wang, J., Kang, W., Foo, C. Y., & Lee, P. S. (2014). Stretchable

- silver-zinc batteries based on embedded nanowire elastic conductors. *Advanced Energy Materials*. <https://doi.org/10.1002/aenm.201301396>
- Yang, C.-P., Yin, Y.-X., Zhang, S.-F., Li, N.-W., & Guo, Y.-G. (2015). Accommodating lithium into 3D current collectors with a submicron skeleton towards long-life lithium metal anodes. *Nature Communications*, 6(1), 1–9.
- Yang, Chongyang, Sun, M., Wang, X., & Wang, G. (2015). A novel flexible supercapacitor based on cross-linked PVDF-HFP porous organogel electrolyte and carbon nanotube paper@ π -conjugated polymer film electrodes. *ACS Sustainable Chemistry & Engineering*, 3(9), 2067–2076.
- Yang, Cuiru, Jia, Z., Guan, Z., & Wang, L. (2009). Polyvinylidene fluoride membrane by novel electrospinning system for separator of Li-ion batteries. *Journal of Power Sources*, 189(1), 716–720.
- Yang, L., Wang, Z., Feng, Y., Tan, R., Zuo, Y., Gao, R., Zhao, Y., Han, L., Wang, Z., & Pan, F. (2017). Flexible Composite Solid Electrolyte Facilitating Highly Stable “Soft Contacting” Li–Electrolyte Interface for Solid State Lithium-Ion Batteries. *Advanced Energy Materials*, 7(22), 1–9. <https://doi.org/10.1002/aenm.201701437>
- Yang, P., Liu, L., Li, L., Hou, J., Xu, Y., Ren, X., An, M., & Li, N. (2014). Gel polymer electrolyte based on polyvinylidene fluoride-co-hexafluoropropylene and ionic liquid for lithium ion battery. *Electrochimica Acta*, 115, 454–460.
- Yang, X., Gao, X., Sun, Q., Jand, S. P., Yu, Y., Zhao, Y., Li, X., Adair, K., Kuo, L., & Rohrer, J. (2019). Promoting the transformation of Li₂S₂ to Li₂S: significantly increasing utilization of active materials for high-sulfur-loading Li–S batteries. *Advanced Materials*, 31(25), 1901220.

- Yang, X., Jiang, M., Gao, X., Bao, D., Sun, Q., Holmes, N., Duan, H., Mukherjee, S., Adair, K., & Zhao, C. (2020). Determining the limiting factor of the electrochemical stability window for PEO-based solid polymer electrolytes: main chain or terminal–OH group? *Energy & Environmental Science*.
- Yang, Y., Yuan, W., Zhang, X., Ke, Y., Qiu, Z., Luo, J., Tang, Y., Wang, C., Yuan, Y., & Huang, Y. (2020). A review on structuralized current collectors for high-performance lithium-ion battery anodes. *Applied Energy*, 276, 115464.
- Yao, J., Bewlay, S., Konstantinov, K., Drozd, V. A., Liu, R. S., Wang, X. L., Liu, H. K., & Wang, G. X. (2006). Characterisation of olivine-type $\text{LiMn}_x\text{Fe}_{1-x}\text{PO}_4$ cathode materials. *Journal of Alloys and Compounds*, 425(1–2), 362–366.
- Yao, Jian, Bastiaansen, C. W. M., & Peijs, T. (2014). High strength and high modulus electrospun nanofibers. *Fibers*, 2(2), 158–186.
- Yao, Z., Xia, X., Zhou, C., Zhong, Y., Wang, Y., Deng, S., Wang, W., Wang, X., & Tu, J. (2018). Smart construction of integrated CNTs/ $\text{Li}_4\text{Ti}_5\text{O}_{12}$ core/shell arrays with superior high-rate performance for application in lithium-ion batteries. *Advanced Science*, 5(3), 1700786.
- Ye, J., Zhang, H., Yang, R., Li, X., & Qi, L. (2010). Morphology-controlled synthesis of SnO_2 nanotubes by using 1D silica mesostructures as sacrificial templates and their applications in lithium-ion batteries. *Small*. <https://doi.org/10.1002/sml.200901815>
- Ye, Y.-S., Rick, J., & Hwang, B.-J. (2013). Ionic liquid polymer electrolytes. *Journal of Materials Chemistry A*, 1(8), 2719–2743.
- Yildiz, O., Dirican, M., Fang, X., Fu, K., Jia, H., Stano, K., Zhang, X., & Bradford, P. D. (2019). *Hybrid Carbon Nanotube Fabrics with Sacrificial Nanofibers for Flexible High*

- Performance Lithium-Ion Battery Anodes*. 166(4), 473–479.
- <https://doi.org/10.1149/2.0821902jes>
- Yokokawa, H., Tu, H., Iwanschitz, B., & Mai, A. (2008). Fundamental mechanisms limiting solid oxide fuel cell durability. *Journal of Power Sources*, 182(2), 400–412.
- Yoo, E., Kim, J., Hosono, E., Zhou, H., Kudo, T., & Honma, I. (2008). Large reversible Li storage of graphene nanosheet families for use in rechargeable lithium ion batteries. *Nano Letters*, 8(8), 2277–2282.
- Yu, B.-C., Jung, J.-W., Park, K., & Goodenough, J. B. (2017). A new approach for recycling waste rubber products in Li–S batteries. *Energy & Environmental Science*, 10(1), 86–90.
- Yu, C., Masarapu, C., Rong, J., Wei, B. Q. M., & Jiang, H. (2009). Stretchable supercapacitors based on buckled single-walled carbon nanotube macrofilms. *Advanced Materials*.
<https://doi.org/10.1002/adma.200901775>
- Yu, P., Popov, B. N., Ritter, J. A., & White, R. E. (1999). Determination of the lithium ion diffusion coefficient in graphite. *Journal of The Electrochemical Society*, 146(1), 8.
- Yu, S., Schmidt, R. D., Garcia-Mendez, R., Herbert, E., Dudney, N. J., Wolfenstine, J. B., Sakamoto, J., & Siegel, D. J. (2016). Elastic properties of the solid electrolyte Li₇La₃Zr₂O₁₂ (LLZO). *Chemistry of Materials*, 28(1), 197–206.
- Yu, Xiao-Yuan, Xiao, M., Wang, S., Zhao, Q., & Meng, Y. (2010). Fabrication and characterization of PEO/PPC polymer electrolyte for lithium-ion battery. *Journal of Applied Polymer Science*, 115(5), 2718–2722.
- Yu, Xiaohua, Bates, J. B., Jellison Jr, G. E., & Hart, F. X. (1997). A stable thin-film lithium electrolyte: lithium phosphorus oxynitride. *Journal of the Electrochemical Society*, 144(2), 524.

- Yu, Xiaoyuan, Xiao, M., Wang, S., Han, D., & Meng, Y. (2010). Fabrication and properties of crosslinked poly (propylene carbonate maleate) gel polymer electrolyte for lithium-ion battery. *Journal of Applied Polymer Science*, 118(4), 2078–2083.
- Yu, Xinrun, Wang, L., Ma, J., Sun, X., Zhou, X., & Cui, G. (2020). Selectively Wetted Rigid–Flexible Coupling Polymer Electrolyte Enabling Superior Stability and Compatibility of High-Voltage Lithium Metal Batteries. *Advanced Energy Materials*.
- Yuan, C., Li, J., Han, P., Lai, Y., Zhang, Z., & Liu, J. (2013). Enhanced electrochemical performance of poly (ethylene oxide) based composite polymer electrolyte by incorporation of nano-sized metal-organic framework. *Journal of Power Sources*, 240, 653–658.
- Yuan, M., Erdman, J., Tang, C., & Ardebili, H. (2014). High performance solid polymer electrolyte with graphene oxide nanosheets. *Rsc Advances*, 4(103), 59637–59642.
- Yuan, Z., Peng, H., Huang, J., Liu, X., Wang, D., Cheng, X., & Zhang, Q. (2014). Hierarchical free-standing carbon-nanotube paper electrodes with ultrahigh sulfur-loading for lithium–sulfur batteries. *Advanced Functional Materials*, 24(39), 6105–6112.
- Zaeem, M. A., El Kadiri, H., Mesarovic, S. D., Horstemeyer, M. F., & Wang, P. T. (2011). Effect of the compositional strain on the diffusive interface thickness and on the phase transformation in a phase-field model for binary alloys. *Journal of Phase Equilibria and Diffusion*, 32(4), 302–308.
- Zamarayeva, A. M., Ostfeld, A. E., Wang, M., Duey, J. K., Deckman, I., Lechêne, B. P., Davies, G., Steingart, D. A., & Arias, A. C. (2017). Flexible and stretchable power sources for wearable electronics. *Science Advances*.
<https://doi.org/10.1126/sciadv.1602051>

- Zanetto, P., Nervi, C., & De Biani, F. F. (2011). *Inorganic electrochemistry: theory, practice and application*. Royal Society of Chemistry.
- Zhai, H., Xu, P., Ning, M., Cheng, Q., Mandal, J., & Yang, Y. (2017). A Flexible Solid Composite Electrolyte with Vertically Aligned and Connected Ion-Conducting Nanoparticles for Lithium Batteries. *Nano Letters*, 17(5), 3182–3187.
<https://doi.org/10.1021/acs.nanolett.7b00715>
- Zhai, W., Zhu, H., Wang, L., Liu, X., & Yang, H. (2014). Study of PVDF-HFP/PMMA blended micro-porous gel polymer electrolyte incorporating ionic liquid [BMIM] BF₄ for Lithium ion batteries. *Electrochimica Acta*, 133, 623–630.
- Zhang, D., Zhang, L., Yang, K., Wang, H., Yu, C., Xu, D., Xu, B., & Wang, L. M. (2017). Superior Blends Solid Polymer Electrolyte with Integrated Hierarchical Architectures for All-Solid-State Lithium-Ion Batteries. *ACS Applied Materials and Interfaces*, 9(42), 36886–36896. <https://doi.org/10.1021/acsami.7b12186>
- Zhang, H., Li, C., Piszcz, M., Coya, E., Rojo, T., Rodriguez-Martinez, L. M., Armand, M., & Zhou, Z. (2017). Single lithium-ion conducting solid polymer electrolytes: Advances and perspectives. *Chemical Society Reviews*, 46(3), 797–815.
<https://doi.org/10.1039/c6cs00491a>
- Zhang, H. P., Zhang, P., Li, Z. H., Sun, M., Wu, Y. P., & Wu, H. Q. (2007). A novel sandwiched membrane as polymer electrolyte for lithium ion battery. *Electrochemistry Communications*, 9(7), 1700–1703.
- Zhang, Jianjun, Yang, J., Dong, T., Zhang, M., Chai, J., Dong, S., Wu, T., Zhou, X., & Cui, G. (2018). Aliphatic Polycarbonate-Based Solid-State Polymer Electrolytes for Advanced Lithium Batteries: Advances and Perspective. *Small*, 14(36), 1800821.

- Zhang, Jianjun, Zang, X., Wen, H., Dong, T., Chai, J., Li, Y., Chen, B., Zhao, J., Dong, S., & Ma, J. (2017). High-voltage and free-standing poly (propylene carbonate)/Li_{6.75}La₃Zr_{1.75}Ta_{0.25}O₁₂ composite solid electrolyte for wide temperature range and flexible solid lithium ion battery. *Journal of Materials Chemistry A*, 5(10), 4940–4948.
- Zhang, Jianjun, Zhao, J., Yue, L., Wang, Q., Chai, J., Liu, Z., Zhou, X., Li, H., Guo, Y., & Cui, G. (2015). Safety-reinforced poly (propylene carbonate)-based All-solid-state polymer electrolyte for ambient-temperature solid polymer lithium batteries. *Advanced Energy Materials*, 5(24), 1501082.
- Zhang, Jingxian, Zhao, N., Zhang, M., Li, Y., Chu, P. K., Guo, X., Di, Z., Wang, X., & Li, H. (2016a). Flexible and ion-conducting membrane electrolytes for solid-state lithium batteries: dispersion of garnet nanoparticles in insulating polyethylene oxide. *Nano Energy*, 28, 447–454.
- Zhang, Jingxian, Zhao, N., Zhang, M., Li, Y., Chu, P. K., Guo, X., Di, Z., Wang, X., & Li, H. (2016b). Flexible and ion-conducting membrane electrolytes for solid-state lithium batteries: Dispersion of garnet nanoparticles in insulating polyethylene oxide. *Nano Energy*, 28, 447–454. <https://doi.org/10.1016/j.nanoen.2016.09.002>
- Zhang, M., Ma, X., Liu, Y., Ma, J., Chen, F., & Zhang, Q. (2019). High-performance electrospun POSS-(PMMA 46) 8/PVDF hybrid gel polymer electrolytes with PP support for Li-ion batteries. *Ionics*, 25(6), 2595–2605.
- Zhang, M. Y., Li, M. X., Chang, Z., Wang, Y. F., Gao, J., Zhu, Y. S., Wu, Y. P., & Huang, W. (2017). A Sandwich PVDF/HEC/PVDF Gel Polymer Electrolyte for Lithium Ion Battery. *Electrochimica Acta*, 245, 752–759. <https://doi.org/10.1016/j.electacta.2017.05.154>
- Zhang, Q., & White, R. E. (2007). Calendar life study of Li-ion pouch cells. *Journal of Power*

- Sources*, 173(2), 990–997.
- Zhang, S., Shen, J., Qiu, X., Weng, D., & Zhu, W. (2006). ESR and vibrational spectroscopy study on poly (vinylidene fluoride) membranes with alkaline treatment. *Journal of Power Sources*, 153(2), 234–238.
- Zhang, S S, & Jow, T. R. (2002). Study of poly (acrylonitrile-methyl methacrylate) as binder for graphite anode and LiMn₂O₄ cathode of Li-ion batteries. *Journal of Power Sources*, 109(2), 422–426.
- Zhang, S S, Xu, K., & Jow, T. R. (2002). Low temperature performance of graphite electrode in Li-ion cells. *Electrochimica Acta*, 48(3), 241–246.
- Zhang, S S, Xu, K., & Jow, T. R. (2003). Li-ion cell with poly (acrylonitrile-methyl methacrylate)-based gel polymer electrolyte. *Solid State Ionics*, 158(3–4), 375–380.
- Zhang, Sheng S, & Tran, D. T. (2013). How a gel polymer electrolyte affects performance of lithium/sulfur batteries. *Electrochimica Acta*, 114, 296–302.
- Zhang, W., Richter, F. H., Culver, S. P., Leichtweiss, T., Lozano, J. G., Dietrich, C., Bruce, P. G., Zeier, W. G., & Janek, J. (2018). Degradation Mechanisms at the Li₁₀GeP₂S₁₂/LiCoO₂ Cathode Interface in an All-Solid-State Lithium-Ion Battery. *ACS Applied Materials and Interfaces*, 10(26), 22226–22236.
<https://doi.org/10.1021/acsami.8b05132>
- Zhang, Xiuling, Zhao, S., Fan, W., Wang, J., & Li, C. (2019). Long cycling, thermal stable, dendrites free gel polymer electrolyte for flexible lithium metal batteries. *Electrochimica Acta*, 301, 304–311.
- Zhang, Xue, Liu, T., Zhang, S., Huang, X., Xu, B., Lin, Y., Xu, B., Li, L., Nan, C.-W., & Shen, Y. (2017). Synergistic coupling between Li₆.₇₅La₃Zr₁.₇₅Ta₀.₂₅O₁₂ and poly

- (vinylidene fluoride) induces high ionic conductivity, mechanical strength, and thermal stability of solid composite electrolytes. *Journal of the American Chemical Society*, *139*(39), 13779–13785.
- Zhang, Y., Bai, W., Ren, J., Weng, W., Lin, H., Zhang, Z., & Peng, H. (2014). Super-stretchy lithium-ion battery based on carbon nanotube fiber. *Journal of Materials Chemistry A*. <https://doi.org/10.1039/c4ta01878h>
- Zhang, Y., Zhao, Y., Ren, J., Weng, W., & Peng, H. (2016). Advances in Wearable Fiber-Shaped Lithium-Ion Batteries. *Advanced Materials*, *28*(22), 4524–4531.
- Zhao, C., Jia, X., Shu, K., Yu, C., Min, Y., & Wang, C. (2020). Stretchability enhancement of buckled polypyrrole electrodes for stretchable supercapacitors via engineering substrate surface roughness. *Electrochimica Acta*. <https://doi.org/10.1016/j.electacta.2020.136099>
- Zhao, Jianghui, Zhang, J., Hu, P., Ma, J., Wang, X., Yue, L., Xu, G., Qin, B., Liu, Z., & Zhou, X. (2016). A sustainable and rigid-flexible coupling cellulose-supported poly (propylene carbonate) polymer electrolyte towards 5 V high voltage lithium batteries. *Electrochimica Acta*, *188*, 23–30.
- Zhao, Jie, Liao, L., Shi, F., Lei, T., Chen, G., Pei, A., Sun, J., Yan, K., Zhou, G., & Xie, J. (2017). Surface fluorination of reactive battery anode materials for enhanced stability. *Journal of the American Chemical Society*, *139*(33), 11550–11558.
- Zhao, X., Jiang, J., Xue, Z., Yan, C., & Mu, T. (2017). An ambient temperature, CO₂-assisted solution processing of amorphous cobalt sulfide in a thiol/amine based quasi-ionic liquid for oxygen evolution catalysis. *Chemical Communications*, *53*(68), 9418–9421.
- Zheng, B., Zhu, J., Wang, H., Feng, M., Umeshbabu, E., Li, Y., Wu, Q.-H., & Yang, Y. (2018). Stabilizing Li₁₀SnP₂S₁₂/Li interface via an in situ formed solid electrolyte

- interphase layer. *ACS Applied Materials & Interfaces*, 10(30), 25473–25482.
- Zhong, J., Cao, C., Liu, Y., Li, Y., & Khan, W. S. (2010). Hollow core-shell η -Fe₂O₃ microspheres with excellent lithium-storage and gas-sensing properties. *Chemical Communications*. <https://doi.org/10.1039/c0cc00204f>
- Zhou, D. Y., Wang, G. Z., Li, W. S., Li, G. L., Tan, C. L., Rao, M. M., & Liao, Y. H. (2008). Preparation and performances of porous polyacrylonitrile–methyl methacrylate membrane for lithium-ion batteries. *Journal of Power Sources*, 184(2), 477–480.
- Zhou, D., Zhou, R., Chen, C., Yee, W.-A., Kong, J., Ding, G., & Lu, X. (2013). Non-volatile polymer electrolyte based on poly (propylene carbonate), ionic liquid, and lithium perchlorate for electrochromic devices. *The Journal of Physical Chemistry B*, 117(25), 7783–7789.
- Zhou, F., Liao, H., & Zhang, Z. (2020). Mechanical strong polymer cross-linking PVDF nanofiber electrolyte for lithium-ion batteries. *Ionics*, 1–8.
- Zhou, G., Li, F., & Cheng, H.-M. (2014). Progress in flexible lithium batteries and future prospects. *Energy & Environmental Science*, 7(4), 1307–1338.
- Zhou, G., Li, L., Wang, D., Shan, X., Pei, S., Li, F., & Cheng, H. (2015). A flexible sulfur-graphene-polypropylene separator integrated electrode for advanced Li–S batteries. *Advanced Materials*, 27(4), 641–647.
- Zhou, G., Wang, D. W., Li, F., Zhang, L., Li, N., Wu, Z. S., Wen, L., Lu, G. Q., & Cheng, H. M. (2010). Graphene-wrapped Fe₃O₄ anode material with improved reversible capacity and cyclic stability for lithium ion batteries. *Chemistry of Materials*. <https://doi.org/10.1021/cm101532x>
- Zhou, Q., Ma, J., Dong, S., Li, X., & Cui, G. (2019). Intermolecular Chemistry in Solid

- Polymer Electrolytes for High-Energy-Density Lithium Batteries. *Advanced Materials*, 31(50), 1902029.
- Zhou, W., Wang, Z., Pu, Y., Li, Y., Xin, S., Li, X., Chen, J., & Goodenough, J. B. (2019). Double-Layer Polymer Electrolyte for High-Voltage All-Solid-State Rechargeable Batteries. *Advanced Materials*, 31(4), 1–7. <https://doi.org/10.1002/adma.201805574>
- Zhu, M., Tan, C., Fang, Q., Gao, L., Sui, G., & Yang, X. (2016). High performance and biodegradable skeleton material based on soy protein isolate for gel polymer electrolyte. *ACS Sustainable Chemistry & Engineering*, 4(9), 4498–4505.
- Zhu, Yinghua, Cao, J., Chen, H., Yu, Q., & Li, B. (2019). High electrochemical stability of a 3D cross-linked network PEO@ nano-SiO₂ composite polymer electrolyte for lithium metal batteries. *Journal of Materials Chemistry A*, 7(12), 6832–6839.
- Zhu, Yizhou, He, X., & Mo, Y. (2016). First principles study on electrochemical and chemical stability of solid electrolyte-electrode interfaces in all-solid-state Li-ion batteries. *Journal of Materials Chemistry A*, 4(9), 3253–3266. <https://doi.org/10.1039/c5ta08574h>
- Zhu, Yusong, Wang, F., Liu, L., Xiao, S., Yang, Y., & Wu, Y. (2013). Cheap glass fiber mats as a matrix of gel polymer electrolytes for lithium ion batteries. *Scientific Reports*, 3, 3187.
- Zou, M., Yoshio, M., Gopukumar, S., & Yamaki, J. (2003). Synthesis of high-voltage (4.5 V) cycling doped LiCoO₂ for use in lithium rechargeable cells. *Chemistry of Materials*, 15(25), 4699–4702.
- Zito, Ralph., Ardebili, Haleh. (2019) Energy Storage: New Approach, Second Edition, Scrivener Willey.

CHAPTER VIII. APPENDICES

A. Tables

Table 14 Flexible commercial electronics and our lithium ion batteries

Model	Diagonal (In)	Radius of Curvature(mm)	Bending angles(θ)
Samsung Round	5.7	400(16in)	20.4°
LG G Flex	6	700(28in)	12.3°
Samsung KN55S9C	54.6	4500(180in)	17.4°
LG 55EA9800	54.6	5000(200in)	15.6°
Helmet	15.3	185(7.3)	120°
Smart Watch	4.1	33(1.3)	
Our Batteries	2.4	19(0.7in)	180°

Table 15 Polymer electrolyte ionic conductivity comparison

Sample	LiTFSI:LiBOB:PEO:TEGDME (S/cm)	LiBOB:PEO:TEGDME (S/cm)
1	9.37×10^{-6}	4.13×10^{-5}
2	3.28×10^{-6}	2.13×10^{-5}
3	1.41×10^{-5}	2.73×10^{-5}
Average	8.92×10^{-6}	3.00×10^{-5}

Table 16 Flexible LIBs(LiBOB) performance summary for bending test

Bending Angles (°)	Capacity (mAh/cm ²)	Capacity Retention (%)
0	~0.76	100
90	~0.80	105
180	~0.75	99
0 (0C°)	~0.15	20
0(~23°C)	~0.71	93

Table 17 Flexible LIBs (LiBOB) performance summary for thermal test

Temperature(°C)	Capacity (mAh/cm ²)	Capacity Retention (%)
0	~0.14	19
10	~0.31	41
23	~0.75	96
35	~0.86	115
45	~0.98	131
60	~1.00	133

Table 18 Stretchable LIBs performance summary for stretchability test

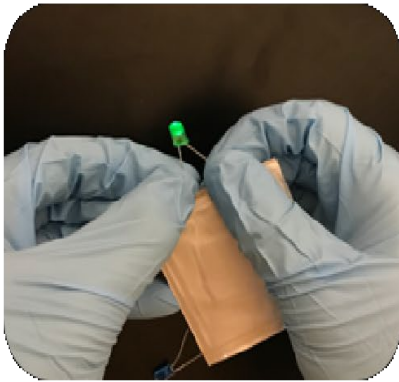
Stretching Percentage (%)	Capacity (mAh/cm ²)	Capacity Retention (%)
0	~0.92	100
3000	~0.59	64
6000	~0.47	51
0	~0.72	78
1000	~0.49	53
3000	~0.46	50
0	~0.33	36

Table 19 Summary of three types polymer electrolyte flexible LIBs

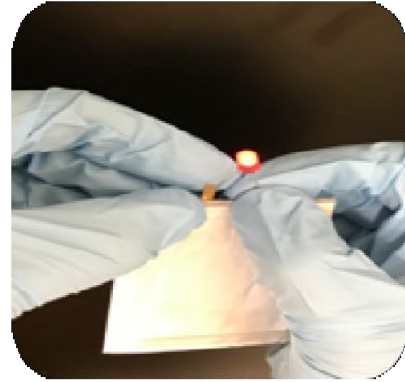
Battery type	Composition	Cut Off Voltage Range (V)	Nominal Voltage (V)	Capacity (mAh/cm ²)	Energy Density (Wh/Kg based on LIBs)	Energy Density (Wh/Kg based on LCO)
Type 1	LCO/PEO:LIBO B:TEGDME /G	3-4.2	3.7-3.8	~0.8	~8.45	~67.71
Type 2	LCO/PEO:LIBO B+LiTFSI:TEG DME/G	3-4.2	3.7-3.8	~0.7	~7.40	~59.29
Type 3	LCO/PEO:LIBO B:TEGDME:FE C/G	3-4.2	3.7-3.8	~1.5	~15.85	~127.0

B. Figures

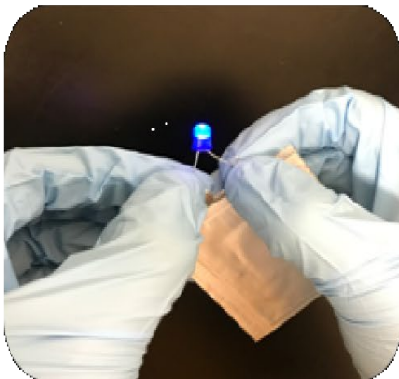
Green LED



Red LED



Blue LED



Flash LED

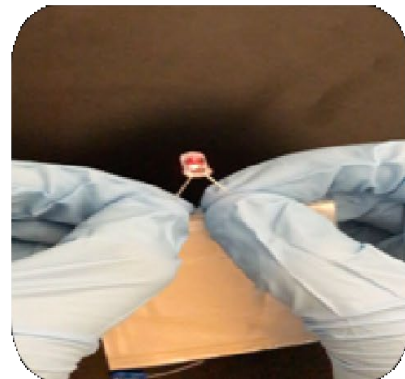
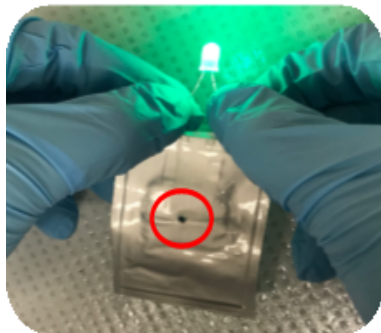


Figure 46 Flexible polymer LIBs powered LED lights

Working after LiB Punctured



Working at 180° Bending

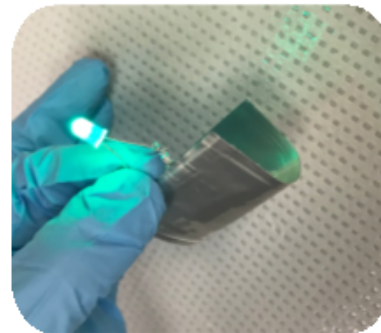


Figure 47 (a) LiB powered LED light after puncture test; (b) LiB powered LED light after bending 180 degrees

